PHYSICS REPORTS (Review Section of Physics Letters) 176, Nos. 5 & 6 (1989) 189–370. North-Holland, Amsterdam

NONSTATIONARY DISSIPATIVE STRUCTURES AND DIFFUSION-INDUCED CHAOS IN NONLINEAR MEDIA

T.S. AKHROMEYEVA, S.P. KURDYUMOV, G.G. MALINETSKII and A.A. SAMARSKII

Keldysh Institute of Applied Mathematics, Academy of Sciences of the USSR, Miusskaya Sq. 4, 125047 Moscow A-47, USSR

Received July 1988

Contents:

0 370-1573/89/$63.70

NONSTATIONARY DISSIPATIVE STRUCTURES AND DIFFUSION-INDUCED CHAOS IN NONLINEAR MEDIA

T.S. AKHROMEYEVA, S.P. KURDYUMOV, G.G. MALINETSKII and A.A. SAMARSKII

Keldysh Institute of Applied Mathematics, Academy of Sciences of the USSR, Miusskaya Sq. 4, 125047 Moscow A-47, USSR

NORTH-HOLLAND – AMSTERDAM

Introduction

In the last decades the study of nonlinear dissipative media has aroused great interest. When analysing these media investigators noticed a reduction of the number of the degrees of freedom effectively describing the system. In some cases several degrees of freedom can be singled out which determine the dynamics of the process, the remaining ones adjusting to them. They are often called *order parameters*. Their existence is very important. In investigating dissipative systems one or a whole *hierarchy of simplified models* is expected to be built. Their analysis is believed to lead to the understanding of many complex nonlinear phenomena.

In this connection the study of the simplest (often called basic) nonlinear models acquires special significance. This approach provided an opportunity to find a number of regularities; it also led to the emergence of new ideas and concepts (such as solitons, strange attractors, dissipative structures) and brought about the discovery of some new phenomena.

Reducing the number of degrees of freedom means that *self-organization* occurs in the system. In other words, the system acquires properties which none of its subsystems possess. The whole assumes qualities which none of its parts possess.

To place special emphasis on this fact, the theory of self-organization is often called synergetics (or the theory of joint action). This term was introduced by H. Haken [13]. He gives the following explanation: "I have called this discipline 'synergetics'. What we investigate is the joint action of many subsystems (mostly of the same or of a few different kinds) so as to produce structure and functioning on a macroscopic scale. On the other hand, many different disciplines cooperate here to find general principles governing self-organizing systems" [13].

The formation of structures closely connected with dissipative processes (often called *dissipative structures*) proved to be a common feature of different nonlinear systems. The term "dissipative structure" was introduced by the Belgian scientist I. Prigogine. The work of the scientists belonging to the Brussels school, of which he is the head, helped to bring out the connection among the formation of structure, phenomenological models and the basic concepts of nonequilibrium thermodynamics. They played an important role in both the theoretical and experimental investigation of order in open systems.

Here is how G. Nicolis and I. Prigogine characterize a new concept appearing in the natural sciences: "... both remoteness from equilibrium and nonlinearity may cause the emergence of order in the system.

The connection among order, stability and dissipation is highly nontrivial. To bring out this connection we shall call ordered configurations, appearing apart from the stability area, dissipative structures... These structures can exist far from the equilibrium position by the expenditure of large fluxes of energy and substance. Dissipative structures themselves are a striking example, illustrating the property of nonequilibrium to be a source of order" [3].

Order formation in open nonlinear systems seems, on the face of it, paradoxical. In equilibrium

systems dissipative processes eliminate order, and thermodynamic equilibrium is established. In nonlinear open systems dissipation comes out in a new quality. Its joint action with other processes leads to pattern formation, which determines their type, shape, dimensions.

In recent years the investigation of open nonlinear systems has resulted in a number of important achievements. Analysis of comparatively simple mathematical models, such as the "reaction–diffusion systems", the Lorenz equations, one-dimensional maps $[x_{n+1} = f(x_n, \lambda)]$ has given rise to new ideas and brought to life a number of mathematical theories. It stands to reason that deep analysis of a concrete situation should not be replaced by simplified models, ideas and concepts of synergetics. However, these concepts can determine the direction of investigation which, in many cases, proves very important. The rapid growth of the number of investigations using the methods and concepts of dissipative structure theory and the appearance of many interesting experimental works devoted to self-organization testify to this. It can be exemplified by the findings in the investigation of the transition-to-turbulence scenarios and the analysis of small-mode chaos in hydrodynamic systems [27], the study of oscillatory chemical reactions [28], and behaviour of active biological media, as well as the dynamics of morphogenetic processes [5, 8], along with a number of other studies.

To solve many concrete problems in plasma physics, microelectronics, hydrodynamics, chemical kinetics, astrophysics and in many other fields, it turned out to be necessary to answer a number of general questions. What are the mechanisms of the formation of spatial–temporal order in nonlinear media? Can simple structures be united into complex ones? What are the organization laws of the structures formed? How does the transition from the simplest ordered regimes to the complex stochastic ones go? Are there any effective methods of controlling processes in dissipative systems?

The attempts to answer these questions helped to single out some features typical of various nonlinear media. Let us consider some of them. As a rule, a whole class of initial data may evolve to the same asymptotic regime. In other words, *the details of the initial data are "forgotten"*. This makes it possible to raise the question of the direction of the processes, of their "aims".

The second law of thermodynamics gives the answer to this question for closed systems. The same answer holds true for a number of nonlinear media. In due course they generate spatially homogeneous stationary distributions. For the models describing them one can plot, by analogy with ordinary differential equations, a Lyapunov function that will define the direction of the processes [29, 30].

However, analysis of many mathematical models shows that the described situation is rather an exception than a rule. The asymptotic regime usually has a more complicated nature. Its mathematical image is a limit set, which attracts the trajectories in the phase space of the system. It is often called an "*attractor*".

In Hamiltonian systems, where energy is conserved, the situation can be quite different; when the values of the energy and other integrals (determined by the initial data) are only slightly different, the solutions do not tend to each other [4]. The fact that the initial data are "forgotten" simplifies the investigation of open dissipative systems to a large extent. The system is expected to consist of a finite number of various structures, and comparatively simple mathematical tools may be used to cope with them.

The investigations showed that, in many cases, the asymptotic regimes in nonlinear dissipative media have an invariant-group structure. In the simplest situations they may be self-similar solutions, stationary solutions, running and standing waves. Two- and three-frequency regimes may often be observed as well. Modern methods of invariant-group analysis provide the possibility to find a complete set of self-similar solutions of the equations under study [68]. For a large class of stochastic regimes

scale invariance is typical [12]. The attractor proves to be similar to itself on different spatial scales. Invariant solutions, more often than not, prove to be the limit of a large class of other solutions rather than an exception or particular case. Thus, depending on the initial data, in comparatively simple dissipative systems there can be a transition to solutions of qualitatively different types, stationary, periodical, multi-frequency and stochastic. Such behaviour has been described in a number of experimental works. For example, it has been noted in ref. [32] that more than 100 different asymptotic regimes have been registered for certain parameter values in Couette–Taylor flow (the flow of a fluid between two rotating cylinders). This means that in one and the same open dissipative system the course of the processes and their "aims" can be different.

The existence of several attractors is closely connected with new possibilities of controlling the processes in nonlinear media. In actual fact, in phase space boundaries can be found that divide the domain of attraction of different attractors. Even a slight change of the initial data near these boundaries can lead to qualitatively different behaviour at a developed stage.

This is a common feature of many open nonlinear systems. In most of them there exists a certain range of parameters or a stage, where the system is especially sensitive to effects coherent with its intrinsic properties. (In a number of works this is called *resonance excitation* of the system.)

We shall see further that the amplitude and duration of these effects are very often less important than their correspondence to the properties of the medium (in the simplest cases it can be a certain profile of the initial data or a certain type of symmetry). Resonance effects can significantly change the course of the process. The study of the intrinsic properties of nonlinear media and the laws of dissipative structure organization is expected to give new instruments for dealing with complicated systems.

Computers play a significant role in the investigation of dissipative structures and self-organization phenomena. Most nonlinear mathematical models can only be analysed by combining analytical methods with computer calculations. This combination today is often called a *numerical experiment*. The study of its results can lead to the appearance of new concepts and notions and, in some cases, to the possibility to predict new phenomena.

If in previous years the problems of synergetics centred around stationary dissipative structures, in recent years investigators have been able to make a step further in understanding the nature of complex spatial and temporal order. This is the subject matter of this survey.

It has been shown that there exists a close connection between the formation of complex temporal order and the emergence of chaos in nonlinear systems. The analysis of stochastic behaviour, in many cases, does not require taking into account a great number of degrees of freedom. It can be well understood in the framework of simplified models with the interaction of several variables taken into consideration. This is why the approach suggested by synergetics, which is connected with the construction of a hierarchy of simplified models, proves very effective here. In a number of cases, their investigation provides an opportunity to find both qualitative and universal quantitative regularities, typical of many nonlinear systems.

Twenty years ago R. Feynman pointed to the analysis of processes in nonlinear media and the development of a qualitative theory of nonlinear partial differential equations as one of the key problems. Recent years have become a landmark in this direction. In the last years several detailed surveys have come to light devoted to the transition to turbulence in hydrodynamic systems. Therefore, we shall centre on other works which study complex spatial and temporal order, and above all systems of the reaction–diffusion type, as well as some other models. We are going to analyse a number of

mathematical results concerning complex spatial and temporal order and to present a number of physical situations in which these results can be effectively used. We consider the hierarchy of simplified models, arising in the theory of reaction–diffusion systems.

The bibliography to this survey does not pretend to be complete. It, mainly, contains either the works where these or other results are presented in a more complete and easier form, or original works, in which one can find important details concerning the problems discussed.

1. Self-organization and stationary dissipative structures

Reaction–diffusion systems reflecting many general properties of nonlinear media, have become an important class of mathematical models. A model of this kind appears to have been used for the first time ever by A. Turing in a mathematical simulation of morphogenesis [1]. His work, published more than 35 years ago, brought to light results which determined the development of the whole direction in science.

A. Turing put forward a hypothesis which furnished an explanation for the appearance of morphological and physiological differences in cells in the course of the development of organisms. He assumed that pattern formation in initially homogeneous tissue could be caused by diffusion processes and simple chemical reactions. The latter could be described by systems of ordinary differential equations.

If diffusion processes are taken into account we obtain a system of parabolic equations

$$\boldsymbol{u}_t = D\boldsymbol{u}_{xx} + \boldsymbol{Q}(\boldsymbol{u}) ,$$

where $\boldsymbol{u}$ is a vector, $\boldsymbol{Q}$ a vector function, D a diagonal matrix. If $\boldsymbol{Q}$ is a linear function and $t \to \infty$, then $\|\boldsymbol{u}\| \sim e^{\lambda t}$ (i.e., either $\|\boldsymbol{u}\| \to 0$, or $\|\boldsymbol{u}\| \to \infty$). To be able to describe the formation of structure, the function $\boldsymbol{Q}(\boldsymbol{u})$ must be nonlinear. Its nonlinearity may be connected either with the law of mass action [in this case $\boldsymbol{Q}(\boldsymbol{u})$ includes products of concentrations], or with other factors.

The formation of stationary dissipative structures can be exemplified by several mathematical models in biology.

1.1. Dissipative structures and simulation of morphogenesis

One of the most important problems facing biology today is the investigation of processes controlling the development of organs, i.e. mechanisms of their development in a certain succession and mutual relationship. Sometimes this problem is called the *problem of morphogenesis*.

Modern biology gives rather a good picture of how genetic information is transferred from one generation to another, and how it is recoded in each cell, thus ensuring the synthesis of enzymes. (Enzymes are organic catalysts of a protein nature produced by living cells to regulate the velocity of practically all biochemical reactions.) However, this knowledge alone does not give an answer to the following question: What causes a cell to differentiate, both morphologically and physiologically, in different organs, and how do these differentiated cells appear? (or: how does the process of cell differentiation go?). In other words, the questions to be answered are as follows:

(1) How is the amount of enzyme, synthesized in a cell, regulated?

(2) Why does this or another enzyme appear at a certain stage of development of an organism?

(3) Why do different types of cells of a multi-cellular organism produce their own protein complexes though they all contain the same genetic information? [2].

A. Turing assumed that the "information" necessary for cell differentiation results from a collective process, of which chemical reactions are the key element. His reasoning was as follows. Let substance X stimulate the development of cells (it is called an "activator") and substance Y inhibit it (it is called an inhibitor). An account of the reactions of X and Y would lead to a system of ordinary differential equations. However, special attention should be paid to the spatial distributions $X(x, t)$, $Y(x, t)$, which are largely affected by diffusion processes. That is why, to model this phenomenon, it is natural to use *reaction–diffusion systems*. Analysing a one-dimensional problem and assuming that at the boundaries no-flow conditions are specified, we obtain the problem

$$
\begin{aligned}
&X_t = D_1 X_{xx} + Q_1(X, Y, \lambda), \qquad Y_t = D_2 Y_{xx} + Q_2(X, Y, \lambda), \\
&a \le x \le b, \quad 0 < t < \infty, \\
&X(x, 0) = X_0(x), \quad Y(x, 0) = Y_0(x), \\
&X_x(a, t) = X_x(b, t) = Y_x(a, t) = Y_x(b, t) = 0,
\end{aligned}
\tag{1.1}
$$

where D_1 and D_2 are the diffusion coefficients for X and Y, which remain constant. The nonlinear right-hand sides, describing chemical reactions, depend on λ. The latter contains the characteristics of the tissue, which changes in the course of the development. The initial data $X_0(x)$, $Y_0(x)$ are assumed to be close to being spatially homogeneous, but they contain small random disturbances. These equations turned out to describe spontaneous order formation, diffusion processes playing a crucial role here.

In fact, assume that in a concentrated system

$$
\begin{aligned}
&\mathrm{d}X/\mathrm{d}t = Q_1(X, Y, \lambda), \qquad \mathrm{d}Y/\mathrm{d}t = Q_2(X, Y, \lambda), \\
&X(0) = X_0, \quad Y(0) = Y_0, \quad 0 < t < \infty.
\end{aligned}
\tag{1.2}
$$

$(\bar{X}, \bar{Y})$, for $\lambda = \lambda_0$, is a stable singular point. Then after simple calculations one can see that for certain relations between the diffusion coefficients D_1, D_2 and the derivatives Q_{1X}, Q_{1Y}, Q_{2X}, Q_{2Y} at the point $(\bar{X}, \bar{Y}, \lambda_0)$, the stationary solution of the system of equations (1.1) will be unstable with respect to small disturbances of the type $e^{ik_c x}$. Diffusion processes have a destabilizing role here. This phenomenon was called a *Turing instability*.

The latter proved to be characteristic of a large class of models in physics, chemistry, biology and other fields. One of the best known models is the *Brusselator*, which under certain circumstances describes the following reaction schemes:

$$
\mathrm{A} \underset{k_{-1}}{\overset{k_1}{\rightleftarrows}} \mathrm{X}, \qquad \mathrm{B} + \mathrm{X} \underset{k_{-2}}{\overset{k_2}{\rightleftarrows}} \mathrm{Y} + \mathrm{D}, \qquad 2\mathrm{X} + \mathrm{Y} \underset{k_{-3}}{\overset{k_3}{\rightleftarrows}} 3\mathrm{X}, \qquad \mathrm{X} \underset{k_{-4}}{\overset{k_4}{\rightleftarrows}} \mathrm{E}.
$$

Nonlinear sources obey the formula

$$
Q_1 = A - (B + 1)X + X^2 Y, \qquad Q_2 = BX - X^2 Y, \tag{1.3}
$$

where B is usually a parameter. One usually studies the behaviour of the solutions at large characteristic time scales. The typical behaviour of the Turing system, as well as that of the Brusselator and many other models, is as follows. For $\lambda < \lambda_0$, the functions $X(x, t)$, $Y(x, t)$ tend to a spatially homogeneous stable solution $(\bar{X}, \bar{Y})$. This solution is often called a thermodynamic branch. For $\lambda > \lambda_0$ things go quite differently. Though the initial data are nearly homogeneous, disturbances grow, and a new pattern, a spatially heterogeneous stationary distribution of concentrations, arises in the medium.

The value of λ_0 can be determined by a standard linear analysis, which shows that, for $\lambda > \lambda_0$, the solution $(\bar{X}, \bar{Y})$ becomes unstable with regard to small disturbances $\sim e^{ik_c x}$ [1]. The profiles of stationary solutions for $\lambda \gtrsim \lambda_0$ can be determined if a more complex nonlinear analysis is conducted using asymptotic methods and the theory of bifurcations [3, 13]. For $\lambda \gg \lambda_0$ calculations must be made.

Figure 1.1 shows a typical behaviour of the amplitudes of stationary structures for $\lambda \gtrsim \lambda_0$. At the point λ_0 the system acquires two more stationary solutions, and branching, or bifurcation, can be observed. For $\lambda \gtrsim \lambda_0$ it may be determined by small external effects, or fluctuations, whether one branch or the other is taken.

The latter gain strength, which leads to macroscopic order formation in nonlinear systems, as is noted in ref. [3]. This behaviour appears to be typical of many nonlinear systems. There can be several ways of development of these systems, and bifurcation points can affect their evolution. A typical form of a stationary solution in the Brusselator can be observed in fig. 1.2. In this model a whole class of initial data end up in one established solution. This "forgetting" of the initial data is characteristic of open dissipative systems. One can observe it in the Turing system and in many other reaction–diffusion systems used to describe morphogenesis mathematically [5–8, 15].

The pattern formation process in one-dimensional and many-dimensional systems has been studied in detail for the model suggested by A. Gierer and M. Meinhardt, in which

$$Q_1 = \rho + kX^2/Y - \mu X, \qquad Q_2 = cX^2 - \nu Y, \tag{1.4}$$

where ρ, k, μ, c, ν are constants. The behaviour of the solutions of the above problem (1, 1), (1, 4) fits the data obtained in the course of other observations and experiments. For example, if a part of the dissipative structure is "removed" (i.e., we assume that at $t = t_0'$, $X = \bar{X}$, $Y = \bar{Y}$ in the interval $0 < L_1 < x < l$), a wave of "self-regeneration" arises and the pattern formation recommences. It would be natural to compare this wave to the regeneration process.

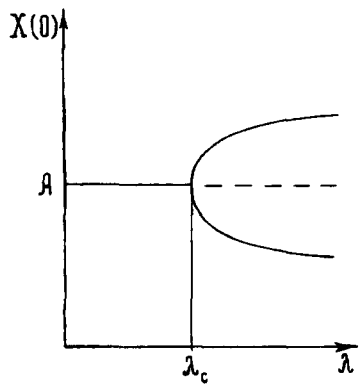

Fig. 1.1

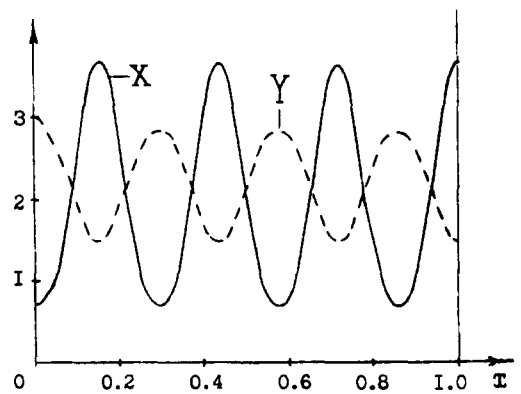

Fig. 1.2. Example of a stationary dissipative structure in the Brusselator. Computation parameters: $A = 2$; $B = 4.6$; $l = 1$; $D_1 = 0.0016$; $D_2 = 0.008$.

The predictions of models (1.1) and (1.4) have been compared to the morphogenesis of the simplest multi-cellular organisms [5–8]. Many-dimensional generalizations of the system make it possible to describe the growth of leaves on the stems of plants. Depending on the model parameters their position is different [7].

To describe morphogenesis in terms of mathematics is a difficult task. Various methods of investigation and new mathematical theories have to be applied, depending on what properties of this phenomenon are thought to prevail. We want to draw attention to several directions developed in recent years.

In a number of cases the activator–inhibitor interaction turned out to be less significant than mechanical strains of the tissue and substances affecting them, which, in fact, proved to be most important. The understanding of this brought about the appearance of mechanical models of morphogenesis. In the simplest cases they can be reduced to a system of a parabolic and an elliptical equation [5, 74]. A more complex model taking into account the changes in cell concentrations, the concentration of the cell matrix and its shifts was built in ref. [9]:

$$n_t = D_1 n_{xx} - D_2 n_{xxxx} - \alpha[n(\rho + \alpha'\rho_{xx})_x]_x - [nu_t]_x + rn(1-n)\,,$$

$$\mu_1 u_{xxt} + \mu_2 u_{xx} + \tau[n(\rho + \beta\rho_{xx})]_x - su\rho = 0\,,$$

$$\rho_t + (\rho u_t)_x = 0\,.$$

Analysis shows that this model can describe a large set of dissipative structures of different types.

In reaction–diffusion systems the length of the interval is important. The number of structures and their configuration can be changed by altering the parameter l (e.g. by arbitrarily increasing it). But in nature any growth has its limits. The dimensions of a growing organism are determined by inner causes and not by external ones. This is why one of the approaches to the modelling of morphogenesis uses equations describing local processes [23]. Intrinsic properties of nonlinear media and not marginal conditions determine dissipative structures in this case. Examples of these systems will be considered in the next chapter.

All models mentioned can be seen as a development of Turing's idea: nonlinear media were investigated in all cases and the processes taking place in them were described by partial differential equations. However, alternative approaches are also possible.

R. Thom presented his model of morphogenesis in a book that has received wide acclaim [10]. The development of an organism goes through a number of qualitative jumps (e.g. those connected with the loss of different symmetries). An effective description of such transitions in systems depending on several parameters can only be given for a comparatively simple class of objects which is considered by *catastrophe theory*,

$$\dot{x} = -\partial U(x, \lambda)/\partial x\,,$$

where x and λ are vectors here. Unlike Turing's approach, information about the spatial structure of an object cannot be obtained here. However, in some cases it is possible to find out how its qualitative properties change with the change of parameters.

Another approach, suggested by G. Neiman, is connected with the transition to a discrete description. It turned out that the simplest discrete media (cellular automata) can be effectively used to produce development and self-reproduction patterns. Each cell is connected with its nearest neighbour

cells. Though its behaviour is determined by simple rules, the evolution of large configurations of cells may be very interesting and diverse. Some examples of such media will be considered in chapter 11.

The models suggested at present appear to be rather far from reality quantitatively. Nevertheless, their construction and investigation were very helpful. They resulted in some general concepts concerning the formation of order in nonlinear media.

1.2. Self-organization

Partial differential equations are the main tool used in the investigation of nonlinear media. Formally they describe systems with an infinite number of degrees of freedom. However, different degrees of freedom play different roles. In a nonlinear dissipative system a finite, and sometimes even small, number of variables can be singled out, the remaining variables "adjusting" to them. These variables are often called order parameters.

Their introduction can be explained by a simple example. Take the function $u(x)$, defined in the interval from 0 to l. It may be expanded in a Fourier series and the amplitude of each harmonic can be found. Let the function $u(x)$ have a complex form (see fig. 1.3a). No order or regularity is observed in its behaviour. The amplitudes of many harmonics a_k are close to each other. On the contrary, the behaviour of the smooth functions in fig. 1.3b is very simple and regularity can easily be observed: it is close to periodical. To show its profile it is sufficient to state the amplitudes for some of the harmonics.

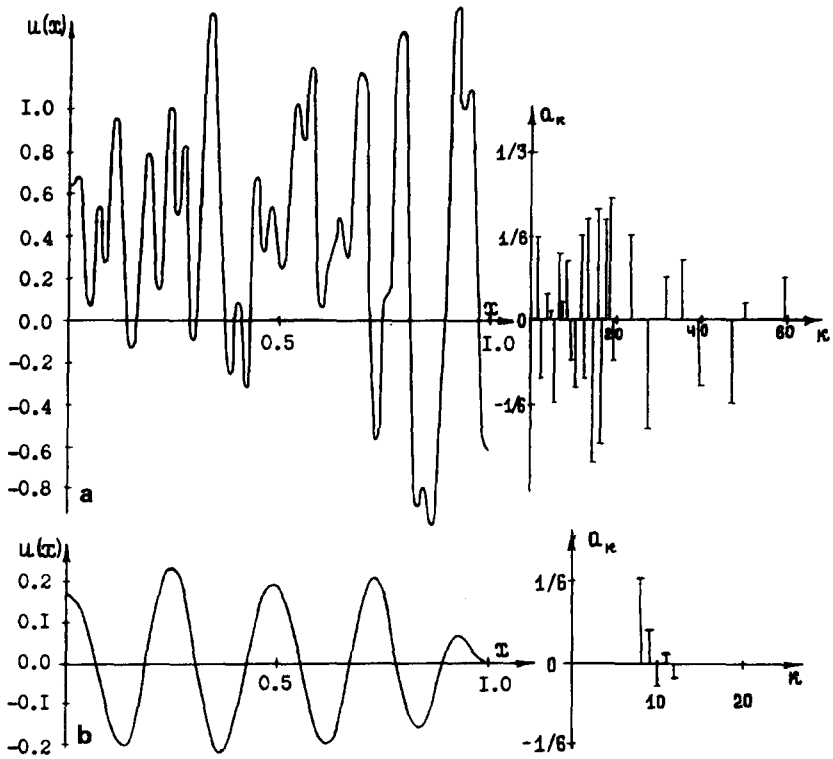

Fig. 1.3

If the number of harmonics with large amplitudes is decreasing, a certain order establishes in the system and self-organization occurs.

Let us see how the amplitudes of the Fourier coefficients of the solutions of the simplest linear and nonlinear equations change with time.

The problem of a linear equation for the thermal conductivity,

$$T_t = aT_{xx}\,, \quad 0 \le x \le l\,,$$
$$T(x,0) = T_0(x)\,, \quad T_x(0,t) = T_x(l,t) = 0\,, \tag{1.5}$$

can be reduced to an infinite system of ordinary differential equations, the function T being expanded into a Fourier series,

$$T(x,t) = \sum_{m=0}^{\infty} C_m(t)\cos(\pi m x/l)\,,$$

which is inserted in eq. (1.5). The problem being linear, all the equations in the system will be independent,

$$\mathrm{d}C_n/\mathrm{d}t = -a(\pi n/l)^2 C_n\,, \quad n = 0,1,2,\ldots, \qquad C_n(0) = C_n^0\,. \tag{1.6}$$

Suppose, we want to solve problem (1.5) for $t > t_1$, and obtain an answer with a rather high accuracy ε. See fig. 1.4, which shows how the amplitudes of the first few harmonics change with time. The larger the number of the harmonic, the faster its amplitude decreases. To obtain an answer with an accuracy $\varepsilon = 0.001$ for $t > t_1$ (see fig. 1.4), we must solve the first five equations in (1.6); for $t > t_2$ solving three

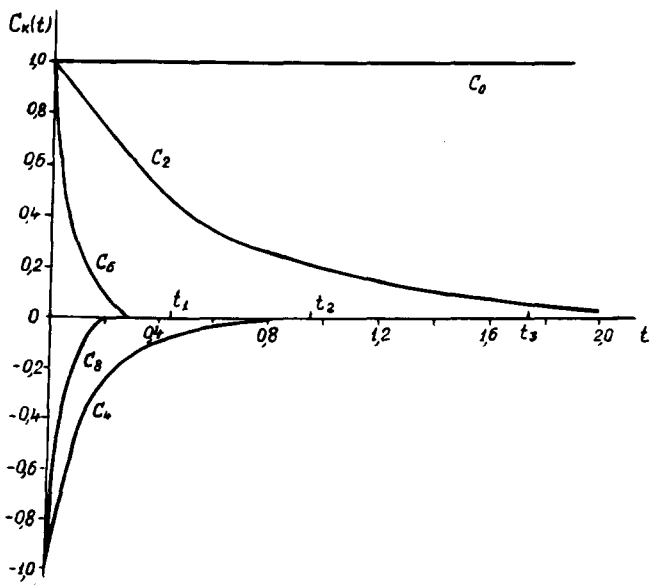

Fig. 1.4. Typical picture of the variation of the function $C_k(t)$ for the linear thermal conductivity equation.

equations is enough, and for $t > t_3$ only two. It is a remarkable fact that, beginning from a certain moment, it is sufficient to solve a few equations instead of solving the infinite system (1.6). Stating the accuracy and the time for which we want to obtain the answer, simplified the problem considerably.

The same approach has been developed by H. Haken to investigate nonlinear dissipative systems [13, 14]. Suppose we know the partial differential equations describing this system. In complete analogy to the derivation of (1.6) from the equation for the thermal conductivity, we can deduce an infinite system of equations

$$dC_m/dt = f_m(C_0, C_1, \ldots) - \gamma_m C_m\,, \quad m = 0, 1, 2, \ldots\,, \tag{1.7}$$

where the C_m are Fourier coefficients, $\gamma_m C_m$ are determined by diffusion (or another dissipative process), $0 < \gamma_1 < \gamma_2 < \cdots < \gamma_m < \cdots$; $f_0, f_1, \ldots, f_m$ are nonlinear functions, which may depend on the amplitudes of all harmonics. The system (1.7) is much more complex than (1.6), all its equations being coupled. However, let us consider computer obtained functions $C_m(t)$ for a nonlinear equation. As an example we shall consider the following equation:

$$u_t = ku_{xx} + Q(u)\,, \tag{1.8}$$

where $Q(u) = u - 2u^3$ (this type of equation is employed in some mathematical models in biology [37]). One can see the same regularity here which holds for the linear equation (fig. 1.5): the amplitudes of harmonics with a larger number decrease faster, and beginning from a certain moment they can be neglected. Having this in mind, an approximate method of system analysis can be developed.

Let us first consider the simple equation

$$dC_m/dt = -\gamma_m C_m + F(t)\,. \tag{1.9}$$

If $F(t) = 0$, then the solution is $C_m = C_m^0\, e^{-\gamma_m t}$.

If the characteristic time of variation of the function is δ and $\tau_m \equiv 1/\gamma_m \ll \delta$, and we take special interest in processes with characteristic times much longer than τ_m, then the variation of the amplitude

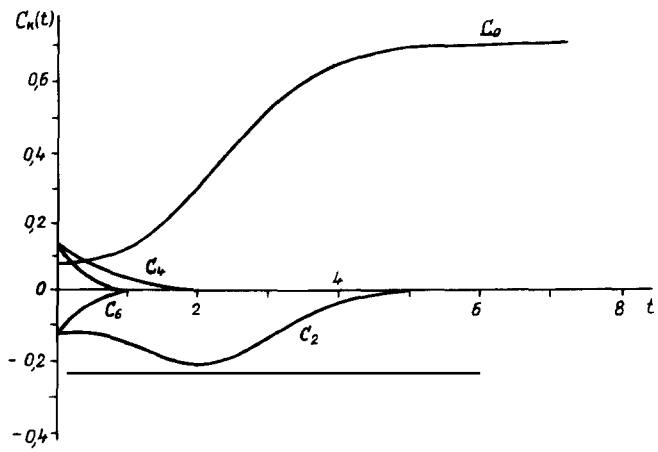

Fig. 1.5

C_m can be described by the algebraic equation

$$-\gamma_m C_m + F(t) = 0 \tag{1.10}$$

instead of a differential equation. (Analysis of the exact solution of eq. (1.9) brings us to the same conclusion.) The fundamental assumption that $\delta \gg 1/\gamma_m$ is referred to as the "*adiabatic approximation*".

Assume that the inequalities $\gamma_m \ll \gamma_{m+1} < \gamma_{m+2} < \cdots$ hold. It means that the processes described by the first $m+1$ equations go much slower than the remaining ones. Besides, if the adiabatic approximation can be used for the function f_m we obtain a system of $m+1$ differential equations and a hierarchy of algebraic equations,

$$\begin{aligned} &dC_n/dt = f_n(C_0, C_1, \ldots) - \gamma_n C_n, \quad n = 0, 1, \ldots, m, \\ &C_p = f_p(C_0, C_1, \ldots)/\gamma_p, \quad p = m+1, m+2, \ldots, \end{aligned} \tag{1.11}$$

which describe the processes with characteristic times $\tau \gg 1/\gamma_m$.

Suppose we have been able to express C_{m+1}, C_{m+2}, and the amplitudes of the other modes, in terms of $C_0, C_1, \ldots, C_m$, from the hierarchy of algebraic equations (or we know that C_{m+1}, C_{m+2} and the other modes are much smaller than the first m); then the purpose has been achieved: stating the accuracy and characteristic time we come to the $(m+1)$ differential equations

$$dC_n/dt = \varphi_n(C_0, C_1, \ldots, C_m) - \gamma_n C_n, \quad n = 0, 1, \ldots m, \tag{1.12}$$

the latter being simpler than the initial system. This approach turned out to be helpful when investigating a number of problems in laser physics and in solving many other problems [13–16].

The reasoning presented above is heuristic. However, in some cases this procedure can be given a rigorous basis. The Tikhonov theorem is one of the main results here [17, 18].

Let us consider the set of differential equations

$$\mu \frac{dz}{dt} = F(z, y, t), \qquad \frac{dy}{dt} = f(z, y, t), \qquad z(0) = z^0, \quad y(0) = y^0, \tag{1.13}$$

where z and F are M-dimensional vector functions, y and f m-dimensional vector functions, $\mu > 0$ is a small parameter. (This is the situation we encounter, if we take the first equations from the infinite system (1.7), supposing that the influence of the other harmonics is very small.)

Assuming that in (1.13) $\mu = 0$, we obtain a system of equations [an analog of (1.11)], the order of which is lower than that of the original system,

$$F(\bar{z}, \bar{y}, t) = 0, \qquad d\bar{y}/dt = f(\bar{z}, \bar{y}, t). \tag{1.14}$$

These problems are called singular-disturbed (as distinct from regular-disturbed, in which, if $\mu = 0$, the order does not decrease). To solve (1.13), it is necessary to express $\bar{z}$ from the equation $F(\bar{z}, \bar{y}, t) = 0$ and to substitute the solution $\bar{z} = \varphi(\bar{y}, t)$ (because the problem is nonlinear, there can be more than one) in the second equation (1.13) and to solve the system obtained,

$$d\bar{y}/dt = f(\varphi(\bar{y}, t), \bar{y}, t), \quad \bar{y}(0) = y^0. \tag{1.15}$$

Our assumption is that in some domain of variable space the equation $F(\bar{z}, \bar{y}, t) = 0$ has a continuous isolated solution $\varphi(\bar{y}, t)$ and that (1.15) has a single solution.

Along with the system (1.13) let us consider the adjoint system

$$d\tilde{z}/d\tau = F(\tilde{z}, y, t), \tag{1.16}$$

in which y and t are parameters. It is clear that $\tilde{z} = \varphi(y, t)$ is an isolated stationary point of the system (1.16). Suppose this point is asymptotically Lyapunov stable in the domain (y, t) under study [i.e., for each $\varepsilon > 0$, there is a $\bar{\delta}(\varepsilon)$ which, when $\|\tilde{z}(0) - \varphi(y, t)\| < \bar{\delta}(\varepsilon)$, obeys the conditions $\|\tilde{z}(\tau) - \varphi(y, t)\| < \varepsilon$ if $\tau \geq 0$ and $\tilde{z}(\tau) \to \varphi(y, t)$ as $\tau \to \infty$]. Let us also assume that $\tilde{z}(\tau) \to \varphi(y^0, 0)$ [that means that z^0 belongs to the domain of attraction of the stationary point $\tilde{z} = \varphi(y^0, 0)$].

If these requirements are fulfilled (as well as some technical conditions, concerning the smoothness of the right-hand sides and their domain of definition), according to Tikhonov's theorem a value of μ_0 can be found for which the problem (1.13) has a single solution $z(t, \mu)$, $y(t, \mu)$ for $0 < \mu \leq \mu_0$ and $0 \leq t \leq T$; it satisfies the limit equations

$$\begin{aligned} &\lim_{\mu \to 0} y(t, \mu) = \bar{y}(t) \quad \text{for } 0 \leq t \leq T, \\ &\lim_{\mu \to 0} z(t, \mu) = \bar{z}(t) = \varphi(\bar{y}(t), t) \quad \text{for } 0 < t \leq T. \end{aligned} \tag{1.17}$$

(They are analogs of eqs. (1.11), (1.12) for the finite-dimensional case.) The Tikhonov theorem does not deal with the behaviour of the solutions of the studied system as $t \to \infty$.

It would also be helpful to know how many equations from the infinite-dimensional system (1.7) should be left to effectively describe the processes in nonlinear media. This is especially important for the analysis of stochastic regimes. In recent years a number of works have been published which make it possible to give an answer to this question for a certain class of hydrodynamic problems [13].

The physical meaning of the results mentioned above is simple: modes with longer characteristic times are order parameters in these systems. Slow orders "subordinate" the fast ones. The amplitudes of the first Fourier harmonics act as order parameters here. Substantiation of this approach is very close to a problem emerging in the theory of numerical methods – how close to each other are the solutions of the initial infinite-dimensional problem and the solutions of the finite-dimensional system obtained by treating the initial equation with the Galerkin method [20].

No less interesting are other phenomena, in which self-organization occurs and dissipative structures emerge. In the 70s investigators of plasma physics focussed their attention on superfast regimes, which enabled them in many cases to use one group of processes and ignore others [21]. It brought about the appearance of a large class of mathematical models where order parameters could be independent of Fourier harmonics and are defined by the fastest processes in the system.

As a simple example of a model of this kind we can treat the nonlinear equation for the thermal conductivity with a bulk source [22–24]

$$T_t = (k(T)T_x)_x + Q(T), \quad -\infty < x < \infty, \quad k(T), Q(T) > 0, \qquad T(x, 0) = T_0(x), \tag{1.18}$$

where T is the temperature of the medium, its combustion simulating the source $Q(T)$. For the sake of simplicity we assume that both the source and the thermal conductivity are power functions of the

temperature,

$$k(T) = k_0 T^{\sigma}, \qquad Q(T) = q_0 T^{\beta}, \qquad k_0, q_0, \beta, \sigma > 0. \tag{1.19}$$

Equation (1.18) has a self-similar solution,

$$T = g(t) f(\xi), \quad \xi = x/\varphi(t), \tag{1.20}$$

where $g(t)$ characterizes the amplitude of the solution, $\varphi(t)$ is its half-width and f its form. It is natural to treat it as a dissipative structure which, unlike patterns in the Turing model and many other models, is nonstationary.

Suppose the initial profile evolves into a self-similar solution [in some cases strict results can be obtained, as far as the evolution to a solution of the type (1.20) is concerned]. To describe this process the method of averaging can be applied [23, 25]. In fact, substituting formula (1.20) into eq. (1.18) one can find expressions for $g(t)$ and $\varphi(t)$, as well as obtain a boundary value problem for the function $f(\xi)$. But we can go another way. After inserting (1.20) into eq. (1.18) one can integrate eq. (1.18) over x, then multiply it by T and integrate again over x. One can see that a dynamic system is obtained,

$$\begin{aligned} \dot{g} &= q_0[c-a] g^{\beta} - k_0 b g^{\sigma+1} \varphi^{-2}, \\ \dot{\varphi} &= -q_0[c-2a] g^{\beta-1} \varphi + k_o b g^{\sigma} \varphi^{-1}, \end{aligned} \tag{1.21}$$

where

$$a = \int_{-\infty}^{\infty} f^{\beta}(\xi)\, \mathrm{d}\xi \Big/ \int_{-\infty}^{\infty} f(\xi)\, \mathrm{d}\xi,$$

$$b = 2 \int_{-\infty}^{\infty} f^{\sigma}(\xi)[f'_{\xi}(\xi)]^2\, \mathrm{d}\xi \Big/ \int_{-\infty}^{\infty} f^2(\xi)\, \mathrm{d}\xi,$$

$$c = 2 \int_{-\infty}^{\infty} f^{\beta+1}(\xi)\, \mathrm{d}\xi \Big/ \int_{-\infty}^{\infty} f^2(\xi)\, \mathrm{d}\xi,$$

and the initial temperature profile acts as f.

Analysis shows that the model (1.21) describes solutions with one maximum of the initial system well, providing an opportunity to predict an interesting effect. There exist such parameter values and initial data $\bar{g}$, $\bar{\varphi}$ [and $T_0(x)$] for which the amplitude decreases, and the half-width grows ($g \to 0$, $\varphi \to \infty$). However, perturbations can push the system into another regime, which has no solution at all times ($g \to \infty$, $\varphi \to 0$, for $t \to t'_f < \infty$, so that $\max_x T(x, t) \to \infty$, if $t \to t''_f < \infty$). Fluctuations turn out to play a fundamental role here as well. Acting as order parameters in formula (1.18), the functions g and φ characterize here the fastest variables. The existence of order parameters in nonlinear dissipative systems is very important. In a number of cases a hierarchy of simplified models can be built with their help, which to a great extent simplifies the analysis of the systems under study.

2. Complex spatial order in nonstationary processes

2.1. Model of thermal structures

It is natural to begin studying nonlinear dissipative media with the simplest models. It turns out that many paradoxical properties of nonstationary structures, typical for nonlinear systems, can be investigated by means of a single nonlinear parabolic equation, i.e. with the aid of a model that is simpler than the one considered by A. Turing,

$$u_t = (k_0 u_x)_x + Q(u) . \tag{2.1}$$

It seems that a parabolic equation with a nonlinear source was first studied in a publication by Kolmogorov, Petrovsky and Piskunov [37]. They investigated the Cauchy problem, where the source satisfied the conditions

$$Q(u) \in C^1[0,1] , \qquad Q(0) = Q(1) = 0 , \qquad Q(u) > 0,\ 0 < u < 1 ; \qquad Q'(0) > 0 .$$

Subsequently this equation was used to describe epidemics, the motion of excitations in a nerve fibre, and the propagation of flames in a combustible medium [38]. A set of running waves was constructed, i.e., solutions of the form $u = f(x - ct)$ were obtained for various values of c; also the *comparison theorem* was proved: if $u_1(x, t)$ and $u_2(x, t)$ are two solutions of eq. (2.1) with initial data $u_1(x, 0)$ and $u_2(x, 0)$, respectively, and if $u_1(x, 0) > u_2(x, 0)$ for all x, then $u_1(x, t) > u_2(x, t)$ for $0 < t < \infty$. (For the linear equation of heat conduction without a source the comparison theorem is proved in standard textbooks of mathematical physics [39]; in a rather simple manner it is generalized to the case when $Q(u)$ is a sink, $Q(u) < 0$, to which the problem is reduced in ref. [37].) Kolmogorov et al. [37] could prove that for $t \to \infty$ the solutions of eq. (2.1) are determined by one of the constructed particular solutions, i.e., the solution with the minimal wave propagation velocity c,

$$c = 2\sqrt{k_0 \alpha} , \quad \alpha = Q'(0) .$$

If the initial data are even, two waves arise, right- and left-running waves.

Obtaining a *self-similar* solution for $t \to \infty$ leads to a reduction of the number of degrees of freedom, i.e. self-organization occurs in the system. The class of sources $Q(u)$ for which analogous behaviour is observed can be made larger [38].

Besides, the behaviour of the solutions was investigated in detail in the first and second boundary value problems for eq. (2.1) for $t \to \infty$. In the case of bounded sources $Q(u)$ stationary solutions were obtained. For these solutions a criterion of stability was analytically determined [29]. From this criterion it follows in particular that in the second boundary value problem the stationary solution with at least one extremum at an internal point of the interval is Lyapunov unstable provided there are no flows at the boundaries. Hence, complex dissipative structures such as in reaction–diffusion systems are impossible here.

The asymptotic behaviour of solutions for $t \to \infty$ is usually investigated in the cases when the slowest processes are of main interest. However, lately nonstationary processes with the smallest characteristic times have attracted growing attention of specialists in plasma physics, chemical kinetics and biology [23]. These processes are idealized as *regimes with peaking*, for which one of the values under

investigation grows infinitely over a finite time, called the time of peaking. Below, it will be denoted by t_f. The equations in which regimes with peaking are possible represent a simplified model of certain stages of processes [23].

For example, in a publication dealing with evolution theory it is stated that natural selection of features giving dominance in the course of evolution has as a result that ". . . the process itself runs with a rate increasing to a certain limit since in the natural selection more perfect forms arising faster than others triumph" [40].

The simplest differential equation in which such regimes are possible has the form

$$\frac{du}{dt} = Q(u), \quad \int_{u_0}^{\infty} \frac{du}{Q(u)} = C < \infty. \tag{2.2}$$

The last inequality describes a necessary and sufficient condition for the existence of a regime with peaking in such a system. It is called the *Osgood criterion* [41]. For example, if $Q(u) = u^{\beta}$, then

$$u \sim (t_f - t)^{1/(1-\beta)}, \quad t_f = u(0)^{1-\beta}/(\beta - 1),$$

i.e., the time of existence of the solution depends on the initial data. The question about the existence of regimes with peaking was also studied for many systems of ordinary differential equations [41].

It is interesting to see how the opinion about such regimes has changed. Even recently the nonexistence of a solution for all times ($0 < t < \infty$) has been considered as an indication that the model is incorrect and not applicable for a description of real processes. Now growing attention is attached to phenomena in which the instability develops in a finite time (this does not happen in linear systems). As examples we can mention the following cases: the classical problem about the cumulation of shock waves to the centre, which was studied by Guderley [42]; some models of turbulent flows where equations with negative viscosity appear [43]; questions connected with effects of nonstationary boundary regimes upon nonlinear media [24]; plasma physics problems, in particular collapse of Langmuir waves [44]; and many other systems [45].

Let us consider again the equation of nonlinear heat conduction,

$$T_t = (k(T)T_x)_x + Q(T), \quad -\infty < x < \infty, \quad T(x, 0) = T_0(x), \tag{2.3}$$

where $T(x, t)$ is interpreted as the temperature of the medium, the combustion of which simulates the bulk source $Q(T)$.

In the linear equation of heat conduction without a source (as well as with a linear source or sink), in the case of finite initial data [$T_0(x) = 0$ outside a certain domain G] the temperature proves to be different from zero through the entire space for $t > 0$: thermal perturbations in such a model propagate with an infinite velocity. Quite different behaviour is observed in systems where the thermal conductivity is nonlinear and

$$\int_0^{T_0} k(u)u^{-1}\,du < \infty. \tag{2.4}$$

With finite initial data and in the absence of a source the velocity of the thermal wave front in such media proves to be finite [46].

The basic qualitative effects in the system (2.3) can be revealed by investigating the equation with power functions $k(T)$ and $Q(T)$ [21–24],

$$k(T) = k_0 T^{\sigma}, \qquad Q(T) = q_0 T^{\beta}.$$

Let $\beta = \sigma + 1$, $\beta > 1$. A typical evolution of the solution of problem (2.3) is shown in fig. 2.1. The maximum temperature first decreases (the time t_2) and then increases (t_3, t_4). As follows from inequality (2.4), at each instant of time the heat is concentrated in a bounded spatial domain. At the moment t_4 the front reaches some points A and B (see fig. 2.1) after which it stops. The heat turns out to be localised in a bounded domain, whose size is designated by L_f. After this the half-width of the heated domain remains constant while the amplitude (maximum temperature) increases. The temperature increase occurs in a regime with peaking (the temperature maximum goes to infinity in a finite time t_f). The result of the calculation appears to be paradoxical: despite an infinite increase of the temperature and dissipative processes the heat proves to be localized in a bounded domain (note that in this case the law of variation of the half-width and the amplitude of the temperature profile agree well with the solutions of the averaged system [23]).

A large number of works performed in recent years have shown that *localization phenomena* are a common feature of many nonlinear media. This may be due to the action of specific boundary regimes [47], or the presence of sinks [48, 49]. In a nonlinear medium a certain configuration of initial data [50] may cause a localization of heat in a finite time.

Let us vary the amplitude and half-width of the initial distribution. Calculations show that this leads to a change in t_f; however, the size of the localization domain [for a wide class of $T_0(x)$] and the shape of the temperature profile (as $t \to \infty$) remain the same. Here we are faced with the phenomenon that the details of the initial data are forgotten. The fact that the distribution, the half-width of which does not change, maintains its form shows that the combustion in a domain of length L_f occurs self-consistently: the law for the temperature increase at each point proves to be the same up to a factor.

Let us turn our attention to the decisive role of dissipative processes in such systems. We assume that $k_0 = 0$. Then according to eq. (2.2) at each point of space, where $T_0(x) \neq 0$, the combustion runs with its own value of t_f. If $k_0 \neq 0$, in the whole domain the combustion runs with the same time of peaking. Therefore, it is natural to consider the order arising in such a medium and developing in a regime with peaking as a nonstationary dissipative structure. (In this connection in some publications the model (2.3) is called a *model of thermal structures* [23, 24].)

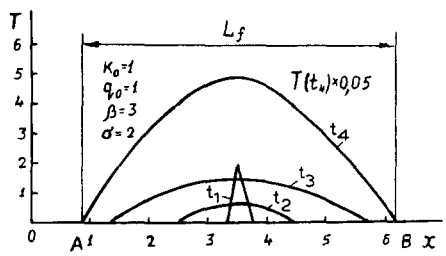

Fig. 2.1. Formation of a dissipative heat structure with a constant half-width (the S-regime): $t_1 = 0.0$; $t_2 = 19.59$; $t_3 = 73.03$; $t_4 = 74.95$.

Maintenance of the shape of the profile for $t \to t_f$ allows us to assume that at a developed stage we obtain a self-similar solution of the form

$$T(x, t) = g(t) f(\xi), \quad \xi = x/\varphi(t). \tag{2.5}$$

By substituting (2.5) into problem (2.3) we can obtain the changes for the amplitude $g(t)$ and the half-width $\varphi(t)$,

$$g(t) = A_1(1 - t/t_f)^{-1/(\beta-1)}, \qquad \varphi(t) = A_2(1 - t/t_f)^{+(\beta-\sigma-1)/2(\beta-1)}. \tag{2.6}$$

Here A_1 and A_2 are constants, which are determined by the parameters β, σ, k_0, q_0. Now we have a nonlinear boundary value problem for the function $f(\xi)$, which defines the shape of the dissipative structure,

$$-\frac{1}{(\beta-1)t_f} f + \frac{\beta-\sigma-1}{2(\beta-1)t_f} f_\xi \cdot \xi = (f^\sigma f_\xi)_\xi + f^\beta, \tag{2.7}$$

$$f_\xi|_{\xi=0} = 0, \quad f^\sigma f_\xi|_{\xi=\xi_\phi} = 0, \quad f|_{\xi=\xi_\phi} = 0. \tag{2.8}$$

The condition at $\xi = 0$ allows one to distinguish only symmetric solutions, which are obtained for $t \to t_f$. The two other conditions allow one to distinguish localized solutions. For problem (2.7), conditions (2.8) lead to an analytical solution describing a localized structure if $\beta = \sigma + 1$,

$$f(\xi) = [\cos^2(\pi\xi/L_f)\, 2(\sigma+1)\sigma^{-1}(\sigma+2)^{-1}]^{1/(\sigma+1)}, \tag{2.9}$$

where

$$L_f = \frac{2\pi}{\sigma}\sqrt{\sigma+1}\sqrt{k_0/q_0} \tag{2.10}$$

is the length of the localization domain. The structure and the value of L_f coincide with the calculated ones. Formulae (2.9), (2.10) enable us to construct many other solutions of (2.7), (2.8). If two similar initial profiles leading to the appearance of localized structures are given at a distance larger than L_f, they have no influence on each other (see fig. 2.2a). If one of the profiles is smaller in amplitude it

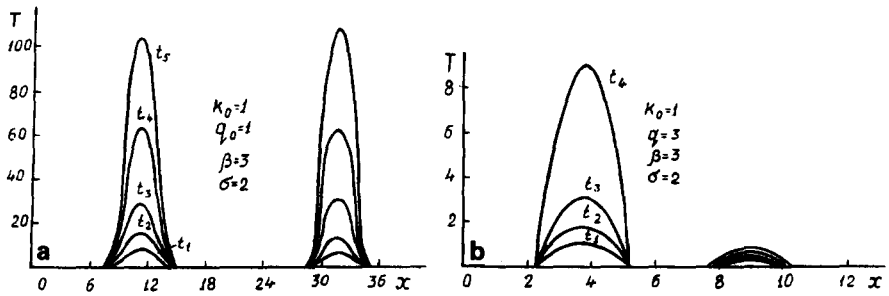

Fig. 2.2. (a) Effect of heat localization. Two heat structures in a nonlinear medium develop independently: $t_1 = 0.0$; $t_2 = 3.56 \times 10^{-2}$; $t_3 = 3.93 \times 10^{-2}$; $t_4 = 3.99 \times 10^{-2}$; $t_5 = 4.00 \times 10^{-2}$. (b) Structure develops with a minimal time of peaking. The rest of the profile "dies down" for $t \to t_f$; $t_1 = 0.0$; $t_2 = 0.147$; $t_3 = 0.220$; $t_4 = 0.245$.

simply "stops" when $t \to t_f$, while the other one grows infinitely (see fig. 2.2b). This is a typical picture for regimes with peaking. Therefore in the nonlinear medium described by (2.3) we should consider only the fastest processes with minimal times of peaking.

So far we have assumed that $\beta = \sigma + 1$. Let us find out what occurs when the parameters of the nonlinear medium β and σ are varied. From (2.6) it follows that for $\beta > \sigma + 1$ we have $\varphi(t) \to 0$ as $t \to t_f$, and $\varphi(t) \to \infty$ as $t \to t_f$, if $\beta < \sigma + 1$. In the first case the half-width of the temperature distribution must decrease, and we are faced with the *LS-regime* with peaking (fig. 2.3a). In the second case it grows infinitely, and we have the *HS-regime* (fig. 2.3b). When $\beta = \sigma + 1$ the half-width remains constant [22–24] (*S-regime*).

For the nonlinear problem (2.3) the superposition principle is not valid. In fact, if we multiply the initial data by some factor this will lead to a process running at a quite different rate and with a different time of peaking rather than to multiplication of the solution by a constant. Here we cannot construct a general solution from the known set of particular solutions. So what is the value of the self-similar solution obtained?

The answer follows from the calculations given in ref. [23] and some rigorous statements made in ref. [24]: any distribution for $t \to t_f$ gives one or several self-similar solutions. Although there is no superposition principle, we know which structures arise at the stage of intense combustion. This is a profound and interesting fact.

One of the traditional methods of analysing linear problems of mathematical physics is connected with separation of variables and subsequent determination of a set of particular solutions. To do this we should find eigenfunctions of the problem under investigation (which are also some self-similar solutions). These essentially depend on the region in which the equation is solved as well as on the boundary conditions. Then by using the same set of particular solutions a general solution is constructed [39].

On the face of it, in the question under discussion the situation proves to be similar: the nonlinear problem (2.3) admits a generalized separation of variables (2.5). Determining the profile of a self-similar solution leads to the *nonlinear eigenvalue problem* (2.7), (2.8). (For given t_f the eigenvalue is ξ_ϕ. The similarity transformation allows us to determine profiles of $f(\xi)$ for other t_f as well. In recent years similar problems have arisen in many fields [51].)

In this connection solutions of equations which describe configurations of nonstationary structures are called the *eigenfunctions of the nonlinear medium* [52, 53]. Unlike the usual eigenfunctions they

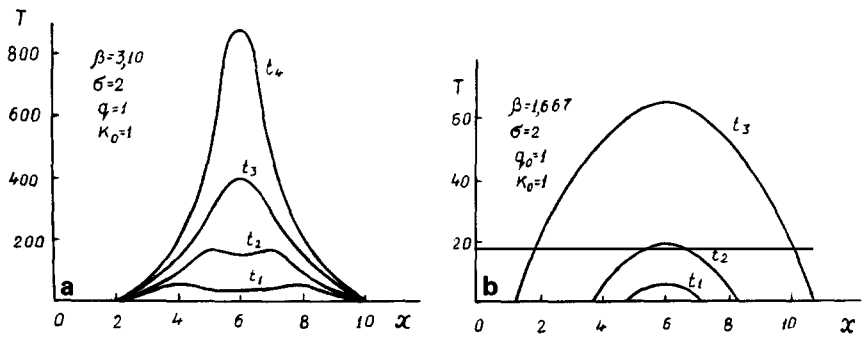

Fig. 2.3. (a) Appearance of a heat structure with decreasing half-width (LS-regime with peaking): $t_1 = 0.0$; $t_2 = 2.15 \times 10^{-4}$; $t_3 = 2.38 \times 10^{-4}$; $t_4 = 2.44 \times 10^{-4}$. (b) Heat waves of growing amplitude (HS-regime with peaking): $t_1 = 0.0$; $t_2 = 0.69$; $t_3 = 0.875$.

describe localized processes and do not depend on boundary conditions. [For example, formula (2.9) can determine the solution of a large class of various boundary value problems for eq. (2.3), in which the length of the domain $L > L_f$.] We may say that they describe intrinsic properties of a nonlinear medium. It is no small wonder that great attention has been attached to the study of these functions [23, 24, 54]. Let us note several results of importance.

The solution (2.9), (2.10) proves to be very simple: the temperature profile which it describes has a single maximum. (We shall say that it determines a *simple structure*.) The question is: Can *complex structures* that have more than one maximum and keep their form exist in the nonlinear media which are described by eq. (2.3)? The physical idea appears to be rather simple. Let two structures exist in the medium and each of them have a localization domain L_f. If the distance between them exceeds L_f they do not influence each other. If the distance is much shorter than L_f they quickly degenerate into a simple structure. In the intermediate case the maxima move to the symmetry axis for a long time; however, the form of the profile changes little. This allows us to speak about the interaction of heat structures.

An example of such an interaction is shown in fig. 2.4. It is seen that four local temperature maxima move to the centre when $t \to t_f$. The spatial symmetry of the initial data plays an important role in the interaction. In ref. [55] the interaction of structures in the multi-dimensional case was studied by numerical methods, and the following example was considered.

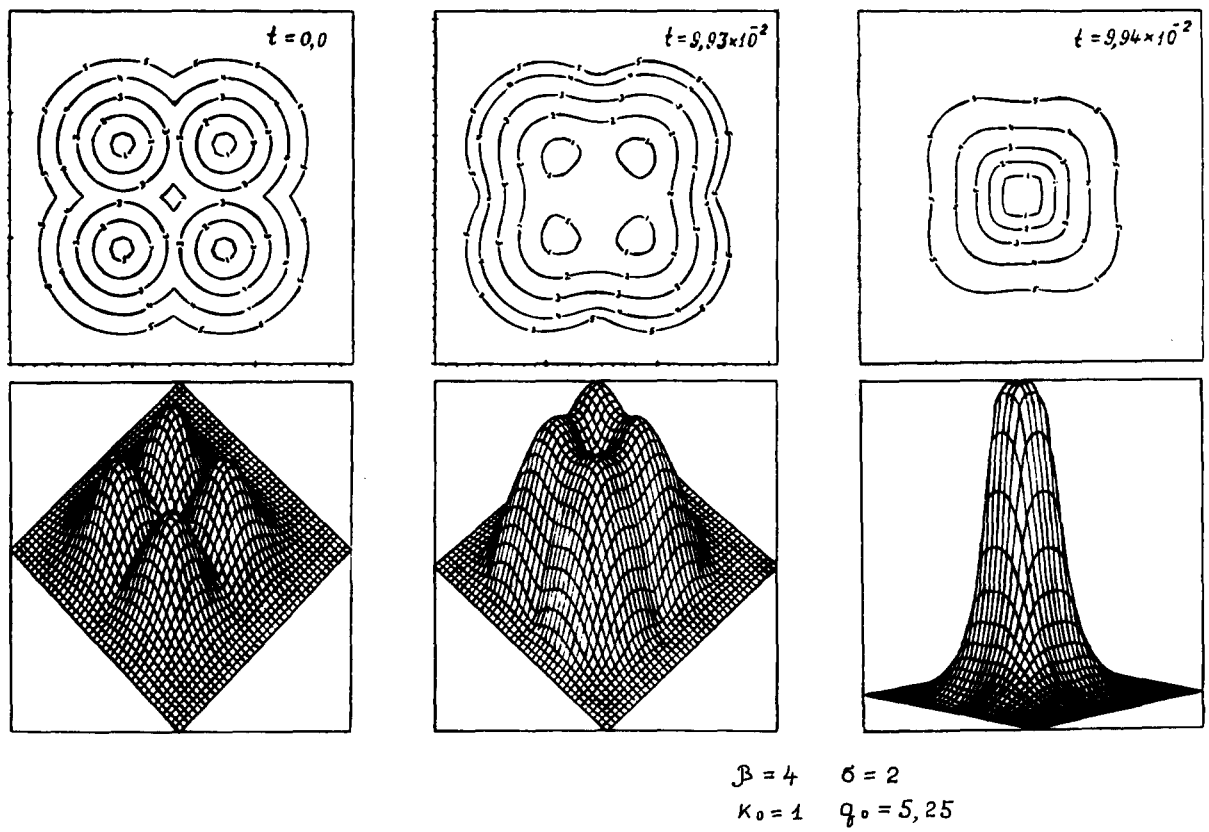

Fig. 2.4. Interaction of four heat structures.

Take initial data of the form

$$T_0(\boldsymbol{r}) = \max_{i \le n} \{A_i \exp[-\alpha_i(\boldsymbol{r} - \boldsymbol{a}_i)^2]\}\,, \tag{2.11}$$

where $\boldsymbol{r}$ and $\boldsymbol{a}_i$ are two-dimensional vectors. Let $n = 3$, $A_1 = A_2 = A_3$, $\alpha_1 = \alpha_2 = \alpha_3$ and the vectors $\boldsymbol{a}_i$ be chosen so that at one time they form an equilateral triangle ($|\boldsymbol{a}_1 - \boldsymbol{a}_2| = |\boldsymbol{a}_1 - \boldsymbol{a}_3| = |\boldsymbol{a}_2 - \boldsymbol{a}_3| = a$) and at another time an isosceles triangle with apex of 120° ($|\boldsymbol{a}_1 - \boldsymbol{a}_2| = |\boldsymbol{a}_1 - \boldsymbol{a}_3| = a$, $\beta = 4.0$; $\sigma = 2.0$; $k_0 = 1.0$; $q_0 = 5.25$; $a = 2.08$; $A = 1.3$; $\alpha = 2.5$). More energy concentrates in a smaller volume in the first case than in the second case. In spite of this $t_{f_1} > t_{f_2}$, i.e., the symmetric configuration exists longer. Various stages of the interaction of the structures can be approximately described, and it can be shown that similar laws are typical for the three-dimensional case.

Profiles of the form (2.11) change their form when $t \to t_f$ (therefore, they are sometimes called quasi-structures). The laws of structure interactions revealed in calculations allow one to assume the existence of complex structures. They are determined by solutions of eq. (2.7) (or a multi-dimensional analog) with several maxima or by the so-called higher eigenfunctions of a nonlinear medium.

In refs. [23, 52, 53] such functions were investigated in the one-dimensional case. They exist in the LS-regime when $\beta > \sigma + 1$. The solution of the self-similar problem does not have a finite front. So since we are interested in localized solutions it is natural to require, instead of conditions (2.8), that the temperature and the flux should to go to zero as $x \to \infty$,

$$\partial f/\partial\xi|_{\xi=0} = 0\,, \quad f^{\sigma} f_{\xi} \xrightarrow[\xi\to\infty]{} 0\,, \quad f \xrightarrow[\xi\to\infty]{} 0\,. \tag{2.12}$$

Hence, it follows that

$$f \xrightarrow[\xi\to\infty]{} C_i \xi^{-2(\sigma+1)/(\beta-\sigma-1)}\,. \tag{2.13}$$

When solving the nonlinear problem (2.7), (2.8) we must determine ξ_ϕ (t_f can be put equal to unity), while here C_i must be determined.

The solutions of (2.7), (2.12) constructed numerically allow us to establish an interesting law [52, 53]. Two different parts can be distinguished in the solution. In one of them the solution represents small oscillations about $f = 1$ [In the original equation the solution $f = 1$ corresponds to a homogeneous background $T(x, t) \sim (1 - t/t_f)^{1/(1-\beta)}$; therefore it is sometimes called *homothermal*.] In the other part fast convergence to the asymptotic form (2.13) occurs. This is seen in fig. 2.5, where a whole set of eigenfunctions is shown for a nonlinear medium which is described by eq. (2.3) with power nonlinearities with $\beta = 3.18$; $\sigma = 2.0$; $q_0 = 1$; $k_0 = 1$.

Such a behaviour of solutions enabled us to estimate the number N of eigenfunctions of a nonlinear medium by analysing the problem linearized about $f = 1$ [52],

$$N \ge [a - [[a]a^{-1}]]\,, \quad a = (\beta - 1)(\beta - \sigma - 1)^{-1}\,, \tag{2.14}$$

and to obtain some rigorous results [56].

It turns out that the solutions of the linearized problem can be connected to asymptotic forms for $\xi \to \infty$; the connection point should be chosen so that the natural conditions of smoothness be fulfilled. Calculations showed that the functions thus constructed are very close to the solutions obtained

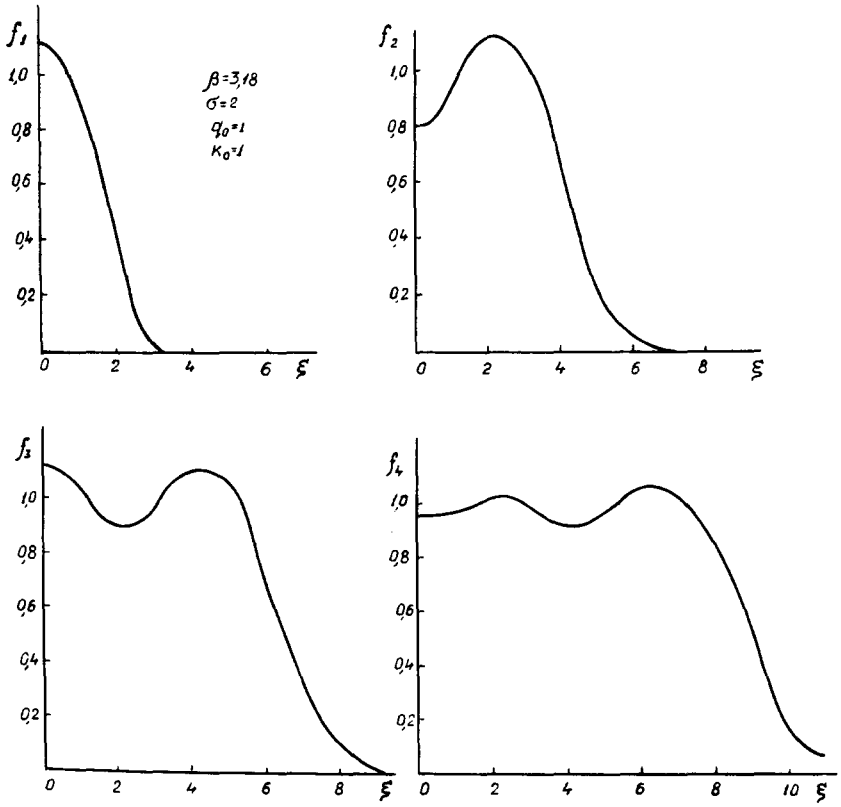

Fig. 2.5. Eigenfunctions of a nonlinear medium.

numerically [57, 58]. So this method allowed us to obtain good approximate solutions (approximations) of the original nonlinear problem (2.7), (2.12). Such approximations were used to construct new numerical algorithms for iteration procedures and the Newton method [58].

On the other hand, these algorithms enabled us to make progress in constructing *multi-dimensional eigenfunctions of a nonlinear medium*. A two-dimensional analog of problem (2.3), in which the term $(k(T)T_x)_x$ is replaced by the operator $\operatorname{div}(k(T)\operatorname{grad} T)$, admits a self-similar solution of the form $T(r, t) = g(t)f(r/\xi(t), \theta)$, where r and θ are polar coordinates. The two-dimensional function f, which determines the complex structure, satisfies the nonlinear elliptic equation

$$\frac{1}{\sigma+1}\Delta y - \frac{\beta-\sigma-1}{2(\beta-1)t_f}\,\xi\,\frac{\partial(y^{1/(\sigma+1)})}{\partial\xi} + y^{\beta/(\sigma+1)} - \frac{y^{1/(\sigma+1)}}{(\beta-1)t_f} = 0,$$
$$y(0) < C, \quad y \xrightarrow[\xi\to\infty]{} 0, \quad |\nabla y| \xrightarrow[\xi\to\infty]{} 0, \quad y \equiv f^{1/(\sigma+1)}(\boldsymbol{\xi}). \tag{2.15}$$

Standard numerical techniques allow us to construct only the simplest centro-symmetric solutions $f(\boldsymbol{\xi}) = f(|\boldsymbol{\xi}|)$. Acting by analogy with the one-dimensional case we should search for a boundary on which the solution of the linearised problem can be connected to asymptotic solutions for $|\boldsymbol{\xi}| \to \infty$. So a problem with a free boundary arises, whose solution involves great difficulties.

An interesting approach was proposed in refs. [57–59]. When investigating open nonlinear systems described by nonlinear parabolic equations, one frequently manages to distinguish a set of order parameters to which all the other degrees of freedom would "tune in". Let us find the order parameters which characterize the function f. We assume that it transforms into itself when we rotate over an angle $2\pi/n$. We expand f in a Fourier series in an angular variable. It is clear that a certain row will contain only the harmonics with numbers $0, n, 2n, \ldots$. Let us assume that only the first harmonics of this row are essential. This enables us to reduce considerably the number of degrees of freedom. But the connection conditions cannot be satisfied on a continuous curve. It is natural to demand that they must be satisfied on several rays within the sector $2\pi/n$. Such an approach yields a whole hierarchy of simplified finite-dimensional models. They allow the prediction of configurations of higher eigenfunctions in a region of nonmonotonicity and give good initial approximations necessary for the numerical construction of such solutions.

In refs. [58, 59] such approximations were widely used and a large class of higher eigenfunctions of nonlinear media was constructed. Projections of some such functions are shown in fig. 2.6. From fig. 2.7 an idea can be obtained about a set of eigenfunctions which were predicted using an approximate analysis and then constructed numerically for a nonlinear medium. The result is very interesting.

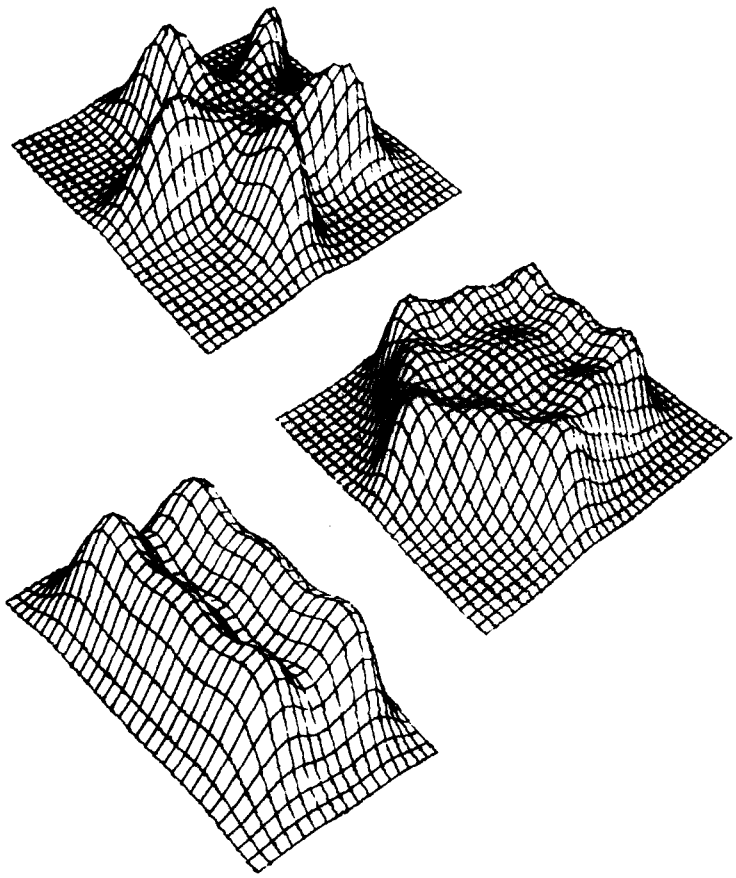

Fig. 2.6. Projections of several eigenfunctions of a nonlinear medium.

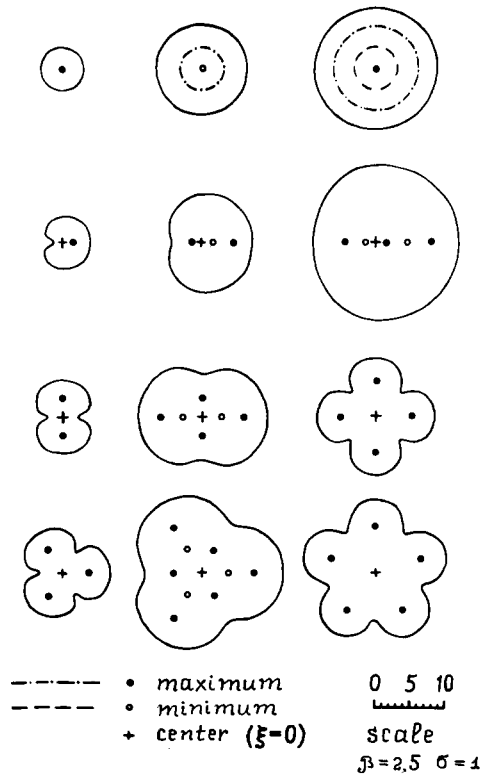

Fig. 2.7. Collection of eigenfunctions predicted by means of an approximate analysis and then constructed numerically.

Besides the simplest configurations consisting of similar quasi-structures there are many other forms. Maxima can have different amplitudes and be located in several layers. The temperature minima prove to be somehow consistent with the maxima. We recall that all these structures describe combustion waves converging to the centre with increasing amplitude.

Thus, in a very simple nonlinear medium a complex organization can exist. There are a finite number of configurations in it, which maintain their forms during evolution. They can be interpreted as several simple structures with different maxima that are combined into a complex structure (see fig. 2.6). The laws for such combinations determine higher eigenfunctions of a nonlinear medium. A more complex order cannot be achieved in the medium with given values of β and σ [23, 58].

Formulation of initial data can be considered as a method of influencing the nonlinear medium. [They can be generated by means of other processes which are not taken into account by the model (2.3).] In the general case one or several simple structures are formed rapidly, each of them localized in a domain G_L. If the initial data are set in accordance with higher eigenfunctions of the nonlinear medium the processes run in a larger domain, the arising heat wave converges to the centre and maintains its shape. In that case the processes behave quite differently as compared with the general case. Such a method of influencing nonlinear media has been called *resonant excitation of a nonlinear system* [23, 52]. Let us point out that for a configuration of initial profiles, their agreement with the eigenfunctions of the nonlinear medium rather than the amplitude are most important here.

Analysis of the eigenfunctions of various nonlinear media appears to be essential for the investiga-

tion of many systems in physics, biology and ecology. When executing control of many systems we cannot impose required behaviour upon them. In this case it would be very alluring to use resonant excitation, phenomena of self-organization, and to lean efficiently upon intrinsic properties of the system. This is particularly expedient in the cases when we cannot apply the cut-and-try method.

It should be said that until now the model of heat structures is one of the few systems for which the laws of organization of the dissipative structures are established. A search for similar laws was carried out in a number of other models as well. In some cases it was successful. It is difficult to outline even the main results obtained recently in the investigations of the model (2.3) and its generalizations. Therefore we shall describe only some of the most important trends of these investigations.

The first one is connected with a generalization of model (2.3) to more complex media and application of it to various physical problems. It was shown that localization and regimes with peaking are typical for systems whose parameters explicitly depend on the spatial coordinates. Cases were considered, when the density and the nonlinear source were power functions of the coordinate r [$r = (x^2 + y^2)^{1/2}$ or $r = (x^2 + y^2 + z^2)^{1/2}$] [60]. Localized structures developing in a regime with peaking arise here also. (They can, for example, represent localized cylindrical or spherical layers.) In some of these cases we can construct the eigenfunctions of the nonlinear medium for both the one-dimensional and two-dimensional problems [57–59].

Similar results were also obtained for a system of two quasi-linear parabolic-like equations with bulk sources,

$$u_t = (k_1 u^{\sigma_1} u_x)_x + q_1 u^{\beta_1} v^{\gamma_2}\,,$$

$$v_t = (k_2 v^{\sigma_2} v_x)_x + q_2 u^{\gamma_1} v^{\beta_2}\,, \tag{2.16}$$

$$q_1, q_2 > 0\,; \quad \sigma_1, \sigma_2 > 0\,; \quad \beta_1, \beta_2, \gamma_1, \gamma_2 > 0\,.$$

Here we also have the LS, S and HS regimes with peaking. For the LS regime the higher eigenfunctions were constructed. It is interesting that eq. (2.16) and eq. (2.3) obey the same law: in the nonmonotonic range they agree well with the solutions of the linearized problem [61, 62].

At the same time, for $t \to t_f$ the behaviour of the system (2.16) is far from being always determined by self-similar solutions. The following simple argument demonstrates this. Let us consider a spatially homogeneous solution ($u_x = v_x = 0$). Then we can verify that eqs. (2.16) have the integral

$$q_2 u^{\alpha_1}/\alpha_1 - q_1 v^{\alpha_2}/\alpha_2 = C\,, \quad \alpha_1 = \gamma_1 + 1 - \beta_1\,, \quad \alpha_2 = \gamma_2 + 1 - \beta_2\,. \tag{2.17}$$

The value of the constant is determined by the initial data. Then it is clear that for $\alpha_1 < 0$, $\alpha_2 < 0$ a regime with peaking occurs in the first component ($u \to \infty$, $t \to t_f$) when $C > 0$, in the second component when $C < 0$, and in both components when $C = 0$. It is natural that the self-similar solution describing a regime with peaking in both components (even the one which determines a simple structure) is unstable. It is this picture that was observed in calculations carried out in ref. [61]. In model (2.3) regimes with peaking exist when $\beta > 1$, and localized structures exist when $\beta \geq \sigma + 1$. It is a rather stiff requirement for many real models. However, such regimes are possible in systems where the source of the component u does not depend on the component itself. An example is the following set of equations:

$$u_t = k_0(uu_x)_x + q_0 vw\,,$$

$$v_t = k_0(vv_x)_x + q_0 uw\,, \tag{2.18}$$

$$w_t = k_0(ww_x)_x + q_0 uv\,.$$

We can verify that the solution (2.5), (2.9) satisfies this problem with $u = v = w$. It is this solution that was obtained for $t \to t_f$ in calculations carried out for (2.18).

In many models of plasma physics the thermal conductivity depends on the temperature as a power function [63]. Therefore model (2.3) was efficiently used to solve a number of physical problems [23, 64]. Using localized processes in the θ-pinch problem allows a reduction of heat losses from butt ends, which may lead to smaller dimensions of laboratory installations [65].

We note that LS regimes with peaking can exist in media with a constant thermal conductivity too. Due to this fact eqs. (2.3) can be used as a simplified model to describe the initial stage of many processes. For example, in ref. [66] such an approach gave an explanation for the effective reduction of the half-width of the temperature profile which was observed in oxidation of some metals by air under laser radiation.

This view on localized processes developing in a regime with peaking proved very useful to solve many other problems in physics and gas dynamics. Those problems are discussed in detail in ref. [67] and in ref. [293].

The analysis of the model of heat structures became much simpler due to a known self-similar solution. The question arises: How wide is the class of thermal conductivity coefficients and sources for which such solutions exist? The question was settled in a number of works where the methods of invariant-group analysis were used. (A detailed reference list of these works can be found in the review [54].) In these studies the groups of transformations admitted by (2.3), i.e., those that introduce no changes in the equation, were obtained for arbitrary $k(T)$ and $Q(T)$. Along with the groups of point transformations

$$t^* = f(t, x, T; a_1, \ldots, a_r)\,,$$

$$x^* = g(t, x, T; a_1, \ldots, a_r)\,, \tag{2.19}$$

$$T^* = h(t, x, T; a_1, \ldots, a_r)\,,$$

where a_r are the parameters of an r-parametric Lie group [68], the Lie–Bäcklund groups were considered. Besides dependent and independent variables these groups contain all derivatives up to infinite order. They are given by the transformations

$$x^* = x + \xi(t, x, T, T_1, T_2, \ldots)a + \mathrm{o}(a)\,,$$

$$t^* = t + \eta(t, x, T, T_1, T_2, \ldots)a + \mathrm{o}(a)\,, \tag{2.20}$$

$$T^* = T + U(t, x, T, T_1, T_2, \ldots)a + \mathrm{o}(a)\,,$$

where $T_i = \partial^i T/\partial x^i$, and a is the group parameter [69]. It turns out that the set of $k(T)$ and $Q(T)$ for

which the self-similar solutions exist is far from being exhausted by the power and exponent functions; it proves to be much wider. In this case one has succeeded not only in solving the problem of invariant-group classification but also in obtaining many particular solutions of physical interest.

For example, the equation

$$u_t = (u^{\sigma_1} u_x)_x + (u^{\sigma_2} u_y)_y + u^{\beta}\,, \quad \sigma_1 > 0,\ \sigma_2 > 0,\ \beta > 1\,, \tag{2.21}$$

which describes heat propagation through an anisotropic medium, has a self-similar solution of the form

$$\begin{aligned} &u(x, y, t) = (t_f - t)^{1/(1-\beta)} \tilde{u}(\xi, \eta)\,, \\ &\xi = x(t_f - t)^{(\sigma_1 + 1 - \beta)/(2\beta - 2)}\,, \qquad \eta = y(t_f - t)^{(\sigma_2 + 1 - \beta)/(2\beta - 2)}\,. \end{aligned} \tag{2.22}$$

From the above formula an unexpected result follows: the heat in such a medium can be localized in one direction [$\xi(t) < C$ for $t \to t_f$] and propagate infinitely along the other direction [$\eta(t) \to \infty$ for $t \to t_f$].

With $\sigma_1 = \sigma_2 = \sigma$ eq. (2.21) has another paradoxical solution [54] ($x \equiv r\cos\varphi$, $y \equiv r\sin\varphi$),

$$\begin{aligned} &u(t, r, \varphi) = (t_f - t)^{1/(1-\beta)} \tilde{u}(R, \Phi)\,, \\ &R = r(t_f - t)^{(\beta - \sigma - 1)/(2 - 2\beta)}\,, \qquad \Phi = \varphi_0 - c_0 \ln(t_f - t)\,, \end{aligned} \tag{2.23}$$

in which local maxima must move along a logarithmic spiral that twists out ($\beta < \sigma + 1$) or in ($\beta > \sigma + 1$) for $t \to t_f$. So far the eigenfunctions of a nonlinear medium of this type [$\tilde{u}(R, \Phi)$ with $c_0 \neq 0$] have not been constructed; nevertheless the mere possibility of the existence of such solutions seems very interesting.

Recently a mathematical theory has been developed due to which the self-similar solutions have proved to be even more useful for an analysis of nonstationary dissipative structures [24]. The theory is based on the idea to compare different solutions of nonlinear parabolic equations. Let us consider fig. 2.1. It is seen that first the amplitude of the solution decreases but then the temperature begins to increase at every point of the profile. The distributions for which $u_t(x, 0) > 0$ for all x were called critical. We can verify that in many problems of type (2.3) critical initial data lead to critical solutions for $t > 0$.

It turns out that a large class of comparison theorems can be proved for different critical solutions. For example, if two solutions $T^{(1)}(x, t)$ and $T^{(2)}(x, t)$ in problem (2.3) are critical and $T^{(1)}(x, 0) > T^{(2)}(x, 0)$, then $T^{(1)}(x, t) > T^{(2)}(x, t)$. This gives, in particular, information about the evolution of the profile $T^{(2)}(x, t)$ if the self-similar solution $T^{(1)}(x, t)$ is known.

Different solutions of different equations (not only of the same equation) can be compared, which is especially important in applications where $k(T)$ and $Q(T)$ may have rather complex forms. Such an approach is called operator comparison [71, 72]. For example, the solutions of the equations

$$u_t^{(\nu)} = k^{(\nu)}(u^{(\nu)}, |\nabla u^{(\nu)}|)\Delta u^{(\nu)} + Q^{(\nu)}(u^{(\nu)}, |\nabla u^{(\nu)}|)\,, \quad \nu = 1, 2\,,$$

can be compared if the inequalities

$$k^{(2)}(p, q) \geq k^{(1)}(p, q), \quad k^{(1)}(p, q)Q^{(2)}(p, q) \geq k^{(2)}(p, q)Q^{(1)}(p, q),$$

$$u^{(1)}(x, 0) > u^{(2)}(x, 0)$$

are satisfied.

A new approach was proposed in refs. [71, 72] for investigating the asymptotic stage of processes (the so-called method of *approximate self-similar solutions*). It turns out that for $t \to t_f$ different equations (2.3), including those which have no self-similar solutions, behave in the same way. Their solutions converge to the solutions of some degenerate basic equations which can have such solutions. Depending on the value of the limit

$$b_k = \lim_{u \to \infty} [k(u)/k'(u)]',$$

the basic solutions will be different. For example, when $b_k \to \infty$, such an approximate self-similar solution, to which the solution of (2.3) converges for $t \to t_f$, satisfies the first-order Hamilton–Jacobi-type equation [71]

$$v_t = \frac{k(v)}{v+1} |\nabla v|^2 + Q(v).$$

At present some strict results have been obtained as to the localization of solutions, evaluation of the peaking time, and stability of the first eigenfunctions of nonlinear media [54].

Thus, in the model of heat structures the self-similar solutions act as degenerate solutions which are not special. They describe the asymptotic behaviour of processes in a wide class of nonlinear media; they are an efficient tool for theoretical analysis and they determine the laws according to which simple structures can combine into the complex ones.

2.2. *Dissipative structures in media with trigger properties*

The model of heat structures as well as other models involving a single parabolic equation lack two important features which are typical for many nonlinear media. Due to the maximum principle, new extrema cannot appear in such systems and, hence, no new structures can emerge. Besides, only simple structures are stable in the media considered; to create complex order the initial data must be given in a special form.

Describing complex stable structures and their generation requires transition to a system of equations. In some cases one has been able to find out how complex structures can be constructed from simple ones, how order arises in such media, or how the course of the processes changes when one goes from one-dimensional to multi-dimensional models. All these questions have been studied for *systems with trigger properties* [73]. We shall discuss some of the results obtained.

Let us consider a system that for $D_1 = D_2 = 0$ (no diffusion) can exist in two stable states, $(\bar{u}_1, \bar{v}_1)$ and $(\bar{u}_2, \bar{v}_2)$, and in one unstable state $(0, 0)$. Such systems are called bistable or trigger systems. Trigger systems with diffusion appear in chemical kinetics, nonlinear optics, and in the simulation of morphogenesis [74].

For simplicity we consider the model

$$\begin{pmatrix} u \\ v \end{pmatrix}_t = \begin{pmatrix} D_1 & 0 \\ 0 & D_2 \end{pmatrix} \begin{pmatrix} u \\ v \end{pmatrix}_{xx} + A \begin{pmatrix} u \\ v \end{pmatrix} + B \begin{pmatrix} u \\ v \end{pmatrix} (u^2 + v^2) ,$$

$$u(x, 0) = u_0(x) , \quad v(x, 0) = v_0(x) , \quad 0 \le x \le l , \tag{2.24}$$

$$u_x(0, t) = u_x(l, t) = v_x(0, t) = v_x(l, t) = 0 .$$

Here u and v are assumed to be deviations from equilibrium of some matter concentrations. It is clear that u and v can be positive or negative. We shall assume that the eigenvalues of the matrix A are complex conjugate with positive real part. [This is a sufficient condition for instability of the zero solution of problem (2.24).] The matrix B is negative definite, which is a sufficient condition in order that the solution be bounded for $0 < t < \infty$. Problem (2.24) is invariant under the transformation $\{u, v\} \to \{-u, -v\}$ since the right-hand sides of the equations contain only odd powers of these functions; therefore $\bar{u}_2 = -\bar{u}_1 = -u^*$, $\bar{v}_2 = -\bar{v}_1 = -v^*$ $[Q_i(\bar{u}_j, \bar{v}_j) = 0;\ i = 1, 2;\ j = 1, 2]$. We shall consider such values of D_1, D_2 and l for which the Turing instability does not occur.

As initial data we first consider "the step distributions" $u_0 = u^*$, $v_0 = v^*$ for $0 \le x \le a$ and $u = -u^*$, $v = -v^*$ for $a \le x \le l$. In calculations quick convergence to the stationary solution shown in fig. 2.8 can be observed. There is a transition region to the left of which we have one *stable background* (u^*, v^*) and to the right of which the other one $(-u^*, -v^*)$. Such a solution is called an *elementary structure* (its meaning will be explained below). We may vary the length l and the parameter a in a wide range; it hardly affects the appearing elementary structure.

Let us note that in the model of heat structures we could have strict localization, $T(x, t) \equiv 0$ beyond G_L for $0 < t < t_f$. Here we have *effective localization*: we can give a small value of ε and indicate the region G_ε outside which

$$\max_{x \notin G_\varepsilon} [(u - u^*)^2 + (v - v^*)^2] < \varepsilon \quad \text{or} \quad \max_{x \notin G_\varepsilon} [(u + u^*)^2 + (v + v^*)^2] < \varepsilon .$$

Unlike the model of heat structures, here localization is connected with sinks rather than sources. (In the vicinity of each of the stable backgrounds the function $Q_1(u, v)$ and $Q_2(u, v)$ behave as sinks.) Besides, if structures emerge in a trigger medium they will later be time independent.

Since the elementary structures are localized, more complex structures can be built from them by giving several "steps" as initial data. Calculations show that they really can be constructed if the

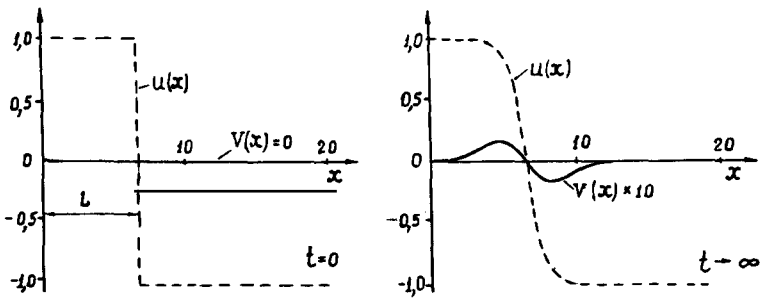

Fig. 2.8. Example of an elementary structure in a trigger medium.

distances between steps are not too small ($L > \tilde{l}$, where $\tilde{l}$ is determined by the properties of the nonlinear medium). An example of the solution appearing in this case is shown in fig. 2.9. All other structures in this medium consist of many elementary structures with different distances between them. The connection method, which has proved very useful in the model of heat structures, in this case also yields good results, i.e. approximate solutions corresponding to elementary structures [59].

One of the most interesting properties of a nonlinear medium is the possibility for dissipative structures to be born and completed by themselves. In order to create complex order it is quite unnecessary to put it in from outside, "to force" it onto the nonlinear medium by giving the required number of steps. Let us see what happens to a small perturbation put against the unstable background. Figure 2.10 illustrates this kind of calculation. It is seen that structures successively appear in neighbouring regions. In the calculations the region where dissipative structures appear has a distinct, observable boundary. This allows one to talk about the wave nature of the process and to identify the boundary with a front of a propagating wave.

Such a behaviour is typical for many other two-component systems when in the beginning there are small perturbations near the thermodynamic branch which has lost its stability. For example, this is typical for the best known two-component system, the Brussels model, which describes a certain class of chemical reactions in open systems [3],

$$Q_1 = A - (B+1)u + u^2 v\,, \quad Q_2 = Bu - u^2 v\,,$$

or the Gierer–Meinhardt model, which arises in the mathematical description of morphogenetic processes,

$$Q_1 = \rho + ku^2/v - \mu u\,, \qquad Q_2 = cu^2 - \nu v\,.$$

Here A, B, ρ, k, μ, c and ν are constants describing the model parameters.

Trigger media of the above type have an interesting feature: the dissipative structures in the one-dimensional and multi-dimensional systems differ qualitatively. In the multi-dimensional case a large set of localized nonstationary structures appears; the time of their existence is finite.

We shall consider a two-dimensional analog of eq. (2.24), in which $D_1 u_{xx}$ and $D_2 v_{xx}$ are replaced, respectively, by $\mathrm{div}(D_1 \,\mathrm{grad}\, u)$ and $\mathrm{div}(D_2 \,\mathrm{grad}\, v)$ in a square with side l, provided there are no flows at the boundary. Let us put a square with side $\bar{l}$ in the right bottom corner as initial data. Within the square $u = u^*$, $v = v^*$, while in the remaining region $u = -u^*$, $v = -v^*$. The quantity $\bar{l}$ is chosen so that

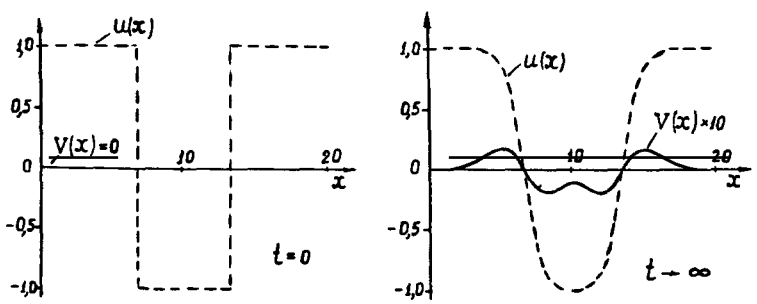

Fig. 2.9. Example of a complex stationary structure.

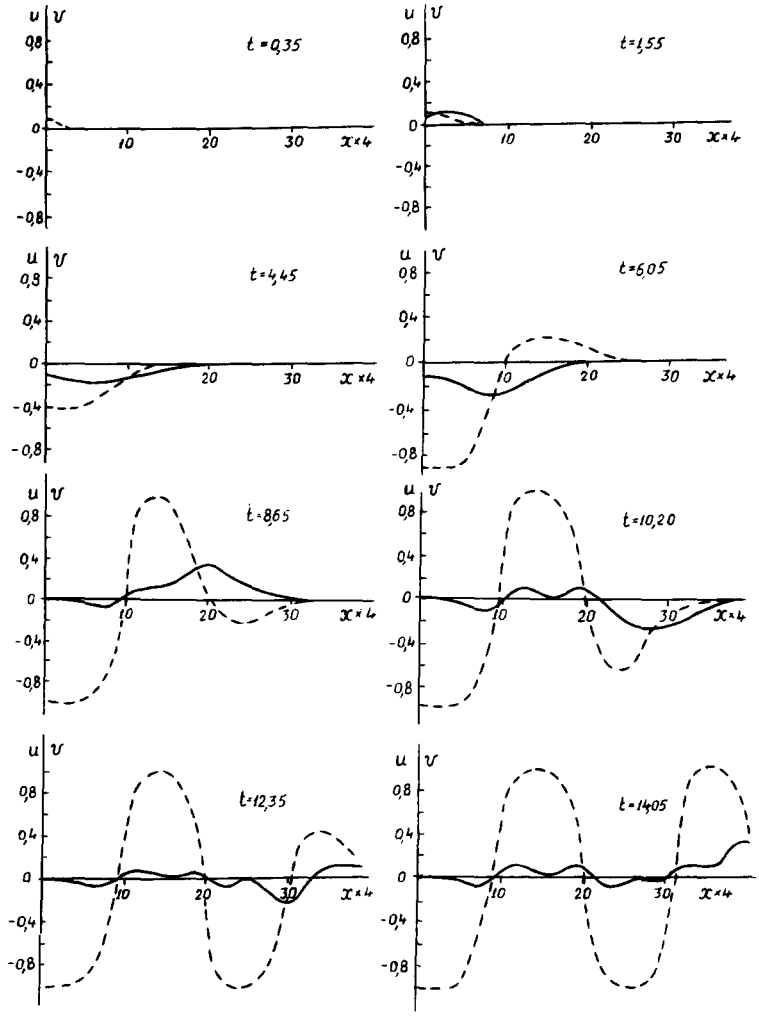

Fig. 2.10. Appearance of structures in neighbouring regions: $D_1 = 0.18$; $D_2 = 0.576$; $A = \begin{vmatrix} 1 & -1 \\ 1 & 1 \end{vmatrix}$; $B = \begin{vmatrix} -1 & 4 \\ -1 & -4 \end{vmatrix}$.

in the one-dimensional case when $u_0(x) = u^*$, $v_0(x) = v^*$ $(0 \le x \le \bar{l})$, $u_0(x) = -u^*$, $v_0(x) = -v^*$ $(\bar{l} \le x \le l)$, stationary structures should appear. A transition region develops over a time τ, whose structure remains constant for different points of the boundary in spite of the fact that the curvature of the contour, Γ_0, enveloping the region G_0, where $u(x, y) > 0$, varies from point to point.

The region G_0 slowly symmetrizes, tending to a circle whose radius decreases with time. Increasing l does not, in fact, change the process; convergence to the stationary solution does not occur for any l. The transition region, the independence from initial data, the efficient localization, and the long existence times, which can exceed τ by a few orders of magnitude, allow us to consider this process to be the evolution of a *nonstationary dissipative structure*.

In the two-dimensional case an initial small perturbation against an unstable background leads, as in the one-dimensional case, to the successive emergence of structures (t_1, t_2, t_3 in fig. 2.11). But here, having once emerged the structures are slowly reconstructed. The radii of the structures with circular configurations slowly decrease (t_4, t_5, t_6 in fig. 2.11).

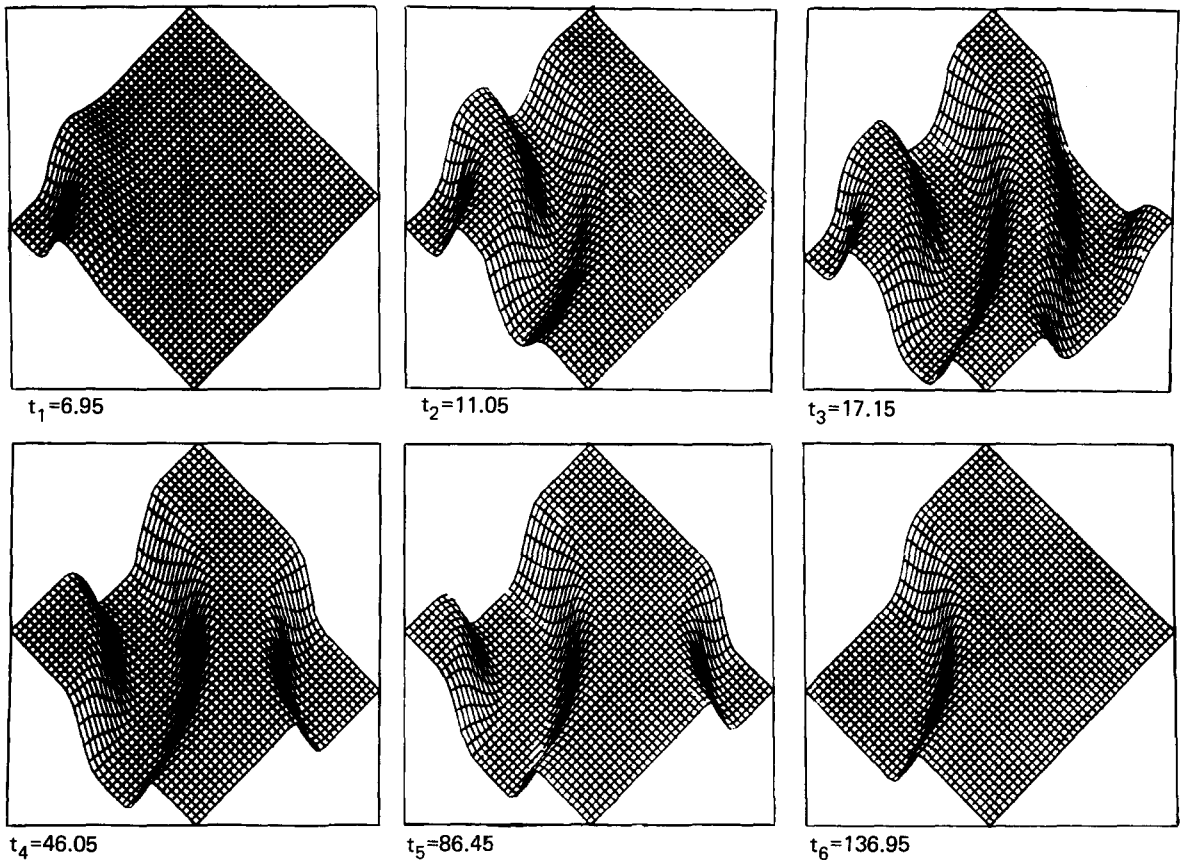

Fig. 2.11. Appearance of structures and their subsequent decay in a two-dimensional problem. Computational parameters are the same as in fig. 2.10.

On the face of things it seems that in the two-dimensional case trigger media have no stationary time-independent structures. However, this is not so. Such solutions can be constructed from symmetry considerations. Indeed, the equation does not change when x is replaced by $-x$, y by $-y$, and u, v by $-u$, $-v$. We shall denote the region where $u<0$ with black, and where $u>0$ with white. The evolution of one structure with circular configuration will look like the reduction of a black circle against a white background or a white circle against a black background.

Now we shall put "black" and "white" into similar conditions, for example, as is shown in the right half of fig. 2.12a. If the black squares began reducing it would mean violation of the symmetry between black and white, which exists in eq. (2.24). Calculations show that in that case a *stationary structure* called a "cross" appears (fig. 2.12a, left). The resonant excitation in such a medium is determined by the symmetry; unlike the model of heat structures the specific form of the initial data proves unimportant here.

It is interesting that the connection method enables us to construct an approximate solution corresponding to this structure with high accuracy [59]. By using this method other stationary configurations can be built too (for example, "windmill" and "parquet", figs. 2.12b and c).

We have considered cases in which the simplest "colour" symmetry (between "black" and "white") plays an important role. In some works which deal with other types of colour symmetry the

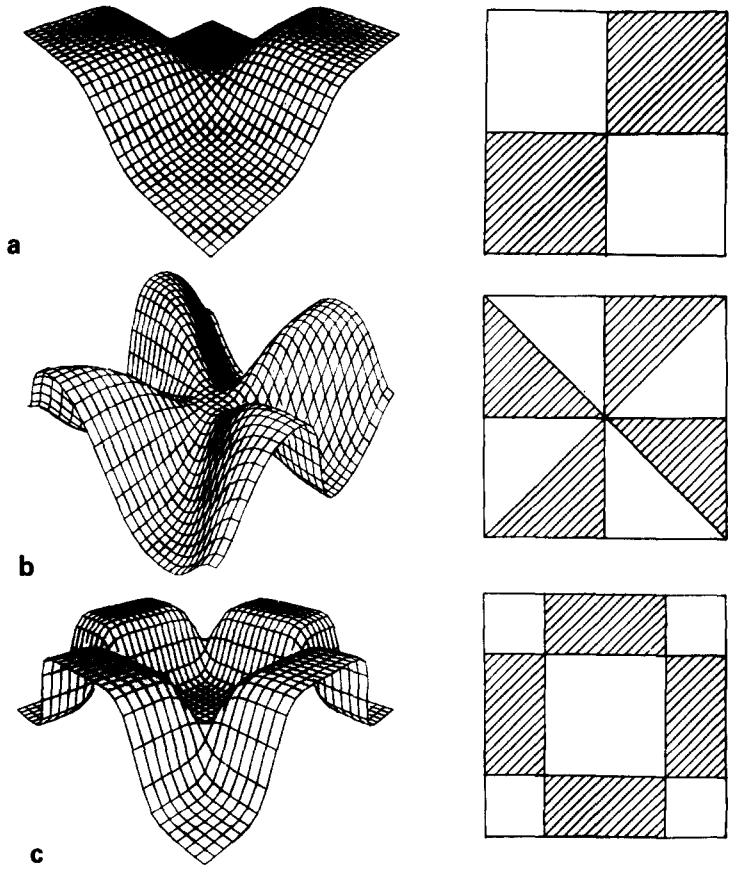

Fig. 2.12. Examples of two-dimensional stationary structures in a trigger medium.

mathematical theory is developed [75]. These ideas may prove useful in analysing partial differential equations, specifically, reaction–diffusion-type systems.

Thus, the laws of the organization of structures in the trigger media considered prove to be linked with localized processes and symmetry.

We have discussed two types of nonstationary dissipative structures, each of which may have complex spatial order. In both cases we managed to find out how the complex structures could be built from the simpler ones. At the present time this line of investigation is developing rapidly. And here a new approch to the problem, viz. studying the internal properties of a nonlinear medium and the laws of the organization of dissipative structures, and searching for efficient ways to influence the processes under investigation, may prove as important as specific mathematical and physical results.

3. Hierarchy of simplified models

In the last decade dozens of different models of the reaction–diffusion-type have been proposed to describe specific systems in chemical kinetics, plasma physics, ecology and many other fields. They have

been analysed by many authors, who considered specific functions $Q_1(X, Y, \lambda)$ and $Q_2(X, Y, \lambda)$ of different kinds. Therefore the following questions arise: Are there common features in the behaviour of the solutions of system (1.1) with different right-hand sides? Can we classify two-component systems by some features? Classification of the systems and distinguishing common features would let us pass from the study of specific models of a particular form to the development of the theory. This would help, in turn, to simplify the analysis of each specific problem.

Computer simulation is a basic tool used to investigate reaction–diffusion systems. Given specific functions $Q_1(X, Y, \lambda)$ and $Q_2(X, Y, \lambda)$, the coefficients D_1 and D_2, the initial data and the boundary conditions, one can observe the evolution of one solution over a certain time interval. However, watching the behaviour of a solution we often cannot observe any law or understand how it operates.

We can speak about understanding when we learn how to predict the behaviour of a solution and its qualitative peculiarities for different parameter values without solving the equation again and again. It would be fine if we could predict also the basic quantitative characteristics by using explicit formulas or simpler models. There may be several simplified models that differ in complexity, in the way they are obtained and in their range of applicability. If we had a sufficiently complete set of approximate models we could treat complex phenomena described by eq. (1.1) using the notions and categories which we encountered while investigating simpler problems. The development of simplified models, the establishment of their relationships, applicability ranges and properties are usually called the construction of a hierarchy of models.

Constructing a hierarchy of simplified models proves very important for the study of many nonlinear dissipative systems. As an illustration we refer to Rayleigh–Bénard convection [76, 77], some problems in nonlinear optics [78], and investigations of terrestrial and solar dynamos [79, 80]. It becomes necessary in cases when the capabilities of modern computers do not yet allow us to solve directly the arising equations (for example, in simulating complex hydro- and magnetohydrodynamic flows, or many-dimensional reaction–diffusion systems with many characteristic times).

In the study of open nonlinear systems, several ranges of the external parameter λ can be conditionally distinguished.

I. Small values of λ. In this range of parameter values the arising structures have small amplitudes and occur in the vicinity of the thermodynamic branch. As a small parameter here we can consider $\varepsilon \sim (\lambda - \lambda_0)$, where λ_0 is the point of loss of stability of the thermodynamic branch.

II. Intermediate values of λ. The amplitude of the arising solutions is not small, but the number of degrees of freedom that effectively determine the process dynamics is not large.

III. Large values of λ. In this range of parameter values complex regimes may arise, whose description involves many spatial and temporal harmonics. Such is, for example, multi-mode developed turbulence.

The first range of parameter values has been most thoroughly studied, and basic concepts as well as efficient mathematical models developed. Let us briefly describe some approaches proposed in this connection.

3.1. Universal description in the vicinity of the thermodynamic branch

One of the most efficient tools for analysing nonlinear systems is the theory of bifurcations. The problem of beam bending is classical in bifurcation theory; it was posed as early as last century.

Imagine a beam of rectangular cross section with load P acting on it from above (fig. 3.1). With increasing load the beam gets shorter and thicker, its axis remaining straight. At some critical value P_c,

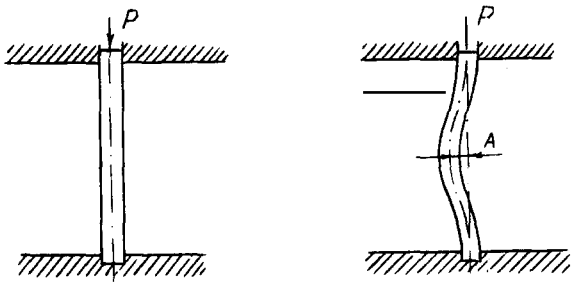

Fig. 3.1

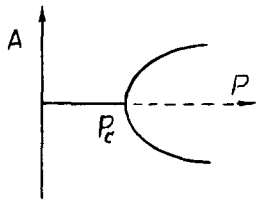

Fig. 3.2

however, the picture qualitatively changes: the beam will lose its rectilinear configuration and bend to the right or left. When $P < P_c$ the beam has only one equilibrium configuration, when $P > P_c$ it has three: the rectilinear configuration, which becomes unstable, and two stable configurations (one corresponding to bending to the right, the other to the left). If we draw the deflection A of the beam axis depending on the value of P the picture will be as in fig. 3.2. Stable equilibrium states in this figure as well as in others below in this chapter are denoted by a solid line and unstable states by dashed lines. When $P = P_c$ the number of equilibrium states and their stability change. The change in the number and stability of solutions is called *branching* or *bifurcation* of solutions. It is a typical nonlinear phenomenon. In the problem of beam bending the classical linear theory of elasticity gives only the rectilinear equilibrium state. The loss of stability of a beam and some other nonlinear models of elasticity theory are discussed in detail in ref. [51].

The problem of the loss of the beam stability was treated by Euler, Bernoulli and Lagrange. The term "bifurcation" was first introduced by C. Jacobi in 1884. But the meaning of bifurcation theory was only fully realized by the outstanding French mathematician Henri Poincaré at the end of last century.

Let the solution of a nonlinear problem be known for $\lambda = \lambda_0$; then we may try to find the solution for $\lambda_0 + \Delta\lambda$, where $\Delta\lambda$ is small. Our analysis becomes local – instead of searching for a general solution we restrict ourselves to what happens with a specific solution in the vicinity of one value of the parameter. It is natural first of all to choose values of the parameter at which the behaviour of the system changes qualitatively, i.e., the *points of bifurcation*. It is the most important task to establish all the basic types of bifurcation in various problems. Poincaré believed that the solution of this extensive and complex problem would help in investigations of many specific nonlinear phenomena.

The research programme proposed by Poincaré was extended in the theory of *normal forms* of differential equations [81], in the theory of catastrophes, where the equilibrium states of dynamic systems described by a potential function are studied [10, 82], and in some other developing fields of mathematics.

We consider the simplest types of bifurcations typical for reaction–diffusion systems. Let us consider a chemical reaction where the variation of concentration of an ingredient, dx/dt, depends on the concentration x and on external effects which are described by λ. This yields the ordinary differential equation

$$dx/dt = F(x, \lambda) . \tag{3.1}$$

The solutions of this equation behave in a simple manner. When $t \to \infty$ the function $x(t)$ tends to a constant value $\bar{x}$ (we shall assume that the equation has no infinite solutions).

There may be several such $\bar{x}$: $\bar{x}_1$, $\bar{x}_2$, $\bar{x}_3$, etc. it is clear that

$$F(\bar{x}, \lambda) = 0 . \tag{3.2}$$

Depending on the initial data $x(0)$ the solution tends to one $\bar{x}_n$. Therefore, we have only to solve eq. (3.2) and find its roots as functions of λ.

We assume that some solution of eq. (3.2) is known. In order to obtain a solution for the value of $\lambda = \lambda_0 + \Delta\lambda$, $\Delta\lambda \ll 1$, we may use the Taylor formula

$$F(\bar{x} + \Delta x, \lambda_0 + \Delta\lambda) = F(\bar{x}, \lambda_0) + \frac{\partial F(\bar{x}, \lambda_0)}{\partial x} \Delta x + \frac{\partial F(\bar{x}, \lambda_0)}{\partial \lambda} \Delta\lambda + \frac{1}{2}\left(\frac{\partial^2 F(\bar{x}, \lambda_0)}{\partial x^2} (\Delta x)^2 + 2 \frac{\partial^2 F(\bar{x}, \lambda_0)}{\partial x \partial \lambda} \Delta x \Delta\lambda + \frac{\partial^2 F(\bar{x}, \lambda_0)}{\partial \lambda^2} (\Delta\lambda)^2\right) + G , \tag{3.3}$$

where G is the residue of the series, containing the terms proportional to $(\Delta x)^3$, $(\Delta x)^2 \Delta\lambda$, $\Delta x (\Delta\lambda)^2$, $(\Delta\lambda)^3$, etc.; its specific form is of no importance to us. Since we are interested in the equilibrium states, $F(\bar{x} + \Delta x, \lambda_0 + \Delta\lambda) = 0$. But then for $\Delta x \to 0$, $\Delta\lambda \to 0$, we obtain

$$\Delta x = -\frac{\partial F(\bar{x}, \lambda_0)}{\partial \lambda} \Delta\lambda \Big/ \frac{\partial F(\bar{x}, \lambda_0)}{\partial x} . \tag{3.4}$$

From this formula it follows that if $\partial F(\bar{x}, \lambda_0)/\partial x$ is different from zero, a new equilibrium state can be approximately determined (fig. 3.3). As follows from formula (3.3), such a state will be unique, i.e., bifurcation does not occur at the point λ_0, $\bar{x}$.

It may happen, however, that $\partial F(\bar{x}, \lambda_0)/\partial x = 0$, and then we should take into account the next terms. If $\partial^2 F(\bar{x}, \lambda_0)/\partial x^2 \neq 0$, then instead of (3.4) we have

$$\Delta x = \pm\left((-2) \frac{\partial F(\bar{x}, \lambda_0)}{\partial \lambda} \Delta\lambda \Big/ \frac{\partial^2 F(\bar{x}, \lambda_0)}{\partial x^2}\right)^{1/2} = \pm\sqrt{c_1 \Delta\lambda} . \tag{3.5}$$

The picture is different here (fig. 3.4): when $\lambda > \lambda_0$ two solutions appear, when $\lambda < \lambda_0$ there is none (if c_1 is assumed to be positive). The problem about the beam load illustrates such a behaviour. Let the beam be not ideally straight in the initial state but a little bent to one side. Then the load function of maximal bending shown in fig. 3.2 will change and take the form given in fig. 3.5.

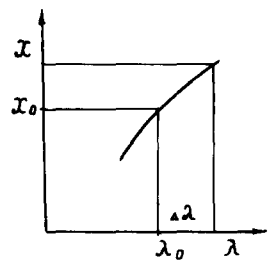

Fig. 3.3

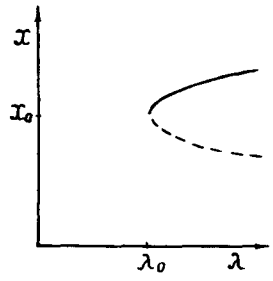

Fig. 3.4

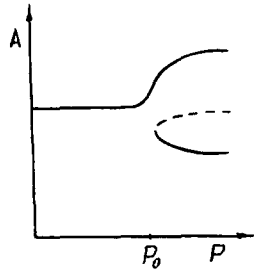

Fig. 3.5

If the beam is in a stable state (on the lower branch of the bifurcation diagram in fig. 3.5) and the load slowly decreases, then for a certain value of P a jump into another equilibrium state will occur (on the upper branch). This phenomenon, called a "*flop*", is used in engineering [83]. The change of the form of the *bifurcation diagram*, for example, for a small violation of symmetry of the system under investigation, is analysed in one of the sections of bifurcation theory, the *theory of imperfections* [84].

If $\partial^2 F(\bar{x}, \lambda_0)/\partial x^2$ and $\partial F(\bar{x}, \lambda_0)/\partial\lambda$ are zero, the next terms $(\partial^2 F(\bar{x}, \lambda_0)/\partial\lambda^2)(\Delta\lambda)^2$, $(\partial^2 F(\bar{x}, \lambda_0)/\partial x\,\partial\lambda)\,\Delta x\,\Delta\lambda$, etc. should be taken into account.

If even one of the second derivatives is not zero, the typical bifurcation will be as those shown in fig. 3.6. We have already seen the picture of fig. 3.6a in the problem of beam bending. Figure 3.6b corresponds to a bifurcation which can conditionally be called "*stability exchange*". The equilibrium states become stable at a point λ_0, $\bar{x}$ if located on one branch, and unstable if located on the other branch. The bifurcation shown in fig. 3.6c is called *subcritical* (in contrast to "*supercritical*" bifurcation, shown in fig. 3.6a). Its specific feature is that the solutions appearing as a result of branching exist in the same range of parameter values ($\lambda < \lambda_0$) where the initial stable branch is located. Analysis shows that in this case they are unstable. As the parameter λ increases the stable equilibrium state simply disappears, and the solution of eq. (3.1) goes to the other region in x. The pictures in fig. 3.6 and the corresponding bifurcations occur for most stationary dissipative structures.

More complex types of bifurcations can be obtained if the next coefficients in the Taylor series are assumed to be zero. However, the more conditions are imposed on these coefficients, the more degenerate and atypical such bifurcations prove to be. They are essential only in families of mathematical models that depend on several parameters or in systems that have a number of symmetries.

In eq. (3.1) bifurcations mean the appearance or disappearance of stationary solutions. In the system of two ordinary differential equations

$$dX/dt = F_1(X, Y, \lambda), \qquad dY/dt = F_2(X, Y, \lambda), \tag{3.6}$$

bifurcation may result in the appearance of periodic regimes. An example of such a process is shown in fig. 3.7, where typical phase trajectories are presented (projections of the solution $X(t)$, $Y(t)$ on the $\{X, Y\}$ plane).

From the point (0, 0), which is a stable focus (fig. 3.7a) for $\lambda < \lambda_0$, a limit cycle originates for $\lambda > \lambda_0$. This cycle determines a stable periodic solution, and all the trajectories in its vicinity tend to it. (In this case all the trajectories except (0, 0).)

By using methods of the theory of normal forms [81, 85] we may show that in the vicinity of the point (0, 0) all systems (3.6) in which such a bifurcation occurs can be reduced to the form

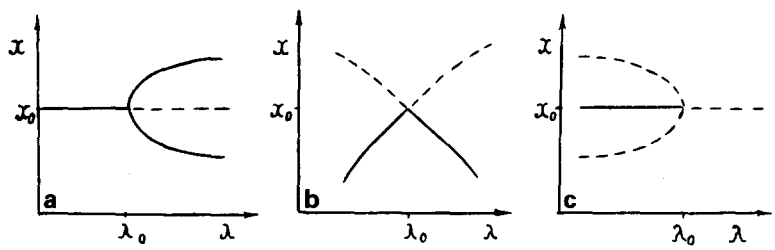

Fig. 3.6

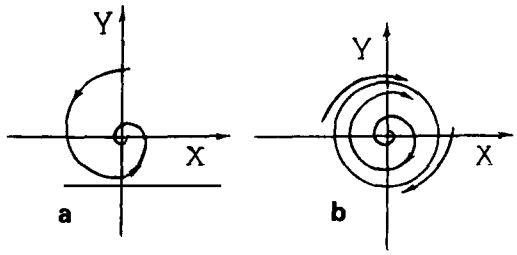

Fig. 3.7

$$dW/dt = \lambda W - (1 + ic_2)|W|^2 W ,$$

where $\lambda_0 = 0$, $W = u + iv$, if we make a change of variables. In polar coordinates $u = r\cos\varphi$, $v = r\sin\varphi$, we have

$$\dot{r} = \lambda r - r^3 , \qquad \dot{\varphi} = c_2 .$$

When λ is positive the focus loses its stability and a limit cycle appears with a radius varying as $\sqrt{\lambda}$.

The bifurcation in which a limit cycle is created was discovered by A.A. Andronov in 1931 and later it was intensively used for the mathematical modelling of systems in radioengineering, and for constructing the theory of oscillations [86]. Hopf carried out an analysis of this bifurcation for multi-dimensional dynamical systems, therefore it is often called a *Hopf bifurcation*.

We have discussed branching in the simplest systems. But as early as the beginning of this century A.M. Lyapunov and E. Schmidt developed methods to study partial differential equations by using bifurcation theory. A typical situation can be described as follows. When there is a unique stable stationary solution, its stability in the linear approximation is determined by the set of eigenvalues μ_i that describe the behaviour of solutions of linearized problems. When $\lambda < \lambda_0$ the real parts of all eigenvalues are negative. When $\lambda = \lambda_0$ we have p eigenvalues with $\mathrm{Re}\,\mu_i = 0$, $(i = 1, \ldots, p)$. For example, in the case of the Hopf bifurcation $\mu_1 = i\omega$, $\mu_2 = -i\omega$.

Lyapunov and Schmidt proposed to split the equation under investigation into two: one equation in a finite-dimensional subspace with dimensionality p, the other in its infinite-dimensional complement. Then we have a system of p equations with p unknowns (the so-called *branch equation*). For many problems we can show that when $\lambda > \lambda_0$ the properties of the solutions of the original equation are determined by the properties of the branch equation [51, 84, 87]. In this case all information about the number of branch solutions and their stability is contained in a finite-dimensional problem. An infinite-dimensional nonlinear system in the vicinity of a bifurcation point behaves as a finite-dimensional system.

This approach proved very useful for solving many applied problems. Many hydrodynamic systems were studied with its aid. Some of them are discussed in detail in ref. [88]. The Hopf bifurcation enables us to explain many important phenomena in hydrodynamics, chemistry and biology [89]. Its specific features in reaction–diffusion systems and, in particular, in the Brusselator model are discussed in ref. [90]. The use of methods of bifurcation theory to investigate two-dimensional dissipative structures will be considered in chapter 10.

In spite of the simplicity of many branch equations, cumbersome calculations and even the use of numerical methods are required to determine the coefficients and to study the stability of branch

solutions. The more complex the solution $\bar{X}$ undergoing bifurcation proves to be, the more severe technical difficulties are involved in using these methods.

In the seventies in the study of hydrodynamic systems and reaction–diffusion models, some physical phenomena initiated a class of problems which were beyond the scope of the traditional methods of bifurcation theory and required a different approach. Let us imagine that a Turing bifurcation occurs in a nonlinear system, and that for $\lambda > \lambda_0$ the system becomes unstable against small perturbations of the form $W(X, T)\,e^{ik_c x}$, where $W(X, T)$ describes a slow spatial–temporal modulation, X and T are "slow" spatial and temporal variables. In studying such systems it seems expedient to go over to simpler equations to describe variations of $W(X, T)$.

This approach is associated with multi-scale expansions and widely used in the theory of nonlinear waves. Applying it we can describe different wave processes with the same equations. As examples we can give the parabolic equation extensively used in nonlinear optics [91] or the cubic Schrödinger equation used to describe waves in deep water and in many other cases [92].

Newell and Whitehead [93] used multi-scale expansions to describe Rayleigh–Bénard convection in a fluid layer of thickness d heated from below. (This system is very frequently discussed in connection with synergetic problems [3, 13].) As an original physical model the hydrodynamic equations in the Boussinesq approximation are considered. The state in which a fluid is at rest, for $R = R_c$, proves to be unstable against perturbations of the form

$$\omega \sim e^{ik\cdot x} \sin(\pi z/d)\,, \quad k^2 = \pi^2/(2d^2)\,,$$

where ω is the vertical velocity component (directed along the z axis). Assuming

$$\omega = (W(X, Y, T)\,e^{ik\cdot x} + W^*(X, Y, T)\,e^{-ik\cdot x}) \sin(\pi z/d)$$

for $R > R_c$ and writing down the corresponding expressions for the pressure, temperature and the other velocity components, we obtain for W the following equation:

$$2\frac{p+1}{p}\frac{\partial W}{\partial t} - 8(\boldsymbol{n}\cdot\nabla_x)^2 W = (3\pi^2\chi - WW^*)W\,, \tag{3.7}$$

where $X = \varepsilon x$, $Y = \varepsilon y$, $T = \varepsilon^2 t$, p is the Prandtl number, χ is a constant, $\boldsymbol{n}$ is a unit vector along the critical mode. The small parameter ε describes the deviation of R from R_c. It is shown in ref. [93] that eq. (3.7) lets us explain a number of experimental results and describe efficiently many phenomena which were beyond the scope of traditional methods. Such an approach was used in 1975 by Y. Kuramoto and T. Tsuzuki [94] to analyse reaction–diffusion systems.

It is convenient to distinguish two classes of systems. If the length scale is not large, $[(\lambda - \lambda_0) \ll l^{-2}]$, standard methods of bifurcation theory can be efficiently used. With large length scales $[(\lambda - \lambda_0) \gg l^{-2}]$, as in the convection problem, it is expedient to pass to slow variables. It is natural to consider two cases: the Turing bifurcation when the linearized problem has zero eigenvalue for $\lambda = \lambda_0$, and the Hopf bifurcation when a pair of complex-conjugate values $\pm i\omega_0$ appears.

In both cases the equation proposed in ref. [94] has the form

$$W_t = (\pm 1 + ic_0)W + (1 + ic_1)W_{xx} - (1 + ic_2)|W|^2 W\,. \tag{3.8}$$

Here $W = u + iv$; c_0, c_1 and c_2 are real constants. In refs. [94, 95] an algorithm is given to determine the values of the constants using the coefficients D_1 and D_2, the functions $Q_1(X, Y, \lambda)$ and $Q_2(X, Y, \lambda)$ and their derivatives. The + sign on the right-hand side of (3.8) corresponds to the parameter range $\lambda > \lambda_0$, the − sign to $\lambda < \lambda_0$.

Let us explain the meaning of the variables W, R and T. The possibility of passing from (1.1) to (3.8) is connected with the existence of the small parameter $\varepsilon \sim (\lambda - \lambda_0)^{1/2}$. In ref. [94] it is shown that in this case the solution of (1.1) should be looked for in the form

$$\begin{pmatrix} X \\ Y \end{pmatrix} = \begin{pmatrix} X_0 \\ Y_0 \end{pmatrix} + \varepsilon \left[W(R, T) f \begin{pmatrix} e_1 \\ e_2 \end{pmatrix} + \text{c.c.} \right] + \cdots, \quad e_1, e_2 = \text{const.},$$

where $\{X_0, Y_0\}$ is the thermodynamic branch, W depends on the slow variables $R = \varepsilon x$, $T = \varepsilon^2 t$; $f = e^{ik_c x}$ if stationary solutions appear, and $f = e^{i\omega_0 t}$ in the Hopf bifurcation case. In other words, R and T are slow variables, which determine the time and space modulations of the simplest solutions f, whose configurations follow from the linear analysis. Below the independent variables in (3.8) will be designated by x and t.

The function $W(x, t)$ describes the deviation of the solutions of eqs. (1.1) from $\{X_0, Y_0\}$. Therefore, eq. (3.8) describes only the cases when the solutions remain in the vicinity of the thermodynamic branch for $t \to \infty$. The equation does not describe degenerate cases when more than two eigenvalues of the linearized problem cross the imaginary axis.

The investigation of eq. (3.8) proves to be closely associated with the problem of a classification of two-component systems. Let the qualitative features of its solutions (type of asymptotic behaviour, symmetry, etc.) be known for any values of c_0, c_1, c_2 and the length scale l. Then all systems of the form (1.1) for which solutions of (3.8) behave similarly, can be combined in the same class. Such an approach would be more useful if we could propose efficient approximate and qualitative methods for analysing different types of solutions.

Equation (3.8) is of great interest for the simulation of wind waves in water [96] and ion-acoustic waves in a plasma [97]. Similar problems were considered when studying the stability of Poisseuille flow [98] and in nonlinear optics [99]. This equation arises in many cases when finite-amplitude perturbations in a nonequilibrium system are investigated for small supercritical values.

In the literature eq. (3.8) is given different names. It is referred to as the λ–ω system in refs. [100, 101], while it is called the Kuramoto–Tsuzuki equation in refs. [102, 103] and the generalized time-dependent Ginzburg–Landau equation in refs. [94, 104].

Meanwhile quite specific equations in the theory of phase transitions of the second kind, which do not coincide with (3.8), are usually meant when the Ginzburg–Landau equation and the time-dependent Ginzburg–Landau equation are considered [105]. At the same time an extensive class of equations including (3.8), equations with a quadratic nonlinearity and many other systems, are called the generalized Ginzburg–Landau equations in the books by H. Haken [13, 14]. Therefore, thinking of the use of (3.8) to analyse reaction–diffusion systems we shall call it the *Kuramoto–Tsuzuki equation*.

Let us dwell on some specific features of eq. (3.8). In the second boundary value problem, provided flows are absent at the boundaries, or in the problem with periodic boundary conditions, $\int_0^l |W(x, t)|^2 \, dx \to 0$ if the Kuramoto–Tsuzuki equation is chosen with the − sign. (We can verify this by multiplying it by W^* and integrating over the entire domain.) Therefore, we shall assume that the sign is plus.

By the change of variable $W = W_1 \exp(ic_0 t)$ we may easily verify that without loss of generality we can put $c_0 = 0$. Below we shall assume that such a replacement has been made. By writing down eq. (3.8) in the variables ρ and φ ($u = \rho \cos\varphi$, $v = \rho \sin\varphi$),

$$\rho_t = \rho - \rho^3 + \rho_{xx} - \rho\varphi_x^2 - 2c_1\rho_x\varphi_x - c_1\rho\varphi_{xx} ,$$

$$\rho\varphi_t = -c_2\rho^3 + 2\rho_x\varphi_x + \rho\varphi_{xx} + c_1\rho_{xx} - c_1\rho\varphi_x^2 ,$$

we can verify the following statement. Let $\{\rho(x, t), \varphi(x, t)\}$ be a solution of (3.8). Then $\{\rho(x, t), -\varphi(x, t)\}$ will be a solution if c_1 and c_2 are replaced by $-c_1$, $-c_2$. This means that it is sufficient to consider the parameter region $c_1 \geq 0$.

The simplest solutions of (3.8) are the zero solution (always unstable in the linear approximation) and the spatially homogeneous solution

$$W = \exp(-ic_2 t + i\alpha) , \tag{3.9}$$

where α is a real constant. It is stable against small perturbations of the form $\exp(ikx)$ provided that [94]

$$(c_1^2 + 1)k^4 + 2k^2(1 + c_1c_2) > 0 , \tag{3.10}$$

i.e., it is stable for all k when $1 + c_1c_2 > 0$.

It can be proven that in the second boundary value problem for $0 < t < \infty$ the solution is bounded in norm L_2 (i.e. the quantity $\|W\|_{L_2} = \{\int_0^l [u^2(x, t) + v^2(x, t)]\, dx\}^{1/2}$ is bounded) provided the flows at the boundaries are absent. It is shown in ref. [106] that if the norm does not decrease in L_2 the solution is bounded in norm C (the quantity $\max_{0<x<l} (|u(x, t)| + |v(x, t)|)$, $0 < t < \infty$, is bounded).

The Kuramoto–Tsuzuki equation is a complex mathematical object. It can have several types of self-similar solutions, and describe two-frequency and stochastic regimes. At the present time it can be considered as one of the most important model equations in the theory of open nonlinear systems. Its investigation helps us to understand the properties of nonlinear media and some physical phenomena. Later we shall discuss in more detail the methods of analyzing this equation and some results of this analysis.

Above we have discussed methods for investigating nonlinear media when λ is close to λ_0 and the amplitudes of the branch solutions are small. As λ increases the amplitudes are no longer small, but even then we can sometimes describe processes in distributed systems by simplified finite-dimensional systems. Most results here were obtained with the use of the Galerkin method. It was assumed that in the solution only some harmonics (a finite number) are important, and instead of the original partial differential equations a system of ordinary differential equations that connects their amplitudes was considered [107].

In other cases a transition to a finite-dimensional system can be made if the original equation is assumed to be a small perturbation of nonlinear equations whose solutions are known. Usually, these are fully integrable systems which have soliton solutions.

We may expect that as λ increases the complexity of the solution will grow. In the simplest cases when we consider only the behaviour of specific types of systems in time the Feigenbaum theory of universality allows a prediction of the behaviour of the solution after an infinite number of bifurcations

[33]. (Below we shall discuss some results of this theory.) However, an efficient description of nonlinear systems in which the number of temporal and spatial modes characterizing the process dynamics increases as λ grows is an open question as yet. An interesting approach to this problem is proposed in ref. [78].

3.2. A hierarchy of simplified models for the Kuramoto–Tsuzuki equation

Reaction–diffusion systems were investigated using different simplified models. Each of them can be applied to a certain range of parameter values and proves to be simpler than the original set of equations. Let us consider a few simplified models arising when nonlinear media in the vicinity of the bifurcation point are described. Note that there is a relationship between these models.

Mathematical models of many specific physical, chemical and biological systems are nonlinear parabolic equations of the form

$$\begin{pmatrix} u_1 \\ \vdots \\ u_N \end{pmatrix}_t = \begin{pmatrix} D_1 & & 0 \\ & \ddots & \\ 0 & & D_N \end{pmatrix} \begin{pmatrix} u_1 \\ \vdots \\ u_N \end{pmatrix}_{xx} + \begin{pmatrix} Q_1(u_1, \ldots, u_N, \lambda_1, \ldots, \lambda_m) \\ \vdots \\ Q_N(u_1, \ldots, u_N, \lambda_1, \ldots, \lambda_m) \end{pmatrix}. \tag{3.11}$$

Considering the processes with the longest characteristic times we can distinguish the order parameters that determine the behaviour of the remaining functions describing the state of system. Methods for distinguishing these parameters were discussed in chapter 1.

In some cases the evolution of the order parameters is described by a system of two nonlinear partial differential equations depending on a single parameter λ. Their behaviour is typically as follows [3, 13]. When $\lambda < \lambda_0$ there is a stable stationary spatially homogeneous solution, called the thermodynamic branch. For $\lambda = \lambda_0$ the thermodynamic branch becomes unstable against small perturbations $f \sim \exp(ik_c x)$ or $f \sim \exp(i\omega_0 t)$.

If the system is sufficiently large it is convenient to consider eq. (3.8) for a variable W which describes the slow spatial–temporal modulation of the function f, whose form follows from the linear analysis [94]. At the present time it seems that the second boundary value problem,

$$\begin{aligned} &W_t = W + (1 + ic_1)W_{xx} - (1 + ic_2)|W|^2 W, \quad 0 \le x \le l, \quad 0 < t < \infty, \\ &W_x(0, t) = W_x(l, t) = 0, \qquad W(x, 0) = W_0(x), \end{aligned} \tag{3.12}$$

has been studied in most detail.

If the length l in (3.12) is not large, the Fourier coefficients of the solutions quickly decrease with increasing number. In the simplest case only the zeroth and first harmonics prove to be essential.

We assume that in the solution under investigation there are only two modes,

$$W = u + iv = (x_0 + iy_0) + (x_1 + iy_1)\cos kx, \tag{3.13}$$

where k is chosen so that the boundary conditions of problem (3.12) be satisfied, i.e., $k = \pi/l$ corresponds to the first harmonic. We substitute (3.13) into (3.12) and ignore all the terms with $\cos(\pi m x/l)$, $m > 1$, by assuming they are negligibly small. This leads to a closed system of ordinary differential equations,

$$\begin{aligned}
\dot{x}_0 &= x_0 - (x_0 - c_2 y_0)(\rho_0^2 + \rho_1^2/2) - s(x_1 - c_2 y_1)\,, \\
\dot{y}_0 &= y_0 - (c_2 x_0 + y_0)(\rho_0^2 + \rho_1^2/2) - s(c_2 x_1 + y_1)\,, \\
\dot{x}_1 &= x_1 - (x_1 - c_2 y_1)(\rho_0^2 + 3\rho_1^2/4) - 2s(x_0 - c_2 y_0) - k^2(x_1 - c_1 y_1)\,, \\
\dot{y}_1 &= y_1 - (c_2 x_1 + y_1)(\rho_0^2 + 3\rho_1^2/4) - 2s(c_2 x_0 + y_0) - k^2(c_1 x_1 + y_1)\,,
\end{aligned} \tag{3.14}$$

where $\rho_0^2 = x_0^2 + y_0^2$, $\rho_1^2 = x_1^2 + y_1^2$, $s = x_0 x_1 + y_0 y_1$. It can be simplified even more if we pass to the variables ρ_0, ρ_1, φ_0, φ_1 by the formulas $x_0 = \rho_0 \cos\varphi_0$, $y_0 = \rho_0 \sin\varphi_0$, $x_1 = \rho_1 \cos\varphi_1$, $y_1 = \rho_1 \sin\varphi_1$, and then to ξ, η, θ [$\xi = \rho_0^2$, $\eta = \rho_1^2$, $\theta = 2(\varphi_0 - \varphi_1)$]. As a result we have three equations,

$$\begin{aligned}
\dot{\xi} &= 2\xi - 2\xi(\xi + \eta) - \xi\eta(\cos\theta + c_2 \sin\theta)\,, \\
\dot{\eta} &= 2\eta - 2\eta(2\xi + 3\eta/4) - 2\xi\eta(\cos\theta - c_2 \sin\theta) - 2k^2\eta\,, \\
\dot{\theta} &= c_2(2\xi - \eta/2) + \sin\theta\,(2\xi + \eta) + c_2 \cos\theta\,(2\xi - \eta) + 2c_1 k^2\,, \\
k &= \pi/l\,.
\end{aligned} \tag{3.15}$$

The relationship between ξ, η, θ and φ_0 is determined by the equation

$$\dot{\varphi}_0 = -c_2(\xi + \eta) + 0.5\eta(\sin\theta - c_2 \cos\theta)\,. \tag{3.16}$$

The ability to go over to the system of equations (3.15) is due to the fact that eq. (3.12) has a symmetry. If $W(x, t)$ is a solution, the function $W(x, t)\,e^{i\alpha}$, $\alpha = \text{const.}$, is also a solution. In eqs. (3.15) ξ and η describe the square amplitudes of the zeroth and first harmonics, θ is the phase difference between them.

The simplest solutions of eqs. (3.15) are the stable singular points ($\xi \to \text{const.}$, $\eta \to \text{const.}$, $\theta \to \text{const.}$, $t \to \infty$). In order to find the coordinates of a singular point (ξ, η, θ), we should put $\dot{\xi}$, $\dot{\eta}$, $\dot{\theta}$ equal to zero and solve the three algebraic equations obtained. Explicit expressions are given in refs. [103, 108] for the singular points and the straight lines for which $\xi = 0$ or $\eta = 0$. It is also shown that the coordinates of the other points are determined by a fourth-order algebraic equation. It may also be considered as a simplified model for problem (3.12).

To study systems of three ordinary differential equations, specifically the system of equations (3.15), it is very useful to investigate a class of *two-dimensional mappings* or mappings of the plane.

Let us consider, for example, a system of three ordinary differential equations relating the functions $x(t)$, $y(t)$ and $z(t)$. We shall give initial data lying in one plane $z = z_0$. From each such point we draw a phase trajectory and see where it crosses again the chosen plane (fig. 3.8). The coordinates of the crossing point (x_1, y_1, z_0) depend on the initial data (x_0, y_0, z_0), i.e.,

$$x_1 = f(x_0, y_0)\,, \qquad y_1 = g(x_0, y_0)\,. \tag{3.17}$$

The functions f and g determine a mapping of the plane $z = z_0$, which is usually called a Poincaré map. As a rule, it is sufficient to consider not the entire plane $z = z_0$ but only a small part which contains an attractor.

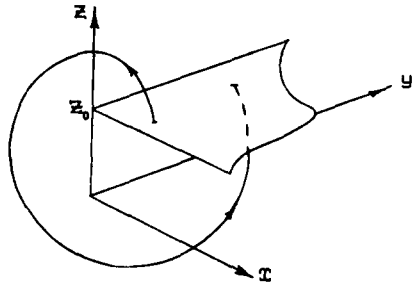

Fig. 3.8

The mapping (3.17) generated by a system of differential equations usually enables us to investigate the most important properties of the system. But it may turn out that the interval which contains elements of the sequence $\{y_n\}$ is much shorter than that with elements of the sequence $\{x_n\}$. (Or there are other variables x', y' for which this condition is satisfied.) Then the *one-dimensional mapping*

$$x_{n+1} = F(x_n)\,, \tag{3.18}$$

i.e. the into mapping of the interval, proves to be a useful simplified model.

A mapping of the form (3.18) may appear not only as a result of analysing a simplified two-mode system but sometimes directly in the course of studying problem (3.12).

In fact, let us expand its solution into a Fourier series

$$W(x, t) = \sum_{m=0}^{\infty} [a_m(t) + \mathrm{i}b_m(t)] \cos(\pi m x/l)\,.$$

We consider the function $\xi(t) = [a_0^2(t) + b_0^2(t)]^{1/2}$, pick out the local maxima $\xi_1\, \xi_2, \ldots, \xi_m, \ldots$ and construct the function $\xi_{m+1}(\xi_m)$. In some cases $\{\xi_m, \xi_{m+1}\}$ do not fill randomly the whole region; instead they very accurately fall on a single continuous curve $\xi_{m+1} = F(\xi_m)$. Such curves usually appear in a whole range of parameters c_2. Therefore, we can consider a family of mappings (3.18) as a simplified model of the distributed system.

Let there exist a steady state regime such that $\xi_n \to \text{const.}$ for $n \to \infty$, $n = 1, 2, \ldots$. Then the single point $(\bar{\xi}, \bar{\xi})$ on the curve F corresponds to this regime. If $\xi(t)$ is periodic and has p local maxima in a period, then p points on the curve F correspond to it. If $\xi(t)$, and this means $W(x, t)$ as well, is aperiodic, the points may fill the entire curve or a few segments of it.

The approach of picking out the local maxima and constructing the function $\xi_{m+1}(\xi_m)$ was proposed by E. Lorenz [76] and was efficiently used to study several systems of ordinary differential equations.

For most nonlinear partial differential equations it proves useful to analyse self-similar solutions. These cases include running waves, whose properties are discussed for the Kuramoto–Tsuzuki equation in refs. [100, 101], and solutions of the form

$$W(x, t) = R(x) \exp[\mathrm{i}\omega t + \mathrm{i}a(x)]\,.$$

This solution was obtained in ref. [109] using invariant-group analysis of eq. (3.8). Below we shall see that in a certain range of parameter values it proves to be stable and determines the asymptotic

behaviour of the system when $t \to \infty$. In this case equations for the functions $R(x)$ and $a(x)$ (or the functions that describe other self-similar solutions) can be considered as a simplified model.

In many cases multi-dimensionality is a necessary factor for understanding various nonlinear phenomena, but it complicates the problem immensely. So to study some phenomena we should consider two-dimensional analogs of eq. (3.12). Such problems arise when we study water waves caused by wind, or simulate morphogenesis and surface reactions. The simplest two-dimensional generalization of (3.12) is the equation

$$W_t = W + (1 + ic_1)(W_{xx} + W_{yy}) - (1 + ic_2)|W|^2 W . \tag{3.19}$$

It has two-dimensional self-similar solutions of the form

$$W(x, y, t) = R(x, y) \exp[i\omega t + ia(x, y)] . \tag{3.20}$$

In the two-dimensional case the Kuramoto–Tsuzuki equation has solutions which are now called spiral waves. They are described by formula (3.20) provided $R(x, y) = R(r)$, $a(x, y) = S(r) + m\varphi$ ($m = 1, 2, \ldots$), $x = r\cos\varphi$, $y = r\sin\varphi$. Their name is understood from fig. 3.9, where a typical picture of the solution with $m = 1$ is shown at time t'. In the dashed region $u(x, y, t') > 0$, in the blank region $u(x, y, t') < 0$.

If $m > 1$ the spiral wave is called multi-armed. Spiral waves can be observed experimentally, in particular in the Belousov–Zhabotinsky reaction [110]. It is important that the existence of spiral waves is not connected with a specific form of the equations – it is a general feature of many open nonlinear systems. Some biologists think that the appearance of spiral waves can explain many biological phenomena, for example, arrhythmia of the heart muscle [111].

The method of multi-scale expansions used to obtain eq. (3.8) was successfully applied to the investigation of convective instabilities in a fluid [93], the analysis of plasma physics problems [112], and in the theory of nonlinear waves [113]. It was also used to analyse eq. (3.8). By assuming that the

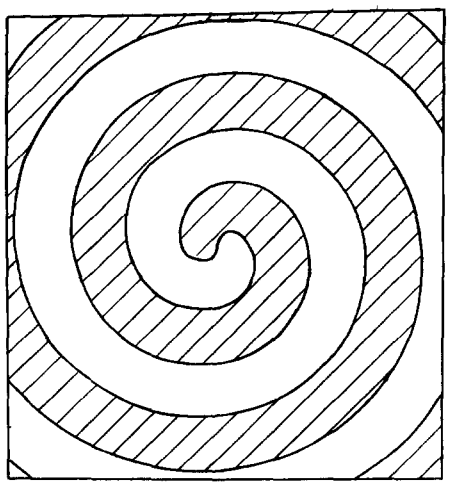

Fig. 3.9

solution of the equation is close to being spatially homogeneous we obtain the equation [114, 115]

$$v_t = \nu\Delta v - \mu\nabla^2\nabla^2 v - \lambda v(\nabla v)\,, \tag{3.21}$$

which is usually called the *Kuramoto–Sivashinskii equation*. Here v is the gradient of the phase W, $\nu = 1 + c_1c_2$, $\lambda = 2(c_1 - c_2)$, $\mu = (1 + c_1^2)/2$. An analytic solution of the Kuramoto–Sivashinskii equation of the running wave type was obtained in ref. [116]. The problem of the instability of the wavefront in active media was formulated in ref. [118] for the two-dimensional case. Using the method of multi-scale expansions leads in this case to eq. (3.8). In such an approach v is connected with the local phase velocity of the running wave.

When $\nu > 0$ the properties of eq. (3.21) resemble those of the Burgers equation [42]. When $\nu < 0$ eq. (3.21) may seem to have complex aperiodic solutions [115]. Indeed, when the term $\mu\nabla^2\nabla^2 v$ is absent solutions can exist for a limited time. By using the Hopf–Cole replacement [42] when $\nu < 0$ we reduce (3.21) to the linear heat conduction equation with a negative coefficient k. Equation (3.21) is of interest as one of the simplest model equations which can describe chaotic processes in the one-dimensional case. Numerical results including complex aperiodic solutions were described in ref. [115]. In ref. [117] a priori estimates of solutions of the boundary value problem ($u_x = u_{xxx} = 0$ for $x = 0$ and $x = 1$ with $u(x, 0) = u^0(x)$, $0 \le t < \infty$) were obtained; also existence and uniqueness theorems were proved, and difference schemes for this equation were considered.

At the same time the calculations show that in many ranges of parameter values the solution $W(x, t)$ of eq. (3.8) is essentially inhomogeneous in space. Therefore the range of applicability of (3.21) is much smaller than that of the original equation, as was noted in refs. [104, 118].

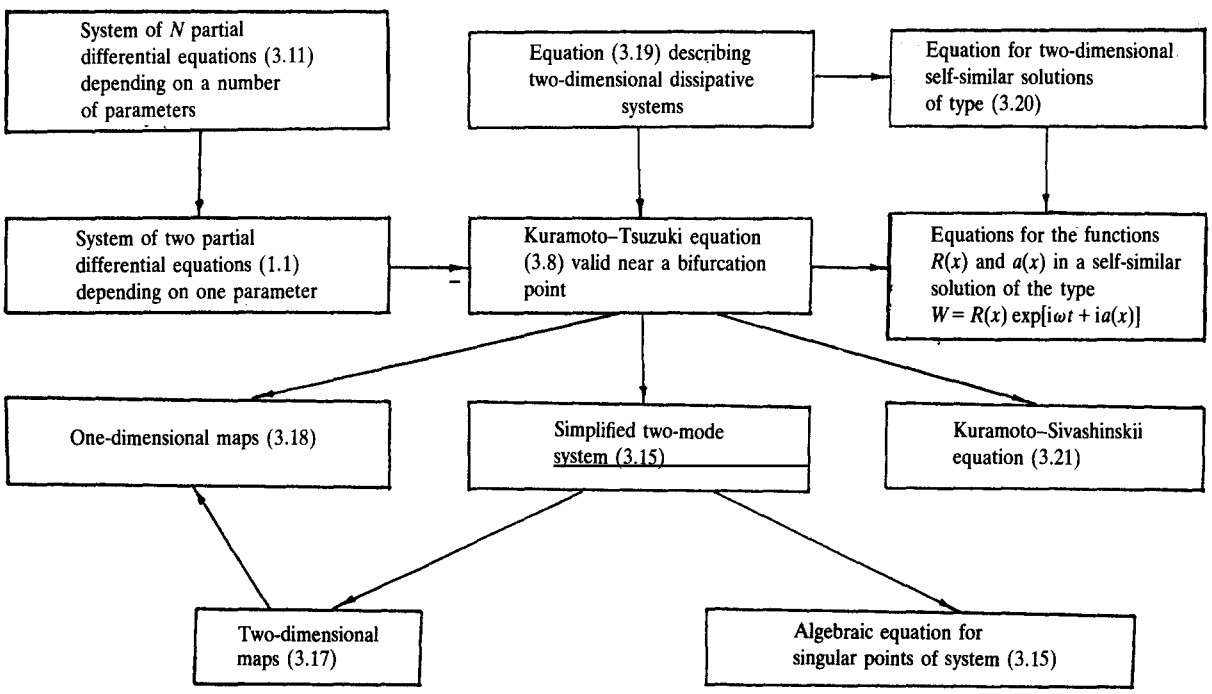

Scheme 1.

Considering the behaviour of two-component systems in the vicinity of a bifurcation point, we have presented a few simplified models. The properties of some models will be discussed below. We illustrate the connections between these models in a diagram (Scheme 1). We shall see that an analysis of any model requires using a computer and various mathematical methods. There are several levels in the hierarchy of models shown in the diagram. The study of the models at any level has not yet been accomplished. There are still problems at each level that require further investigation.

3.3. Other lines of investigation

Besides the simplified models described above and constructed for an analysis of reaction–diffusion systems, some generalizations of the Kuramoto–Tsuzuki equation were proposed. It turned out that a similar approach can be used to investigate certain hydrodynamic systems. Let us discuss some lines of investigation in this connection.

One of the generalizations of the Kuramoto–Tsuzuki equation appears when the next terms in the expansions with respect to a small parameter for reaction–diffusion systems in the vicinity of the thermodynamic branch are taken into account. Let the nonlinear sources in such a system depend on two parameters λ and μ. We write eq. (3.8) in the form

$$W_t = d_0 W_{xx} + (a_1 + a_2|W|^2)W .$$

Let Re $a_2 < 0$ for $\mu < \mu_0$, and Re $a_2 > 0$ for $\mu > \mu_0$. In the second case the Kuramoto–Tsuzuki equation cannot be used: if we vary λ the solution discontinuously changes by a finite amount. The FitzHugh–Nagumo model [119] and other models where threshold effects are important give us examples of such behaviour. To describe these effects the authors of ref. [120] propose to take into account the next terms in the expansion and to use the equation

$$W_t = d_0 W_{xx} + (a_1 + a_2|W|^2 - a_3|W|^4)W , \tag{3.22}$$

where d_0, a_1, a_2, a_3 are complex constants. The possibility to use this equation is connected with the existence of another small parameter, $\sim(\mu - \mu_0)^{1/2}$. Therefore eq. (3.22) does not have the generality of (3.8) and its range of applicability is much smaller.

When we go from the original system (1.1) to (3.8) it is essential that the problem is one-dimensional: the form of the function f can be uniquely determined from the linearized equation. In the multi-dimensional case the situation is more complex – the linearized problem can have several solutions; their number greatly depends on the geometry.

The equations describing two-component systems for the Turing bifurcation were considered in ref. [121] in the two- and three-dimensional formulations. For regions of different geometries they may represent systems containing more than two equations. It would be very useful to analyse them in detail.

In the classical theory of bifurcations and in the theory of normal forms there are standard and strictly justified procedures that allow one to go to the asymptotic local description in typical cases [81, 85]. In the theory of reaction–diffusion systems a strict procedure to go from the boundary value problem for eq. (1.1) to that for the Kuramoto–Tsuzuki equation has not yet been developed up to now. At present, however, studies have been initiated where this question is considered for systems with a small diffusion coefficient,

$$u_t = \varepsilon D u_{xx} + (A_0 + \varepsilon A_1)u + F(u)\,, \quad 0 < \varepsilon \ll 1\,,$$

$$u_x(0, t) = u_x(1, t) = 0\,, \qquad u(x, 0) = u^0(x)\,,$$

where u is an m-dimensional vector, D is a positive definite matrix, A_0 has eigenvalues with zero real parts and no eigenvalues with positive real parts, $F(u)$ is a nonlinear function. Under these conditions the asymptotic analysis may lead to both the Kuramoto–Tsuzuki equation and its more complex analogs [122].

A similar approach associated with constructing a hierarchy of simplified models has been intensively developed recently in connection with investigations of convective instability. In these investigations systems can be considered whose lengths and widths are much longer than the characteristic sizes of cells or convective shafts. A direct numerical simulation of such instabilities requires solving the hydrodynamic problem in a large domain, which includes a large amount of computation. At the same time, solving the equations arising in an analysis of the system in the vicinity of the thermodynamic branch is much simpler. In this case one usually obtains boundary value problems for a system of two parabolic equations in a two-dimensional region.

In such a description frequently equations arise which are more complex than (3.8); they contain fourth derivatives [93],

$$W_T = W + \left(\frac{\partial}{\partial X} - \frac{\mathrm{i}}{\sqrt{2\pi}}\frac{\partial^2}{\partial Y^2}\right)^2 W - |W|^2 W\,.$$

Various physical factors may complicate the equations obtained by asymptotic methods [123]. Different methods to describe the convective instability in a simplified form and the topologic features of the arising flows are discussed in ref. [77]. Numerical solutions of the resulting equations usually give a picture that is in good agreement with experimental results [124].

4. One-dimensional maps

One of the simplest models that allows an investigation of complex temporal order and stochastic regimes in nonlinear media is the map of an interval onto itself or, as it is usually called, the one-dimensional map.

The study of one-dimensional maps led to the introduction of new notions applicable to an extensive class of dissipative systems and the discovery of some new phenomena; as a result some fundamental questions could be answered. How does the transition from the simplest ordered to stochastic regimes proceed? In what manner do the domains where order or chaos is observed, alternate in parameter space? How does order become complicated with a varying parameter? What are the basic types of stochastic regimes in such systems and how can they be described?

Let us note the paradoxicality of these questions. Indeed, a one-dimensional map is a determinate system. Nevertheless, it describes processes that may have some stochastic properties.

To fix the ideas we consider the simplest model that leads to one-dimensional maps. Let us be interested in the variation of the population of some animals in a certain region. We count them once a year and obtain a number x. From these data we construct the sequence $x_1, x_2, \ldots, x_n, \ldots$ ($n = 1$ corresponds to the first count). For brevity we designate it by $\{x_n\}$. It seems that there is a law for these numbers. It is natural to expect that the population in a given year, x_{n+1}, depends on the number of

animals that lived the previous year, i.e. the value of x_n. Thus, in the simplest case

$$x_{n+1} = f(x_n, \lambda) . \tag{4.1}$$

Here f is a continuous function, λ is a parameter, which depends on the specific problem under consideration. We usually use a function f of the form $\lambda x_n(N - x_n)$,

$$x_{n+1} = \lambda x_n(N - x_n) , \quad 0 \le x_n \le N . \tag{4.2}$$

The above formula shows that the population quickly grows so long as it is small ($x_n \ll N$) and starts diminishing when there are too many animals. It is convenient to make the change of variables $x_n = x'_n N$ and $\lambda = \lambda'/N$. Then formula (4.2) becomes

$$x'_{n+1} = \lambda' x'_n(1 - x'_n) , \quad 0 \le x'_n \le 1 . \tag{4.3}$$

Below we shall omit the primes.

Now we are interested in the question: What will happen with different kinds of animals over a sufficiently long time? To answer this question within our simplest model it is sufficient to determine the form of the sequence $\{x_n\}$, $n \to \infty$, for different λ. The maps of the form (4.1) are used for the phenomenological description of many other events.

4.1. Transition to chaos. The Feigenbaum scenario

For small values of λ ($0 < \lambda < 1$) we have $x_n \to 0$ with $n \to \infty$ regardless of the choice of x_1. In this and other cases it is convenient to describe the behaviour of the sequence graphically.

Let us draw the plot $y = f(x)$ for a chosen λ and the straight line $y = x$ in fig. 4.1. We take x_1 on the abscissa, draw a vertical up to the intersection with the curve $y = f(x)$ at point A, then draw a horizontal from A until it intersects the curve $y = x$ (point B). Now we draw again a vertical to the intersection with the x-axis. It is easy to see that $x_2 = f(x_1)$. Taking now the point x_2 as a starting point and repeating the same operations we obtain x_3, then x_4, etc. From fig. 4.1 it is seen that $x_n \to 0$ when $n \to \infty$.

From formula (4.3) it follows that the function $f(x)$ maps the interval $[0, 1]$ onto $[0, \lambda/4]$. If $\lambda \le 4$, all values of x_n are on $[0, 1]$ provided that $0 \le x_1 \le 1$. This is why formula (4.3) is said to give maps of an interval into itself.

Now let λ be slightly more than 1. The sequence $\{x_n\}$ behaves differently (fig. 4.2) and tends to a

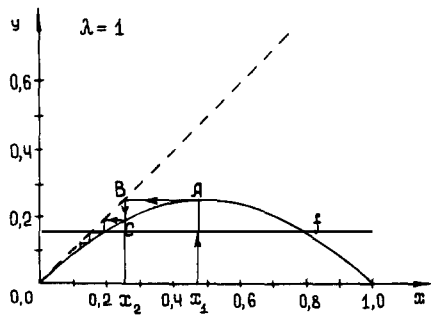

Fig. 4.1

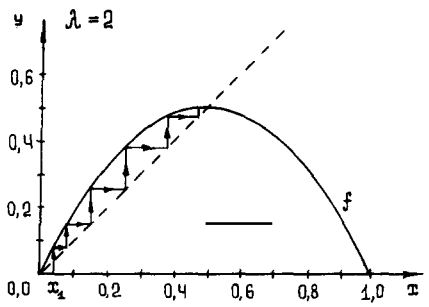

Fig. 4.2

constant value $x^* > 0$. As applied to the original biological problem, it means that the population of a given species becomes stable after several years and stops changing with time.

The value of x^* can be obtained from the equation

$$x^* = f(x^*, \lambda) . \tag{4.4}$$

All the points satisfying this equation are called the *fixed points* of the map, since $x_n = x^*$ for all n if $x_1 = x^*$. If $\lambda < 1$, the quadratic equation $x^* = \lambda x^*(1 - x^*)$ has one nonnegative root $x^* = 0$. If $\lambda > 1$ there are two nonnegative roots: $x^* = 0$ and $x^* = (\lambda - 1)/\lambda$. When $\lambda = 1$ the fixed point $x = 0$ loses its stability, and the newly appeared point becomes stable.

It is easy to determine if the fixed point x^* of the map $f(x)$ is stable. Let $x_n = x^* + \Delta x_n$, where Δx_n is a small number. If the point is stable the value of $|\Delta x_n|$ must decrease with increasing n. We rewrite formula (4.1) in the form

$$x^* + \Delta x_{n+1} = f(x^* + \Delta x_n) = f(x^*) + \frac{\mathrm{d}f(x^*)}{\mathrm{d}x} \Delta x_n + \mathrm{o}(\Delta x_n^2) .$$

In the analysis of the stability of singular points of ordinary differential equations it is shown that in the nondegenerate case the linear terms dominate the situation (the first method of Lyapunov stability theory). Using analogous arguments here we can verify that the stability of x^* is determined by the behaviour of the map

$$\Delta x_{n+1} = \frac{\mathrm{d}f(x^*)}{\mathrm{d}x} \Delta x_n . \tag{4.5}$$

In order that $\Delta x_n \to 0$ for $n \to \infty$ the inequality

$$|\mathrm{d}f(x^*)/\mathrm{d}x| < 1 \tag{4.6}$$

should be satisfied. It is the sufficient condition for stability of the point x^*. (If the opposite inequality is satisfied we may infer that x^* is unstable. If the derivative is equal to unity we should consider the next terms in the Taylor series.)

Let us further increase λ. The behaviour of the system changes again: Starting from sufficiently large n in the sequence $\{x_n\}$ two numbers a_1 and a_2 will be alternating. (Speaking more exactly, the sequence $\{x_n\}$ is composed so that $x_{2n+1} \to a_1$, $x_{2n} \to a_2$ for $n \to \infty$.) We shall say that in this case the map (4.3) has a *stable cycle* of period 2, which will be designated by S^2. Figure 4.3 shows S^2.

The transition from the fixed point (we may consider it as a cycle S^1) to the cycle S^2 occurred as a result of bifurcation, which is called a *period-doubling bifurcation*. The point x^* did not disappear but the value of $\mathrm{d}f(x^*)/\mathrm{d}x$ became smaller than -1.

As λ increases further the sequence $\{x_n\}$ changes again. The cycle S^4 arises: $x_{4n} \to a_1$, $x_{4n+1} \to a_2$, $x_{4n+2} \to a_3$, $x_{4n+3} \to a_4$, for $n \to \infty$ and $a_2 = f(a_1)$, $a_3 = f(a_2)$, $a_4 = f(a_3)$, $a_1 = f(a_4)$ (see fig. 4.4).

Still increasing λ we may observe the cycles S^8, S^{16}, S^{32} etc. Every time S^{2^p} loses stability, a period-doubling bifurcation takes place, and the cycle $S^{2^{p+1}}$ becomes stable. Finally, at a certain value of λ (sometimes denoted by λ_∞) formula (4.3) yields an aperiodic sequence $\{x_n\}$.

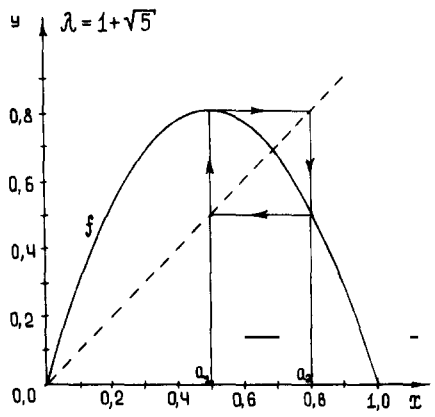

Fig. 4.3

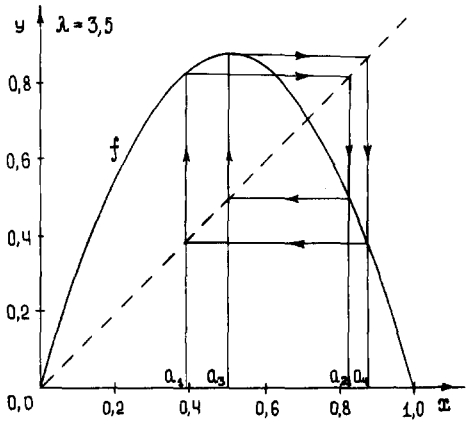

Fig. 4.4

The observed picture turns out to be very interesting. First, there is very complex behaviour in the remarkably simple model (4.1). Second, a large number of bifurcations leading to a more complex solution can be discovered. It is much more difficult to do this in more complex models. Third, when $0 < \lambda < \lambda_\infty$ only cycles of period 2^p are stable. It would be interesting to see why this is so and to study the behaviour of the model in more detail.

Besides the map (4.1) it is convenient to consider the map

$$x_{n+1} = f(f(x_n)) \equiv f^2(x_n)\,. \tag{4.7}$$

In this chapter $f^n(x)$ will always correspond to the nth *iteration* of the function f, $f^n(x) = f(f \cdots (x))$ (n times). In our case the form of the function $f^2(x)$ is shown in figs. 4.5 and 4.6. The first figure corresponds to the stable fixed point, the second to the stable cycle S^2. The plot of $f^2(x)$ intersects the straight line $y = x$ at all fixed points of the map and also at points belonging to cycles S^2 [because $a_2 = f(a_1) = f(f(a_2))$, $a_1 = f(a_2) = f(f(a_1))$]. By increasing the parameter λ we stretch the function $f^2(x)$ along the y-axis, and if at some λ the lines $y = x$ and $y = f^2(x)$ intersect at one point (see fig. 4.5), then

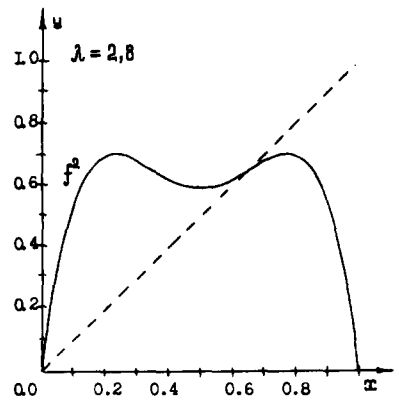

Fig. 4.5

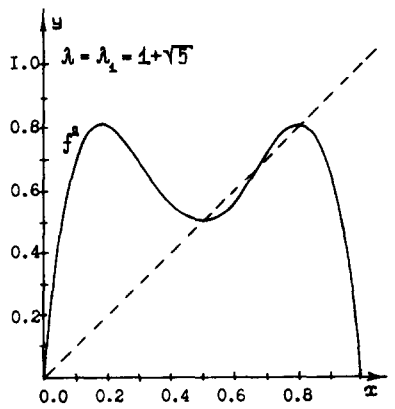

Fig. 4.6

two new intersection points may appear as λ increases (see fig. 4.6). These points will determine the cycle S^2. The transition $S^1 \to S^2$ in the map $f(x)$ will be due to the fact that in the map $f^2(x)$ one of the fixed points loses its stability, and two new stable fixed points appear in its neighbourhood. The bifurcation diagram here proves to be like that shown in fig. 3.6a. By considering the functions $f^4(x)$, $f^8(x)$ etc. we can see how the next doublings occur. In each of these cases one group of points loses its stability and two other stable groups of points appear, and as a result the cycle period doubles.

Acting in the same way as in the case of a fixed point, we can show that the stability of the cycle S^p with elements $x_1, \ldots, x_p$ will be determined by the formula $|df^p(x_k)/dx| < 1$, $k = 1, \ldots, p$. By differentiating this formula we can easily verify that it is equivalent to the inequality

$$\left| \frac{df(x_1)}{dx} \times \cdots \times \frac{df(x_p)}{dx} \right| < 1 . \tag{4.8}$$

From the formula for $|df^p/dx|$ it follows that the value of $|df^p/dx|$ will be the same at all points of the cycle S^p.

It turns out that by the example of model (4.3) we can understand not only the qualitative but also the quantitative laws of the transition to chaos. In order to observe them we shall draw the plot $x(\lambda)$. We shall put $x_1, x_2, \ldots, x_p$ belonging to the stable cycle along the x-axis, and the parameter values along the λ-axis. Two points on the same vertical line will correspond to cycle S^2, four points to cycle S^4, etc. We denote the parameter values where doublings occur by Λ_1, Λ_2, $\Lambda_3, \ldots$, and the values for which $x = 1/2$ is an element of cycles S^2, S^4, S^8 etc. by λ_1, λ_2, $\lambda_3, \ldots$ (these cycles are called superstable). Let us also introduce the quantities $d_1, d_2, \ldots, d_n$, the distances between $x = 1/2$ and the closest element of the cycle S^{2^n} at $\lambda = \lambda_n$. All these notations are shown in fig. 4.7. Computations show that the numerical values of Λ_n and λ_n with large n behave like a geometrical progression with

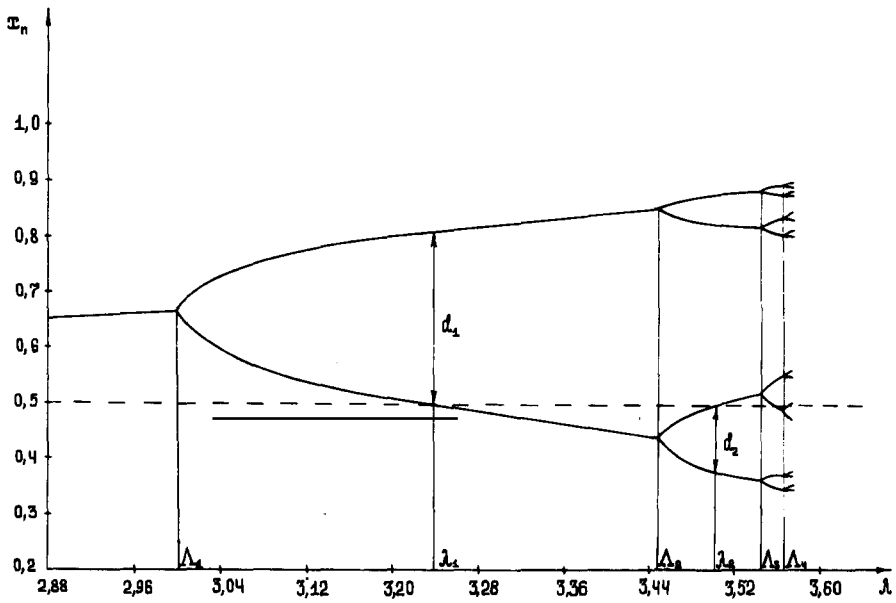

Fig. 4.7

denominator $\delta = 4.669\,201\,6\ldots$. In other words,

$$\frac{\Lambda_{n+1} - \Lambda_n}{\Lambda_{n+2} - \Lambda_{n+1}} \xrightarrow[n\to\infty]{} \delta\,. \tag{4.9}$$

The ratio d_n/d_{n+1} also has a limit equal to α, where $\alpha = 2.502\,907\,8\ldots$.

Instead of (4.3) we may consider some other family of symmetric functions that have one maximum on $[0, 1]$, are close to a quadratic parabola near its apex, and in which an infinite cascade of period-doubling bifurcations occurs with varying λ. It turns out that in any such model the numbers α and δ are the same. Moreover, regardless of the form of $f(x)$, the limit

$$\lim_{n\to\infty} (-\alpha)^n f^{2^n}((x - 0.5)/(-\alpha)^n, \lambda_n)$$

exists and is the same. It is called the universal function $g_0(x)$.

These remarkable laws were established and explained by M. Feigenbaum in 1978 [33, 126, 127]. He proposed the functional equations to determine α, δ and $g_0(x)$. Due to the universal nature of α, δ and $g_0(x)$ and other similar functions, this theory is called the *universality theory*.

In this theory the renorm-group method is applied. It is widely used in quantum field theory and statistical physics. With this approach the constant α can be determined from an equation that has a graphic geometric meaning.

Let us compare figs. 4.3 and 4.8. An element of the curve $f^2(x)$ located within the left square is very much like the arc of the function $f^1(x)$ located in the square in fig. 4.3. In fact, they differ only by a scale and the orientation of the axes. Calculations show that the same law holds for the functions f^{2^n}, $n > 1$, when $\lambda = \lambda_n$. The larger the n, the more accurately it is satisfied. From these considerations it follows that

$$g(x) = -\alpha g(g(x/\alpha)) \equiv (Tg)(x)\,, \tag{4.10}$$

which allows us to determine both the function $g(x)$ and the value of α. The function g is determined on $[-1, 1]$; it is assumed to have only one maximum at $x = 0$ and to be symmetric, $g(x) = g(-x)$. Near the

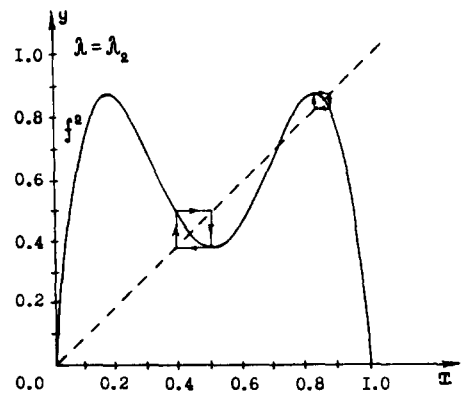

Fig. 4.8

maximum $g(x)$ must be close to a quadratic parabola, and $g(0)=1$. T is called the *doubling transformation* [128, 131].

In the universality theory the space of maps of the interval $[-1, 1]$ into itself is considered so that $f(x) \in C^2[-1, 1]$, where $x=0$ is a maximum of $f(0)=1$. This space is invariant with respect to the transformation T.

The *Feigenbaum equation* (4.10) determines the fixed point of the doubling transformation. The spectrum $DT(g)$ of the linearized transformation at the point g lies within a unit circle except for the eigenvalue $\delta = 4.699\,2\ldots$, which determines the Feigenbaum constant. This eigenvalue corresponds to the one-dimensional unstable separatrix $\Gamma^{u}(g)$, which consists of the maps moving away from $g(x)$ under the effect of the transformation T (fig. 4.9). Along other directions, belonging to the stable separatrix $\Gamma^{s}(g)$, the maps tend to this point.

Let us denote the surface in the functional space on which the first period-doubling bifurcation occurs by Σ_1. We also write

$$\Sigma_2 = T^{-1}\Sigma_1, \quad \ldots, \quad \Sigma_k = T^{-1}\Sigma_{k-1}.$$

At the intersection of the surface Σ_k the kth period doubling occurs: the stable cycle of period 2^k arises from the stable cycle of period 2^{k-1}.

The surfaces Σ_k prove to converge to $\Gamma^{s}(g)$, and for large k the distances between Σ_{k+1} and $\Gamma^{s}(g)$ are δ times shorter than those between Σ_k and $\Gamma^{s}(g)$. Therefore, the bifurcation values of the parameters for any family of maps $f(x, \lambda)$ form a geometric progression.

Some rigorous results of the universality theory and references to the original works can be found in detail in the book [131] and the review [128]. The proofs available are mainly based on numerical results. By using a computer the Feigenbaum equation is solved, and the constants α and δ are determined. For these problems different techniques can be employed [127, 129]. The universality theory can be applied in the case when the apex is smooth but not quadratic. However, α and δ prove to be different [127].

An interesting object is the limit set arising after an infinite cascade of period-doubling bifurcations ($\lambda = \lambda_\infty$). It is called the *Feigenbaum attractor* and has a complex structure, which repeats itself on smaller scales. In particular, there are an infinite number of unstable cycles of the type S^{2^p} coexisting

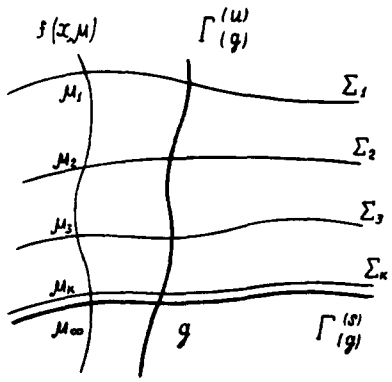

Fig. 4.9

with the Feigenbaum attractor. The structure and ergodic properties of limit sets of one-dimensional maps at $\lambda = \lambda_\infty$ are discussed in detail in ref. [128]. In the neighbourhood of the point λ_∞ the attractors have a typical power spectrum from which we can see that this scenario of the transition to chaos is implemented [131].

In many dissipative systems as well as in some nonlinear media the transition to chaos occurs according to the Feigenbaum scenario [35, 36, 103]. Therefore, it is particularly interesting to generalize the results of the universality theory to maps of higher dimensions. For example, two-dimensional transformations $\mathbb{R}^2 \to \mathbb{R}^2$ were studied in ref. [131]. They are close to the map F,

$$F\begin{pmatrix} x \\ y \end{pmatrix} = \begin{pmatrix} g(\sqrt{x^2 - y}) \\ 0 \end{pmatrix},$$

where g is the universal function which is a solution of eq. (4.10),

$$g(x) \approx 1 - 1.527\,63\,x^2 + 0.104\,815\,x^4 - 0.026\,705\,7\,x^6 + \cdots .$$

Every one-parameter family of maps $\mathbb{R}^2 \to \mathbb{R}^2$ which passes sufficiently near F will exhibit an infinite sequence of period-doubling bifurcations at values λ_k. The λ_k will have a limit λ_∞ and $|\lambda_n - \lambda_\infty| \sim \text{const.}\ \delta^{-n}$.

Thus, the transition from the simplest ordered to aperiodic regimes according to the *Feigenbaum scenario* is connected with an infinite cascade of period-doubling bifurcations. The bifurcation points are located according to a geometric progression with denominator δ. Here chaos (aperiodic sequence at λ_∞) acts as a limit of supercomplex temporal order.

4.2. *Intermittency*

The transition to chaos can occur differently even in very simple physical systems. For example, in hydrodynamics the following phenomenon has been described. If flow is observed for a sufficiently long time without a change in its parameters, it may be seen that in ordered laminar flow suddenly vortices appear whose behaviour seems to be random. Then the picture of the flow again becomes simple and regular before the next vortices appear. This phenomenon is called *intermittency*. Regular regimes alternate with islands of chaos.

The simplest model that provided an explanation for this phenomenon was proposed by Manneville and Pomeau in 1980 [130]. It can be illustrated by an example of a family of one-dimensional maps (4.3).

For a certain value of λ ($\tilde{\lambda} = 3.83$) the stable cycle S^3 abruptly appears from chaos. In order to understand the situation we consider the one-dimensional map $f^3(x, \lambda) = f(f(f(x, \lambda)))$ before the cycle appears, $\lambda < \tilde{\lambda}$ (see fig. 4.10a), and after that, $\lambda > \tilde{\lambda}$ (see fig. 4.10b). As the parameter λ increases, the curve $f^3(x, \lambda)$ becomes steeper, and new points of intersection with the straight line $y = x$ appear. These points are denoted by $M_{1,2,3}$ and $N_{1,2,3}$ in fig. 4.10b. They are all fixed points of the map $f^3(x, \lambda)$. The derivative of $f^3(x, \lambda)$ at the points M_1, M_2, N_3 [see formula (4.8)] is the same and its absolute value does not exceed 1. It is these points that determine the stable cycle S^3. The slopes at the points N_1, N_2, M_3 are also the same but their absolute value is larger than 1. In the map f they correspond to an unstable cycle S^3 which appears simultaneously with the stable one (see fig. 4.11).

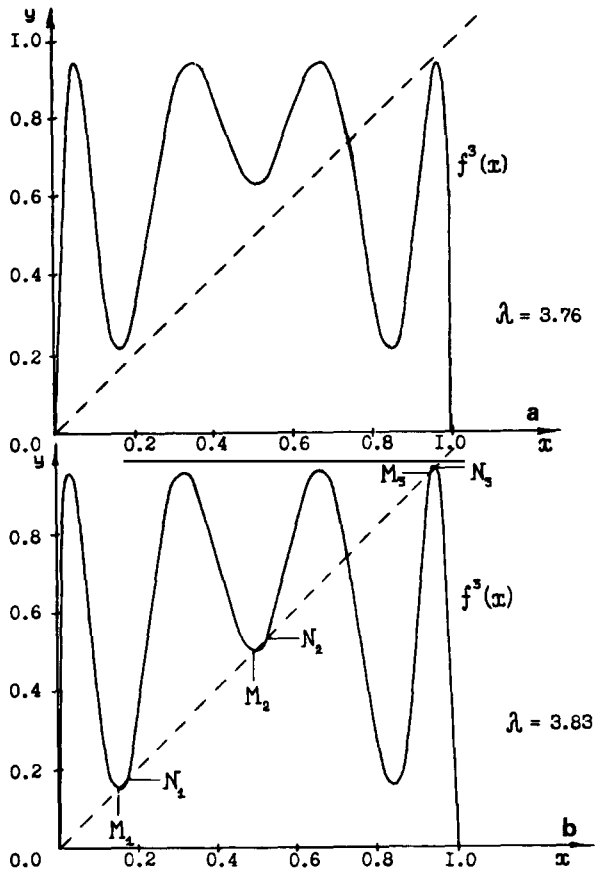

Fig. 4.10

The simultaneous appearance of stable and unstable singular points is called a *tangent bifurcation*. It is due to the fact that at the bifurcation point the curve $f(x)$ is tangent to the diagonal $y = x$. Accordingly, the derivative df/dx at this point is equal to unity.

We give an initial value x_1 and see how the map f^3 behaves when $\lambda > \tilde{\lambda}$ and when $\lambda < \tilde{\lambda}$. (In other words, we observe every third element of the sequence $\{x_n\}$.) Computations show that in the first case after a long transient process the points are attracted to the cycle S^3. In the second case slow motion to the point M can be observed first, but then the elements of the sequence quickly diverge from this

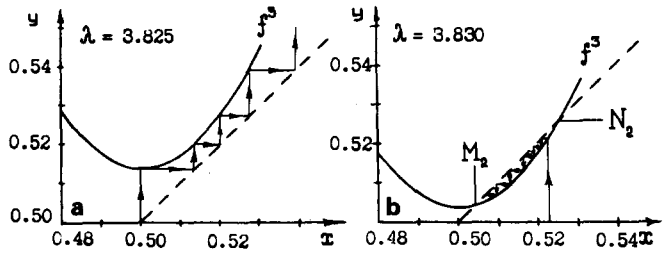

Fig. 4.11. The function f^3 on a larger scale. (b) $\lambda = 3.830$; the point M_2 corresponds to the stable cycle S^3 and the point N_2 to the unstable cycle. (a) $\lambda = 3.825$; the cycle S^3 has not yet appeared.

point. Subsequently they start approaching it again. Such a behaviour for a map with a sharp apex is illustrated in fig. 4.12. It is seen that intervals of motion to the point M, when the solution looks regular, alternate with quick chaotic rejections. We have intermittency in this very simple model.

We may estimate how the duration of "the laminar phase" depends on the parameter λ. Let the tangent bifurcation occur for $\lambda = 0$. From fig. 4.11 it is clear that for the interval of interest the map $f^3(x)$ [or $g(x)$ in fig. 4.12] can be approximated by the map

$$x_{n+1} = x_n + ax_n^2 - \lambda\,. \tag{4.11}$$

Since $x_{n+1} - x_n \ll 1$ for $\lambda \to 0$, formula (4.11) can be approximated by the differential equation

$$\mathrm{d}x/\mathrm{d}\tau = ax^2 - \lambda\,. \tag{4.12}$$

By integrating it we can verify that the time Δt (and thus the number of iterations) in which the trajectory $x(\tau)$ is near zero, is proportional to $\lambda^{-1/2}$. It is this law which can be observed in computations. Transition to chaos connected with intermittency is observed in many concentrated systems and seems to be typical for a large class of nonlinear media too.

4.3. *Attractors of one-dimensional maps*

Considering one-dimensional maps we have not specified so far with what initial data some or other stationary regimes are obtained. At the same time it seems natural that in many cases the choice of initial data may determine the behaviour of the system when $n \to \infty$. We shall discuss this in detail.

An intuitive idea about the stationary regime may be associated with the notion of an attracting set or *attractor* [290]. An attractor is the closed set A which is invariant under the map f [$f(A) = A$] and has the domain of attraction U_0 ($U_0 \supset A$) of all the points that go into A [i.e. $A = \cap_{n=1}^{\infty} f^n(U_0)$]. Sometimes the definition of an attractor includes the property of indecomposability: the set A cannot be divided into some closed invariant nonintersecting sets.

We shall give examples of attractors. Let the map (4.3) have a stable fixed point x^* for $\lambda = \bar{\lambda}$ (for example, $\bar{\lambda} = 2$). It is an attractor. Indeed, $f(x^*) = x^*$, and we can see that there is a sufficiently small neighbourhood of the point x^* from where all points tend to x^*. At the same time we cannot say that iterations of all points tend to x^* [$f^n(0) = 0$, $n = 1, 2, \ldots$].

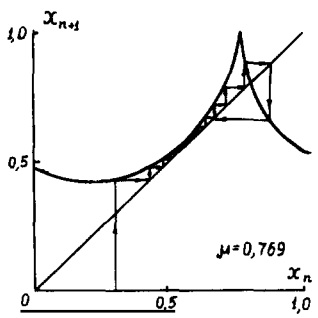

Fig. 4.12

The stable cycle S^n must be another example. We may expect that generally a one-dimensional map has several attractors which are obtained depending on the initial data. This question was studied in detail for the class of so-called S-unimodal maps [131, 135], which can be obtained, in particular, after a transformation of variables in the family (4.3). The map f of the interval $[-1, 1]$ into itself is *unimodal* if

(1) f is continuous,
(2) $f(0) = 1$,
(3) f is strictly decreasing on $[0, 1]$ and strictly increasing on $[-1, 0]$.

We shall call f C^1-*unimodal*, if in addition

(4) f is once continuously differentiable, and $f'(x) \neq 0$ if $x \neq 0$.

The Schwartzian derivative of f is defined by the formula

$$Sf(x) = \frac{f'''(x)}{f'(x)} - \frac{3}{2}\left(\frac{f''(x)}{f'(x)}\right)^2 .$$

Then f is called *S-unimodal* if

(1) f is C^1-unimodal,
(2) $f \in C^3$,
(3) $Sf(x) < 0$ for all $x \in [-1, 1]$; at $x = 0$ we allow the value $-\infty$ for $Sf(x)$,
(4) f maps $j(f) = [f(1), 1]$ into itself,
(5) $f''(0) < 0$.

The following theorems are valid.

Theorem I. If f is S-unimodal, then it has at most one stable periodic orbit, plus possibly a stable fixed point in the interval $[-1, f(1)]$.

Theorem II. If f is S-unimodal and has a stable periodic orbit, then the measure of those points which do not converge to it is zero.

Theorem III. If f is S-unimodal and has a stable periodic orbit, then the initial point $x_1 = 0$ will be attracted to it.

The last theorem provides a method to construct maps that have no stable cycles – to do this we should see that one of the iterations of zero comes at an unstable point or into an unstable cycle.

The simplest example of such a function was given by S. Ulam and J. von Neumann in 1947. This is the function $f(x) = 1 - 2x^2$: $f(0) = 1$, $f^2(0) = -1$, $f^k(0) = -1$ $(k > 2)$ but $f'(-1) = 4$.

Iterations of this map exhibit an example of *chaotic behaviour*. We consider it in more detail. We can verify that the change of variables

$$y = \frac{4}{\pi}\left[\arcsin\sqrt{(x+1)/2}\right] - 1$$

reduces the map to the form

$$y_{n+1} = 1 - 2|y_n| . \tag{4.13}$$

We investigate the properties of the sequence $\{y_n\}$ by using very simple considerations. Let y_1 have k

digits after the decimal point (the $(k+1)$st, $(k+2)$nd and all later digits are zero). Then we may verify by using (4.13) that y_2, y_3 and all the other elements of the sequence $\{y_n\}$ will have the same number or less digits. However, there are at most $N_k = 10^k$ numbers with k digits and the rest zeros. Hence, after some $N < N_k$ elements the same numbers will appear in the sequence $\{y_n\}$. Similar arguments can be used if y_1 is a rational number, $y_1 = p/q$, $-1 \le y_1 \le 1$, p and q integers. All these cycles will be unstable since $|df/dy| = 2 > 1$ at each point of the interval, and the product

$$\left| \frac{df(y_1)}{dy} \times \cdots \times \frac{df(y_n)}{dy} \right| = 2^n > 1$$

for any cycle S^n [see formula (4.8)]. The opposite statement is also valid: if the map (4.13) has a cycle, all its elements and their pre-images are rational numbers. (It is easy to prove this statement by using a reductio ad absurdum.)

We obtained an interesting qualitative conclusion: any rational number gives a cycle, any irrational number an aperiodic trajectory. While all rational numbers lying in the interval $[-1, 1]$ can be numbered (they form a countable set), the irrational numbers cannot. We can construct a system of intervals that will have as small a total length as desired and contain all rational numbers. The coordinate of a point taken at random will nearly always prove to be irrational and determine chaos. (If in analysing the map (4.13) we used only numerical results we would have come to the opposite conclusion: cycles would always be observed since all initial values of y_1 are stored in a computer with a finite number of decimal digits.)

How can we describe aperiodic trajectories of the map (4.13)? It is natural to act in the same way as in investigations of random processes: determine with what probability the elements of $\{y_n\}$ come into the neighbourhood of the point y. The measure ν on $[-1, 1]$ will be called the *invariant measure* for the map (4.1) if for every measurable subset E of the interval $[-1, 1]$, $\nu(E) = \nu(f^{-1}(E))$. We assume that $\nu([-1, 1]) = 1$. Let μ_1 and μ_2 be two measures on $[-1, 1]$. It is said that μ_1 is absolutely continuous with respect to μ_2 if for any subset A from $\mu_2(A) = 0$ it follows that $\mu_1(A) = 0$. When the measure ν is absolutely continuous with respect to the Lebesgue measure *the measure density* $\rho(x) = d\nu/dx$ [$\nu(dx) = \rho(x)\,dx$] is definite and belongs to the space L_1.

For many maps we may prove the following statement. If we give a measure μ and calculate its n iterations, the sequence $(1/n)\sum_{k=0}^{k=n-1} f^k(\mu)$ converges to the invariant measure that describes an attractor of this map [131, 133].

Let us present some examples. The cycles S^p correspond to measures for which $\rho(x) = (1/p)\sum_{k=1}^{p} \delta(x - x_k)$ represents p δ-functions. For the map (4.13) $\rho(x) = 1/2$. For the transformation $f(x) = 1 - 2x^2$, $\rho(x)$ has the following peculiarities: $\rho(x) = (\pi\sqrt{1 - x^2})^{-1}$ (see fig. 4.13a); $\rho(x)$ can be a linear function [see fig. 4.13b, $f(x) = 1 - 2\sqrt{|x|}$, $\rho(x) = (1 - x)/2$].

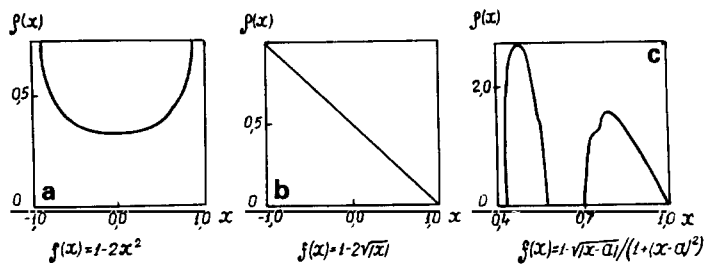

Fig. 4.13. Examples of invariant measures of one-dimensional maps. The map in (c) is given by formula (4.15).

There are other attractors of one-dimensional maps which stand between stable cycles and stochastic regimes, and for which the points $\{x_n\}$ come into the neighbourhood of every point of the interval. They are called *noisy cycles* or *semi-periodic trajectories*. In this case $\rho(x)$ is concentrated on p "islands" (fig. 4.13c). Such attractors will be denoted by χ^p. The order of going around the islands proves to be strictly fixed; therefore we can exactly predict in the limit of which of the islands the element x_n occurs for any n. (This makes noisy cycles resemble cycles.) However, as the position of typical points within each island changes in a random way they are more like stochastic regimes.*)

For some classes of one-dimensional maps we can prove the existence of an absolutely continuous (with respect to the Lebesgue measure) invariant measure. Among them are, in particular, the everywhere stretching maps [131, 133], for which

$$|\mathrm{d}f/\mathrm{d}x| \geq c_1 > 1 .$$

An idea of the invariant measure may be obtained by considering a histogram of the sequence $\{x_n\}$ constructed on a computer. We divide the interval $[-1, 1]$ into equal segments of length ε, each segment being compared with a number n_i. First $n_i = 0$ for all i. The value of n_i increases by one if element x_n comes into the ith interval. Then n_i is divided by the total length of the sample N. In many cases

$$\rho(x) = \lim_{\varepsilon \to 0} \lim_{N \to \infty} n_i/N .$$

However, large samples are required to obtain $\rho(x)$ with a sufficiently high accuracy.

We may act differently. Using the definition of invariant measure an equation is derived to determine $\rho(x)$. It is called the *Perron–Frobenius equation*,

$$\rho(x) = \sum_{y \in f^{-1}(x)} \frac{\rho(y)}{|f'(y)|} , \tag{4.14}$$

where the summation is over all pre-images of the point x. The solution of this equation for one map arising in the theory of numbers was already known to Gauss. In most cases, however, analytical solutions cannot be obtained. Here various numerical methods may be used [134].

The opposite problem is also of interest: given an invariant measure (statistical characteristic) the map f (system dynamics) must be determined. For example, it turns out that there are an infinite variety of unimodal maps that generate the measure of density $\sim \mathrm{e}^{-x^2/\sigma^2}$ (with given σ) on the interval $[-1, 1]$. The method to solve the inverse problem and the conditions for which there is a unique solution are discussed in ref. [134].

Let us discuss the question of the stability of iterations of one-dimensional maps. We consider the iterations of the point x_1 and the neighbouring point $x_1' = x_1 + \Delta x$. Using the same arguments as we used for the cycle S^p and letting Δx tend to zero we may verify that the stability of the trajectory $\{x_n\} \equiv \{x_1, f(x_1), f^2(x_1), \ldots\}$ is determined by

$$\lambda(x_1) = \lim_{n \to \infty} \frac{1}{n} \log \left| \frac{\partial f^n(x_1)}{\partial x} \right| ,$$

*) In this case as well as in the case of the Feigenbaum attractor the set U in the definition of the attractor is determined in a specific way [142].

where $\lambda(x_1)$ is called the *Lyapunov exponent*. In many cases we may prove that almost all points x_1 yield the same values of λ [131].

If $\lambda < 0$ the trajectory $\{x_n\}$ is stable, and all adjacent trajectories tend to it. If $\lambda > 0$ the paths of two neighbouring points exponentially diverge. This property is often called a *sensitive dependence on initial conditions*. If this sensitive dependence is exhibited in a system we cannot, in fact, forecast its behaviour in the future.

As applied to model (4.1) this means the following. If x_1 and x_1' are sufficiently close, the first terms of the sequences $\{x_n\}$ and $\{x_n'\}$ will be close as well, but starting from a certain number N the terms will be quite different. We can conclude that chaos, which, in fact, does not allow us to predict the time evolution of a system, may be described by the very simple explicit formula (4.1).

Let us note that in real systems our knowledge of initial conditions is always inaccurate, even if only slightly. Therefore, the behaviour of a system sensitive to initial conditions proves to be unpredictable. In 1963 E. Lorenz suggested that this circumstance might be closely associated with the weather forecast problem [76]. Even recently specialists believed that advances in computer technology would lead to the appearance of correct long-term weather forecasts (even if for two-week periods). This, however, has not happened. It seems that the equations describing the atmospheric state are sensitive to initial conditions.

4.4. Metastable chaos, crises

When simulating various phenomena one may encounter one-dimensional maps with sharp apexes, several maxima or sometimes maps that are not continuous [103, 137, 150]. In order to simulate such situations one should study maps which are not S-unimodal; they may have several attractors.

As a simple example we consider the family of one-dimensional maps

$$f(x, \lambda) = 1 - |x - \lambda|^{1/2}/[1 + (x - \lambda)^2]\,. \tag{4.15}$$

For $\lambda_1 < \lambda < \lambda_2$ ($\lambda_1 = 0.432$ and $\lambda_2 = 0.448$) the map has a stable cycle S^2. It coexists with the noisy cycle χ^4 on the interval $\lambda_3 < \lambda < \lambda_2$ ($\lambda_3 \approx 0.445$). When $\lambda = \lambda_3$ the region of attraction of the cycle S^2 discontinuously decreases, and a stochastic attractor appears.

In order to explain this picture it is convenient to pass to the map $g \equiv f^4$. Let us consider a square with sides j, constructed as shown in fig. 4.14. For illustrative purposes we have shown several iterations of the point x_1. Let the point x_1 be inside the square and $\lambda > \lambda_3$ (fig. 4.14b). It is seen that the function g

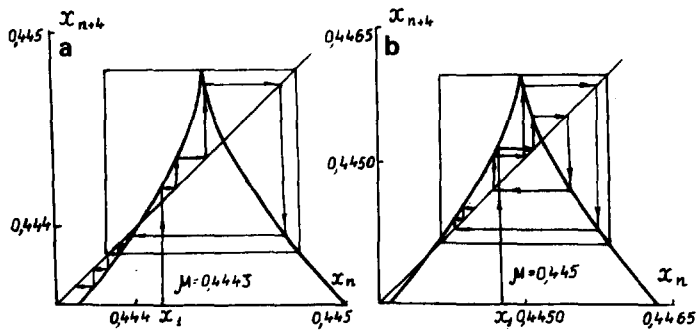

Fig. 4.14

defines a map of interval j onto itself; therefore all iterations (images) of x_1 will be inside the square. Since $|dg/dx| > 1$ inside j, there are no stable cycles and fixed points in it, and the images of the points inside it behave in a stochastic way. (In fig. 4.14 only one segment of the function g is shown for illustration. If we consider the whole interval $(0, 1)$ it may be verified that for $\lambda = \lambda_3$ four segments appear simultaneously, each of which goes into itself, i.e. the noisy cycle χ^4 arises.)

For $\lambda > \lambda_3$, a stable singular point (x^* in fig. 4.15) may exist in the map g along with a stochastic attractor. For the map g this point corresponds to an element of the stable cycle S^2 (in figs. 4.14 and 4.15 $\mu = \lambda$).

Quite a different picture is observed for $\lambda < \lambda_3$. In this case the segment j does not go into itself. Images of the point x_1 leave the square through a small segment near its lower left corner (fig. 4.14a). The smaller the value of $\lambda - \lambda_3$, the longer time the images of x_1 spend within the square. Thus, if x_1 is in the interval j a chaotic regime will be observed for a long time. However, the life time of this regime is limited. When $n \to \infty$ (or when $t \to \infty$ in systems with continuous time) convergence to a stable point or cycle occurs. In case the transient process connected with chaotic oscillations can be arbitrarily long if $\lambda \to \lambda_3$, J. Yorke and E. Yorke [136] called this interesting phenomenon *metastable chaos*. It was discovered in the Lorenz system, which was proposed as a simplified model of the Bénard instability. It is possible that metastable chaos and the appearance of stochastic regimes described above may be observed in some nonlinear media too.

The example considered lets us introduce another important notion associated with the analysis of nonlinear systems. For $\lambda > \lambda_3$ there are a stochastic attractor and an unstable fixed point (fig. 4.14); at $\lambda = \lambda_3$ they collide and as a result, the stochastic attractor disappears. "The collision" between an attractor and an unstable fixed point or cycle is called an *attractor crisis* [138, 139, 212].

Crises are typical for a large class of nonlinear systems [139]; they are connected with fast qualitative variations of chaotic regimes. We can distinguish *boundary crises*, which usually lead to the sudden disappearance of a chaotic attractor (an example of such a crisis has been discussed above), and internal crises. As a result of an *internal crisis* the size and attraction regions of the stochastic attractor suddenly vary. It can be observed even in the simplest S-unimodal maps [138].

The scenario of the transition to chaos in maps with several extrema may be quite different from the traditional picture. For example, in ref. [147] it is shown that a cascade of the period-doubling bifurcations in odd maps has an interesting peculiarity. Here the bifurcation points may not tend to a geometric progression as $n \to \infty$.

Maps with a sharp apex may have complex properties. In ref. [148] the family of maps (4.15) was considered. In this case it is convenient to denote cycles by the indices m and n: $S^p_{(m,n)}$ $(m + n = p)$; they

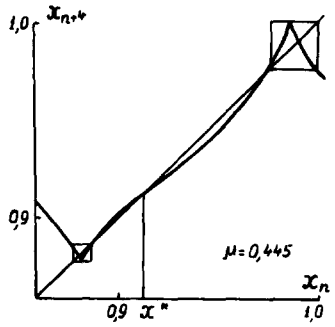

Fig. 4.15

show how many elements lie to the right and left of the apex ($x = \mu$). Computations show that there may be a large class of transitions in which the topology of stable cycles changes, $S^p_{(m,n)} \to S^p_{(m+1,n-1)}$. Such transitions may be accompanied by cascades of bifurcations, crises, appearance of chaotic regimes.

In experiments we usually deal with determinate processes which are affected by a small-amplitude noise. In the simplest case the situation is described by the map

$$x_{n+1} = f(x_n) + \xi_n , \tag{4.16}$$

where ξ_n is a small random function. It is shown in refs. [128, 149] that despite the noise effects many phenomena predicted by the theory of one-dimensional maps are typical for systems of the form (4.16).

4.5. *Categories of cycles*

Computations show that a "*window structure*" is typical for the map (4.3). As the parameter λ increases ($\lambda > \lambda_\infty$), both chaotic regimes and stable cycles of any period can be observed. The question arises: What rules determine the order of appearance of cycles as the parameter changes?

Considering the Feigenbaum scenario it can be verified that along with the stable cycle S^{2^p} there are unstable cycles of periods $S^{2^{p-1}}, S^{2^{p-2}}, \ldots, S^1$ for the same value of the parameter. Then it is important to find out under what conditions cycles of different periods can coexist.

The above questions were settled for a large class of one-dimensional maps [131, 141, 142, 143]. Let us pay attention to some results obtained in this field.

We shall say that there is an order relation, $m \succ n$, between the integers m and n if from the existence of the cycle S^m it follows that there is also a cycle S^n for the same map. The Soviet mathematician A.N. Sharkovskii proved in 1964 that with the above relation the cycles of continuous maps are ordered in the following way:

$$3 \succ 5 \succ 7 \succ \cdots \succ 3\cdot 2 \succ 5\cdot 2 \succ 7\cdot 2 \succ \cdots \succ 3\cdot 2^2 \succ 5\cdot 2^2 \succ 7\cdot 2^2 \succ \cdots \succ 2^3 \succ 2^2 \succ 2 \succ 1 . \tag{4.17}$$

The last relation in this series means that if there is a cycle S^2 then there is a fixed point (cycle S^1). It can easily be proved. Since there is a cycle S^2, values a_1 and a_2 can be found such that $a_1 = f(a_2)$, $a_2 = f(a_1)$, $a_2 > a_1$. Now we consider the function $g = x - f(x)$ at the points a_1 and a_2: $g(a_1) = a_1 - f(a_1) = a_1 - a_2 < 0$ and $g(a_2) = a_2 - a_1 > 0$. Since $f(x)$, and hence $g(x)$, are continuous there is a point a^* where $g(a^*) = 0$, i.e., $f(a^*) = a^*$. The other relations cannot be proved so easily.

To judge from (4.17), the cycle S^3 is most complex. The American mathematicians T. Li and J. Yorke proved the following theorem. If for a continuous map F points a, b, c, d, such that $b = F(a)$, $c = F(b)$, $d = F(c)$, and $d \le a < b < c$ can be found, then this map has cycles of any period and an infinite set of aperiodic trajectories [140].

In the Sharkovskii theorem any continuous maps and all cycles regardless of their stability are considered. In many cases, however, stable cycles are the main interest. It turns out that for families of smooth maps, continuous together with their first derivative, the window structure does not depend on the specific form of the function $f(x, \lambda)$. As the parameter λ changes the cycles appear in a certain order [131, 143].

We shall assume that the functions $f(x, \lambda)$ are given on the interval $[-1, 1]$ and have a maximum at $x = 0$. Let the elements of the cycles S^n be numbered in increasing order: $x_1 < x_2 < \cdots < x_n$. Beside the period of the cycle we introduce two other characteristics. The first one determines the order in which the elements of the cycle are visited. For example, for the cycle S^4 there are two possibilities, shown in

Fig. 4.16

fig. 4.16. The picture in fig. 4.16a corresponds to $f(x_1) = x_3, f(x_3) = x_2, f(x_2) = x_4, f(x_4) = x_1$, i.e. 1324. In the second case the visiting order is: 1234 (fig. 4.16b).

The sign of the elements of the cycle is also of importance. According to the sign we construct a sequence of symbols R, L and C. We have R if $f(x) > 0$, C if $f(x) = 0$ and L if $f(x) < 0$. For example, the sequence RLRL means that $x_1 > 0, f(x_1) < 0, f^2(x_1) > 0, f^3(x_1) < 0$. Such a sequence can be constructed for any initial point x_1. Generally speaking, it is infinite and called an *itinerary* of this point. But if convergence to a stable cycle occurs in $\{x_n\}$, a certain combination of elements in the itinerary repeats itself.

Now let us look at table 4.1 which contains information on the stable cycles whose period does not exceed six. The left column shows the cycle period, the middle one indicates the order in which the points are visited, while the right column gives the itinerary. We can prove that in one-parametric families of C^1-unimodal maps the stable cycles are encountered in the order shown in the table. Jumps are impossible in this list.

For example, if we have found that at $\lambda = \lambda_1$ there is a stable cycle S^4 with itinerary RLRL and at λ_2 the cycle S^3 with RLR, then necessarily λ_3 and λ_4, $\lambda_1 < \lambda_3 < \lambda_4 < \lambda_2$, can be found such that at λ_3 the cycle S^6 is stable with itinerary RLRRRL and at λ_4 the cycle S^5 is stable with itinerary RLRRR. The order in which the elements of the cycle are visited (if they are numbered in increasing order) will be exactly as indicated in the second column.

From the table it follows that all intermediate cycles will be encountered between two different cycles. They may be encountered not once but several times. For the map (4.3) the cycles are encountered only once as λ increases.

The sequence in which the cycles appear is called the *U (universal) sequence*. An algorithm to determine it and proofs of the corresponding statements are considered in refs. [143, 131].

This result is very important. It proves that there is a deep intrinsic connection between the characteristics of one-dimensional maps and the itineraries of different points. If we study the itineraries for different initial data x_1, it will turn out that nearly all of them coincide provided there is some order (a stable cycle) in the system. And vice versa, if there is chaos almost all itineraries are different. The

Table 4.1

Period	Order of points	Itinerary
2	12	RR
4	1324	RLRL
6	143526	RLRRRL
5	13425	RLRRR
3	123	RLR
6	135246	RLLRLL
5	12435	RLLRL
6	124536	RLLRRR
4	1234	RLLR
6	123546	RLLLRL
5	12345	RLLLR
6	123456	RLLLLR

properties of sequences of several symbols are closely associated with the properties of one-dimensional maps. The theory that studies these properties is called *symbolic dynamics*. It is useful for analysing different nonlinear models. In particular, its methods were extensively used to obtain table 4.1.

The classification of stable cycles is used to analyse many nonlinear dissipative systems. Let us give two examples. A theorem proved by M. Jakobson [145] states that the set of parameters for which the iterations of the map $x_{n+1} = \lambda x_n(1 - x_n)$ determine aperiodic trajectories, has a *positive Lebesgue measure*. In ref. [146] numerical results are given which allow us to determine this measure. Then, by following from the U-sequence the superstable cycles and the windows of periodicity where these cycles are located, can be obtained. Information about the itineraries of the cycles proved very useful. (Every element x_n in symmetric maps with one maximum has two pre-images x'_{n-1} and x''_{n-1}: $f(x'_{n-1}) = f(x''_{n-1}) = x_n$. However, knowing its itinerary we can compute not only direct but inverse iterations too. This proved essential in the construction of numerical methods.)

The total size of all "windows" whose dimensions exceed ε is denoted by $h(\varepsilon)$. Computation shows that

$$\mu(\varepsilon) = 1 - h(\varepsilon) \approx \mu(0) + A\varepsilon^{\beta} ,$$

$$\mu(0) = 0.897\,95 \pm 0.0005 , \quad \beta = 0.45 \pm 0.04 .$$

It was suggested that β is universal and does not depend on the specific family [146].

In refs. [28, 144] results of experimental studies of the Belousov–Zhabotinsky reaction in a flow reactor with mixing are discussed. (Mixing is introduced so that diffusion effects can be ignored.) It turns out that the maxima in one of the variables which describe the reaction, often generate one-dimensional maps $x_{n+1} = f(x_n)$ of the form shown in fig. 4.17. When the control parameter (the flow velocity of the reagents) increases, the amplitude of the map monotonically increases. Transition to chaos occurs according to the Feigenbaum scenario, and then the stable cycles predicted by the classification are observed (see table 4.1).

In some cases every cycle is encountered only once. However, adding Fe as an ingredient (even in concentrations not more than thousandths of a percent) changes the system dynamics. Some cycles from the table are encountered not in a single but in three intervals of the parameter [144]. The sequence of stable cycles may be an indicator to show how the concentrations of some reagents vary.

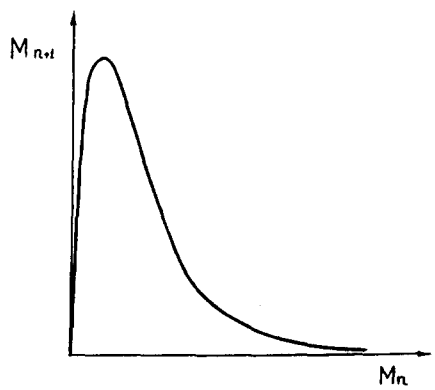

Fig. 4.17.

5. Two-dimensional maps and dissipative systems

One-dimensional maps describing complex ordering and stochastic regimes are *irreversible*. At least two pre-images $y = f(a) = f(b)$ correspond to some values of y. Therefore, we cannot reconstruct the previous values $x_0, x_{-1}, x_{-2}, \ldots$, from a given value of x_1. Most mathematical models used in science have quite different properties. From a set of variables $x(t')$ describing the phenomenon under study at a given time we may predict the future, $x(t' + T)$, and reconstruct the past, $x(t' - T)$.

Hamiltonian systems are invariant under the replacement $t \to -t$, and the processes they describe turn out to be reversible. However, in dissipative systems we usually can reconstruct the values of $x(t' - T)$ from $x(t')$ (at least for a finite interval $t < \bar{T}$).

Two-dimensional maps,

$$x_{n+1} = f(x_n, y_n), \qquad y_{n+1} = g(x_n, y_n), \tag{5.1}$$

are the simplest dynamic systems which may have the *reversibility* property and describe complex stochastic processes. An analysis of the system (5.1) as well as one-dimensional maps allows us to find new scenarios for the transition to chaos, and to discover some interesting phenomena typical for many nonlinear dissipative systems. From the study of such maps mathematical theories could be constructed for a direct investigation of differential equations appearing in various physical problems. These approaches sometimes help to find out to what extent the objects under study are stochastic, and to obtain some rigorous assertions about their properties.

In this chapter we shall discuss some two-dimensional maps which have proved useful for understanding chaotic regimes in nonlinear media.

5.1. Characteristics of chaotic regimes. Hyperbolicity

One of the simplest and most important maps describing chaotic regimes is determined by the formulae

$$x_{n+1} = (2x_n + y_n) \mod 2\pi, \qquad y_{n+1} = (x_n + y_n) \mod 2\pi, \tag{5.2}$$

or

$$\begin{pmatrix} x_{n+1} \\ y_{n+1} \end{pmatrix} = \left[A \begin{pmatrix} x_n \\ y_n \end{pmatrix} \right] \mod 2\pi .$$

Since the residue from division by 2π enters into x_{n+1} and y_{n+1}, it is natural to consider this map as defined on a torus. It is convenient to present the torus as a rectangle whose opposite sides are identified. That is, $(0, a)$ and $(2\pi, a)$, $0 \le a \le 2\pi$, as well as $(b, 0)$ and $(b, 2\pi)$, $0 \le b \le 2\pi$, are supposed to be the same point.

Let us see what will happen with a figure given on the torus after the use of the map (5.2) (see fig. 5.1). It can be seen that after the first iteration, different parts of the figure turn out to be expanded and shifted in a complicated way. We may expect that after a great number of iterations the "black" parts will be uniformly spread all over the torus. Note that the determinant A of the matrix in (5.2) is equal to unity, therefore the area of the figure does not change in the course of the iterations.

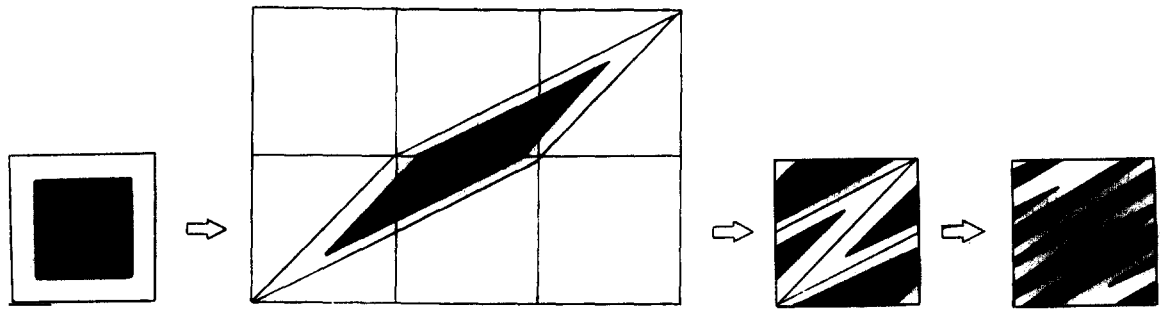

Fig. 5.1

From fig. 5.1 it is seen that a pre-image of any set is also situated on the torus while the map (5.2) is reversible. (We can determine uniquely the pre-image from the points of the image.) For brevity we shall denote it by A.

Depending on the initial point, trajectories of the map (5.2) may be both periodic and aperiodic. A *cycle* of the map (5.1) is called a set of points $(x_1, y_1), \ldots, (x_p, y_p)$ such that $x_{n+1} = f(x_n, y_n)$, $y_{n+1} = g(x_n, y_n)$, $1 \le n \le p-1$, $x_1 = f(x_p, y_p)$, $y_1 = g(x_p, y_p)$.

It is easy to verify that all points (x, y) whose coordinates are both a product of π and a rational number, determine the cycles of the map. It is clear that their number is countable. We may also verify that all the points whose coordinates cannot be presented in the above form, determine aperiodic trajectories (in this connection the cycle A resembles the cycles of the map $x_{n+1} = 1 - 2|x_n|$).

The matrix A of the map has eigenvalues $\lambda_{1,2} = (3 \pm \sqrt{5})/2$, $\lambda_1 > 1 > \lambda_2$, and eigenvectors $\boldsymbol{e}_1, \boldsymbol{e}_2$. The map A carries into itself the family of straight lines parallel to the eigenvector $\boldsymbol{e}_1$. The distance between two nearby points lying on such a straight line becomes λ_1 times as large after each iteration (fig. 5.2). These straight lines determine the family of everywhere dense windings of the torus, which is transformed by the map into itself. Such a family is called an *expanding foliation* of the map A. The family of straight lines parallel to the vector $\boldsymbol{e}_2$ determines a *contracting foliation*.

The map (5.2) has many remarkable properties. In the beginning of the sixties the Anosov theorem was proved, which states that the map A is *structurally stable*. (That is, a small change of the dynamic system does not affect the qualitative behaviour of the system. A detailed discussion of the structural stability may be found in the book [85].) In particular, any map which is sufficiently near A has a countable set of cycles and an infinite number of aperiodic trajectories. Therefore, it may be expected that such systems as well as their multi-dimensional analogs will have complex aperiodic trajectories. When generalizing the representations on the map A it is natural to introduce the notions of *U-systems*

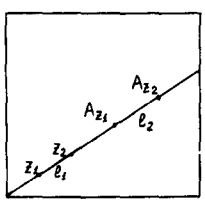

$\ell_2/\ell_1 = \lambda_1$

Fig. 5.2

(*Anosov diffeomorphisms*) and of hyperbolic systems, which represent a large class of mathematical objects, the ergodic properties of which can be studied in detail [151].

Before we discuss these objects let us consider, following refs. [152, 153], what can be a criterion for stochasticity in dynamic systems, or by what features we can judge the extent of stochasticity of a solution.

1. In many cases the typical behaviour of trajectories is the main interest. So we shall assume that there is a set of similar systems which differ only in initial data. In this case the initial data are chosen in phase space with probability P_0, $\mathrm{d}P_0(x)/\mathrm{d}x = \rho(x)$. (The introduction of P_0 may be considered as a manifestation of a random mechanism operating at the initial time.) The simplest stochastic property is the existence of an *invariant distribution of probabilities* $\bar{P}(x)$ in the phase space of the system. An invariant distribution $\bar{P}(x)$ means that for any function f the integral

$$I(f) = \int f(x(t))\,\mathrm{d}\bar{P}(x) \tag{5.3}$$

is independent of time. Suppose the trajectory visits some fractions of phase space rarely, and others frequently. In order to calculate average time-independent values of a function f we should take into account the relation between the probabilities of hitting different points of phase space. This gives the information necessary for averaging.

The Krylov–Bogolubov theorem proves that in the case of a continuous map and a compact phase space there is at least one invariant measure. Even in the simplest cases many invariant measures may exist. For example, in the map $x_{n+1} = 1 - 2|x_n|$ all distributions of the form

$$P = \frac{1}{r}\sum_{i=1}^{r} \delta(x - x_i), \quad i = 1, \ldots, r,$$

where x_r are elements of the cycle S^r, and the distribution $P(x) = 1/2$ are invariant. However, when considering strange attractors in dissipative dynamic systems we may distinguish the measures which are most important for studying typical solutions which are, in a certain sense, stable. It turns out that in some cases we may, first, give an arbitrary initial measure $P_0(x)$, then watch its evolution in time and verify that

$$\lim_{t\to\infty} \int f(x)\rho(x, t)\,\mathrm{d}x = \int f(x)\,\mathrm{d}\bar{P}(x). \tag{5.4}$$

In this case $\bar{P}(x)$ determines the probability with which a typical trajectory hits different points of phase space. Sometimes the existence of the limit (5.4) can be proved [154, 155].

2. The average values that characterize the dynamic system may be calculated by averaging over the invariant measure (the set of trajectories) or over time if only one trajectory is considered. When both average values coincide it is said that the system

$$\lim_{T\to\infty} \frac{1}{T}\int_0^T f(x(t))\,\mathrm{d}t = \int f(x)\,\mathrm{d}\bar{P}(x) \tag{5.5}$$

is *ergodic*. [This equality is fulfilled with probability 1 in the measure $\bar{P}(x)$.]

The system may have a continuous invariant measure and be ergodic but behave in a rather regular manner. For example, like the map of a circle onto itself,

$$\theta_{n+1} = \theta_n + \alpha \,, \tag{5.6}$$

where $\alpha/2\pi$ is an irrational number.

Here the invariant measure is equal to $1/2\pi$, the map is ergodic, but the distance between any two trajectories does not change (if $\theta_1' - \theta_1'' = a$ we have $\theta_n' - \theta_n'' = a$ for any n). Stronger criteria of stochasticity must take into account how different trajectories behave with respect to each other.

3. A map T acting on sets M and having an invariant measure $\bar{P}(x)$ is called *mixing* if for any f, $g \in L_2$

$$\lim_{n\to\infty} \int_M f(T^n(x))g(x)\,\mathrm{d}\bar{P} = \int_M f\,\mathrm{d}\bar{P} \int_M g\,\mathrm{d}\bar{P} \,. \tag{5.7}$$

The meaning of this definition becomes clearer if we consider the transformation A of the torus [see formula (5.2)]. In this case the invariant measure has a constant density. We denote the set on which A acts by S, and two arbitrary domains by F and G. Then it follows from relation (5.7) that

$$\lim_{n\to\infty} \frac{\operatorname{mes}(A^n F) \cap G}{\operatorname{mes} F} = \frac{\operatorname{mes} G}{\operatorname{mes} S} \,.$$

This means that an arbitrary set will be uniformly smeared all over the torus after a sufficiently large number of iterations. The "black" parts (see fig. 5.1) turn out to be mixed with the white ones. (The proof may be found in ref. [85].) The definition is naturally generalized for the case of continuous time. From the mixing property the ergodic property follows.

It is rather difficult to verify relation (5.7) in real systems. Therefore, in order to establish the mixing property the self-correlation functions $b(t)$,

$$b(t) = \int f(x(t))f(x(0))\,\mathrm{d}\bar{P}(x) - \int f(x(t))\,\mathrm{d}\bar{P}(x) \int f(x(0))\,\mathrm{d}\bar{P}(x) \,,$$

are usually considered. In ergodic systems it is convenient to replace the measure-averaged value by the time-averaged value for a typical trajectory,

$$b(t) = \lim_{T\to\infty} \frac{1}{T} \int_0^T f(x(t+\tau))f(x(\tau))\,\mathrm{d}\tau - \left(\lim_{T\to\infty} \frac{1}{T} \int_0^T f(x(\tau))\,\mathrm{d}\tau \right)^2 . \tag{5.8}$$

If a dynamic system has the mixing property, $b(t) \to 0$ for $t \to \infty$, which shows that the process under study is stochastic [152]. In physics it is known as the property of decomposition of temporal correlations [156]. (Specifically, the map (5.6) does not have the mixing property.)

The law of creasing $b(t)$ and the spectral characteristics of dynamic systems are closely connected. We present $b(t)$ in integral form,

$$b(t) = \int_{-\infty}^{\infty} e^{i\omega t} a(\omega)\, d\omega\,. \tag{5.9}$$

The spectrum of ergodic motion without mixing is discrete,

$$a(\omega) = \sum_k a_k \delta(\omega - \omega_k)\,; \tag{5.10}$$

with mixing it is continuous [156].

4. It is natural to expect that many properties of independent stochastic quantities will be typical for dynamic systems with chaotic behaviour. One of them is the *central limit theorem*. We introduce the quantity

$$T^{1/2}\left\{\frac{1}{T}\int_0^T f(x(t))\, dt - \int f(x)\, d\bar{P}(x)\right\}. \tag{5.11}$$

The quantity in the braces usually decreases as $T^{-1/2}$. Therefore by analogy with probability theory it may be expected that for $T \to \infty$ the quantity (5.11) must obey a Gaussian probability distribution. From a physical point of view, this means that the integral $\int_0^T f(x(t))\, dt$ is near a sum of poorly dependent terms.

5. One of the strongest stochastic properties is the *exponential decrease of correlations*,

$$b(t) \to \exp(-h_0 t) \quad \text{for large } t\,, \quad h_0 = 1/\tau_0\,. \tag{5.12}$$

In this case the function $a(\omega)$ [see formula (5.9)] is analytic. The time τ_0 is often called the *time of correlation decomposition* or the *correlation radius*.

For the investigation of the map (5.2) the existence of contracting and expanding foliations is important. In the neighbourhood of each trajectory there are infinitely many nearby trajectories, some of them tending to it for $t \to \infty$ and the others for $t \to -\infty$. It turns out that, if all the trajectories of a dynamic system are thus arranged, we may study the global properties of the system using the local properties of the trajectories. Such an approch is developed in *hyperbolic theory*. Let us discuss some of its results.

The hyperbolicity property naturally generalizes the properties of the map (5.2) to multi-dimensional maps with more complex phase spaces.

Let us consider a dynamic system with discrete time in the phase space M. (In the map (5.2) it is a torus.) We denote a trajectory by $\{S^t(x)\}$, and the space tangent at a point x by T_x (fig. 5.3). (If there

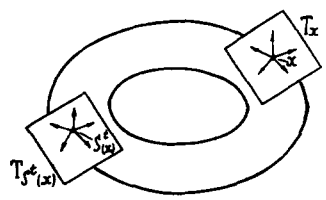

Fig. 5.3

are a point $x \in M$ and infinitely many nearby points $x' \in M$, all possible vectors $x' - x$ make up the tangent space T_x.) According to ref. [151] the trajectory $\{S^t(x)\}$ is called *uniformly fully hyperbolic* if the space $T_{S^t(x)}$ can be decomposed into a direct sum of subspaces,

$$T_{S^t(x)} = E^s(S^t(x)) \oplus E^u(S^t(x)) .$$

In this case these subspaces are T-invariant,

$$dS^\tau E^s(S^t(x)) = E^s(S^{t+\tau}(x)) , \qquad dS^\tau E^u(S^t(x)) = E^u(S^{t+\tau}(x)) ,$$

and there are constant numbers $0 < \lambda < 1 < \mu$ such that for all t and $\tau > 0$,

$$\|dS^\tau v\| \le C\lambda^\tau \|v\| , \quad v \in E^s(S^t(x)) ,$$

$$\|dS^\tau v\| \ge c^{-1}\mu^\tau \|v\| , \quad v \in E^u(S^t(x)) ,$$

$$\gamma(S^t(x)) \ge \text{const.} ,$$

where $\gamma(S^t(x))$ is the angle between the subspaces $E^s(S^t(x))$ and $E^u(S^t(x))$ (fig. 5.4). By $\|dS^\tau v\|$ we mean the distance between the trajectory originating at the point $S^0(x)$ and an infinitely nearby trajectory leaving the point $S^0(x) + v$ at time τ. In order to determine $dS^\tau v$, in systems with continuous time $\dot{x} = X(x)$, the *equation of variations* $\dot{v} = X_x(x)v$ is solved on the interval $0 < t < \tau$, and in systems with discrete time $x_{n+1} = f(x_n)$, the map $v_{n+1} = f_x(x_n)v_n$ is considered ($X_x = \partial X/\partial x$, $f_x = \partial f/\partial x$, where f, X, x are vectors).

A dynamic system is called a *U-system* or an *Anosov diffeomorphism* if each trajectory in it is uniform and completely hyperbolic, while the constants C, λ and $\mu = \lambda^{-1}$ may be chosen the same for all points.

Anosov diffeomorphisms like the map (5.2) are structurally stable. There are not so many problems where they arise in pure form. One of them is the problem of motion along geodesic trajectories on surfaces of a constant negative curvature [151].

Hyperbolic trajectories are typical for an interesting class of dynamic systems called *billiards*. A billiard is a system corresponding to the inertial motion of a material point within a domain with a

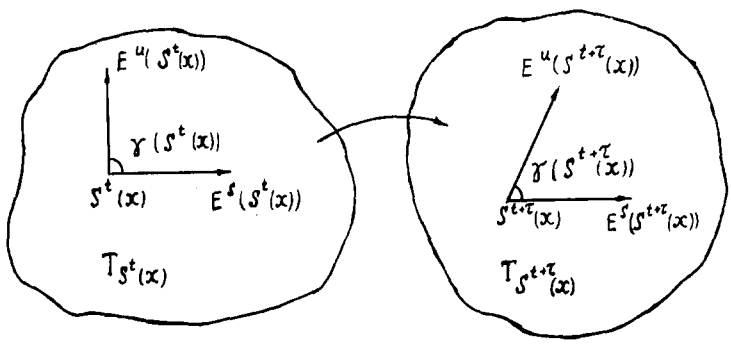

Fig. 5.4

piecewise smooth boundary and with elastic reflection from the boundary. If the domain is bounded by smooth concave curves, and the curvature is positive for each regular point of the boundary, the billiard is called dispersing and represents an analog of smooth hyperbolic systems. Billiards appear in problems of acoustics, radiophysics, and quantum mechanics. Their chaotic behaviour usually can be studied in detail [157].

It is very interesting that for the analysis of strange attractors in dissipative systems we may use results of hyperbolic theory.

An attractor of a dynamic system is called *hyperbolic* if it consists entirely of trajectories satisfying the condition of uniform complete hyperbolicity with the same constants C and λ.

Hyperbolic systems have good stochastic properties. Specifically, the map T is mixing with respect to the probability distribution $\bar{P}$ if the attractor satisfies the hyperbolicity conditions (under some additional restrictions [154, 155]). In this case for any initial distribution P_0 with density ρ_0, which is concentrated in the vicinity of the attractor $\bar{W}$, the iterations $T^n P_0$ converge to $\bar{P}$. It is clear, however, that using the definition of hyperbolicity we can investigate the properties of a rather narrow class of dynamic systems. In ref. [152] the conditions for hyperbolicity were given, which can be verified in many cases with the aid of a computer. In the literature they are usually called the *Sinai criterion*. It may be used to analyse mathematical models of different phenomena for which chaotic regimes are typical.

Let us present this criterion according to ref. [152] for systems with discrete time. Along with the map T at the point x we shall consider its Jacobi matrix $\mathrm{d}T(x) = \partial f/\partial x$ [the map T transforms the N-dimensional vector x into the N-dimensional vector $f(x)$]. A vector e is called *expanding* if $\|\mathrm{d}T(x)e\| > \|e\|$. The collection of all expanding vectors at a given point x forms a cone of *expanding vectors*. Reversing the sign of the inequality we obtain a definition of a *contracting* vector and a cone of contracting vectors. For $N = 2$ these definitions would be sufficient. In the multi-dimensional case we have to define yet *expanding* and *contracting subspaces*, $L^{(\mathrm{u})}$ and $L^{(\mathrm{s})}$, or subspaces consisting of expanding and contracting vectors.

Let us assume now that for a pair of integers k and l, $k + l = N$, and a constant λ $(1 < \lambda < \infty)$ an open set $\mathscr{L}^{(\mathrm{u})}(x)$ of k-dimensional expanding subspaces $L^{(\mathrm{u})}$ and an open set $\mathscr{L}^{(\mathrm{s})}(x)$ of contracting l-dimensional subspaces $L^{(\mathrm{s})}(x)$ are given at each point x in a domain Q containing the attractor $(TQ \subset Q)$ (see fig. 5.5). Then

(1) $(\mathrm{d}T(x))\mathscr{L}^{(\mathrm{u})}(x) \subset \mathscr{L}^{(\mathrm{u})}(Tx)$, i.e. for any $L^{(\mathrm{u})} \in \mathscr{L}^{(\mathrm{u})}(x)$ the image $(\mathrm{d}T)L^{(\mathrm{u})} = L_1^{(\mathrm{u})} \in \mathscr{L}^{(\mathrm{u})}(Tx)$; moreover, any vector $e \in L^{(\mathrm{u})} \in \mathscr{L}^{(\mathrm{u})}(x)$ obeys the inequality

$$\|\mathrm{d}T(x)e\| \geq \lambda\|e\| ;$$

(2) $(\mathrm{d}T(Tx))^{-1}\mathscr{L}^{(\mathrm{s})}(Tx) \subset \mathscr{L}^{(\mathrm{s})}(x)$, i.e. for any $L^{(\mathrm{s})} \in \mathscr{L}^{(\mathrm{s})}(Tx)$ the image $(\mathrm{d}T)^{-1}L^{(\mathrm{s})} = L_1^{(\mathrm{s})} \in \mathscr{L}^{(\mathrm{s})}(x)$; moreover, any vector $e \in L^{(\mathrm{s})} \in \mathscr{L}^{(\mathrm{s})}(Tx)$ obeys the inequality

$$\|(\mathrm{d}T)^{-1}(Tx)e\| \geq \lambda\|e\| .$$

These conditions may be explained by means of fig. 5.5 $(N = 2)$.

The first condition means that the operator carries the expanding vectors into the cone in which there are expanding vectors on the next iteration. The second condition is obtained if the cone of expanding vectors is replaced by the cone of contracting vectors, and T by T^{-1}.

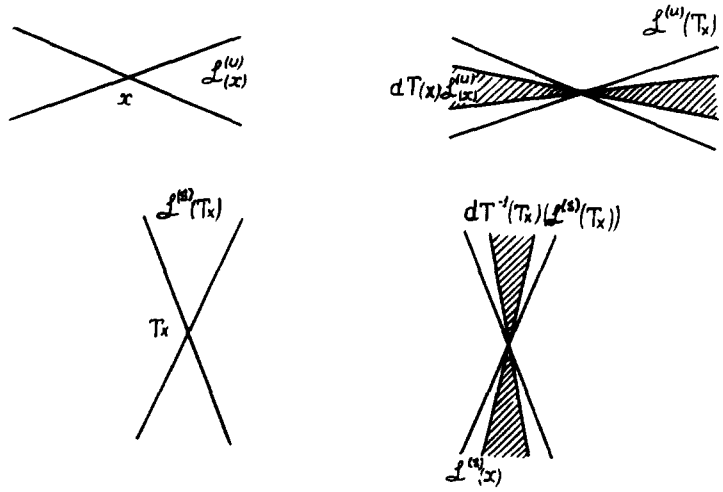

Fig. 5.5

It the case of the two-dimensional maps (5.1) these conditions are simplified and may be explicitly expressed through derivatives of f and g [158],

$$\|\partial f/\partial x\| < 1\,, \quad \|(\partial g/\partial y)^{-1}\| < 1\,;$$

$$\left\|\left(\frac{\partial g}{\partial y}\right)^{-1} \frac{\partial f}{\partial y}\right\| \left\|\frac{\partial g}{\partial x}\right\| < \left(1 - \left\|\frac{\partial f}{\partial x}\right\|\right)\left(1 - \left\|\left(\frac{\partial g}{\partial y}\right)^{-1}\right\|\right); \tag{5.13}$$

$$1 - \left\|\left(\frac{\partial g}{\partial y}\right)^{-1}\right\| \left\|\frac{\partial f}{\partial x}\right\| > 2\sqrt{\left\|\left(\frac{\partial g}{\partial y}\right)^{-1}\left(\frac{\partial f}{\partial y}\right)\right\| \left\|\left(\frac{\partial g}{\partial y}\right)^{-1}\right\| \left\|\frac{\partial g}{\partial x}\right\|}\,,$$

where $\|h(x, y)\| = \max_{(x,y)\in Q} |h(x, y)|$.

The hyperbolicity criterion was used in such a form, for example, in ref. [158] to investigate the Lorenz model and in ref. [159] to study the strange attractor in a system of differential equations connected with reaction–diffusion-type equations.

Invariant sets in hyperbolic systems may have a complex structure and unusual properties. As an example we may consider an invariant set of the map called the *Smale horseshoe*.

Let T be a map of a fraction of the plane into itself, for which the square S with vertices ABCD transforms into the curvilinear figure A′B′C′D′ shown in fig. 5.6. For purposes of illustration we describe this in two stages. First the square is contracted in one direction and expanded in the other. At the second stage the strip obtained is folded in the form of a horseshoe. It is clear what the structure of the set $T^2(S) \cap S$ will be. Instead of each strip, two strips with a smaller width will appear. They are shown by the shaded area in fig. 5.7. At the next iteration, each of the strips will be split into two until there are 2^n strips at the nth step. Hence, the limit set $\lim_{n\to\infty} T^n(S) \cap S$ will have a structure that repeats itself on small scales. Such sets are called *Cantor* sets. They are typical for attractors of many systems showing chaotic behaviour. Below we shall consider in more detail examples of such systems, properties of Canor sets and their quantitative characteristics.

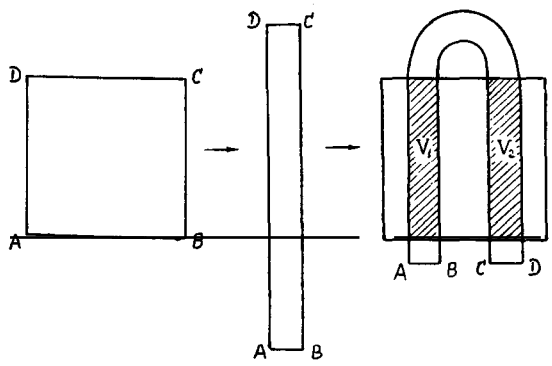

Fig. 5.6

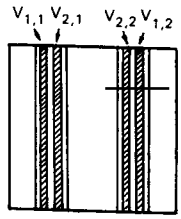

Fig. 5.7

We propose a simple symbolic description of iterations of different points on the square. We denote the two strips appearing at the first step by V_1 and V_2. Then at the second step the strips V_{11} and V_{12} will appear from the first strip, and V_{21} and V_{22} from the second strip, etc. With every point remaining within the square S we associate an infinite sequence of 1 and 2 according to the following rule. If the image of the point at the first step falls in the strip V_1, the first entry in this sequence will be 1; if it falls in V_2 it will be 2. Let at the kth step the point fall in the strip $V_{i_1 i_2 \cdots i_k}$. The image of this strip consists of two parts, left and right. If the $(k+1)$th iteration of the point falls in the left-hand part then we put 1 in the $(k+1)$th position in the sequence; if it falls in the right-hand part we write 2. Each iteration of the map T is equivalent to a shift by an element to the right. In the limit set $\lim_{n\to\infty} T^n(S) \cap S$ all the points with the same y-coordinate are described by the same sequence of 1 and 2. Different sequences correspond to points with different values of y (fig. 5.7). Indeed, the strip V_1, for example, obtains only points with ordinate $0 \le y < 1/2$, the strip V_2 those with ordinate $1/2 < y \le 1$. Since at each step the map T expands the pre-image along the y-axis, at a certain step the points $y' - y''$ come into different strips for an arbitrary small initial distance along the y-axis between these points.

This symbolic description of iterations of the map T proves to be exactly the same as in the random process of coin tossing. We consider an infinite series of tossings. If head shows up for the nth time there will be 1 in the nth position in the sequence, if tail shows up we write 2. One tossing is equivalent to a shift by one element of the sequence. Thus, there is a one-to-one correspondence between the y-coordinate of a point in the limit set $\lim_{n\to\infty} T^n(S) \cap S$ and an infinite series of coin tossings. This is a very important fact. It testifies to a deep connection between deterministic invertible dynamic systems and traditional objects of probability theory. Such an approach of associating different trajectories with symbolic descriptions is called symbolic dynamics and has proved very fruitful. Methods of symbolic dynamics helped to investigate chaotic regimes in some interesting dynamic systems [152, 160, 161]. In order to construct an invariant set we shall act in the following way.

Let us note that $S \cap T^{-1}(S)$ consists of two horizontal strips, $S \cap T^{-2}(S)$ of four strips, etc. (fig. 5.8). They may be numbered as before by a sequence of 1 and 2. We consider the set $T^{-1}(S) \cap S \cap T(S)$ (fig. 5.9), it represents four squares. (After applying T or T^{-1} these squares are iterated into themselves.) The set $T^{-2}(S) \cap T^{-1}(S) \cap S \cap T(S) \cap T^2(S)$ represents 16 squares. The set $\cap_{n=-\infty}^{\infty} T^n(S) = \Lambda$ is invariant. For a symbolic description of trajectories of points in the set Λ we should consider a sequence of 1 and 2 which is infinite in both directions. It may be proved that there is a

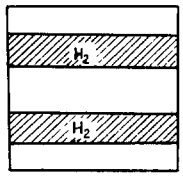

Fig. 5.8

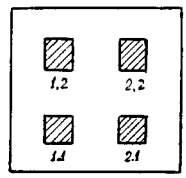

Fig. 5.9

one-to-one correspondence between points $(x, y) \in \Lambda$ and the set of in both directions infinite sequences of two symbols [160, 161]. Iteration of the map leads to a shift by one element to the right.

Suppose that in the sequence $\{a_i\}$, $-\infty < i < \infty$ ($a_i = 1$ or 2) there is a periodically recurring group of numbers. Watching the trajectory of the point of the square which corresponds to the sequence, we may verify that it belongs to a cycle of the map T. By considering aperiodic sequences $\{a_i\}$ we can construct an infinite set of aperiodic trajectories of different types.

A similar approach based on the construction of a symbolic sequence may be developed by analysing the so-called baker transformation, which is widely used as a simple efficient model in the theory of dynamic systems [162] and in thermodynamics [292]. A *generalized baker transformation* is determined by the formula

$$\begin{aligned} &x_{n+1} = \lambda_a x_n\,, \quad y_{n+1} = y_n/\alpha\,, \quad y_n < \alpha\,, \\ &x_{n+1} = \tfrac{1}{2} + \lambda_b x_n\,, \quad y_{n+1} = (y_n - \alpha)/(1-\alpha)\,, \quad y_n > \alpha\,. \end{aligned} \tag{5.14}$$

The effect of this map upon the unit square is shown in fig. 5.10. The baker transformation has a sensitive dependence on initial conditions and the mixing property. In ref. [162] different quantitative characteristics of the map (5.14) are considered in detail.

Under the hyperbolicity condition the existence of contracting and expanding directions which cross at a nonzero angle at each point is important. However, in many dynamic systems describing chaotic regimes this condition is not satisfied. An example is the *Hénon map*,

$$x_{n+1} = y_n + 1 - ax_n^2\,, \qquad y_{n+1} = bx_n\,, \tag{5.15}$$

which is shown in fig. 5.11. In ref. [163] Hénon gave numerical results showing that the attractor has a

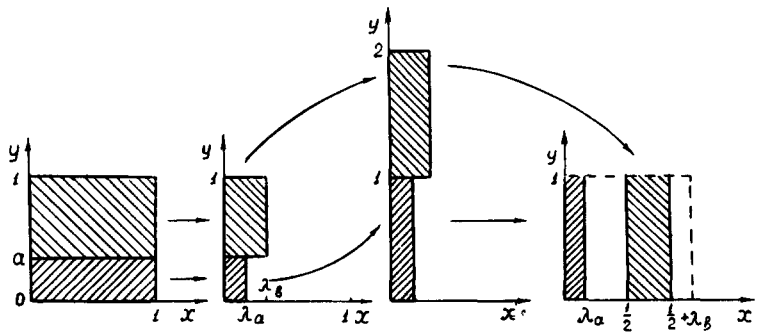

Fig. 5.10

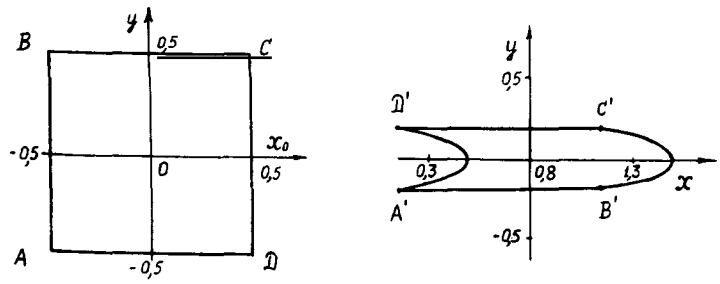

Fig. 5.11

Cantor structure along one direction. The map (5.15) is a complex object. The results in ref. [164], where the stability domains of the cycles S^n ($n \leq 6$) are studied in the parameter plane (a, b), testify to this fact.

An analysis of one-dimensional maps shows that in many cases it is easier to study the stochastic properties of maps with sharp rather than smooth vertexes. We may expect that the situation will be analogous in the two-dimensional case. This is indeed so. For the attractor of the map

$$x_{n+1} = 1 - y_n - a|x_n|\,, \qquad y_{n+1} = bx_n\,,$$

called the *Lozi attractor*, the existence of an invariant measure was proved, the hyperbolicity of the attractor was verified and its mixing property was demonstrated in a certain range of parameters [166, 167].

5.2. *Breakdown of invariant tori. The Ruelle–Takens scenario*

Before extensive investigations of stochastic regimes began it was assumed that turbulence in hydrodynamics appears as a result of bifurcations. This is now called the Hopf–Landau scenario [168, 169].

We shall assume that the phenomenon is described by a finite-dimensional dynamic system. (This seems natural since we may assume that the effect of higher spatial harmonics will not be strong due to viscosity.) Let laminar flow correspond to a singular point of this system. We change one of the flow parameters λ (for example, the Reynolds number). At a certain value of λ the singular point loses its stability, a Hopf bifurcation occurs and a limit cycle develops. As a result of the next Hopf bifurcation an invariant torus appears (fig. 5.12). Two independent frequencies may be distinguished in such a solution. Indeed, let us go over to the system of coordinates R, φ, θ shown in fig. 5.13. In these

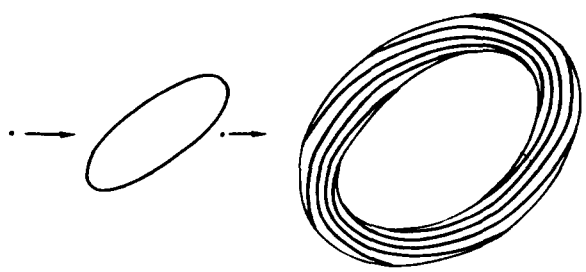

Fig. 5.12

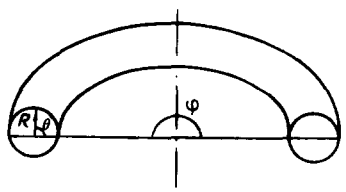

Fig. 5.13

variables the simplest spiral wound about the torus is described by the formulas $R = R_0$, $\varphi = \omega_1 t + \varphi_0$, $\theta = \theta_0 + \omega_2 t$, where R_0, φ_0, θ_0, ω_1, ω_2 are constants. If the ratio ω_1/ω_2 is irrational the solution will be aperiodic and the trajectory will uniformly cover the torus surface.

The next Hopf bifurcation will lead to the appearance of an invariant torus of higher dimension. In this case the solution may resemble a spiral that winds with frequency ω_3 about the spiral which appeared after the previous bifurcation. The trajectory that appears after many Hopf bifurcations in the Hopf–Landau scenario is considered to be the turbulent regime.

Modern experimental technology permits us to see whether a multi-frequency regime can be observed in real systems and how many different frequencies exist in this regime [27, 32]. Usually we cannot observe flow with more than three independent frequencies. It is natural to expect that a different scenario must exist, in which Hopf bifurcations play an essential role (in contrast to the Feigenbaum and Pomeau–Manneville scenarios discussed earlier).

Such a scenario was proposed in 1971 by D. Ruelle and F. Takens [170]. Let a system of equations describe the simplest three-frequency regime $\varphi_1 = \omega_1 t$, $\varphi_2 = \omega_2 t$, $\varphi_3 = \omega_3 t$, where φ_n are the angles in the corresponding space, $n = 1, 2, 3$, and let $f(\varphi_n) = f(\varphi_n + 2\pi)$, where f is any of the functions entering in these equations. Ruelle and Takens proved that when an arbitrary small change is introduced into the right-hand side of the system of equations, then the solution will qualitatively change. Instead of the three-frequency regime a strange attractor will appear, and the behaviour of the solution will become chaotic. The set of such deformations changing the type of solutions proves to be rather extensive. Thus, the scenario may be as follows: two Hopf bifurcations and chaos developing after the third bifurcation.

The question how the chaotic regime arises from the invariant torus has proved complex and has been intensively investigated recently [171, 211]. The main object of these investigations are two-dimensional maps. Many established laws have proved universal, independent of the specific form and dimension of the system. In ref. [171] the transition to chaos was studied for the map

$$x_{n+1} = y_n\,, \qquad y_{n+1} = a y_n (1 - x_n)\,. \tag{5.16}$$

It may be written in the form

$$x_{n+2} = a x_{n+1}(1 - x_n)\,.$$

It appears as a natural generalization of model (4.2). In the whole range of the parameter a a point on the (x, y)-plane lies on a smooth closed curve Γ as $n \to \infty$. The same situation is typical for invariant tori in dynamic systems with continuous time (the curve Γ acts as the cross section of the torus and the Poincaré plane). In the case of a periodic solution there are a finite number of points on this curve (fig. 5.14); if the solution is aperiodic, the points will cover the whole contour.

In both cases the contour is an invariant set, and the behaviour of trajectories on it (and this means the behaviour of trajectories in the two-dimensional map for $n \to \infty$) is defined by the map of a circle into itself,

$$\theta_{n+1} = F(\theta_n)\,, \quad F(\theta_n + 2\pi) = F(\theta_n) + 2\pi\,. \tag{5.17}$$

Let us consider some properties of the model. The limit

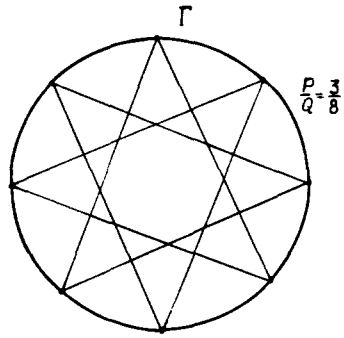

Fig. 5.14

$$\rho(\theta_0) = \lim_{n\to\infty} \frac{F^n(\theta_0) - \theta_0}{2\pi n} \tag{5.18}$$

is called the *winding number* at a given point θ_0. Let $\rho(\theta_0) = P/Q$, where P and Q are integers. Then a certain point $\bar{\theta}$ returns to the initial position after Q iterations and P rotations about the contour (fig. 5.14). For illustration the points $F^n(\bar{\theta})$ and $F^{n+1}(\bar{\theta})$ are connected by thin lines.

Maps of the type (5.17) appear in connection with the analysis of differential equations on a torus, which is of interest in some problems of celestial mechanics and in the study of other Hamiltonian systems. They were investigated by Poincaré (1885) and Denjoy (1932). Specifically, it was shown that the limit in the definition of the winding number exists and does not depend on the initial point. It is rational if and only if the map F^q has a fixed point for a certain q.

A circle map with $F'(\theta) > 0$, which keeps its orientation, is structurally stable if and only if the winding number is rational and all the cycles are nondegenerate (i.e., the eigenvalue of the derivative of the map F^q at the points of the cycle of period q is not 1). The structurally stable diffeomorphisms*) form an open everywhere dense set in the space C^2 of all twice differentiable orientation-preserving maps of a circle. This means, in particular, that near any transformation of this class there is a map with a cycle.

As the simplest transformation of a circle we consider a rotation by a constant angle, eq. (5.6). It turns out that any orientation-preserving transformation F of class C^2 with an irrational winding number μ is *topologically equivalent* to a rotation of the circle by an angle $2\pi\mu$ [eq. (5.6)]. (Proofs can be found in ref. [85].)

In spite of the structural stability of circle maps with cycles, the measure of the set of parameter values for which the winding number ρ is irrational may be rather large. This is shown by the family of maps

$$\theta_{n+1} = \theta_n + \alpha + \varepsilon \sin\theta_n\,, \quad \alpha \in [0, 2\pi]\,, \quad 0 \le \varepsilon < 1\,. \tag{5.19}$$

The division of the parameter plane into regions where ρ is rational (shaded) and irrational (unshaded) is schematically shown in fig. 5.15. A "*tongue*" bounded by a pair of smooth curves emerges from each point on the α-axis such that $\alpha = \pi \cdot p/q$. (Only some of such "tongues" are shown in the figure.) As q

*) A diffeomorphism is a one-to-one differentiable map with return map being one-to-one and differentiable.

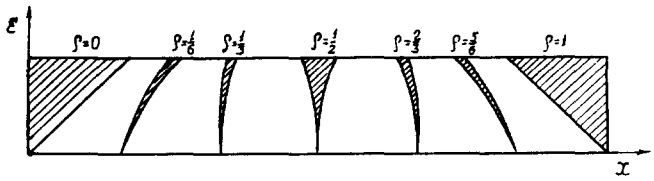

Fig. 5.15

increases the tongues grow thinner. Despite the fact that the rational numbers represent a dense set on the interval, the measure of the set of points (α, ε) for which ρ is rational is small in the region $0 \le \varepsilon \le \varepsilon_0$, $0 \le \alpha \le 2\pi$ compared with the measure of the entire region. Thus, a map that is randomly taken from the family (5.19) has an irrational winding number with an overwhelming probability. The same result is valid if, instead of $\sin\theta$, any analytic function θ is considered.

The analysis of such families is closely associated with the *Kolmogorov–Arnold–Moser theory*, which considers the breakdown of n-dimensional invariant tori under small perturbations. The results of this theory played an important role in the analysis of many Hamiltonian systems and in some problems of statistical physics [156, 172, 173, 291].

Let us note two important facts. First, for each value of the parameter the number ρ is unique and independent of the initial point. Second, the properties of the one-parameter family of maps (5.19) prove to be simpler and more understandable than those of the one-parametric families that correspond to various curves in the parameter plane (α, ε).

As a consequence of these facts, in ref. [171] maps of the form (5.16) are also considered as an element of the two-parameter family

$$x_{n+1} = y_n + bx_n\,, \qquad y_{n+1} = ay_n(1 - x_n)\,. \tag{5.20}$$

Suppose the map (5.20) is written in polar coordinates,

$$(r_{n+1}, \theta_{n+1}) = F(r_n, \theta_n)\,. \tag{5.21}$$

Let it map the domain B $(1 < r < 2)$ onto itself (fig. 5.16), and let $\arg(r, \theta) \equiv \theta$, $\arg F(r, \theta + 2\pi) = 2\pi + \arg F(r, \theta)$, for all $(r, \theta) \in B$. The winding number $\rho(r, \theta)$ is given by the formula

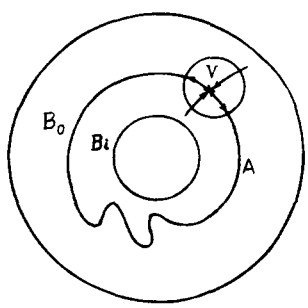

Fig. 5.16

$$\rho(r,\theta)=\lim_{n\to\infty}\frac{\arg F^n(r,\theta)-\theta}{2\pi n}. \tag{5.22}$$

Using numerical techniques, in ref. [171] boundaries of the regions in the (a, b)-plane are constructed where the cycles are stable with a given winding number P/Q (analogs of the tongues or, as they are called, the *resonant "horns"* in fig. 5.15). It turns out that there are parts of the plane where the cycles are stable with different winding numbers. (For different initial data we obtain different cycles.) Hence, the invariant torus is broken down. In other words, there is no transformation of coordinates with which the figure emerging in the Poincaré plane could be reduced to a circle. (If there were a contour topologically equivalent to a circle, the winding number would be unique.)

To investigate Hamiltonian systems the *criterion of resonance overlap* is used in many physical problems [174]. It states that stochasticity may arise in a region where at least two "tongues" overlap. A similar situation is typical for the map (5.16).

First, it is natural to understand in what cases the winding number is unique and when there are several values. Sufficient conditions for this were obtained in ref. [171]. Before discussing these results we introduce some definitions.

Let a compact invariant set containing all the points $z\in A=\cap_{n\geq 0}F^n(B)$ divide the region into two parts—an internal, B_i, and an external part B_0 (fig. 5.16). A fixed point z of the map F is called a *saddle* if the Jacobian matrix $DF(z)$ has one eigenvalue $|\lambda_1|<1$ and the other eigenvalue $|\lambda_2|>1$. The points z of a cycle of period q are called *periodic saddle points* if the same inequalities are satisfied for the eigenvalues of the matrix DF^q. Let z be a fixed point of F; then the sets

$$W^s(z,F)=\{x\colon F^n(x)\to z \text{ as } n\to+\infty\},\qquad W^u(z,F)=\{x\colon F^n(x)\to z \text{ as } n\to-\infty\},$$

will be called the *stable* and *unstable manifolds* of the point z, respectively. Note that these manifolds may behave in a different way from integral curves of differential equations: they may intersect without coinciding entirely.

In ref. [171] two theorems are proved.

Theorem 1. Suppose that the map F satisfies the following conditions.

(a) There exists a periodic saddle point $y\in A$ with positive eigenvalues.

(b) $W^s(y,F^q)\cap A=\{y\}$, where q is the period of y.

(c) One branch of $W^s(y,F^q)$ intersects only B_i, while the other branch intersects only B_0 (fig. 5.16).

Then $\rho(z)=\rho(y)$ for all $z\in B$.

Theorem 2. Let $y\in A$ be a periodic point of period q and winding number p/q, where p and q are relatively prime. Suppose that $W^u(y,F^q)$ intersects $W^s(F^k(y),F^q)$ transversely (at a nonzero angle) for some $0<k<q$. Then there exists a nondegenerate interval I containing p/q such that for every $\alpha\in I$ there is $z\in A$ with $\rho(z)=\alpha$. Furthermore, there exist points for which the winding number is not defined.

Figure 5.17 shows the saddles marked by asterisks and several iterations of a point x_0 near $y'=F^k(y)$. For the iterations of such points we may construct the symbolic dynamics, which allows us to prove the theorem.

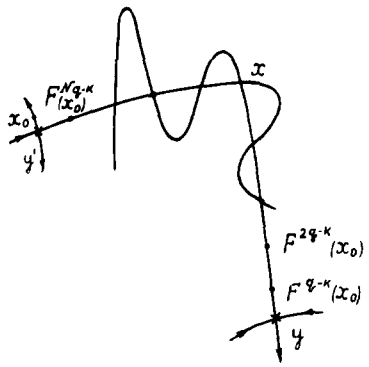

Fig. 5.17

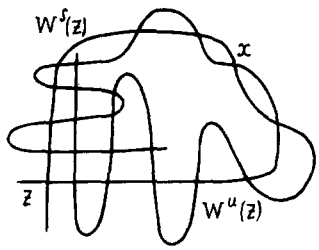

Fig. 5.18

The definition of a stable and unstable manifold naturally is generalized to the case of a cycle Y of period q ($Y \equiv \{y, F(y), \ldots, F^{q-1}(y)\}$, $F^q(y) = y$, $F^n(y) \neq y$ for $0 < n < q$):

$$W^s(Y, F) = \{x: \mathrm{d}(F^n(x), Y) \to 0 \text{ as } n \to +\infty\},$$

$$W^u(Y, F) = \{x: \mathrm{d}(F^n(x), Y) \to 0 \text{ as } n \to -\infty\}.$$

A point $x \in B$ is called *homoclinic* to Y if

$$x \in W^s(Y, F) \cap W^u(Y, F) - Y.$$

The conditions of the second theorem imply that there is a homoclinic point.

In this and many other problems, where the maps arising are invertible, the existence of a homoclinic point proves important. We may verify that the existence of one homoclinic point implies that there are infinitely many of them. Indeed, due to the invariancy of $W^s(z, F)$ and $W^u(z, F)$ we have $F^k(x) \in W^s(z, F)$ and $F^k(x) \in W^u(z, F)$ for all k. Hence, they are all homoclinic points.

By assuming that the points $x, F(x), \ldots, F^m(x)$ form a cycle we obtain a contradiction to the fact that $F^k(x) \in W^s(z, F)$, which implies that $F^k(x)$ must tend to z as $k \to \infty$. Therefore, from the existence of one nondegenerate homoclinic point (i.e., a point in which W^s and W^u intersect, and are not tangent) it follows that there is a very complex set called a *homoclinic structure*. Due to the infinite number of intersection points it cannot be drawn; however, some idea of it can be obtained from fig. 5.18.

A homoclinic structure was first discovered by Poincaré when he investigated the classical three-body problem. The existence of such structures is connected with the appearance of stochastic regimes [156, 161, 173]. In the analysis of maps resulting in these structures, a set appears which is affected by the map in a way similar to the Smale horseshoe. From this the existence of invariant Cantor sets follows, and they may be studied using the apparatus of hyperbolic theory. It may be said that the iterations of F behave as a random sequence of coin tossings. References to original studies dealing with this problem may be found in refs. [151, 175].

Thus, if the transition to chaos occurs according to the Ruelle–Takens scenario, *frequency locking* may take place after two Hopf bifurcations and an invariant torus may be generated. In this case a cycle

appears, and the conditions of theorem 1 are usually satisfied. Then a complex reconstruction of the invariant set occurs, and as a result homoclinic points appear (the conditions of theorem 2 are satisfied). Hysteresis is observed in the system—for different initial data cycles with different winding numbers and chaotic regimes develop.

It is interesting to know what happens with the invariant set A when the parameters change and how it loses its smoothness. These questions were considered in refs. [151, 174, 177]. Possible versions of the reconstruction of A and the development of homoclinic points are graphically shown in refs. [176, 211].

Let us note the difference between the scenario under discussion and those considered earlier. In the earlier cases, in order to determine the type of attractor it was sufficient to consider iterations of a randomly taken point (or several points). Here the situation is different and much more complex. When considering the sequence $\{x_n\}$ we may expect that under a change of parameters the sequence "singular point→cycle→2-torus→cycle→chaos" will be discovered. However, in order to understand the mechanism of torus breakdown, a mathematical model of the phenomenon should be constructed. Then we should carefully investigate it: study a two-parameter family of dynamic systems, construct stable and unstable manifolds, find homoclinic points. As a result, performing numerical experiments appears to be a rather complex task.

We discussed the appearance of chaos as a result of the breakdown of invariant tori. However, in the two-parameter families of two-dimensional maps other scenarios are also possible when an aperiodic regime (in this case trajectories with an irrational value of ρ) is preceded by a sequence of cycles. Moreover, for this sequence some universal laws valid for different families and invariant tori have been established [176, 178, 179].

The two-dimensional map

$$\begin{pmatrix} \theta_{n+1} \\ r_{n+1} \end{pmatrix} = T\begin{pmatrix} \theta_n \\ r_n \end{pmatrix} \equiv \begin{pmatrix} \theta_n + \Omega + br_n - (k/2\pi)\sin 2\pi\theta_n \\ br_n - (k/2\pi)\sin 2\pi\theta_n \end{pmatrix} \tag{5.23}$$

with a constant Jacobian equal to b is a convenient model for studying such behaviour. For $b = 1$ the map conserves its area; it is widely used in analysing Hamiltonian systems. In the other limit ($b = 0$) it transforms into the one-dimensional map

$$\theta_{n+1} = f(\theta_n) = \theta_n + \Omega - (k/2\pi)\sin 2\pi\theta_n . \tag{5.24}$$

When $0 \le k < 1$, f and f^{-1} are invertible and analytic. For $k = 1$, f^{-1} exists; however, it has a singularity $\theta^{1/3}$ and, hence, is non-differentiable at $\theta = 0$. If $k > 1$, f^{-1} does not exist.

In this case the winding number is determined by the formula

$$\rho(k, \Omega) = \lim_{n\to\infty} \frac{1}{n}\,(f^n(\theta) - \theta) .$$

We choose an irrational number $0 < \bar{\rho} < 1$. It is convenient to choose a number which can be presented most simply in the form of a continued fraction. For example, the golden mean is given by

$$\bar{\rho} = \frac{\sqrt{5}-1}{2} = \langle 1\,1\,1\,1\,1\cdots\rangle = \cfrac{1}{1+\cfrac{1}{1+\cfrac{1}{1+\cdots}}}$$

Then we construct a sequence of rational numbers $\rho_i = P_i/Q_i$ such that $\lim_{i\to\infty} \rho_i = \bar{\rho}$,

$$\rho_1 = \langle 1 \rangle = 1/1\,, \quad \rho_2 = \langle 1\,1 \rangle = 1/2\,, \quad \rho_3 = \langle 1\,1\,1 \rangle = 2/3\,, \quad \rho_i = \langle 1\,1\,1 \cdots 1 \rangle = F_i/F_{i+1}\,,$$

where the F_i are the *Fibonacci numbers* determined by the relation $F_{i+1} = F_i + F_{i-1}$, $F_0 = 0$, $F_1 = 1$. In this case

$$\lim_{i\to\infty} \frac{\rho_{i+1} - \rho_i}{\rho_i - \rho_{i-1}} = -l^2\,.$$

Here $l = \bar{\rho}$. Suppose that K is fixed and determine a sequence of the Ω values in the map (5.24) such that

$$f^{Q_i}(0) = P_i \quad \text{for } \Omega = \Omega_i\,.$$

This implies that the point $\theta = 0$ in the map belongs to the cycle of period Q_i and winding number ρ_i. In ref. [178] the suggestion was made that there is a unique limit point

$$\lim_{i\to\infty} \Omega_i(K) = \bar{\Omega}(K)\,, \quad \rho(K, \bar{\Omega}(K)) = \bar{\rho}\,.$$

Let

$$\delta_i(K) = [\Omega_{i-1}(K) - \Omega_i(K)]/[\Omega_i(K) - \Omega_{i+1}(K)]\,.$$

The computations carried out in ref. [179] show that

$$\begin{aligned} &\lim_{i\to\infty} \delta_i(K) = -l^{-2}\,, \quad 0 \le K < 1\,; \\ &\lim_{i\to\infty} \delta_i(K) = -l^{-y} \equiv \delta\,, \quad K = 1\,, \quad y = 2.164\,43 \pm 0.000\,02\,. \end{aligned} \tag{5.25}$$

By analogy with the Feigenbaum theory it is natural to consider the distance between the point $\theta = 0$ and nearby elements of the cycle (modulo 1) with period Q_i. It has the form

$$d_i = f^{Q_{i-1}}(0) - P_{i-1}\,.$$

Let $\alpha_i(K) = d_{i-1}/d_i$. The computations show that

$$\begin{aligned} &\lim_{i\to\infty} \alpha_i(K) = -l^{-1}\,, \quad 0 \le K < 1\,; \\ &\lim_{i\to\infty} \alpha_i(K) = -l^{-x} \equiv \alpha\,, \quad K = 1\,, \quad x = 0.526\,87 \pm 0.000\,02\,. \end{aligned} \tag{5.26}$$

By analogy with the theory of one-dimensional maps we may expect that application of the renorm-group approach to this system will enable us to find universal functions and relations (analogs of

the Feigenbaum equation). By these x and y may be found. Such a theory was constructed in refs. [176, 178].

In refs. [176, 179] the important question is discussed as to how the experiment should be formulated and its results processed in order to detect the phenomena predicted by the theory. As an illustration of such an experimental study we may cite the work of ref. [180], which deals with Rayleigh–Bénard convection in mercury. The parameters are chosen so that the winding numbers of the observed cycles lie in the vicinity of the golden or silver mean, $\bar{\rho} = (\sqrt{5} - 1)/2 = \langle 1\,1\,1 \cdots \rangle$ or $\bar{\rho} = \sqrt{2} - 1 = \langle 2\,2\,2 \cdots \rangle$.

The questions connected with the breakdown of invariant tori are now of great interest. Let us consider a few directions of investigations. One of them is connected with investigations of the Ruelle–Takens scenario in various mathematical models, for example, in systems with symmetry. In ref. [181] the map

$$x_{n+1} = 1 - Ax_n^2 + D(y_n - x_n), \qquad y_{n+1} = 1 - Ay_n^2 + D(x_n - y_n)$$

was studied. A complex sequence of cycles and invariant tori was discovered. It turned out that the values of A_n at which cycles of length $Q_n = 8n - 1$ appeared, converged to A_∞ as $n \to \infty$ and $A_\infty - A_n \sim Cn^{-2}$. Complex sequences of cycles and invariant tori were discovered in some problems of radiophysics too [182, 183].

The other direction is concerned with an analysis of global properties of maps in which the Ruelle–Takens scenario is implemented. For example, if we construct ρ as a function of Ω for the map (5.24), its behaviour proves to be very complex. Each "resonant horn" (fig. 5.15) with $\rho = P/Q$ has a step in the plot. Between every two steps P/Q and P'/Q' there is a step $(P + P')/(Q + Q')$, and so on ad infinitum. The plot which appears (and other curves of this type) is usually called a "*devil's staircase*". It appears that a renorm-group theory [184] may be constructed in order to predict with what probability a random value of the parameter Ω yields a cycle (or with what probability we may get on the steps of the devil's staircase).

Now studies are available where the developed ideas have been generalized onto tori of higher dimensions [185]. In some cases an analysis of two-dimensional maps allows us to predict new phenomena typical for many nonlinear dissipative systems. Among them are crises of attractors. Besides internal and boundary crises there exist *cyclic crises*. These are simultaneous collisions of several co-existing attractors with boundaries which separate their domains of attraction [186]. After the crisis ($\lambda > \lambda^*$) the points in phase space visit one by one all the attractors that existed for $\lambda < \lambda^*$. However, the time they spend at each attractor proves to be stochastic.

In a certain range of parameters the map

$$x_{n+1} = 4\lambda x_n(1 - x_n) + \gamma x_n y_n, \qquad y_{n+1} = 4\lambda y_n(1 - y_n) + \gamma x_n y_n, \tag{5.27}$$

may have three attractors. The attraction domain of each has a complex geometry. In phase space a "parquet" appears [186]. It seems that the "parquet" structure exists down to infinitely small scales. The boundary of the attraction domain may be smooth for $\lambda < \bar{\lambda}$, and becomes a complicated jagged curve repeating itself on small scales [187]. They are called metamorphoses in ref. [187], where such reconstructions are studied. Analogous phenomena may possibly be present in various systems of differential equations too.

6. Quantitative characteristics of chaos

When studying chaotic regimes in nonlinear media a number of interesting questions arise. Let us assume that the phenomenon under investigation is well described by a map (in one, two or more dimensions) with chaotic regimes. How can we compare theory and experiment in this case? Let the map be sensitive to the initial conditions and let two nearby trajectories be quickly diverging. Then we may expect that the disagreement between the trajectory of the map and the experimental data will grow in time. In this case, the nature of the phenomena under investigation rather than faults in the model is the cause of disagreement.

When physical theories are verified usually a small number of measured values (frequencies, lengths, times, etc.) or quantities averaged over a long time interval are compared. However, there is a large class of problems where not only specific numerical values at a given time and at a given point or quantities averaged over long time intervals are of interest but the dynamics of the process must be studied. For example, such are the problems associated with forecasts of the behaviour of nonlinear systems (e.g. the weather forecast). In this case the model efficiency should be judged by determining how accurately and over how long a time the model gives a forecast of the system behaviour rather than how well it can calculate values averaged over long intervals.

In such problems we often should compare not trajectories of two systems (a model and an object) for the same times but some more complex characteristics that determine intrinsic properties of the processes. Usually this requires the development of new algorithms for data processing and extensive use of computers.

There is another important aspect. Processes in nonlinear media are described by infinite-dimensional systems; therefore it is important to understand how many and which variables should be measured, how often the measurements should be made, and in which way they should be processed.

In many physical problems there is a single most important scale of measurement. However, considering the Feigenbaum attractor, or a series of two-dimensional maps, we see quite a different picture – the appearance of a complex structure that repeats itself on smaller and smaller scales. It is this picture that is typical for many stochastic regimes. We must know how this structure should be described.

The investigations undertaken in recent years, analysing these questions have led to the discovery of some interesting physical effects, and new insight into some phenomena has been gained as a result. Let us consider them in more detail.

6.1. Fractals and complex ordering

At the end of the last and the beginning of the present century examples of sets with a complex structure were very popular in connection with the problem of the rigorous justification of mathematical analysis. They drew the attention of outstanding mathematicians such as Weierstrass, Hermite, Cantor and Peano. An example of a continuous, nowhere differentiable function constructed by Weierstrass has determined for many years the direction of a number of investigations in the field of functional analysis and has led to higher standards of rigour of mathematical arguments.

One of the best known sets of such a type was constructed by G. Cantor [189]. We take a unit segment $[0, 1]$, divide it into three parts and eliminate the middle [an open interval $(1/3, 2/3)$]. Each of the two remaining segments is divided again into three equal parts and the middle is rejected (fig. 6.1). We repeat the procedure infinitely many times. The residual set C has many remarkable properties.

Fig. 6.1

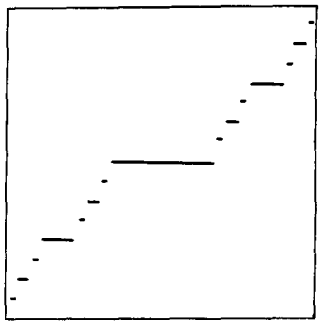

Fig. 6.2

This closed set is perfect (i.e. each point C is a limit point of the set). It is easy to verify (arguing by reductio ad absurdum) that it does not contain a single interval. At the same time the set C proves to be uncountable, i.e., there is no algorithm that allows us to number all its points. It has zero measure. This can be verified by caculating the length of the rejected intervals,

$$p + (1-p)p + (1-p)^2 p + \cdots = \frac{p}{1-(1-p)} = 1 \quad (p = 1/3) .$$

It is interesting that the residual measure is zero for any $0 < p < 1$. However, for different values of p these sets will be quite different, and hence other qualitative characteristics not coinciding with the usual measure are needed.

Another interesting object arising in the analysis of nonlinear systems is connected with the *Cantor set* and its generalizations. It is a continuous monotonic function whose derivative is zero almost everywhere (in the literature it is often called the "*devil's staircase*"; fig. 6.2). Here also a third part of each remaining interval is eliminated in each step. At the first step all the points of the interval $[1/3, 2/3]$ are given the value $1/2$, at the second step the value $1/4$ is given to all the points from the interval $[1/9, 2/9]$ and the value $3/4$ to the points from $[7/9, 8/9]$, etc. The "devil's staircase" appears after an infinite number of steps.

Along with the set C some other, similar sets are also called Cantor sets. Some of them may have a positive measure despite the fact that they do not contain a single interval. We may construct them in the following way [189]. We take an arbitrary number α, $0 < \alpha < 1$. At the first step we remove from the segment $[0, 1]$ all the points of the open interval with length $\alpha/2$ and centred about the point $1/2$. From the two remaining closed intervals $[0, 1/2 - \alpha/4]$ and $[1/2 + \alpha/4, 1]$ we remove middle open intervals of length $\alpha/8$. From the four remaining intervals we remove the middle open intervals of length $\alpha/32$. After an infinite number of steps the measure of the removed open intervals will be equal to $\alpha(1/2 + 1/4 + 1/8 + \cdots)$ and the measure of the remaining Cantor set will be $1 - \alpha$.

Another remarkable example showing that the usual topological idea about dimensions may sometimes prove ineffective was proposed by the Italian mathematician G. Peano in 1890. He constructed a curve which filled a unit square (the curve may cross some points of the square several times). A method to construct this curve is shown in fig. 6.3. In spite of the fact that the topological dimension of the curve is one, in a certain sense it is close to a two-dimensional figure – the square.

In all these examples the set proves to be self-similar – it is invariant to variation of scale and has a complex inner structure (such objects may be considered as an example of supercomplex organization).

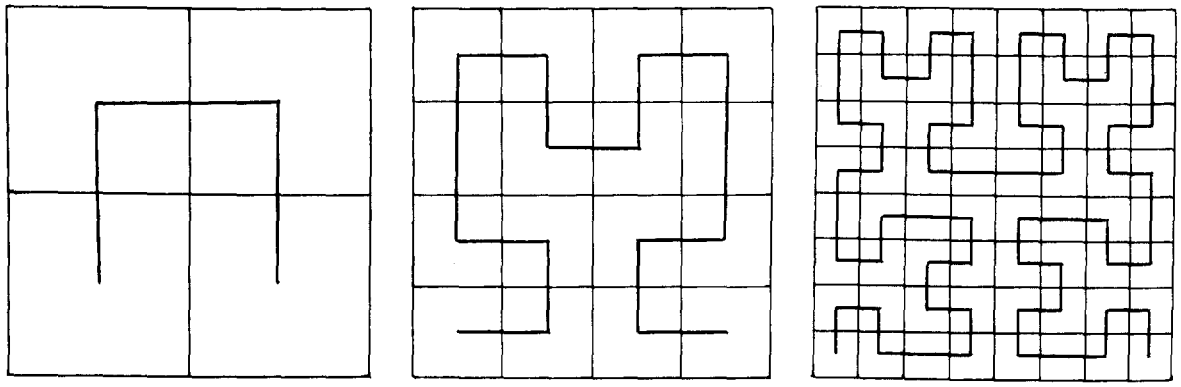

Fig. 6.3

It looks the same at both smaller and larger scales. The invariance is connected with a certain symmetry. Objects with such properties have been called *fractals* [12].

Fractals may be constructed using either simple deterministic rules or probability algorithms. The obtained sets prove to be self-similar in the statistical sense. They are of interest in many physical problems. To characterize fractals a large class of so-called *fractal dimensions* is used. The first dimension of this kind seems to have been introduced by Hausdorff in 1919. Let the set under investigation be contained in a p-dimensional Euclidean space. We consider its covering by p-dimensional spheres of radii $\varepsilon_i < \varepsilon$ and determine $l_d(\varepsilon)$ as

$$l_d(\varepsilon) = \inf \sum_i \varepsilon_i^d \,, \tag{6.1}$$

where the infimum is taken over all possible coverings such that $\varepsilon_i < \varepsilon$. Let

$$l_d = \lim_{\varepsilon \to 0} l_d(\varepsilon) \,. \tag{6.2}$$

We have $l_d = 0$ for large values of d and $l_d = \infty$ for small values. Hausdorff showed that there is a critical value d_H for which the value of l_d is finite*). It is called the *Hausdorff dimension* of the set. For simple geometric objects the Hausdorff dimension coincides with the topological one (for a line segment $d_H = 1$, for a square $d_H = 2$, for a cube $d_H = 3$). However, for the Cantor set the Hausdorff dimension is fractional. When the Cantor set is constructed, 2^n segments of length $(1/3)^n$ appear at each step; therefore

$$\lim_{n \to \infty} (1/3)^{d_H \cdot n} \cdot 2^n = C \,, \quad d_H = \ln 2 / \ln 3 \,. \tag{6.3}$$

[When $p \neq 1/3$ we obtain $d_H = \ln 2 / \ln(2/(1-p))$.]

At the beginning of this century J. Perrin suggested that fractal sets and nowhere differentiable functions would be useful in many physical problems, specifically those dealing with Brownian motion. Nevertheless, until recently such geometrical objects have not been in wide use. The situation has

*) Strictly speaking $d_H = \inf \{d: l_d = 0\} = \sup \{d: l_d = \infty\}$.

changed drastically with the appearance of the book by B. Mandelbrot [12], where it is shown that fractal sets allow us to explain (and, in some cases, predict) experimental results obtained in various fields of physics. Generalization of some earlier known results, discussion of adequate mathematical means, suggestion of new possible applications, and graphic examples presented in the book allow us to form a new view of fractals as a promising field of investigations in science.

An unexpected example of fractals is the coast line of many islands. When the coast length L is measured a complex jagged line is replaced by a broken line which consists of segments with length larger than ε. It has been proved that for Great Britain the value of L depends on ε as a power law, $L(\varepsilon) \sim C/\varepsilon^d$, where $d \approx 1.3$, for $10\,\text{km} < \varepsilon < 1000\,\text{km}$, which is a typical feature of a fractal curve. In a certain range of parameters the power law determines the coast length of many other islands, the length of some rivers, or the path length traversed by a particle in Brownian motion.

Many paradoxes connected with the distribution of stellar matter may be explained if we assume this matter to form fractal clusters. Great potentialities of using fractals in cosmology, turbulence theory, chemical kinetics, or the physics of polymers have been indicated in some recent publications [12, 190]. Fractal structures known as percolation clusters arise when fluid passes through solid bodies, or in the growth of certain crystals [191, 192].

At the same time other important progress has been achieved recently. Some authors have investigated a mechanism for the appearance of such structures in various physical problems, and a series of experiments have been carried out where spatial ordering of this type has been analysed. The formation of a complex spatial structure may be explained by means of rather simple mechanisms. One of them is *diffusion-limited aggregation* [192]. Let us imagine particles performing random wanderings; the particles may settle down on a surface. Once they stick to the surface they remain there and change its shape. It is clear that the probability of running into a hill on the surface is higher than that of getting into a hole. This is why the hills begin to grow, and a growth instability arises. Starting from a certain size, on each of them branches appear and as a result a fractal structure forms (fig. 6.4).

Another mechanism of fractal formation may be due to the combined effect of diffusion and an electrical field. It offers an explanation for the appearance of a complex structure in the electrochemical sedimentation of zinc. In this case the total current going to the cathode determines the probability for a particle to be absorbed. The lesser the curvature of the electrode surface, the higher the field strength; ions sedimentate quicker and growth occurs [193]. Thus, nonequilibrium irreversible growth may lead to the formation of fractals.

It is interesting that in spite of the relative simplicity of models of fractal growth they predict the Hausdorff dimension of the arising structures well enough. This is due to the fact that the fractal dimension is an average characteristic of a set; it reflects only the basic features and does not account for many details.

Above we have considered several examples of sets with a fractal (sometimes called Cantor)

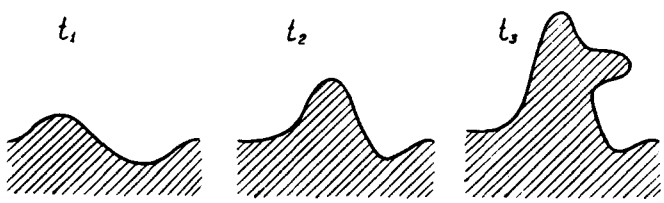

Fig. 6.4

structure. Such sets turn out to arise when one analyses many systems in which stochastic regimes or complex temporal order occur. In this case the concept of fractal dimension proves very useful for distinguishing the order parameters and constructing a hierarchy of simplified models. Let us discuss the main quantitative characteristics of these systems.

6.2. *Dimensions of strange attractors*

According to ref. [162] it is convenient to distinguish two large classes of dimensions: *metric* and *probabilistic*. The former characterizes sets as geometric objects which are determined by their metric properties. (In ref. [12] it is called the fractal dimension.) The probabilistic dimension (or *dimension of the natural measure*) takes into account with what probability a typical trajectory of a dynamic system visits different parts of an attractor.

The above mentioned Hausdorff dimension and the *capacity* of a set, d_c (also called the limit capacity [194]) are metric dimensions. The capacity is determined by the value of the limit

$$d_c = \lim_{\varepsilon \to 0} \log N(\varepsilon)/\log(1/\varepsilon)\,, \tag{6.4}$$

where $N(\varepsilon)$ denotes the minimal number of balls of radius ε needed to cover the set in p-dimensional space. It may be said that the value of d_c determines how much information is needed to specify the location of the set to accuracy ε.

Since the set of all possible covers in the calculation of d_H [see (6.1) and (6.2)] turns out to be wider than that in the calculation of d_c, we have

$$d_c \geq d_H\,. \tag{6.5}$$

Considering the upper and lower limits in formula (6.4) we may introduce, respectively, the upper and lower capacity [151].

We may imagine a situation when rarely visited points make an appreciable contribution to d_c or d_H (examples of simple two-dimensional maps have been constructed, where all happens exactly in this way [162]). In this case it is useful to take into consideration how often the point that determines the state of the dynamic system appears in different parts of the attractor. This probability is given by the natural measure.

It may be determined in the following way [151, 152]. For each ball C containing points of the attractor and for each point x of the domain of attraction we define $\mu(x, \mathrm{C})$ as the fraction of time the trajectory originating in x spends in C. (Averaging over an infinite interval of time is assumed.) If almost every such point x gives the same value of $\mu(x, \mathrm{C})$ we designate it by $\mu(\mathrm{C})$ and call μ the natural measure of the attractor.

The natural measure allows defining some probabilistic dimensions. One of them is the *information dimension*, which is given by

$$d_I = \lim_{\varepsilon \to 0} I(\varepsilon)/\log(1/\varepsilon)\,, \tag{6.6}$$

where

$$I(\varepsilon) = \inf \sum_{i=1}^{N(\varepsilon)} p_i \log(1/p_i)\,.$$

Here $p_i = \mu(C_i)$, C_i is a cube of side ε. (Some authors consider a covering with balls of radii not exceeding ε. They introduce the upper and lower information dimensions $\bar{d}_I$ and $\underline{d}_I$, and take the upper and lower limits in formula (6.6) [151].) The quantity d_I is sometimes called the *Renyi dimension*. If all the cubes are visited with equal probability, $I(\varepsilon) = \log N(\varepsilon)$ and $d_c = d_I$; if the probabilities are not equal, $I(\varepsilon) < \log N(\varepsilon)$ and

$$d_c \geq d_I . \tag{6.7}$$

We may determine probabilistic dimensions by assuming that only a fraction of the attractor visited most frequently is covered. For example, the *θ-capacity* is determined by the limit [162]

$$d_c(\theta) = \lim_{\varepsilon \to 0} \log N(\varepsilon, \theta)/\log(1/\varepsilon) , \tag{6.8}$$

where $N(\varepsilon, \theta)$ is the minimum number of cubes of side ε necessary to cover at least a fraction θ of the natural measure of the attractor. The quantities

$$\begin{aligned} \underline{d}_L(\mu) &= \overline{\lim_{\theta \to 1}}\, \underline{\lim_{\varepsilon \to 0}} \log N(\varepsilon, \theta)/\log(1/\varepsilon) , \\ \bar{d}_L(\mu) &= \overline{\lim_{\theta \to 1}}\, \overline{\lim_{\varepsilon \to 0}} \log N(\varepsilon, \theta)/\log(1/\varepsilon) \end{aligned} \tag{6.9}$$

are called, respectively, the lower and upper *Ledrappier capacities of the measure* μ [151].

So far all the introduced dimensions have defined sets as a whole. In some cases, however, it is convenient to consider the dimension in the vicinity of a given point,

$$d_p(x) = \lim_{\varepsilon \to 0} \log \mu(B_\varepsilon(x))/\log \varepsilon . \tag{6.10}$$

Beyond the above mentioned fractal dimensions there are many others. Meanwhile, in ref. [162] the suggestion is made that for typical attractors the value of different metric dimensions proves to be the same. According to this suggestion the values of all probabilistic dimensions will also be equal. There are several rigorous statements that establish relationships between different dimensions.

Let μ be the probability measure on the compact metric space X. We assume that for almost any point with respect to the measure μ

$$d_p(x) = \alpha \tag{6.11}$$

(i.e., the measure μ of the set of points, where α is different, is zero). Then we may prove [151] that

$$\underline{d}_L(\mu) = \bar{d}_L(\mu) = \bar{d}_I = \underline{d}_I = \alpha . \tag{6.12}$$

Computation of the above mentioned dimensions of strange attractors is connected with serious difficulties. It requires an immense memory or a large number of operations. For example, computing the Hausdorff dimension directly cannot be done presently because it requires minimization of the sum $\Sigma_i \varepsilon_i^d$ in all possible covers. To determine the θ-capacity we need special covers where the trajectory

must spend a strictly determined portion of time. On the other hand, to compute the limit entering the definition of the pointwise dimension we need a minimal memory, but the trajectory of the dynamic system should be observed over times $T \gg \bar{\tau} \sim \varepsilon^{-p}$, where $\bar{\tau}$ is the time of return into the sphere $B_\varepsilon(x)$, which may be very large even for small p. Computing the capacity and the information dimension proves more feasible. Below we shall consider some algorithms for their computation.

Some authors note the following difficulties arising in direct computations of the fractal dimensions.

1. An immense memory or a large amount of computation are required.

2. The number of significant digits in the value of d depends on the length of the sample N according to a logarithmic law.

3. Large samples are necessary, $N > 1/\min_i p_i$, where p_i is the probability of finding a point in the ith cube (in computations of metric dimensions).

Let us note the essential difference between fractals characterizing spatial ordering (numerous examples of which are given in the book by B. Mandelbrot) and the sets arising in investigations of temporal ordering, the strange attractors. In the first case the fractals are determined in a space of low dimension, and their fractional part is rather large. It allows considering small samples, and in some cases avoiding computations.

As a typical example of such a situation we consider the calculation of the capacity of the Cantor set ($p = 1/3$ in formula (6.3), $d_c = \ln 2/\ln 3 \approx 0.6309$) [195]. We plot $\log_2 \varepsilon$ (ε is the length of the sides of the cube) along the abscissa and $\log_2 N$ (the number of cubes necessary to cover the set) along the ordinate. If $N \sim \varepsilon^d$, the points in this plot will lie on a straight line, whose slope determines the value of d_c. (The points belonging to the Cantor set are given by the sequence $a_1 = 0$, $a_{2^k+i} = a_i + 2/3^{k+1}$, where $i = 1, \ldots, 2^k$, $k = 0, 1, 2, \ldots$ [196].) Figure 6.5 shows $\log_2 N(\varepsilon)$ versus $\log_2(\varepsilon)$ for samples of different

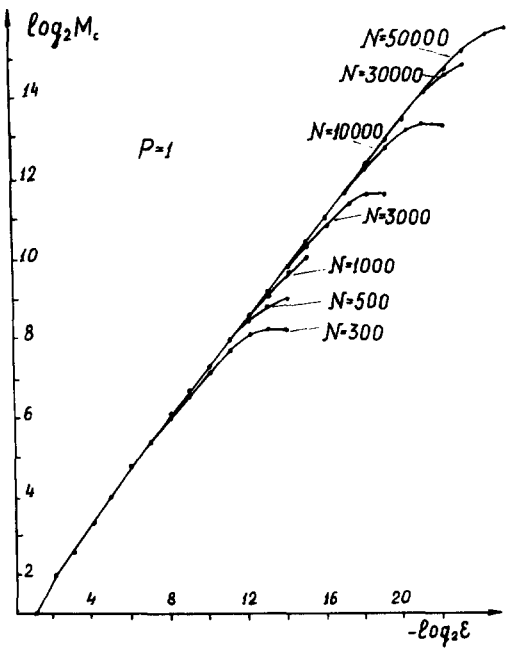

Fig. 6.5

lengths. It is seen that the slope of the straight line can be determined rather accurately even for small samples. In fact, $d_c = 0.642 \pm 0.036$ for $N = 300$, and $d_c = 0.6717 \pm 0.026$ for $N = 500$. Increasing N leads to a growth of the linear part of the curve and a higher accuracy of d_c ($d_c = 0.631 \pm 0.006$ for $N = 200\,000$).

When we study strange attractors it turns out that the fractional part of a dimension is usually small. (This is typical for the Lorenz system and other systems of three ordinary differential equations.) Therefore the dimension has to be determined rather accurately. On the other hand, investigating the processes in nonlinear media or analysing experimental data we often have to consider attractors embedded in a space of high dimension, which leads to serious difficulties [196]. (When d is computed directly the memory size is proportional to ε^{-p}.)

All this requires the development of alternative approaches to estimating fractal dimensions. Two of them are of most interest. The first one is connected with the calculation of the dynamic characteristics of systems under investigation (specifically, the Lyapunov exponents) that enable us to estimate the dimension [197]. The second approach introduces new fractal dimensions which are more feasible for numerical analysis, and then a relationship between these and the actual fractal dimension can be established [198].

We consider the first approach in more detail. Let $\varphi^t(x_0)$, $\varphi^t(x_0 + \Delta x)$ be two nearby trajectories of a dynamic system, which originate from the points x_0 and $x_0 + \Delta x$ (fig. 6.6). The *Lyapunov exponent* $\chi(x_0, \boldsymbol{\omega})$ is

$$\chi(x_0, \boldsymbol{\omega}) = \lim_{t\to\infty} \lim_{d(0)\to 0} \frac{1}{t} \ln d(t)/d(0) . \tag{6.13}$$

It may be shown that this definition is equivalent to

$$\chi(x_0, \boldsymbol{\omega}) = \lim_{t\to\infty} \frac{1}{t} \ln \| y^t(\boldsymbol{\omega}) \| / \| \boldsymbol{\omega} \| , \tag{6.14}$$

where $y^t(\boldsymbol{\omega})$ is the solution of the equation linearized in the vicinity of the trajectory $\varphi^t(x_0)$ (the so-called equation of variations), $\boldsymbol{\omega}$ is an arbitrary vector directed from x_0 to $x_0 + \Delta x$. In a p-dimensional dynamic system the Lyapunov exponents $\chi(x_0, \boldsymbol{\omega})$ have the form of a finite set of values $\lambda_1, \lambda_2, \ldots, \lambda_p$ (further we shall assume that $\lambda_1 \geq \lambda_2 \geq \cdots \geq \lambda_p$).

If the attractor is a singular point z then $\chi(x, \boldsymbol{\omega})$ are determined by the eigenvalues of the matrix of the system of equations linearized in the vicinity of the point z. (When all the eigenvalues are real the Lyapunov exponents coincide with them, $\lambda_k < 0$, $k = 1, \ldots, p$.) In the case of a stable limit cycle $\lambda_k < 0$, $k = 2, \ldots, p$.

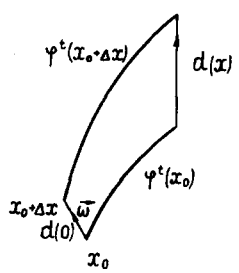

Fig. 6.6

The Lyapunov exponents characterize the rate at which nearby trajectories diverge. They are very important characteristics of a dynamic system. In many problems their values are the same for any initial x_0. The existence of positive Lyapunov exponents testifies that the system is sensitive to initial conditions and has a stochastic behaviour. We note that in a p-dimensional dynamic system with continuous time, all of whose solutions are limited, one of the Lyapunov exponents is zero (if the attractor is not a stable point). The sum of all Lyapunov exponents must be negative (otherwise there would be no trajectories tending to $\varphi(t)$ when $t\to\infty$, which means that $\varphi(t)$ would not belong to the attractor).

Some results concerning the Lyapunov exponents were obtained by Lyapunov and Perron. However, their wide use for the analysis of nonlinear systems began after V. Oseledec has proved his *multiplicative ergodic theorem*, which provided a theoretical basis [199]. The following statement is a particular case of it [153].

Let $x_{n+1} = Tx_n$ be a dynamic system (here x is a vector) with phase space M and invariant measure μ. Let $G(x)$ be a measurable function with values in the space of square matrices of order m ($m \geq 1$), $G_x^{(n)} \equiv G(x)\cdots G(T^{n-1}x)$, and let $\max[0, \ln \|G(x)\|] \in L^1$. Then

(1) there exists an invariant set Γ, $\mu(\Gamma) = 1$, such that for all $x \in \Gamma$ the limit

$$\Lambda_x = \lim_{n\to\infty} [(G_x^{(n)})^* G_x^{(n)}]^{1/2n}$$

exists, and Λ_x is a symmetric nonnegative definite matrix of order m; the positive root is taken, * denotes the conjugate matrix;

(2) if $\exp \lambda_x^{(1)} < \exp \lambda_x^{(2)} < \cdots < \exp \lambda_x^{(s)}$ ($x \in \Gamma$) is the ordered set of different eigenvalues of the matrix Λ_x and $E_x^{(1)}, E_x^{(2)}, \ldots, E_x^{(s)}$ is the corresponding set of eigensubspaces, while $m_x^{(r)} \equiv \dim E_x^{(r)}$, $1 \leq r \leq s$, the functions $x \to s(x)$, $x \to \lambda_x^{(r)}$, $x \to m_x^{(r)}$ ($1 \leq r \leq s$) are measurable and invariant under T;

(3) if $x \in \Gamma$, then for any vector $u \in \mathbb{R}^m$, $u \neq 0$, the limit

$$\lim_{n\to\infty} \frac{1}{n} \ln \|G_x^{(n)} u\|,$$

exists and is equal to one of the $\lambda_x^{(r)}$, $1 \leq r \leq s$, where r is uniquely determined from

$$u \in E_x^{(1)} \oplus E_x^{(2)} \oplus \cdots \oplus E_x^{(r)}, \qquad u \notin E_x^{(1)} \oplus E_x^{(2)} \oplus \cdots \oplus E_x^{(r-1)}$$

where $\oplus$ denotes the direct sum.

(By measurable functions we mean functions which are finite almost everywhere and representable as the limit of a converging sequence of real bounded functions.)

Hence, in order to calculate the Lyapunov exponents of the map T we should take its Jacobian $J(x) = \partial T(x)/\partial x$, calculate the matrix $J_n = [J(x_n) \cdot J(x_{n-1}) \cdots J(x_1)]$, which will play the part of the matrix $G_x^{(n)}$ in the theorem stated above. Then we take the conjugate matrix $(G_x^{(n)})^*$, consider the limit $\Lambda_x = \lim_{n\to\infty} [(G_x^{(n)})^* G_x^{(n)}]^{1/2n}$, and determine the eigenvalues of the matrix Λ_x.

In many cases it is necessary to calculate the Lyapunov exponents in dynamic systems with continuous time. For this class of problems, fast and efficient algorithms have been constructed [197].

If we act in accordance with the definition of the Lyapunov exponents and take two different nearby trajectories, the distance between them will increase due to divergence and the double limit in (6.13) cannot be determined.

Therefore, besides the initial equation

$$\dot{x} = f(x) \tag{6.15}$$

it is convenient to solve the *problem of variations*

$$\dot{w} = A(x)w\,, \tag{6.16}$$

where A is the matrix of the linearized system, $A = \partial f/\partial x$. It guarantees that all the time we shall be considering trajectories infinitely close to the integral curve under investigation. If x is a p-dimensional vector we shall solve simultaneously p systems of equations of variations such that their initial vectors $w_1, \ldots, w_p$ are linearly independent. Moving along the trajectory we shall compute simultaneously the volumes of parallelepipeds formed by the vectors $w_1(t)$ [for $w_1(t)$ it will simply be the length of the segment $\|w_1(t)\|$]; $w_1(t)$, $w_2(t)$; ...; $w_1(t)$, $w_2(t)$, ..., $w_p(t)$:

$$\lim_{t\to\infty} \frac{1}{t} \ln \mathrm{Vol}^k[w_1(t), \ldots, w_k(t)] = \lambda_1 + \cdots + \lambda_k\,, \tag{6.17}$$

where $k \le p$, Vol^k is the k-dimensional volume. (We recall that $\lambda_1 \ge \lambda_2 \ge \cdots \ge \lambda_p$.)

Two problems arise when this procedure is implemented. The first one is connected with the fact that $\|w_1(t)\| \to \infty$ as $t \to \infty$ for almost all initial vectors because of the positive exponent. The second problem is due to a variation in the direction of the vectors $w_k(t)$. When $t \to \infty$ these vectors tend to $w_1(t)$, where $w_1(t)$ corresponds to the maximal Lyapunov exponent. As a consequence the angles between the vectors $w_k(t)$ tend to zero, which does not permit calculating the corresponding k-dimensional volume with sufficient accuracy (fig. 6.7).

In order to overcome the first difficulty we may renormalize the vectors $w_k(t)$ over an interval ΔT (for example, make them unitary), calculate the value of $\lambda_1, \ldots, \lambda_p$ in this interval and then average these values along the entire trajectory. If we orthogonalize the vectors $w_k(t)$ simultaneously with renormalizing the second difficulty will also be overcome.

This algorithm, proposed in ref. [197], is now widely used when dynamic systems are analysed. Since the amount of computation in this method is directly proportional to the dimension of the dynamic system, in some cases we can manage computing about 20 Lyapunov exponents. In ref. [201] a routine is presented where this algorithm is implemented for the simplest cases.

The Lyapunov exponents determine the dynamic properties of the system, such as the above discussed fractal dimensions – the geometric parameters of the sets under investigation. Therefore, it is

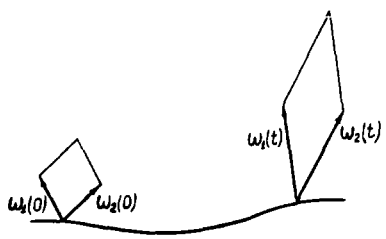

Fig. 6.7

interesting to find the relationships between those quantities. One of these relationships was established by Kaplan and Yorke [200].

For its justification the following arguments are used [162]. Let a two-dimensional map have Lyapunov exponents $\lambda_1 > 0$, $\lambda_2 < 0$ or *Lyapunov numbers* $\chi_1 > 1 > \chi_2$ (the Lyapunov number $\chi = \exp \lambda$) for almost all points. We are interested to know the capacity of the strange attractor in this case. We shall cover the attractor with $N(\varepsilon)$ squares of side ε and integrate the map q times. Now we consider an image of one of the squares (fig. 6.8). It may be expected [see formula (6.17)] that the area of the figure obtained after q iterations will be equal to $(\chi_1 \cdot \chi_2)^q \varepsilon^2$. We now take smaller squares of side $\chi_2^q \varepsilon$ that have an area $\chi_2^{2q} \varepsilon^2$. In order to cover the image of the original square after q iterations, about $(\chi_1/\chi_2)^q$ small squares will be required. If we assume that most original squares covering the attractor behave in such a way the total number of the squares in the finer graining may be estimated as

$$N(\chi_2^q \varepsilon) \approx (\chi_1/\chi_2)^q N(\varepsilon) .$$

By assuming a power law dependence $N(\varepsilon) \approx k(1/\varepsilon)^{d_c}$, we have

$$k(1/\chi_2^q \varepsilon)^{d_c} \approx k(\chi_1/\chi_2)^q (1/\varepsilon)^{d_c} .$$

After going to the limit we obtain an expression for the capacity,

$$d_c = 1 - \lambda_1/\lambda_2 . \tag{6.18}$$

Generalizing these arguments to the maps of higher dimension results in the formula

$$d_L = k + \frac{\lambda_1 + \lambda_2 + \cdots + \lambda_k}{|\lambda_{k+1}|} , \tag{6.19}$$

where k is the largest value for which $\lambda_1 + \lambda_2 + \cdots + \lambda_k > 0$. If $\lambda_1 < 0$ we define $d_L = 0$. The quantity d_L, which is the lower estimate of the fractal dimension, is usually called the Lyapunov dimension.

The Lyapunov exponents are averaged characteristics of a dynamic system, therefore the most often visited domains of attractors must make the largest contributions to $\lambda_1, \ldots, \lambda_p$. So in ref. [162] the suggestion was made that for a typical attractor the probabilistic dimensions d_μ are equal to d_L. The numerical results obtained for a series of attractors confirm this relation.

The Lyapunov exponents allow us to estimate another important characteristic of dynamic systems – the *topological entropy*. The topological entropy $h(T)$ of the map T may be determined in the following

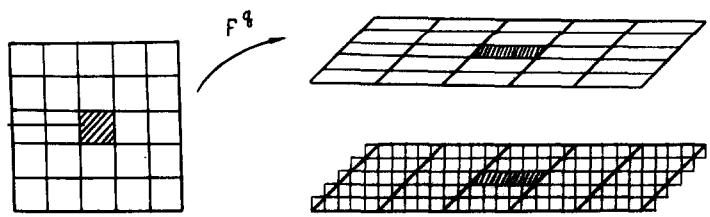

Fig. 6.8

way [151]. We fix $n>0$ and introduce the distance $\rho_n(x, y)$ in the phase space X as

$$\rho_n(x, y) = \max_{0\le i\le n} \rho(T^i(x), T^i(y)) .$$

For $\varepsilon>0$ we denote the minimum number of spheres of radius ε in the metric ρ_n, which are necessary to cover X, by $N(n, T, \varepsilon)$. Then

$$h(T) = \lim_{\varepsilon\to 0} \overline{\lim_{n\to\infty}} \frac{\log N(n, T, \varepsilon)}{n} = \lim_{\varepsilon\to 0} \underline{\lim_{n\to\infty}} \frac{\log N(n, T, \varepsilon)}{n} .$$

The quantity $h(T)$ for maps of the class C^1: $M\to M$, may be estimated as

$$h(T) \le \int_M \sum_{i=1}^{k(x)} q_i(x)\lambda_i(x)\, d\mu(x) , \tag{6.20}$$

where $\lambda_1(x)\ge\cdots\ge\lambda_k(x)\ge 0\ge\lambda_{k+1}(x)\ge\cdots\ge\lambda_p(x)$, $p=\dim M$, are the Lyapunov exponents at the point x, and $q_i(x)$ are their multiplicities. For smoother maps with nonzero exponents inequality (6.20) transforms into an equality [151]. The relation becomes even simpler if $\lambda_i(x)$ happens to be the same for almost all points x. Then $h(T)$ is simply equal to the sum of the positive Lyapunov exponents.

In ref. [289] it was shown that for sufficiently smooth two-dimensional maps with $\lambda_1>0>\lambda_2$ the suggestion that d_L coincides with other probabilistic dimensions proves to be true. It was shown that in this case

$$\lim_{\varepsilon\to 0} \frac{\log \mu(B(x, \varepsilon))}{\log \varepsilon} = \alpha = h_\mu(T)\left(\frac{1}{\lambda_1} - \frac{1}{\lambda_2}\right) , \tag{6.21}$$

and hence, the θ-dimension, the upper and lower Ledrappier dimensions, $\bar{c}_L(\mu)$ and $\underline{c}_L(\mu)$, as well as the upper and lower capacities coincide and are equal to each other. Since the topological entropy $h_\mu(T)$ here is λ_1, α is determined by the Kaplan–Yorke formula.

Calculation of the Lyapunov exponents and estimates of the fractal dimension with their use prove to be very efficient if the finite-dimensional dynamic system of equations that describe the process under investigation and the equations of variations are known. However, in many cases (in particular, when experimental data are analysed) this is not so, and other approaches are needed. One of them is connected with the introduction of new probabilistic dimensions. Grassberger and Procaccia [198] introduced the so-called *correlation exponent*, which proved very useful for studying stochastic regimes in nonlinear media. In order to calculate this exponent we have to find the distances $\rho(x_i, x_j)$ between all points of the set in p-dimensional space, and then determine the function $C(\varepsilon) = \lim_{N\to\infty}(1/N^2)\times$ {the number of distances $\rho(x_i, x_j)$ less than ε}.

The correlation exponent is

$$\nu = \lim_{\varepsilon\to 0} [\ln C(\varepsilon)/\ln \varepsilon] . \tag{6.22}$$

In most cases the correlation exponent is close to the information dimension but its calculation is much simpler. It requires a small memory and about N^2p operations. (Below we shall discuss algorithms that allow us to decrease the number of operations.) Calculating ν with a given accuracy requires much

smaller samples than the other dimensions discussed above. This can be illustrated in the following way. To calculate the capacity and the information dimension N coordinates of attractor points are processed statistically, and to calculate ν, N^2 distances are treated, which enhances the accuracy for a fixed length of sample. In the cases when increasing the length of the sample in the course of a physical or numerical experiment requires too much effort the above considerations prove very important.

In ref. [198] arguments are given to show that

$$\nu \leq d_{\mathrm{I}} \leq d_{\mathrm{c}} . \tag{6.23}$$

For a certain class of fractals these relations can be justified rigorously, and equations to determine ν, d_{I}, d_{c} can be obtained [202]. These fractals have the following hierarchical structure.

The zeroth level. On the coarsest scale there are N points in the volume l_0^d.

The first level. On a finer scale these points get into one of the cubes of side $(l_0/s_1)^d$ (there are M_1 such cubes), one of side $(l_0/s_2)^d$ (M_2 cubes), . . . , $(l_0/s_r)^d$ (there are M_r cubes), see fig. 6.9. The fraction of points getting into the cube of side l_0/s_k is denoted by p_k.

The $(n+1)$st level. Each of the cells that existed at the nth level is replaced by the configuration of cells that existed at the first level (fig. 6.9).

The simplest example of such fractals is the Cantor set. From the above given definition it follows that

$$\sum_{\alpha=1}^{r} M_\alpha p_\alpha = 1 . \tag{6.24}$$

It may be shown that the capacity and the correlation exponent may be determined from the relations

$$\sum_{\alpha=1}^{r} M_\alpha s_\alpha^{-d_{\mathrm{c}}} = 1 , \qquad \sum_{\alpha=1}^{r} M_\alpha p_\alpha^2 s_\alpha^{\nu} = 1 . \tag{6.25}$$

In ref. [202] an infinite number of various generalized dimensions were introduced. They may be determined by using one of the formulas

$$D_q = \frac{1}{q-1} \lim_{\varepsilon \to 0} \frac{\log \Sigma_i p_i^q}{\log \varepsilon} ,$$

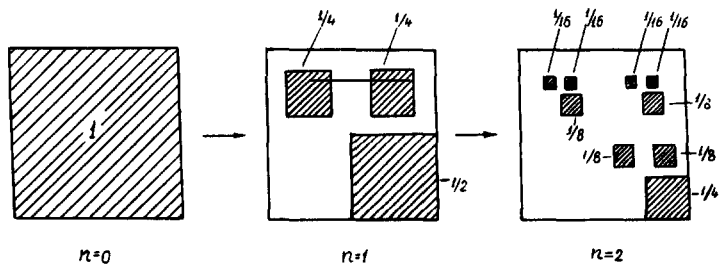

Fig. 6.9

or

$$D_q = \frac{1}{q-1} \lim_{\varepsilon \to 0} \frac{\log \int \mathrm{d}\mu(x)\, \mu(B_\varepsilon(x))^q}{\log \varepsilon}\,, \tag{6.26}$$

where p_i is the probability of hitting the ith cube of side ε by a point of the set, the summation is over all the cubes, $\mu(B_\varepsilon(x))$ is the probability of hitting the sphere of radius ε with its centre at the point x (it appears also in the definition of the pointwise dimension). The values of D_q are defined for any $q > 0$, and $D_q > D_{q'}$ if $q < q'$. However, in some cases they coincide with the known dimensions [202],

$$\lim_{q \to 0} D_q = d_c\,, \qquad \lim_{q \to 1} D_q = d_I\,, \qquad D_{q=2} = \nu\,.$$

Thus, calculating the Lyapunov dimension, the correlation exponent, and other dimensions we determine the quantitative characteristics of a large class of fractals. And here the important question arises: Is the temporal dynamics observed in real physical systems determined by a strange attractor of low dimension, stochastic fluctuations or is it a nonstationary transient process? Let us discuss this.

6.3. Determining the fractal dimension from measurements

Suppose we have a device to measure one of the characteristics of a system under investigation at different times at intervals Δt. The measurements yield a bounded sequence $\{a_i\}$, $0 \le i < \infty$.

It is interesting to know whether, on the basis of this sequence, we are dealing with a complex deterministic process which is described by a smooth differential equation $\dot{x} = X(x)$ in the phase space $\mathbb{R}^n$ or with a stochastic function. The answer was obtained by F. Takens [194, 203].

According to ref. [203] the measurements *may be described by a smooth deterministic model* if there are a smooth differential equation $\dot{x} = X(x)$ on the phase space $\mathbb{R}^n$ with a smooth function X and a smooth function $f: \mathbb{R}^n \to \mathbb{R}$ such that

(i) for each observed sequence $A = \{a_i\}$, $0 \le i < \infty$, of experimental data there is a point $\bar{x}_0 \in \mathbb{R}^n$ such that $a_i = f[\bar{x}(i\,\Delta t)]$, where $\bar{x}(t)$ is the solution of the differential equation $\dot{x} = X(x)$ with $x(0) = \bar{x}_0$;

(ii) for each initial point $x_0 \in \mathbb{R}^n$, the solution $x(t)$, $x(0) = x_0$, for $t > 0$ is bounded.

If for some sequence $A = \{a_i\}$ we can construct the functions f, X and the integral curve $\bar{x}_0(t)$ we say that the results of the above experiment may be explained with the aid of a smooth deterministic model.

In order to formulate the criterion of Takens we introduce several definitions. Let $A = \{a_i\}$, $0 \le i < \infty$, be a bounded sequence of real numbers (experimental data). For $\varepsilon > 0$ and $n \in \mathbb{N}$, where $\mathbb{N}$ is the set of integers, we define the set $\mathscr{C}_{n,\varepsilon} \subset \mathbb{N}$ as follows: $0 \in \mathscr{C}_{n,\varepsilon}$; for $i > 0$, $i \in \mathscr{C}_{n,\varepsilon}$ if and only if for all $0 \le j < i$ with $j \in \mathscr{C}_{n,\varepsilon}$ we have

$$\max\{|a_i - a_j|, |a_{i+1} - a_{j+1}|, \ldots, |a_{i+n} - a_{j+n}|\} \ge \varepsilon\,.$$

The number of elements of $\mathscr{C}_{n,\varepsilon}$ is denoted by $C_{n,\varepsilon}(A)$. Since the sequence A is bounded, $C_{n,\varepsilon}(A)$ is finite.

In ref. [203] the following statements were formulated. The experimental results determined by the sequence A may be explained by a smooth deterministic model if the expression

$$\frac{\ln C_{n,\varepsilon}(A)}{n - \ln \varepsilon} \tag{6.27}$$

is uniformly bounded as $(n - \ln \varepsilon) \to \infty$. But if this limit is unbounded the sequence A cannot be explained by a smooth deterministic model.

In the criterion of Takens the infinite sequence A is employed. In fact, experiment gives a finite number of measurements, and we have to deal with the function $C_{n,\varepsilon,m}(A)$, where m is the sample length, rather than with $C_{n,\varepsilon}(A)$. The quantity $\ln \varepsilon$ is also bounded (for example, by the finite accuracy of measurements); the boundedness of the limit can be checked only for a finite number n. However, if by using a computer we can verify that, as m and n increase while ε decreases, the limits do not, in fact, change, it may be assumed that the physical system is well described by a finite-dimensional deterministic model. (A somewhat different algorithm is usually used; it will be considered later on.)

It is important that the existence of deterministic chaos in a nonlinear medium can be established by measuring any of the dynamic variables at one point for almost any interval Δt in which measurements are made. This conclusion is based on the result by Takens, who showed that, for a compact manifold M of dimension p, a diffeomorphism $g: M \to M$ and a smooth function $f: M \to \mathrm{R}$, the map $\Phi_{g,f}(x) = (f(x), f(g(x)), \ldots, f(g^{2m}(x)))$ is generally an embedding. (That is, the operator Φ is a continuous, one-to-one map of M into $\mathbb{R}^{2m+1}$, $m > p$.)

As g in the system of equations $\dot{x} = X(x)$ we may consider the operator of displacement along a trajectory in the time Δt; as the function f we may take one of the dynamic variables $\xi(t)$ (i.e. one of the coordinates of the vector x). In this case the map Φ is determined by the values $\xi(s\,\Delta t)$, $s = 0, 1, \ldots, 2m$. Hence, the fractal dimension of the limit set can be determined by a discrete collection $\xi(t_i)$ (where $t_i \to \infty$): $\xi_1, \ldots, \xi_n$. With these data we can construct a collection of m-dimensional vectors

$$\zeta_k = (\xi_k, \xi_{k+1}, \ldots, \xi_{k+m-1}) \tag{6.28}$$

for $m = 1, 2$ etc. and determine the dimension (usually the correlation exponent ν) of the set $\{\zeta_k\}$ in the m-dimensional phase space. If the dimension of the attractor M is finite and equal to p it may be expected that for $m > 2p + 1$ the values obtained will be independent of m.

This means that there is a collection of $2p + 1$ order parameters, to which all the degrees of freedom of the system "adjust". Such a behaviour is typical for many mathematical models studied by synergetics [3, 13], including non-linear systems with an infinite number of degrees of freedom, which are described by partial differential equations. Sets that consist of vectors of the form (6.28) are usually called sets in *ζ-space* while their construction is called the reconstruction of the attractor.

Analysing sets in ζ-space allows us to propose a number of algorithms for computing the fractal dimension, which are more efficient than those developed in ref. [198], where the attractors are investigated in the usual phase space (X-space).

As is mentioned above, using the standard algorithm of computing the correlation exponent ν requires storing N vectors (Np numbers) and $\sim N^2 p$ operations to compute the function $C(\varepsilon)$ [see formula (6.22)].

Meanwhile, computation of the correlation integral $C(\varepsilon)$ for the set in ζ-space requires storage of N words and $\sim N^2 + Np$ operations. In fact,

$$\rho^2(\zeta_k, \zeta_m) \equiv \left| \sum_{i=0}^{p-1} (\xi_{k+i} - \xi_{m+i})^2 \right|^{1/2},$$

$$k = 1, \ldots, N - p - 1, \quad m = 1, \ldots, N - p - 1, \quad m - k = \text{const.}, \tag{6.29}$$

$$\rho^2(\zeta_{k+1}, \zeta_{m+1}) = \rho^2(\zeta_k, \zeta_m) + (\xi_{k+p} - \xi_{m+p})^2 - (\xi_k - \xi_m)^2 .$$

Formula (6.29) determines the so-called "sliding sum" algorithm [195] and enables us to compute $\rho^2(\zeta_{k+1}, \zeta_{m+1})$ by adding to and subtracting from $\rho^2(\zeta_k, \zeta_m)$ one term regardless of the dimension of the space.

More efficient algorithms may be proposed for computing capacity and information entropy. They require a storage of less than $4N$ and a number of operations less than N^2 [195]. The idea of such algorithms is connected with the ordering of ζ-vectors by the first component, due to which the number of required comparisons can be decreased.

Besides, preliminary ordering allows us to construct algorithms for computing the correlation exponent in which the number of operations does not depend on the sample length N. They may be very helpful when the samples are large, $N > (l_0/\varepsilon_{\min})^d$, where l_0 is the characteristic length of the attractor, d is the dimension of the attractor, and $\varepsilon_{\min}$ is the minimal distance between vectors ζ_m and ζ_n that can be measured with confidence.

In recent years algorithms have been developed to estimate the Lyapunov exponents from experimental data a_i [201, 204]. To do this, an arbitrary p-dimensional vector $\zeta_k = (a_k, \ldots, a_{k+p-1})$ is constructed and nearby ζ-vectors $\zeta_{m_1}, \ldots, \zeta_{m_s}$ are searched for,

$$\|y_i\| = \|\zeta_k - \zeta_{m_i}\| < \varepsilon\,, \quad 1 \le i \le s\,.$$

Then images of these vectors, $\zeta_{m_1+r}, \ldots, \zeta_{m_s+r}$, are considered in r steps.

Due to the close proximity of these vectors we may consider that there is a linear operator $B_{ij}(r)$ such that

$$z_i = B_{ij}(r) y_j\,, \quad z_i \equiv \zeta_{m_i+r} - \zeta_{k+r}\,, \quad 1 \le i, j \le p\,.$$

This operator transforms the sphere with the vectors y_i into an ellipsoid containing the vectors z_i. The semi-axes of this ellipsoid are determined by the eigenvalues of the linearized problem.

After this, calculating the Lyapunov exponents is reduced to determining the operator B and its eigenvalues with a set of vectors y_i and z_i. Then new vectors ζ_k are chosen, and the same procedure is repeated. Finally, the eigenvalues obtained are averaged over the trajectory of the dynamic system.

It is not difficult to find the maximum Lyapunov exponent. Algorithms that give a set of positive exponents are discussed in ref. [201]; there one may also find a bibliography of previous publications. In ref. [204] a technique is proposed for constructing and analysing the operator B to find then the complete set of Lyapunov exponents. From the tests given in ref. [243] it follows that the approach may be useful for a restricted class of problems.

6.4. Experimental study of few-mode chaos

Analysis of the general properties of dynamic systems enabled us to suggest that complex stochastic regimes in non-linear media are usually associated with complex interactions of several variables (i.e. with a strange attractor of low dimension) rather than with the excitation of an infinite number of harmonics as was earlier supposed [76, 170]. It should be stressed that this suggestion is of a general nature and refers not only to the transition from laminar to turbulent flows in hydrodynamics but to stochastic regimes in oscillatory reactions, to some systems in nonlinear optics, and to many other phenomena as well. Algorithms developed lately for analysing fractals, and strange attractors allow experimental tests of this suggestion.

One of the systems where the transition from the ordered laminar regime to chaotic turbulence can be observed is Taylor–Couette flow. This is fluid flow between two coaxial cylinders of length L, whose radii are, respectively, a and b. The external cylinder rotates with an angular velocity Ω_2 and the internal one with Ω_1. The Reynolds number in this problem is given by the formula $\mathrm{Re} = \Omega_1 a(b-a)\nu^{-1}$ for $\Omega_2 = 0$ (ν is the kinetic viscosity).

When the Reynolds numbers are small the fluid flow is laminar and may be described by an explicit expression. Then, as the rotational speed Ω_1 increases dissipative structures (so-called Taylor vortices) emerge. Increasing Ω_1 further, the Taylor vortices lose their stability, and the fluid motion becomes periodic (an analog of the limit cycle). At even larger Reynolds numbers a two-frequency regime appears (similar to the invariant torus), and then the motion becomes turbulent. Thus, the transition to chaos observed in the experiment at certain values of Ω_1, a, b, L, ν occurs according to the Ruelle–Takens scenario [205].

In order to analyse this flow an effective experimental technique involving laser Doppler spectrometry was proposed. By measuring the Doppler shift of the laser beam propagating through the fluid we may measure one of the velocity components at a given point. Successive measurements of this component yield the set $a_1, \ldots, a_N$. In ref. [27] more than 32 000 points were statistically processed. By considering the variable $a(t)$ we may distinguish the average time T over which this variable takes the same value $\bar{a}$ ($\mathrm{d}a/\mathrm{d}t > 0$). In dynamic systems it is the average time of return to the Poincaré plane. In the experiment a time interval of about $300T$ (300 orbits) was chosen to cover approximately 100 points along the orbit ($\Delta t \sim 10^{-2}T$). From these data the correlation exponent and the positive Lyapunov exponents were computed, and the topological entropy was independently calculated. With these values the dimension of the attractor in the system under investigation was then estimated. It turned out that as the Reynolds number grew ($\mathrm{Re} > \mathrm{Re}_c$) the dimension of the attractor increased; however, in the interval $\mathrm{Re}_c \lesssim \mathrm{Re} \lesssim 1.3\,\mathrm{Re}_c$ it did not exceed 5.4.

Thus, it was shown with confidence that in this infinite-dimensional system few-mode chaos exists. The suggestion that there exists a strange attractor of low dimension which describes this flow, proved valid. This important experimental result testifies that such phenomena may be described, in principle, by a relatively small number of ordinary differential equations. There are similar relationships for fluid flow between rotating spheres [206]. Such a system is interesting in terms of atmospheric physics problems.

Another example of a transition from dissipative structures to turbulent regimes is Rayleigh–Bénard convection in a fluid layer heated from below [207]. The corresponding experiment included 15 000 measurements made over intervals Δt ($T/\Delta t \sim 2$–10) and the correlation exponent was determined. First, the dimension p of the ζ-vectors was given and the correlation exponent was calculated. Then the value of p increased until ν stopped changing. Note that some authors did not perform computations for all N^2 distances but for the distances from n_1 points to the remaining points of the set (in ref. [207] $n_1 = 100$, in ref. [208] $n_1 = 15$). This approach does not have a sufficiently rigorous justification; however, it is widely used in physical experiments because it manages with much smaller amounts of computation. Experimental studies of the Rayleigh–Bénard instability showed that in many convective flows the turbulent regime was defined by a strange attractor of low dimension ($2.5 \lesssim \nu \lesssim 6$). Increasing the Reynolds number and passing to the systems where other complicated factors needed to be taken into account usually led to a growth in the dimension [207].

In the above mentioned works the fluid motion was considered in a bounded volume. Therefore, it is natural to expect that due to viscosity the motion will be damped on small scales, and the attractor will prove to be finite dimensional. In view of this, it is of particular interest to study experimentally

stochastic flows where the fluid motion occurs in an unbounded domain. As examples the motion of a periodically excited isothermal jet [209] and "submerged spray" type flow were considered. In these studies the correlation exponents were computed and the behaviour of the system depending on the spatial coordinate was examined. It turned out that in these cases the motion was also determined by a strange attractor of low dimension.

The results of physical and numerical experiments where few-mode chaos has been investigated allow a new insight into the phenomenon of turbulence, and a new understanding of the role played by fractals and strange attractors in science. At the same time, many methodological problems are still to be solved. Test computations show that with bounded samplings the ratio $\Delta t/T$ is an important parameter. The choice of the linear portion of the curve of $\ln C$ versus $\ln \varepsilon$ is also of importance. Solving these questions of technique would allow enhanced accuracies in determining the fractal dimension, help in studying few-mode chaos, and extend the class of systems where such effects might be discovered.

7. Transition to chaos and differential equations

In the last century mathematical models were constructed with main attention paid to Hamiltonian systems typical of celestial mechanics problems. However, in the thirties of this century a large class of problems appeared in connection with investigations of dissipative systems. Their appearance was due to the rapid development of radio physics and the theory of oscillations. The system of two ordinary differential equations that depend on a parameter,

$$\mathrm{d}X/\mathrm{d}t = P(X, Y, \lambda)\,, \qquad \mathrm{d}Y/\mathrm{d}t = Q(X, Y, \lambda)\,, \tag{7.1}$$

proved to be an efficient model which could explain many phenomena observed.

The class of nonlinear functions P and Q may be very extensive; however, it is natural to use such P and Q for simulating real systems that the solution would not change qualitatively under small perturbations of these functions. It is these we should consider in the first place. The mathematical formulation of such representations was given by A.L. Andronov and L.S. Pontryagin, leading to the concept of *crudeness* or *structural stability* of a system [86].

This concept is common for many sections of mathematics, and it may be explained by a simple example of a family of functions that depend on one parameter,

$$F(x, \varepsilon) = 0\,. \tag{7.2}$$

For illustration we consider two different functions (fig. 7.1a,b). It is easy to see that the number of zeroes of the first function will not change under small deformations of the curve. In the second case things are different. The equation $F(x) = 0$ has two solutions, $F(x) + \varepsilon = 0$ has one solution (fig. 7.1c), and $F(x) - \varepsilon = 0$ three solutions, however small we choose the positive number ε. It is natural to consider the system described by (7.2) with the function of fig. 7.1b as noncrude. The two other functions F describe crude systems. Crude cases are sometimes called the *cases of a general position*.

Considering a specific model we may always assume that it is crude. But if we are interested in a whole family of models depending on a parameter λ, noncrude situations will sometimes be en-

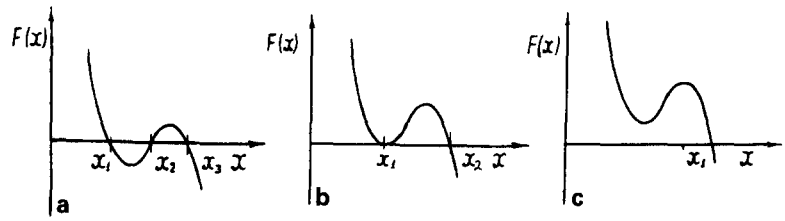

Fig. 7.1

countered too. For example, when the parameter ε changes we transfer from one crude system (see fig. 7.1a) to another (see fig. 7.1c) through a noncrude system (see fig. 7.1b).

The notion of crudeness can be clarified. It is natural to require that differential equations close to the one given be reduced to it as a result of a change of variable. In such a definition, however, the derivative on the right-hand side at the singular point proves to be invariant. Therefore, the systems $\dot{x} = ax$ and $\dot{x} = (a + \varepsilon)x$ cannot be considered close. In order to avoid this a more general definition based on topological representations is introduced. It requires that a continuous one-to-one correspondence should exist between the phase curves of the first and the second system [85, 175].

We can give examples of crude dynamic systems on two-dimensional surfaces. Among them are equations whose attractor is a singular point if an eigenvalue of the linearized equations at this point is not zero. For example, such is the stable focus (see fig. 7.2a) or the node (fig. 7.2b). If the eigenvalue is zero a small change in the parameter alters the number of points or their stability.

The Poincaré map of the limit cycle in crude systems has no eigenvalue whose absolute value is equal to unity. Noncrude systems are those of the form of (7.1) in which there are homoclinic (fig. 7.3a) or heteroclinic (fig. 7.3b) trajectories.

It was proved that eqs. (7.1) determine structure-stable systems if they have a finite number of nondegenerate singular points and cycles and have no homoclinic and heteroclinic trajectories.

It has been proved that structurally stable systems of the form of (7.1) form an open, everywhere dense set in the space of all such systems [85].

This important result agrees with the intuitive idea that in the space of parameters crude systems must exist as close as desired to noncrude ones. By considering crude systems in detail we may understand all the basic types of qualitative behaviour of the models (7.1).

The question arises: Can analogous results be obtained for systems of higher dimension? In generalizing the crudeness conditions an important class of crude multi-dimensional systems (the Morse–Smale systems) was introduced. In the equations that determine them all the solutions tend to

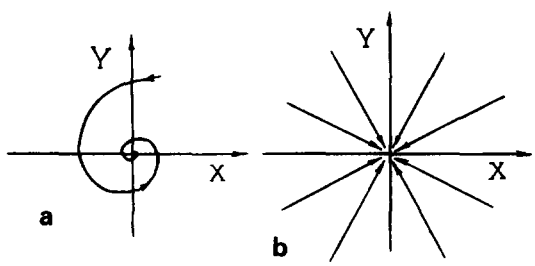

Fig. 7.2

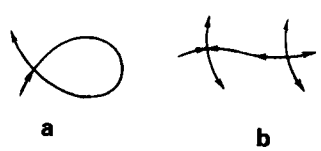

Fig. 7.3

periodic trajectories or singular points for both $t \to \infty$ and $t \to -\infty$. There are a finite number of periodic trajectories and fixed points, all of them hyperbolic, their stable and unstable manifolds intersecting only transversally (at a nonzero angle). (A point is called hyperbolic when the real parts of all eigenvalues λ_i of the linearized system of equations are different from zero. A cycle is called hyperbolic if its Poincaré map does not have λ_i with $|\lambda_i| = 1$.)

Fundamental results dealing with the properties of dynamic systems in the multi-dimensional case were obtained by S. Smale. They are discussed in detail in the reviews [175, 213].

It has turned out that not all crude systems are Morse–Smale systems. For example, U-systems are structurally stable but have an infinite number of closed trajectories. (Simple examples of U-systems are given in chapter 5.) Besides, Smale constructed an example of a dynamic system in the vicinity of which there are no crude systems.

Such a behaviour is due to the existence of chaotic regimes and the appearance of complex invariant sets (such as in the Smale horseshoe).

These results show that the problem of a complete topological classification of differential equations of rather high dimension cannot be solved.

However, studying chaotic regimes in dynamic systems with continuous time appears to be very interesting. The analysis proves rather complex and requires extensive numerical experiments. This is why the investigated systems with chaotic behaviour are not great in number. Nevertheless, some interesting phenomena have been discovered, new approaches and methods of investigation developed, and important concepts applicable to many models created. Let us consider some of them.

7.1. The Lorenz system. Homoclinic explosion

The Lorenz system is a system of ordinary differential equations which appears to have aroused much interest in recent years. The methods of the qualitative theory of ordinary differential equations, topology, hyperbolic theory and other sections of mathematics have been widely used for its analysis. Due to this approaches and ideas useful for studying strange attractors in other dynamic systems have been extended. An extensive bibliography of works dealing with the Lorenz system may be found in the book [137] and the review [214].

The system was proposed as a simplified model for describing Bénard convection in a fluid layer heated from below. In this problem the fluid motion depends on two dimensionless parameters. The first parameter is the Rayleigh number

$$R = \alpha g d^3 \Delta T / \nu \kappa ,$$

where α is the volume expansion coefficient of the fluid, g is the free-fall acceleration, d is the fluid layer thickness, ΔT is the temperature difference between the lower and upper layers of the fluid, ν is the viscosity, and κ is the heat conductivity coefficient. The second parameter is the Prandtl number,

$$\mathrm{Pr} = \nu / \kappa .$$

The equations describing the fluid motion have an equilibrium solution when the fluid is at rest, and its temperature varies linearly with depth. Rayleigh discovered that when $R > R_c = 27\pi^4/4$ the solution is unstable and convection develops.

In the simplest case, using the Galerkin method we can obtain a system of three ordinary differential equations [76],

$$\dot{X} = -\sigma X + \sigma Y\,, \quad \dot{Y} = -XZ + rX - Y\,, \quad \dot{Z} = XY - bZ\,, \tag{7.3}$$

where $r = R/R_c$, $b = 8/3$. The attractors on the line $\sigma = 10$ were investigated in most detail.

The system (7.3) is dissipative. The volume V of the small domain of phase space where each point moves according to (7.3) varies by the law

$$\dot{V} = \Omega V\,, \qquad \Omega = \frac{\partial \dot{X}}{\partial X} + \frac{\partial \dot{Y}}{\partial Y} + \frac{\partial \dot{Z}}{\partial Z} = -(\sigma + b + 1)\,. \tag{7.4}$$

It is invariant under the transformation $X \to -X$, $Y \to -Y$, $Z \to Z$.

When $r < 1$ the coordinate origin is globally attracting: $X \to 0$, $Y \to 0$, $Z \to 0$. There is no convection.

For $r = 1$ the linearized problem that determines the stability of the point $(0, 0, 0)$ has a zero eigenvalue. Bifurcation occurs, and as a result the point $(0, 0, 0)$ loses its stability and two symmetric equilibrium states appear,

$$X = \pm\sqrt{b(r-1)}\,, \quad Y = \pm\sqrt{b(r-1)}\,, \quad Z = r - 1\,.$$

An example of such a bifurcation is shown in fig. 3.6a. As r increases a pair of complex-conjugate eigenvalues of the stable equilibrium states appears.

When $r > 1$ the origin of coordinates is a saddle which has two stable directions and one unstable direction. Trajectories entering it near zero belong to a certain surface – the stable manifold. Two symmetric trajectories – the unstable manifolds of zero – come out of it. Then they spiral about the stable points (fig. 7.4a).

As the parameter r increases the turns of the spirals become larger and larger, and when $r = r' \approx 13.926$ a pair of trajectories (called homoclinic) appears. The points move along them tending towards the origin for both $t \to \infty$ and $t \to -\infty$ (fig. 7.4b).

The appearance of such trajectories proves to be very important. In order to determine how their appearance changes the dynamics of the system it is convenient to consider a small box near zero and two tubes round the unstable manifolds of zero.

According to ref. [137] we may explain what happens with the aid of several diagrams. We consider a small rectangle ABCD on the top face of the box. Points A and D belong to the stable manifold of the origin, and the trajectories crossing AD tend to it when $t \to \infty$. Hence, the integral curves going through ABCD will cross the side face of the box within the triangle MNP (figs. 7.5, 7.6).

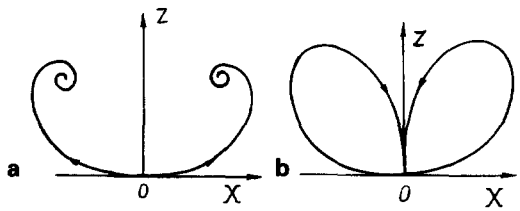

Fig. 7.4

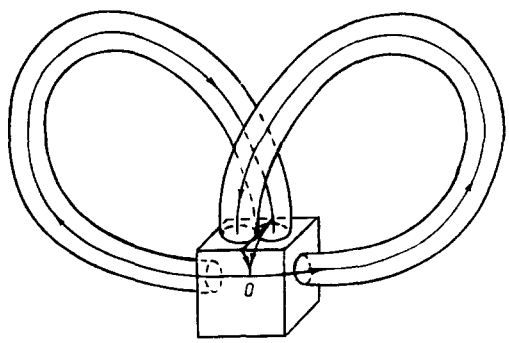

Fig. 7.5

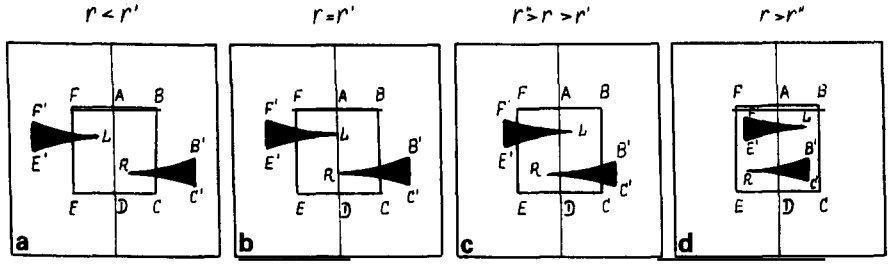

Fig. 7.6

There are no singular points on the trajectory going along the tube from the side to the top face of the box. Therefore the triangle MNP will not be "strongly deformed". After the first return of the trajectories onto the plane of the top face the image of the rectangle ABCD is the triangle RB'C' (fig. 7.6), where R is the point of intersection of the right-hand unstable manifold with this plane. Since there is a homoclinic trajectory at $r = r'$, R hits exactly the line AD (fig. 7.6b). The images of the rectangles ABCD and ADEF, which change depending on the parameter r, are shown in fig. 7.6. The Lorenz system determines a two-dimensional map of the top face of the box into itself.

When $r > r'$ there is an extension along the horizontal direction and compression along the vertical direction. Due to this behaviour the concepts of hyperbolic theory could be used to investigate the Lorenz model [158, 214]. Since the rectangles stretch and fold in a certain way we may expect that this two-dimensional map will behave like the Smale horseshoe and generate complex invariant sets for $r > r'$.

In fact, we choose four small symmetric squares 1, 2, 3, 4 in the rectangle FBCE and see how they will intersect their images $\psi(1)$, $\psi(2)$, $\psi(3)$ and $\psi(4)$. A schematic view is shown in fig. 7.7a. We exclude from our considerations all the points whose iterations do not get into these squares. Then the trajectory of each remaining point may be described by the sequence of four symbols 1, 2, 3, 4. The rules for combining these symbols so that they should correspond to the trajectory of some point may be presented in the schematic form shown in fig. 7.7b.

It is clear that here, as in the Smale horseshoe, an infinite set of periodic trajectories and an uncountable infinity of various aperiodic trajectories may be constructed. This phenomenon occurring immediately after the appearance of a homoclinic trajectory was called the *homoclinic explosion*.

Homoclinic explosions in other systems with symmetry may differ from that discussed above (they can be imagined if before the explosion the triangle C'B'R does not get into ABCD but into ADEF). In dynamic systems a complex sequence of homoclinic explosions may occur [137].

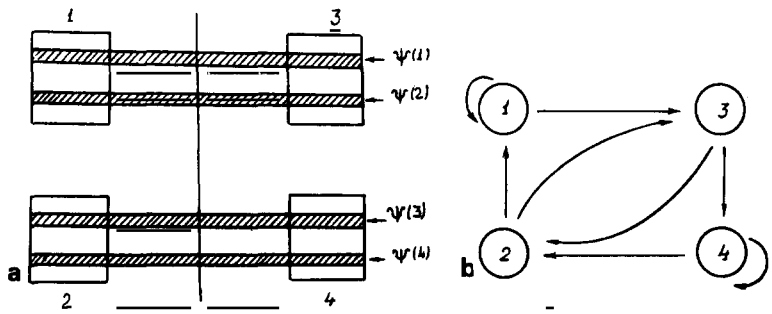

Fig. 7.7

The phenomena typical for the Lorenz model, for $r > r'$, are intrinsic to many nonlinear equations. In fact, the behaviour of trajectories in a small box around the origin agrees with the behaviour of solutions of the system linearized about zero (which is determined by the eigenvalues and eigenvectors of the matrix obtained). This important circumstance can be used to analyse the solutions near homoclinic trajectories [215, 216]. In order that the picture be qualitatively like the one in the Lorenz system at the first homoclinic explosion it is sufficient that the three ordinary differential equations have the same symmetry and the eigenvalues of the matrix of the linearized system of equations near the origin be real and satisfy the inequalities $-\lambda_2 > \lambda_1 > -\lambda_3$, where λ_3 is the eigenvalue corresponding to the eigenvector lying on the symmetry axis [137].

The invariant sets which appear are not attractors for $r = r'$ as in the Smale horseshoe case. In fact, it is seen from fig. 7.6 that the rectangle ABCD does not transform into itself – after each iteration some trajectories leave it. However, there is a value of r'' for which the triangles C'B'R and E'F'L are entirely within ABCD. For $r = r''$ a strange attractor emerges.

If $r \to r''$ $(r < r'')$ metastable chaos is observed. Nearly all the trajectories from ABCD behave in a complex aperiodic way but then tend towards one of the stable points.

For $r = r'''$ the singular points lose their stability due to an inverse Hopf bifurcation, and the asymptotic behaviour of almost all trajectories is determined by the strange attractor. In this region of parameters it is often called the *standard Lorenz attractor.*

The existence of homoclinic trajectories proves to be important not only for analysis of the Lorenz model and other systems with symmetry but for the study of a large class of other equations.

L.P. Shil'nikov [216] considered dynamic systems of the form

$$\dot{x} = \rho x - \omega y + P(x, y, z), \quad \dot{y} = \omega x + \rho y + Q(x, y, z), \quad \dot{z} = \lambda z + R(x, y, z), \tag{7.5}$$

where P, Q, R are functions that are equal to zero together with their first derivatives at the point $(0, 0, 0)$. It was assumed that the singular point at the origin was a saddle focus $\rho < 0$, $\lambda > 0$ and also $\lambda > -\rho$ (see fig. 7.8). If one of the trajectories Γ_0 starting from the saddle focus returns to it as $t \to \infty$ we may prove that in any vicinity of Γ_0 there are an infinite number of periodic trajectories. This statement is called the *Shil'nikov theorem.*

Moreover, the two-dimensional maps generated by these equations have complex invariant sets. A bibliography of works dealing with an analysis of various physical phenomena that lead to eqs. (7.5) may be found in the book [161].

7.2. *Complication of attractors in the dynamic system* (3.15)

Let us see how the solutions become complicated with varying the parameters of a dynamic system. According to refs. [103, 108, 159, 217] we consider the system of equations (3.15). Unlike the Lorenz

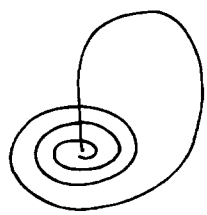

Fig. 7.8

system, it is not invariant under a change of sign of the variables. We may expect that its behaviour will be simpler and more typical.

From the first two equations it follows that

$$2\dot{\xi} + \dot{\eta} = 2(2\xi + \eta) - (2\xi + \eta)^2 - \eta^2/2 - 2k^2\eta - 4\xi\eta(1 + \cos\theta) \leq 2(2\xi + \eta) - (2\xi + \eta)^2 .$$

From the last inequality it follows that $2\xi + \eta \leq z$, where $z(t)$ is the solution of the equation

$$\dot{z} = 2z - z^2 , \quad z(0) = 2\xi(0) + \eta(0) \geq 0 .$$

Since $z(t)$ is bounded and $\xi \geq 0$, $\eta \geq 0$, the functions $\xi(t)$ or $\eta(t)$ are also bounded.

An important characteristic of the dynamic system is the quantity Ω which determines the rate of change of a small volume moving along the trajectories, $\dot{V} = \Omega V$. This parameter describes the dissipative properties of the system and shows how quickly its solutions converge to the attractor. In this case

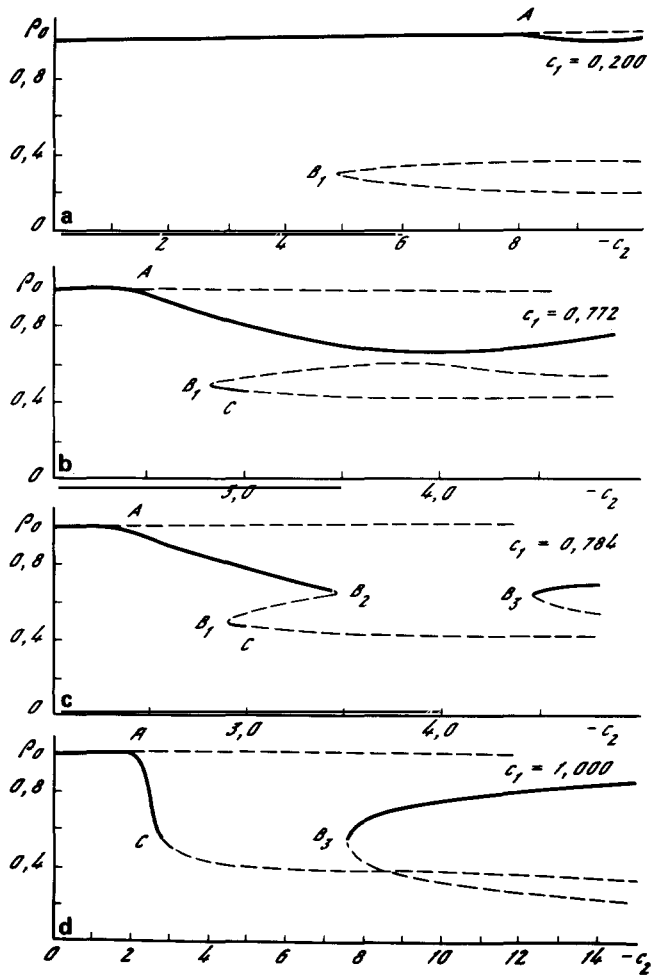

Fig. 7.9. Patterns of singular points for different values of c_1. The solid line marks stable singular points, the dashed line unstable points. The axis $\rho_0 = 0$ is unstable.

$$\Omega = \frac{\partial \dot{\xi}}{\partial \xi} + \frac{\partial \dot{\eta}}{\partial \eta} + \frac{\partial \dot{\theta}}{\partial \theta} = 4 - 2k^2 - 8\xi - 5\eta\,. \tag{7.6}$$

When $k < \sqrt{2}$, in phase space a region appears where $\Omega > 0$. No stable points and to stable limit cycles can lie in this region. However, the attractors which we shall consider below are entirely outside this region.

The simplest solutions of eqs. (3.15) may be obtained by putting $\dot{\xi} = 0$, $\dot{\eta} = 0$. One of them is the invariant straight line

$$\xi = 0\,, \quad \eta = 0\,, \quad \theta = 2c_1 k^2 t + \text{const.}\,,$$

as well as the singular points or invariant straight lines

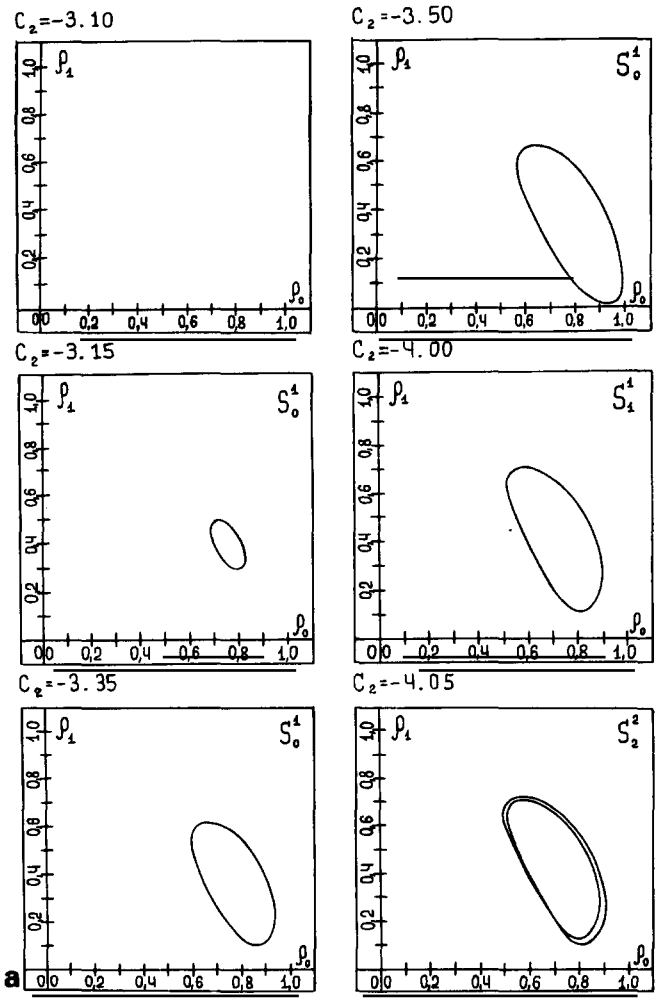

Fig. 7.10(a)

$$\xi = 1\,, \quad \eta = 0\,.$$

The invariant straight line $\theta = \theta(t)$ exists if the inequality

$$c_1^2 k^4 + 2c_1 c_2 k^2 - 1 > 0 \tag{7.7}$$

is fulfilled [217]. A pair of singular points $\xi = 1$, $\eta = 0$ (the saddle and the stable node) arises on the curve $c_1^2 k^4 + 2c_1 c_2 k^2 - 1 = 0$. The node loses its stability on the line

$$(c_1^2 + 1)k^4 + 2k^2(1 + c_1 c_2) = 0\,. \tag{7.8}$$

Another family of particular solutions may be obtained by assuming $\xi = 0$.

By assuming $\dot{\xi}$, $\dot{\eta}$, $\dot{\theta}$ to be equal to zero we may obtain the equation that determines the coordinates

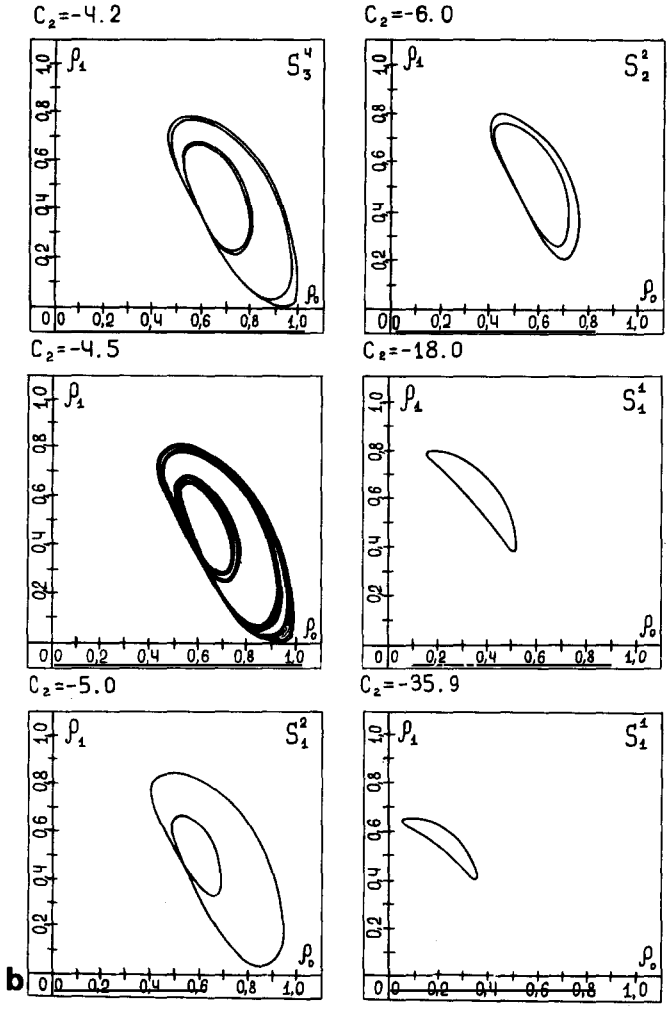

Fig. 7.10(b)

of singular points (ξ, η, θ). After changes of variables and algebraic transformations it is reduced to the fourth-order equation [103, 108]

$$y^4 + by^2 + cy + d = 0 . \tag{7.9}$$

The coefficients b, c, d depend on c_1, c_2, k in a rather complex way. Instead of using the explicit expressions it is convenient to solve eq. (7.9) numerically. Figure 7.9 gives a graphic illustration of the occurrence of equilibrium states. We decrease the parameter c_2 for fixed c_1. The change of $\rho_0 = \xi^{1/2}$ for all the singular points $\xi > 0$, $\eta > 0$ and $\xi = 1$, $\eta = 0$ obtained in calculations is shown in the figure for various values of c_1. The values of the parameter c_2 for which the number of singular points and their stability change are denoted by A, B_1, B_2, B_3, C.

First there is only one singular stable point $\xi = 1$, $\eta = 0$ in the system. At point A a bifurcation of "the stability exchange" type, as in fig. 3.6b, occurs. To the left of point A only one solution is shown in fig. 7.9, since the second solution has $\eta < 0$ and corresponds to complex values of ρ_1.

A pair of equilibrium states appears at points B_1 and B_3 and disappears at point B_2. We saw this type of bifurcation when considering the bending of an asymmetric beam (fig. 3.4).

At point C a bifurcation of the origin of the limit cycle occurs, and due to this a periodic solution appears in the system of equations (3.15). Here we encounter the same simple bifurcations in different combinations.

From fig. 7.9 it is seen that there are two stable singular points simultaneously here and there. Depending on the initial data $\xi(0)$, $\eta(0)$, $\theta(0)$ the solution tends towards one of them. There are regions without stable points, and the attractor in the system must be different.

We fix the parameter $c_1 = 3$ and see what will happen with the solution as c_2 decreases (fig. 7.10). First, there is a stable singular point ($c_2 = -3.10$), then the limit cycle ($c_2 = -3.15$) appears. The cycles in the system of equations (3.15) may be different. It is convenient to distinguish them by the number of revolutions n which they perform around a central region. From formulae (3.15) it is seen that if the functions ξ and η periodically vary with period T, then $\cos\theta$, $\sin\theta$ and $\dot{\theta}$ will have the same period. In this time the phase θ increases by $2\pi m$ ($m = 0, \pm 1, \pm 2, \ldots$): $\theta(t + T) - \theta(t) = 2\pi m$. In the simplest case ($m = 0$) the cycles correspond to closed curves in ξ, η, θ space (fig. 7.11a). If $m > 0$ the functions $\xi(t)$, $\eta(t)$, $\theta(t)$ determine spirals (fig. 7.11b). The cycle described by m and n will be denoted by S^n_m.

At the time of the Hopf bifurcation the limit cycle S^1_0 appears, and as the parameter c_2 decreases it goes over into S^1_1. With decreasing c_2 the amplitude of the stable cycle S^1_0 grows. As the transition point c_2^* is approached the cycle comes closer to the saddles $\xi = 1$, $\eta = 0$ (fig. 7.10). After the transition, $c_2 < c_2^*$, the cycle moves away from them. At $c_2 = c_2^*$ the cycle goes across two singular points. It is natural to expect that in this case $T(c_2) \to \infty$ as $c_2 \to c_2^*$.

Then the period-doubling bifurcations $S^n_m \to S^{2n}_{2m}$ as well as the transitions $S^n_m \to S^n_{m+1}$ occur. Later on chaotic regimes arise (fig. 7.10, $c_2 = -4.5$). As c_2 decreases the attractor of the system becomes simpler. Here inverse period-doubling bifurcations may occur [217, 218].

As was shown in ref. [218], for $k = 1$ the system of equations (3.15) is well described by families of one-dimensional maps in a certain range of parameters. An example of such a family will be given below. It is an interesting and profound fact. It speaks in favour of many simplified models.

Combining numerical and analytical methods allows us to obtain a chart of attractors which shows the type of solution of the system of equations (3.15) for different values of c_1 and c_2 (fig. 7.12). The parameter k is everywhere assumed to be equal to unity.

In a large region of parameters above the line ABC the stable singular point is $\xi = 1$, $\eta = 0$. It adjoins to a region with other singular points whose appearance was noted above. In many cases, for

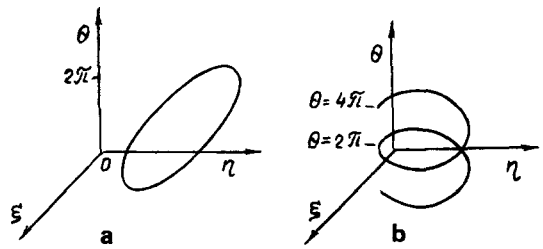

Fig. 7.11

$t \to \infty$ the asymptotic behaviour of the system of equations (3.15) is determined by a simple cycle S^1 or a double cycle S^2. The stability regions of more complex cycles and the regions with as many as two attractors are narrow and not shown in fig. 7.12. The chart of attractors gives a classification of solutions of the system of equations (3.15) for $k = 1$ by their behaviour for $t \to \infty$. The picture obtained is rather simple.

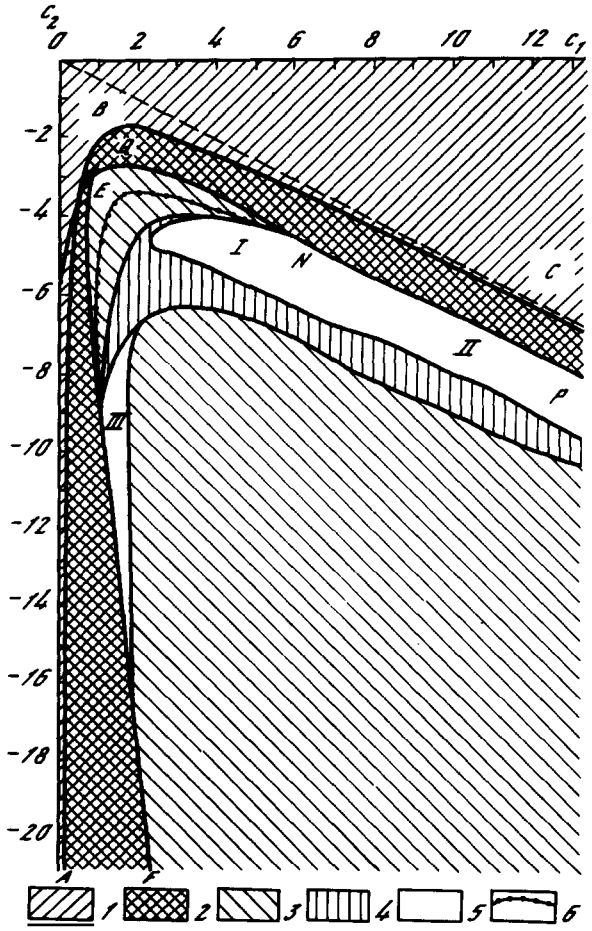

Fig. 7.12. Types of attractors for the system of equations (3.15) for $k = 1$; 1: solution $\xi = 1$, $\eta = 0$; 2: singular point with $\xi > 0$, $\eta > 0$; 3: simple cycle S^1; 4: cycle S^2; 5: more complex solutions; 6: the line where the transition $S_0^1 \to S_1^1$ occurs; QNP is the Hopf bifurcation line. The picture is obtained by numerical solution of eqs. (3.15). A step $h_1 = 1.0$ is taken in c_1 and $h_2 = 0.5$ in c_2. Between the domains the step was decreased to 0.1. Initial data in the problem with parameters $\{c_1, c_2 - h_2\}$ below the line ABC was the point belonging to the attractor of the system of equations (3.15) for values of $\{c_1, c_2\}$. Computations began at $c_2 = 0$.

7.3. *Strange attractor in the dynamic system* (3.15)

We consider one aperiodic solution of the system of equations (3.15) in detail. For this example it is convenient to see how the investigation methods discussed above may be used to study strange attractors of specific ordinary differential equations.

At the present time the number of strange attractors studied in detail is not very large. Therefore, the ideas about systems where dynamic chaos is possible may prove useful for constructing models of various physical phenomena.

In the further discussion we shall pay attention mainly to the attractor of eqs. (3.15) with $c_1 = 7$, $c_2 = -6$, $k = 1$. Its projection on the (ξ, η)-plane is shown in fig. 7.13. It is entirely in the region where the system is dissipative. It is seen that the trajectory may come into the vicinity of saddles $\xi = 1$, $\eta = 0$ and hence, it may stay there for a long time. The mean time T of one revolution about the central region is approximately equal to 1.63, and the mean value of Ω is -4.189. Hence, the phase volume will decrease by a factor 900 per revolution.

We consider successive intersections of the trajectory with the plane $\theta = \text{const}$. Since $\dot{\xi}$, $\dot{\eta}$, $\dot{\theta}$ depend only on $\cos\theta$ and $\sin\theta$ (θ is a cyclic coordinate) it is necessary to consider the intersections with all the planes $\theta = \text{const.} + 2\pi n$, $n = 0, \pm 1, \pm 2, \ldots$. The intersection of the attractor with the plane $\theta = 2\pi n$ is the simplest. Now we shall discuss some of its properties.

The system of equations (3.15) uniquely determines the map of this plane into itself (the *Poincaré map*),

$$\xi_1 = \bar{f}(\xi_0, \eta_0), \quad \eta_1 = \bar{g}(\xi_0, \eta_0). \tag{7.10}$$

Here ξ_1 and η_1 are the coordinates of the point of the first intersection of the trajectory with initial data $\{\xi_0, \eta_0, 0\}$ with the plane $\theta = 0$ ($\theta = 2\pi n$). We shall consider only the intersections for which $\dot{\theta} > 0$. In the (ξ, η)-plane we may distinguish a region which iterates into itself under the map (7.10). It contains the attractor.

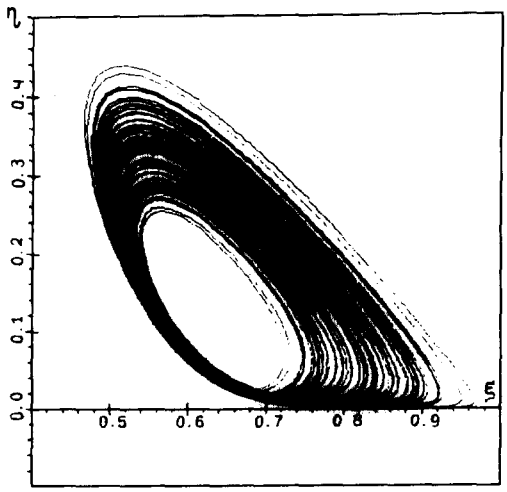

Fig. 7.13

To investigate the Poincaré map it is natural to go over to new coordinates, one of which, x, is close to the stretching direction, while the other, y, is orthogonal to it,

$$x = [3(\xi - 0.45) - 7(\eta - 0.38)]/\sqrt{58}\,, \qquad y = [7(\xi - 0.46) + 3(\eta - 0.38)]/\sqrt{58}\,.$$

The region ABCD that iterates into itself and its image A′B′C′D′ are shown in the new coordinates in fig. 7.14. (We note that figs. 7.14 are strongly stretched along y.) In these coordinates the image of a rectangle is a complex curvilinear figure that consists of two parts. The region APQD is mapped into the lower part. The corresponding trajectories get a phase increment $\Delta\theta = +2\pi$ per revolution. The upper part of the curvilinear figure is the image of BPQC. For the trajectories originating here the phase increment is zero. The segment PQ is entirely mapped onto the point R. We note an analogy between this map and the Smale horseshoe.

The functions f and g that determine the Poincaré map in the new coordinates x, y,

$$x_1 = f(x_0, y_0)\,, \qquad y_1 = g(x_0, y_0)\,, \tag{7.11}$$

are shown in fig. 7.15. These functions are continuous but their derivatives have a discontinuity on the line PQ. On this line the value of f is equal to the x-coordinate of the point R (fig. 7.14); the y-coordinate of this point determines the value of g on the line PQ. The partial derivatives of f and g increase infinitely in the vicinity of the line PQ.

The section of the attractor corresponding to a chaotic regime must have a complex inner structure. The calculations carried out for several models allowed us to reveal this structure. This can also be done for the system under investigation.

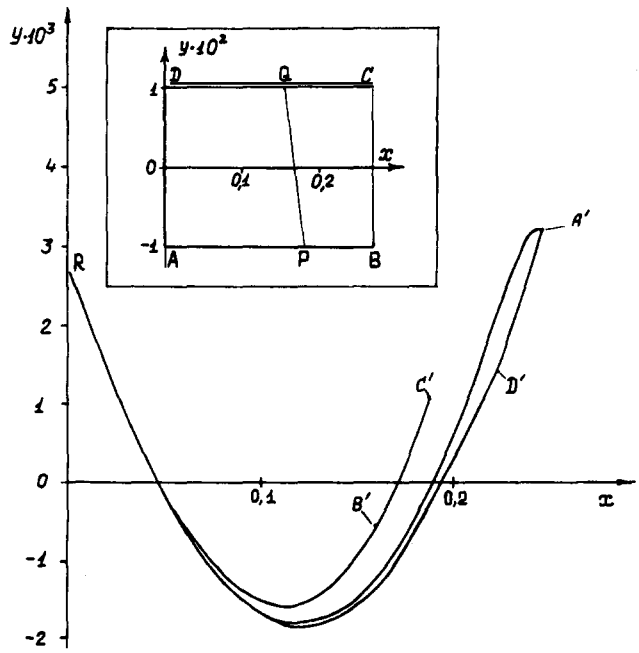

Fig. 7.14

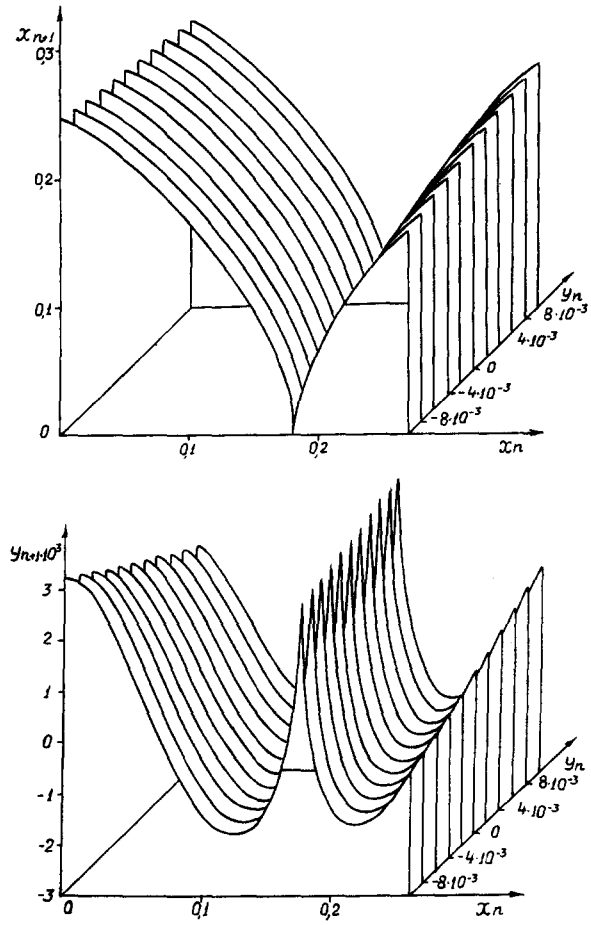

Fig. 7.15

Let us turn to fig. 7.16. Here, the points of intersection of the plane $\theta = 0$ with one of the trajectories are shown on different scales. An enlarged view of the rectangle marked in fig. 7.16a is given in fig. 7.16b. In its turn the rectangle marked in fig. 7.16b is presented on an enlarged scale in fig. 7.16c. The section of the attractor in the upper figure consists of two lines. By the 500-fold increase of resolution each line splits into two. (Note that the distance between lines is very small and does not exceed 4×10^{-7}.) We may expect that this process occurs also on smaller characteristic distances. That is, the attractor along one of the directions has a Cantor structure.

Figure 7.17 shows x_{n+1} versus x_n. On the scale of the figure the points are located on a continuous unique curve F. We note that $|dF/dx| > 1$ everywhere except for one portion on the left end of the segment. The one-dimensional map $x_{n+1} = F(x_n)$ may be considered as a simplified model for the problem (3.15). For its analysis many results obtained in the theory of maps of an interval into itself may be used.

Figure 7.13 shows that the projections of different turns of the trajectory onto the (ξ, η)-plane are qualitatively the same. However, observing their variations in (ξ, η, θ)-space we can distinguish two different types of turns. In one type the phase changes by 2π when the trajectory returns to the plane

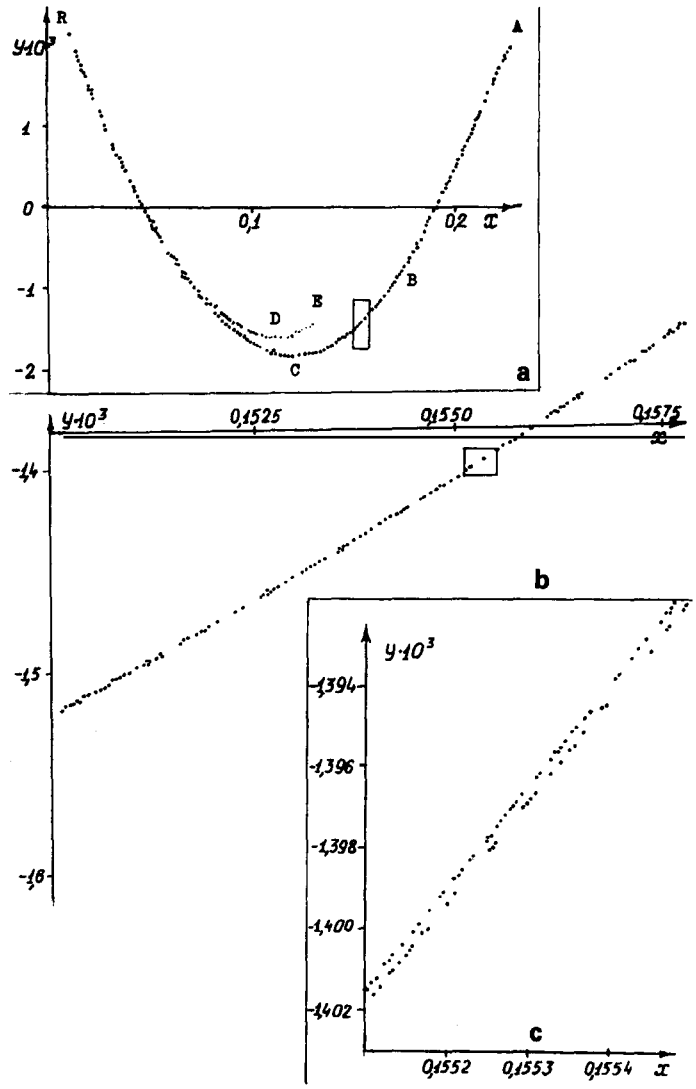

Fig. 7.16

$\theta = 2\pi n$, $n = 0, \pm 1, \pm 2, \ldots$; in the other it does not change. In the one-dimensional map (fig. 7.17) the first type corresponds to the left arm of the curve, the second type to the right arm. If the time of each revolution were bounded from above the functions f and g in the map (7.11) would be continuous and differentiable, and the phase increment $\Delta\theta$ could not suffer a discontinuity. In this case this is not so. We may suggest that this is due to the effect of a certain singular point of the dynamic system (3.15) in whose vicinity the time of revolution may increase infinitely.

An analysis of the behaviour of the trajectories in the vicinity of singular points allows us to understand the specific features of one- and two-dimensional maps arising in this problem. An important property of the system (3.15) is that the plane $\eta = 0$ is an invariant manifold: if $\eta(0) = 0$ then $\eta(t) = 0$ too. In this plane there are two singular points A and B with $\xi^2 + \eta^2 \neq 0$. By considering the

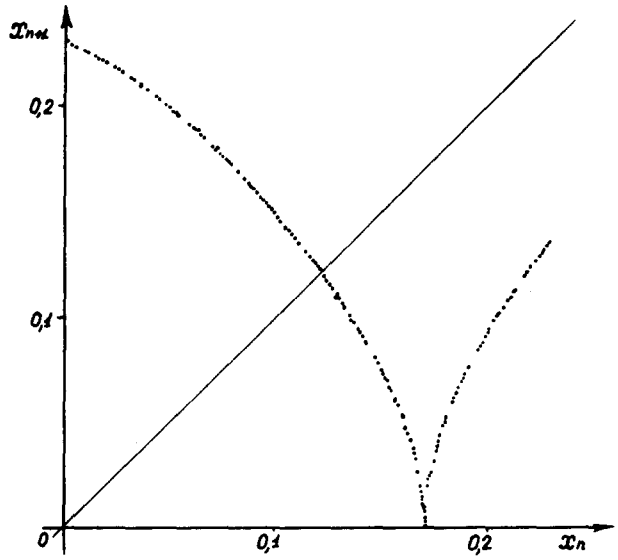

Fig. 7.17

dynamic system linearized in the vicinities of these points we may determine eigenvalues and eigenvectors of the arising matrix. From the analysis it follows that the points A and B are saddles, each having one unstable direction. The line $\xi = 1$, $\eta = 0$, $\theta = \theta(t)$ that connects these points is an integral curve of the system (3.15) for all values of the parameters. The approximate positions of the singular points A and B as well as the eigenvectors of the corresponding matrix are shown in fig. 7.18. The eigenvectors are numbered so that $\lambda_1 < \lambda_2 < \lambda_3$, $\lambda_1' < \lambda_2' < \lambda_3'$. The surface M is a stable two-dimensional

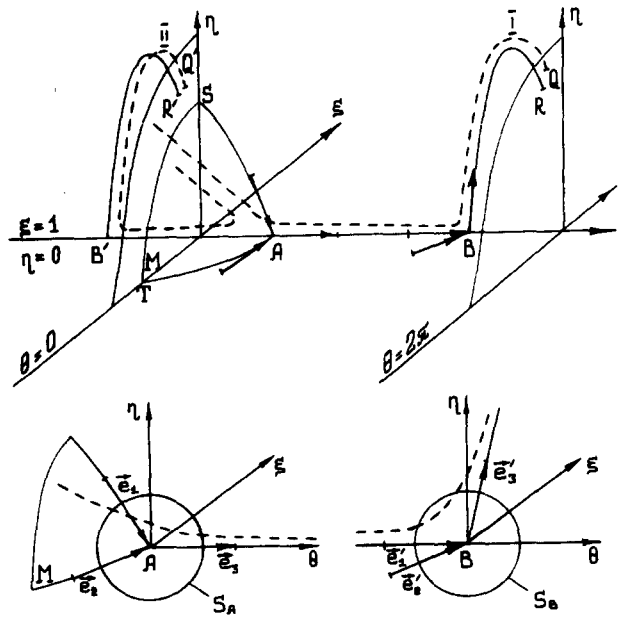

Fig. 7.18

manifold of the point A. The straight line $\xi = 1$, $\eta = 0$ is an unstable manifold of the point A. The plane $\eta = 0$ is a stable manifold of B. The unstable manifold of B intersects the plane $\theta = 2\pi$ at the point R.

Following fig. 7.18 we may present the integral curve originating near the surface M (above it) in the following way. At first the point on the trajectory near M moves towards the point A and further along the line $\xi = 1$, $\eta = 0$ towards the saddle B. Then it moves along the arc BR and intersects the plane $\theta = 2\pi$ at a point Q in the vicinity of the point R. This is curve I in fig. 7.18. Note that the trajectory cannot go out from B downward into the region $\eta < 0$ because then it would have to intersect the plane $\eta = 0$, which consists entirely of integral curves.

Now let the trajectory start below the surface M (curve II in fig. 7.18). In this case the point moves over M but near A it turns left. It comes to the saddle B′ and then gets onto the plane $\theta = 0$ along the curve B′R′. In the first case the phase changed by 2π, in the second case it did not change. The phase increment on the next turn depends on the mutual positions of the manifold M and the points Q and Q′.

The arc B′R′ is obtained from BR by a shift in θ of 2π. Therefore, points R and R′ have the same coordinates ξ and η. The points Q and Q′ lying in their vicinities are also close in ξ and η. This explains the continuous form of f and g in the map (7.11).

The surface M intersects the plane $\theta = 0$ along a line TS. An image of the whole line is the point R (or R′). Formally the Poincaré map is not defined on TS because the trajectories go across two singular points, which requires an infinite time. However, its definition can be completed by continuity. The line PQ in fig. 7.14 is a portion of the arc TS.

From the qualitative picture described it is clear that as the initial point in the plane $\theta = 2\pi n$ comes closer to the line TS the time of revolution will grow infinitely. Analysing the trajectories close to the singular points enables us to determine the function $T(\varepsilon)$, where T is the time of return onto the Poincaré plane and ε is the distance from the initial point to the surface M (the stable manifold of the saddle A). Such an analysis also allows us to calculate the exponent α determining the peculiarities of the arising two- and one-dimensional maps.

In order to obtain this information we should study the behaviour of the trajectories in the vicinity of the points A and B (within the spheres S_A and S_B of small radius r in fig. 7.18). The problem is simplified by the fact that for small r (though greatly exceeding ε) we may consider a linearized system instead of the initial problem. In refs. [159, 217] such an investigation was carried out, and it was shown that

$$T(\varepsilon) = \frac{1}{\lambda_3}\left(1 + \frac{|\lambda_1|}{\lambda_3'}\right)\ln\frac{1}{\varepsilon}\,.$$

Thus the function $T(\varepsilon)$ has a logarithmic singularity. The calculations performed confirm it. In the vicinity of the line PQ (see fig. 7.14) the functions $\bar{f}$ and $\bar{g}$ may be represented in the form

$$\begin{aligned} x_{n+1} &= \bar{f}(x_n, y_n) = f_0 + A(x_n, y_n)[x_n - \bar{x}_0(y_n)]^{\alpha}\,, \\ y_{n+1} &= \bar{g}(x_n, y_n) = g_0 + B(x_n, y_n)[x_n - \bar{x}_0(y_n)]^{\alpha}\,, \end{aligned} \tag{7.12}$$

where

$$\alpha = \min\{|\lambda_1\lambda_1'|/\lambda_3\lambda_3', |\lambda_2|/\lambda_3 + |\lambda_1\lambda_2'|/\lambda_3\lambda_3'\}\,.$$

For $c_1 = 7$, $c_2 = -6$, $k = 1$ we have $\alpha = 1/2$. The value of α near the singularity for $f(x, y)$ with $y = 0$ was obtained to be equal to about 0.51, which testifies to the good agreement between the numerical results and the analytical estimates. From formula (7.12) an important qualitative conclusion follows. For $c_2 > \bar{c}_2$ with

$$\bar{c}_2 = -\frac{(c_1^2+1)k^4 + 6k^2 + 8}{2c_1k^2},$$

the vertex of the arising one-dimensional map must be smooth, $\alpha > 1$; for $c_2 < \bar{c}_2$, it is sharp. As we could see when discussing one-dimensional maps, this may lead to quite different scenarios for the transition to chaos. It also agrees with numerical results.

As has been mentioned above the projection of the trajectories onto the (ξ, η)-plane does not give a complete idea of the geometry of the attractor in three-dimensional space. A portion of the integral curve of the system (3.15) is drawn in the coordinates $x' = \xi \cos\theta$, $y' = \xi \sin\theta$, $z' = \eta$ in fig. 7.19. It is put on a certain surface because the fine structure of the attractor cannot be seen on the scale of the figure. The surface consists of two parts which are connected in the upper region; the point starts moving towards the saddle A, then it moves to the right or left depending on the initial data. Having gone past the saddle B it gets again into the upper part of the attractor. The right band stretches and changes its orientation. The left part of the surface also stretches but does not change orientation.

Hence, it is clear that the attractor in this space may be represented as a Möbius band (the right part) that is attached to the usual ring (the left part). Performing a turn along the right part of the attractor the trajectory increases its phase by 2π, and when moving along the left part it keeps its phase constant.

Such a behaviour allows a symbolic description of the trajectory by comparing it to an infinite sequence of symbols R and L. At the nth place there will be R if the trajectory moves along the right part at the nth turn and L if along the left part. It appears that the topological methods that have been developed for studying the Lorenz attractor [137] may be used here too.

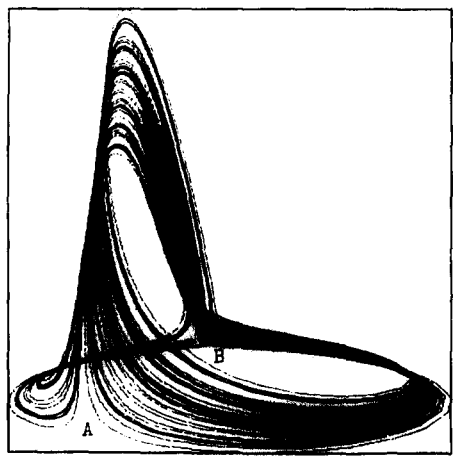

Fig. 7.19

Now let us consider the qualitative characteristics of the attractor discussed. We shall observe the values of the ξ-coordinate at successive intersections of the trajectory with the plane $\theta = 2\pi n$. We construct a histogram from the sequence $\{\xi_n\}$ and normalize it so that the area below the curve is equal to unity. The calculations show that the curve becomes smoother and then constant as the sample length increases. The histogram constructed from $N = 20\,480$ points is shown in fig. 7.20. The number N depends on the interval ε chosen along ξ. The smaller the interval, the larger N for which the histogram in fact stops changing. The same $\rho(\xi)$ was obtained for other initial data. This fact suggests that in three-dimensional phase space also there is an invariant measure which defines the statistical properties of all trajectories converging to the strange attractor.

A typical property of strange attractors is the sensitive dependence on initial conditions. The existence of positive Lyapunov exponents in the solution under investigation testifies to this property.

The attractor of the system of equations (3.15) studied in this case ($c_1 = 7$, $c_2 = -6$, $k = 1$) is described by the following exponents: $\lambda_1 = +0.234$, $\lambda_3 = -4.423$, λ_2 is close to zero within the accuracy of the computations. These values of λ_i were obtained in the computations for different initial conditions. Summing the exponents gives a mean value of Ω, $\lambda_1 + \lambda_2 + \lambda_3 = \langle \partial\dot{\xi}/\partial\xi + \partial\dot{\eta}/\partial\eta + \partial\dot{\theta}/\partial\theta \rangle$, which determines the rate of variation of the phase volume.

An important characteristic of the attractor is its dimension. By knowing the Lyapunov exponents and using the Kaplan–Yorke formula we can estimate the probability dimension of the attractor (dimension of the natural measure) [102]. In this case

$$D = 2 + (\lambda_1 + \lambda_2)/|\lambda_3| \approx 2.05 . \tag{7.13}$$

Since the value of D has a small fractional part it is natural to expect that the behaviour of trajectories on the attractor is described to high accuracy by a one-dimensional map. This agrees with the numerical results in fig. 7.17.

Knowing the trajectory of the system, we may estimate the probability dimension if we compute the correlation exponent. Appropriate results are given in fig. 7.21. For the calculations a fourth-order Runge–Kutta method with step $\tau = 0.01$ was used. The values of ξ were taken as the coordinate in ζ-space with step $\Delta t = 0.25$. A sample length $N = 15\,000$ was considered. Best results were achieved when the attractor was put in ten-dimensional space. The brackets in the plot mark the part closest to

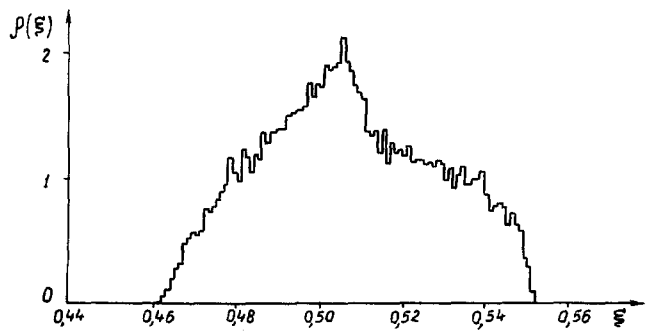

Fig. 7.20

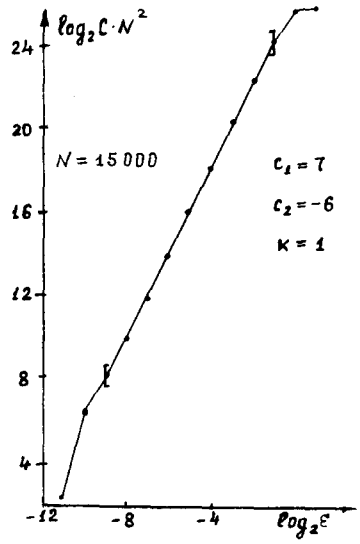

Fig. 7.21

linear. The calculated value of $\nu = 2.035 \pm 0.019$ agrees with the estimate obtained by the Kaplan–Yorke formula (7.13).

Let us stress that here the range of scales over which similarity can be observed is much smaller than in the case of one- and two-dimensional maps. This is also typical for other systems of differential equations.

Another quantitative characteristic of a strange attractor is the self-correlation function

$$b(t) = \frac{\langle \xi(\tau)\xi(\tau + t)\rangle - \langle \xi(\tau)\rangle^2}{\langle \xi^2(\tau)\rangle - \langle \xi(\tau)\rangle^2}, \qquad \langle a(\tau)\rangle = \lim_{T\to\infty} \frac{1}{T} \int_0^T a(x)\,\mathrm{d}x .$$

When $b(t) \to 0$, $t \to \infty$ there is mixing in the system, and it shows that the process under consideration is stochastic. The exponential decrease of correlations proves to be a most prominent stochastic property [152].

Computing $b(t)$ requires determining average values over large portions of the trajectory. In ref. [159] the length of such a portion was estimated, and the function $b(t)$ was given for this attractor. However, we may act differently: go over to a discrete analog of the distribution function $B_N(k)$, where N is the sample length. Again we consider the sequence $\{\xi_n\}$, where ξ_n is the coordinate of the nth intersection of the trajectory and the plane $\theta = 2\pi m$, and the corresponding auto-correlation function $B_N(k)$. Figure 7.22 shows the plots of $B_N(k)$ and its logarithm. It is seen that on this interval $|B_N(k)|$ ($N = 19\,456$) decreases faster than const. $\times \exp(-\lambda k)$, where $\lambda \approx 0.0675$.

In this case an important question is the relationship between N and the number of terms in $B_N(k)$ which can be computed rather accurately. It may be shown that the sums

$$I_1 = \frac{1}{N} \sum_{n=1}^{N} \xi_n \xi_{n+k}, \qquad I_2 = \frac{1}{N} \sum_{n=1}^{N} \xi_n f^k(\xi_n),$$

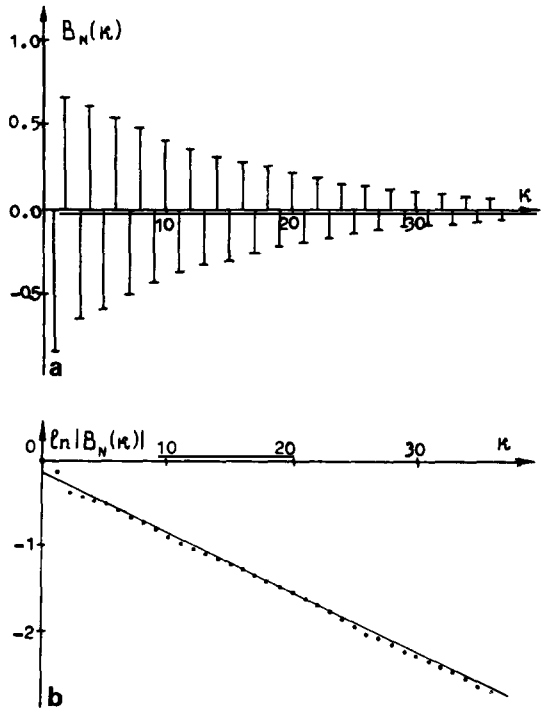

Fig. 7.22

prove to be associated with each other (here f is a continuous function with a single extremum). The sum I_2 approximates the integral

$$I = \int_{\xi_{\min}}^{\xi_{\max}} \xi f^k(\xi)\rho(\xi)\,\mathrm{d}\xi\,,$$

in which the integrand quickly oscillates. The function $f^k(\xi) = f(f(\cdots f(\xi)))$ has 2^{pk} extrema, where $0 < p < 1$, $p = \text{const}$. This follows from the form of f. For numerical integration it is natural to require that there be at least s points for each extremum, so that $N = s \cdot 2^{pk}$. Hence, the number of correct values depends on the sample length according to the logarithmic law

$$k_{\max} = \frac{1}{p}\log_2(N/s)\,, \quad s = 4\text{–}6\,.$$

For $N = 19 \times 2^{10}$ the maximum k is of order 30.

The attractor considered corresponds to one point in the three-dimensional space of the parameters c_1, c_2, k. The questions arise: Is it typical, and will chaotic regimes be observed for nearby parameter values? In order to answer these questions it is convenient to consider the family of maps $M_{n+1} = f(M_n)$ along a line. For M_n we take the nth local maximum of the quantity $\rho_0(t) = \xi^{1/2}(t)$. The maps arising on the line $c_1 = 5$ are shown in fig. 7.23. It is seen that they are close to one dimensional, have a sharp vertex and contain noisy cycles of the type χ^2. It may be expected that due to the sharp vertex chaotic

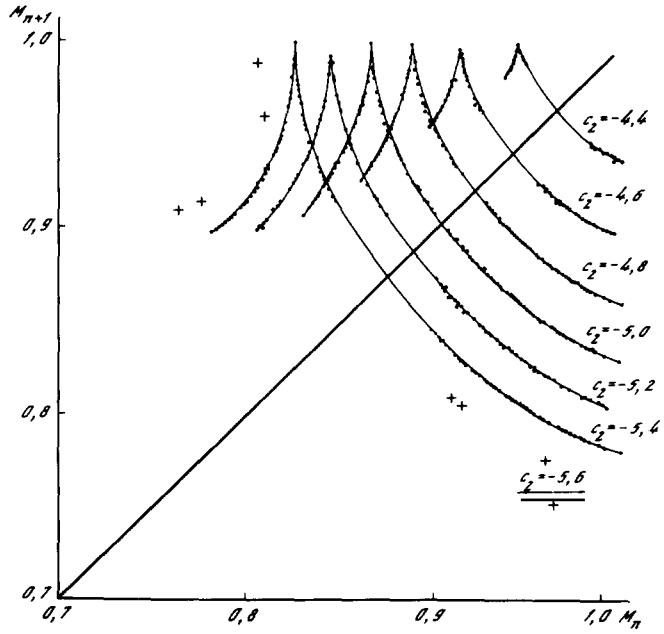

Fig. 7.23

attractors will exist on the whole interval of c_2, and the largest Lyapunov exponent in this interval will be positive. The calculations confirm this premise. In fig. 7.24 it is shown how the Lyapunov exponent changes along the line $c_1 = 7$ (for $-6.4 \lesssim c_2 \lesssim -5.2$, $\lambda_1 \approx 0.2$).

Moreover, it can be verified that the two-dimensional maps generated by the system of equations (3.15) for $c_1 = 7$, $c_2 = -5.25$ and $k = 1$ satisfy the hyperbolicity conditions. We shall again consider the Poincaré section in the plane $\theta = 2\pi n$. It is convenient to introduce new coordinates by directing one of the axes along the singularity (an analog of the line PQ in fig. 7.14). These coordinates are

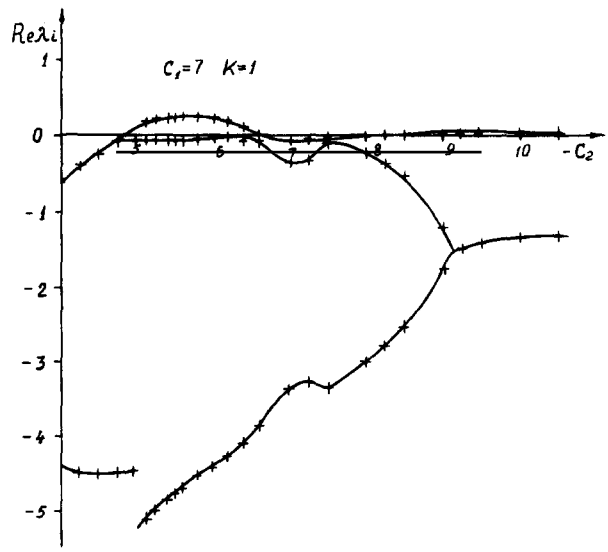

Fig. 7.24

$$x = \frac{1}{\sin\alpha}\left[\xi\cos(\beta-\gamma)+\eta\sin(\beta-\gamma)\right] - 11.241/\sqrt{389}$$

$$y = \frac{1}{\sin\gamma}\left[\xi\cos\beta+\eta\sin\beta - 11.89/\sqrt{389}\right],$$

$$\operatorname{tg}\gamma = 1.3\,,\quad \operatorname{tg}\beta = 10/17\,,\quad \gamma,\beta\in[0,\pi/2]\,.$$

Near the singularity of the two-dimensional map we can verify the inequalities (5.13) analytically when we know the exponent α [see formula (7.12)]. Beyond it ($x \le 0.054$, $x \ge 0.056$) calculations let us estimate the norms of the functions appearing in relations (5.13) as

$$\|(\partial f/\partial x)^{-1}\|_c = 0.902 < 1\,; \qquad \|\partial g/\partial y\|_c = 1.150\,88\times10^{-2} < 1\,;$$

$$\|(\partial f/\partial x)^{-1}(\partial g/\partial x)\|_c = 7.431\,21\times10^{-2} < 0.0744\,; \qquad \|\partial f/\partial y\|_c = 2.416\,56\times10^{-1} < 0.242\,.$$

Substituting these values into inequalities (5.13) we may verify that they are all satisfied. Thus, in the analysis of the stochastic properties of this attractor many results of the hyperbolic theory can be used.

7.4. *Strange attractors in higher-dimensional systems*

Studying systems of three ordinary differential equations shows that they represent complex mathematical objects. They may show several scenarios of the transition to chaos as well as hysteresis, intermittency, attractor crises, metastable chaos, and many phenomena studied by means of one- and two-dimensional maps. However, to investigate some phenomena more complex systems have to be used as simplified models.

Let us give two typical examples. One measures an average magnetic field if one deals with large-scale long-time characteristics of solar activity. It is connected, in particular, with the changing number of solar spots, which have regularly been observed since 1750 (fig. 7.25). It is known that the average magnetic field varies with a basic period of 22 years. A special analysis shows that the field is modulated by oscillations with a characteristic period of 57 years [220]. The variation of the number of spots found by Wolf, $W(t)$, or the total area is shown in fig. 7.25. It is seen that here at least a two-frequency regime is observed. There is every reason to believe that oscillations exist with a period

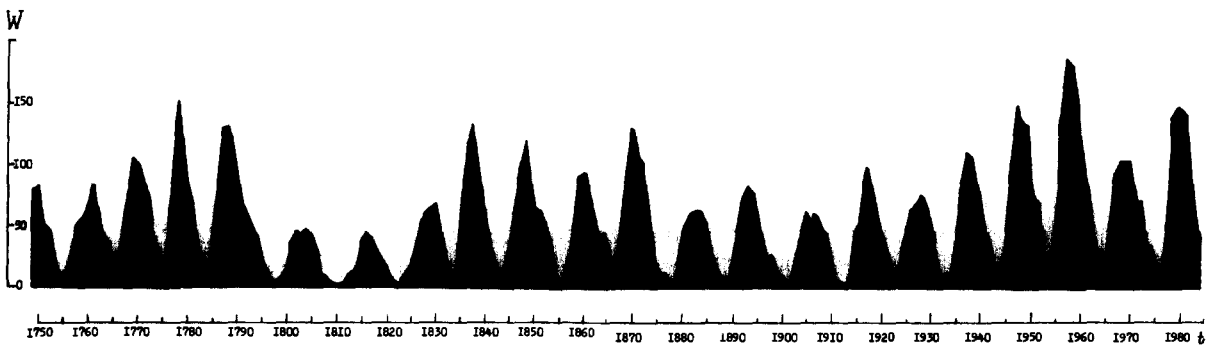

Fig. 7.25

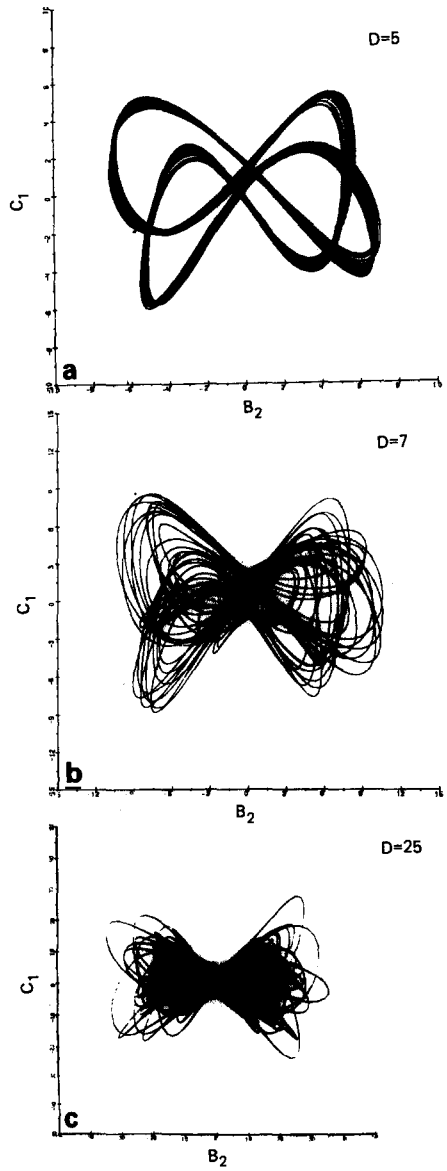

Fig. 7.26

of order 360 years [221]. Besides, a global reduction of the solar activity (the Maunder minimum) is observed.

Such a complex temporal behaviour suggests that the oscillations observed have a stochastic nature and there is a strange attractor in the dynamic system that determines the solar activity [222].

Following refs. [223, 224] we shall approximately consider a convective shell of the Sun as a plane layer of thickness h. Let the z coordinate be perpendicular to the layer while the x and y coordinates lie in it. The divergenceless magnetic field can be described by two scalar functions: the y-components of the vector potential and magnetic induction,

$$\boldsymbol{B} = \mathrm{curl}(A(x, z, t)\boldsymbol{e}_y) + B(x, z, t)\boldsymbol{e}_y .$$

The dynamo equations are a parabolic system for A and B with sources that are proportional to these components and are determined by the gradient of the angular velocity of the plasma rotation and the mean helicity – the quantity connected with the mirror symmetry of turbulent motions due to the effects of Coriolis forces and inhomogeneity. Taking into account the effect of the magnetic field on the helicity, the equations may be written in dimensionless form as

$$\begin{aligned} &\partial A/\partial t = (\alpha + C)B + \Delta A , \\ &\partial B/\partial t = D\,\partial A/\partial x + \Delta B , \\ &\partial C/\partial t = -\nu C + pAB - q(\alpha + C)B^2 , \end{aligned} \tag{7.14}$$

where C is the helicity variation caused by the magnetic field.

The parameter D is proportional to the product of the sources, i.e. the characteristic values of the angular velocity and the mean helicity, and inversely proportional to the square of the coefficient of turbulent diffusion. It is the major parameter to determine bifurcations of the system (7.14). The other parameters can be fixed from theoretical or phenomenological estimates.

By averaging the system (7.14) over z and involving only one harmonic in x we can obtain a system of seven differential equations that connect three complex functions a, b, c and one real one, c_0 [225],

$$\begin{aligned} &\dot{a} = -\sigma a + (\alpha + c_0)b + \tfrac{1}{2}b^*c , \qquad b = -b + \mathrm{i}Da , \\ &\dot{c}_0 = -\nu_0 c_0 + p\,\mathrm{Re}(ab^*) - q[(\alpha + c_0)bb^* + \tfrac{1}{2}\,\mathrm{Re}(b^2c^*)] , \\ &\dot{c} = -\nu c + pab - q[(\alpha + c_0)b^2 + bb^*c] . \end{aligned} \tag{7.15}$$

For $\nu_0 \gg \nu$ we may consider the system of three complex equations

$$\begin{aligned} &\dot{a} = -\sigma a + \alpha b + cb^*/2 , \qquad \dot{b} = -b + \mathrm{i}Da , \\ &\dot{c} = -\nu c + pab - q(\alpha b^2 + cbb^*) . \end{aligned} \tag{7.16}$$

We emphasize that even for a qualitative description of the observations systems of more than three real equations should be considered. The existence of two frequencies in the picture of the observed solar activity gives reason to believe that the solution is located in the vicinity of the torus. Meanwhile an invariant torus is usually observed in systems with at least four degrees of freedom.

Attractors becoming more complex as D increases in a system with only square terms $q = 0$ are considered in ref. [225] for $p = -1$. Dynamo models that lead to such equations are discussed in ref. [226].

It was shown that as D increases the point $(0, 0, 0, 0, 0, 0)$ loses its stability, and a Hopf bifurcation occurs. If D increases further the amplitude of the limit cycle grows and then a second Hopf bifurcation ($D = D_2 \lesssim 5.0$) occurs. A second frequency ω_2 appears, and an invariant torus arises. Then as D increases still further, a three-frequency regime is observed in the computations. The situation differs from the Ruelle–Takens scenario due to the system's symmetry.

In fact, eqs. (7.16) can be simplified by going over to the variables

$$a = \rho\, e^{i\theta}, \quad b = \rho x\, e^{i\theta}, \quad c = y\, e^{2i\theta}, \quad \xi = \rho^2, \tag{7.17}$$

where ρ and θ are real functions, and x and y are complex functions. It may be shown that the equations for ξ, x and y do not depend on θ, which allows us to go over from (7.16) to a system of five real equations. Singular points in this system correspond to points or cycles in (7.16), cycles to 2-tori, 2-tori to 3-tori.

Then chaotic regimes appear. A typical form of trajectories of the system (7.16) is shown in fig. 7.26.

An analysis of the systems of equations (7.15) and (7.16) showed that they can describe three-frequency, two-frequency or stochastic regimes. In any case a typical picture arises, and two basic frequencies can easily be distinguished. Many stochastic solutions have the following property: a trajectory may exist near the origin for a long time. Hence, the system (7.15) satisfies the requirements necessary for a qualitative description of the phenomenon of the deep minima in the solar activity.

If we assume that the model (7.16) accurately describes the basic qualitative properties of the activity modulation it may be concluded that phenomena such as the Maunder minima must be observed further on.

Following eqs. (7.14) and assuming that the basic source of the generation of the magnetic field is inhomogeneous rotation, we can obtain other finite-dimensional models of the solar dynamo [228]. In the simplest case they reduce to complex generalizations of the Lorenz equations,

$$\dot{x} = \sigma y - \sigma x, \quad \dot{y} = Rx - x^* z - y, \quad \dot{z} = xy - \nu z.$$

The quantity R here is proportional to D. Complex ordered and chaotic regimes in such a system were considered in refs. [228]. In some cases as R increases, the Ruelle–Takens scenario is implemented here too. Complex Lorenz equations may arise in many other physical problems [229].

Another example occurs in the theory of oscillatory reactions. After experimental investigations were introduced [230, 231] the simulations of such phenomena began [232]. It turns out that the mechanisms of the Belousov–Zhabotinsky, Briggs–Raucher and other reactions are rather complex. These reactions may run in many stages with tens of substances involved. In spite of an improvement in the experimental apparatus we can usually observe only a few degrees of freedom that characterize the system [28].

However, it has been shown that these problems may be successfully solved for some biological systems [233]. This lets us distinguish the most important from a variety of reactions to simulate oscillations and to determine the coefficients in the appropriate equations. Unlike the models of oscillatory reactions which are characterized by power nonlinearities, in these models sources of the form $f(x) = ax/(1 + bx)$ arise.

Although the dimension of the arising models is rather large (usually more than 10), they may be used successfully for a description of the picture observed in experiments. It has proved that for the models obtained an extensive class of stochastic regimes is typical [233].

8. From finite-dimensional systems to nonlinear media

We have discussed above some finite-dimensional dynamical systems. There are different types of attracting sets in them – cycles, fixed points, invariant tori, strange attractors. In this connection some

questions arise: Do these attractors have analogs in the partial differential equations which describe nonlinear media? What is the applicability region for few-mode systems, which often represent simplified models for the problems of partial differential equations? Is there quantitative or qualitative agreement between their solutions?

The rigorous results available in this field deal with two limiting cases. In the first case, using bifurcation theory it is shown that the existence and stability of solutions of partial differential equations of a certain type can be established by analysing a finite-dimensional system. The small parameter here is the deviation from the bifurcation point. Searching for the coefficients of the emerging system appears to be a rather complex problem [84, 89]. Using another approach it can be shown that when $N \gtrsim \bar{N}$ the solutions of the initial partial differential equations and $\bar{N}$ ordinary differential equations obtained by the Galerkin method are close to each other in a certain norm. The value of $\bar{N}$ in such estimates turns out to be usually rather large [234].

From the physical point of view a quite different situation is often of interest. The simplest model (with p ordinary differential equations, $p \ll \bar{N}$) is favoured which could be used to predict the behaviour of the solutions for different types of initial data in a certain range of parameters. (The Lorenz system is a typical example.) The use of such models is usually based on various physical considerations and numerical results. It is important that an increase in the number of harmonics in a finite-dimensional system would not lead to a qualitative change in its behaviour.

Unfortunately, the Lorenz system and many other simplified models emerging in hydrodynamic problems do not possess this property [235]. An analysis of reaction–diffusion systems, however, shows that the picture may be quite different here – there may not only be qualitative but also quantitative agreement between the solutions of the initial problem and the simplest few-mode system. An example of such a problem, which will be considered below in detail, is the behaviour of solutions of the Kuramoto–Tsuzuki equation in the case of small spatial domains. This example will let us determine what regimes in nonlinear media can correspond to various types of attractor of the simplified model, and what its applicability region is; moreover, some general questions will be considered.

8.1. Self-similar solutions and simple cycles

Following refs. [102, 108, 217, 236] we compare the behaviour of solutions of eqs. (3.15) and of problem (3.12) as $t \to \infty$. The numerical results for the partial differential equation for $l = \pi$ ($k = 1$) are shown in fig. 8.1. As initial data we use functions without spatial symmetry,

$$W_0(x) = \left(\sum_{m=0}^{3} \cos(2\pi m x/l) \right) + \mathrm{i} \left(\sum_{m=0}^{3} \cos((2m+1)\pi x/l) \right).$$

In the plane of the parameters (c_1, c_2) it is convenient to distinguish several domains where the solutions have similar asymptotic behaviour. Above the curve ABC [whose equation is determined by formula (7.8)] both systems have similar properties. In the linear approximation the spatially homogeneous solution (3.9) is stable here. In the system of ordinary differential equations (3.15) it corresponds to the solution with $\xi = 1$, $\eta = 0$. When crossing the line ABC it loses its stability, and a new stable singular point with $\xi \neq 1$ emerges. Therefore, as $t \to \infty$ we have $\xi \to$ const., $\eta \to$ const. and $\theta \to$ const. The functions x_0, x_1, y_0, y_1 in the system (3.14) vary according to a harmonic law.

For the partial differential equation we obtain in this range of parameters also solutions with constant values of ρ_m, $m = 0, 1, 2, \ldots$ and Ψ_m, $m = 1, 2, \ldots$. Here

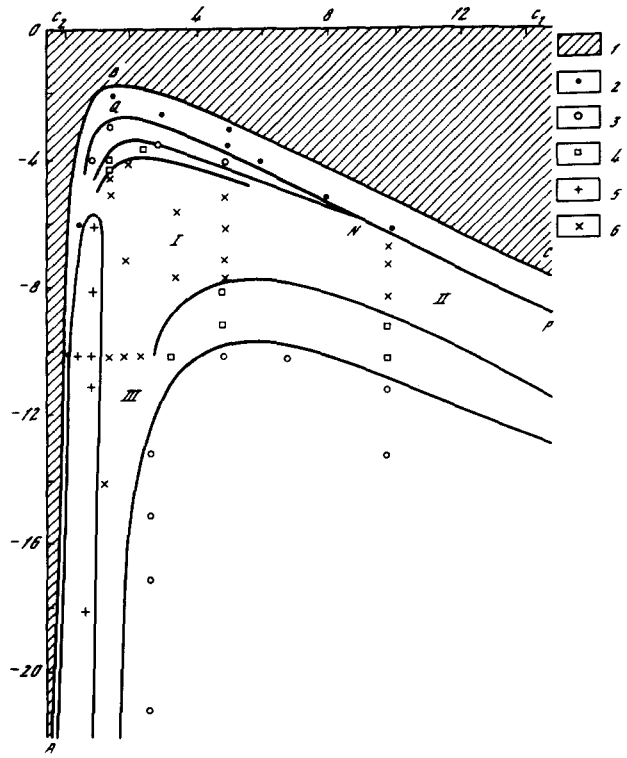

Fig. 8.1. Types of asymptotic solutions of the Kuramoto–Tsuzuki equation in the region ($l = \pi$) for $t \to \infty$; 1: the spatially stable homogeneous solution; 2: the solution whose ρ_n does not depend on time; 3: the periodic solution in which $\rho_0(t)$ and $\rho_1(t)$ determine a simple cycle; 4: $\rho_0(t)$ and $\rho_1(t)$ determine a double cycle; 5: the even solution; 6: more complex regimes. Solid lines approximately indicate the boundaries between different types of solution.

$$W = \sum_{m=0}^{\infty} [a_m \cos(\pi m x/l) + \mathrm{i} b_m \cos(\pi m x/l)] ,$$
$$a_m = \rho_m \cos \varphi_m , \quad b_m = \rho_m \sin \varphi_m , \quad \Psi_m = \varphi_m - \varphi_0 . \tag{8.1}$$

It means that a *self-similar solution* arises in the problem under investigation. The following lemma is valid [103, 108].

Lemma. Let $W(x, t)$ be a solution of problem (3.12). If and only if $\rho_n(t) = \text{const.}$, $\Psi_n(t) = \text{const.}$, $n = 0, 1, 2, \ldots$, does a self-similar solution exist of the form

$$W = R(x) \exp[\mathrm{i}\omega t + \mathrm{i} a(x)] . \tag{8.2}$$

Thus, self-similar solutions correspond to singular points of the simplified system. The typical form of the function $u(x, t)$ ($u = \mathrm{Re}\, W$) in such a solution is shown in fig. 8.2. It is seen that it can describe a rather complex process in the course of which local extrema of the functions u and v appear and disappear periodically; nevertheless the quantity $R = (u^2 + v^2)^{1/2}$ does not depend on time and $u(x, t) = v(x, t + \pi/(2\omega))$.

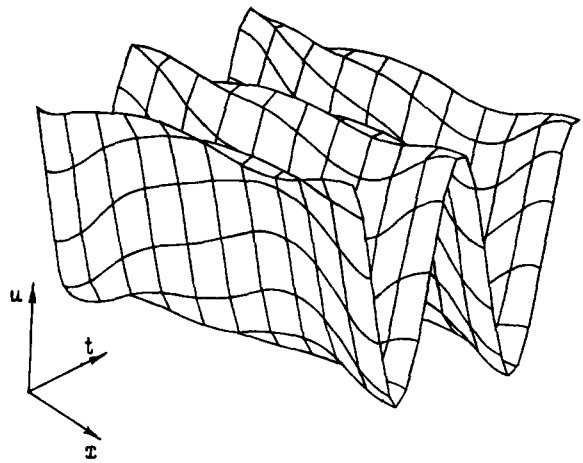

Fig. 8.2

It is natural to compare $\rho_0(t)$ and $\rho_1(t)$, which characterize the solution of problem (3.12), with the values of $\xi^{1/2}(t)$ and $\eta^{1/2}(t)$ in the system (3.15). A remarkable peculiarity of the model is the good quantitative agreement between these functions. A comparison between the parameters of the self-similar solutions and the singular points given in refs. [108, 238] shows that, in this range of parameters, the agreement is perfect up to a few percent. The lower boundary of the domain where the asymptotic behaviour is determined by the self-similar solution (the curve QNP in fig. 8.1) is also close to that existing in the simplified system (the curve QNP in fig. 7.12). A Hopf bifurcation occurs on this boundary. A limit cycle is generated in the approximate system. In the initial problem the solutions appear with functions $\rho_0(t)$ and $\rho_1(t)$ which change periodically.

If for different initial conditions we have the same solution for the partial differential equation, in which $|W|$ periodically depends on time, such a solution is called a cycle. We distinguish the functions $\rho_0(t)$ and $\rho_1(t)$ in the solution. Here again it is convenient to use the notation S^n, where n is the number of revolutions which are made by the projection of the solution onto the (ρ_0, ρ_1)-plane in a period.

We can verify the validity of the following statement [236].

Lemma. Let the solution of problem (3.12) be such that

$$\rho_n(t+T) = \rho_n(t)\,, \quad n = 0, 1, 2, \ldots,$$

$$\Psi_n(t+T) = \Psi_n(t) + 2\pi m_n\,, \quad m_n \in \{0, \pm 1, \pm 2, \ldots\}\,,$$

with $\rho_0 \neq 0$ for $t \in [0, \infty)$. Then it may be represented in the form

$$W(x,t) = R(x,t)\exp[\mathrm{i}(\omega_0 t + \omega_1(t) + a(x,t))]\,, \tag{8.3}$$

where

$$R(x, t+T) = R(x,t)\,, \qquad \omega_1(t+T) = \omega_1(t)\,,$$

$$a(x, t+T) = a(x,t) + 2\pi p\,, \quad p \in \{0, \pm 1, \pm 2, \ldots\}\,, \qquad \omega_0 = \text{const}.$$

Thus, the Hopf bifurcation in problem (3.12) is connected with a change from self-similar solutions of the form (8.2) to more complex solutions of the form (8.3), which contain two, in general independent, frequencies.

A comparison of figs. 7.12 and 8.1 shows that the solutions of the two-mode system (3.15) and the partial differential equation behave qualitatively in the same manner as the parameters c_1 and c_2 are varied. In both cases the parameter plane is divided into similar domains in which the solutions are of a certain type. The domain boundaries, however, are slightly displaced, which is natural: since the solutions bifurcate on these lines the higher harmonics affect their position.

Above the transition to complex solutions (see fig. 8.1) the amplitudes and the periods of simple cycles in the system (3.15) and in the partial differential equation differ not more than 10–15%. Below the domain of complex solutions the periods of cycles are close to each other although the lengths are several times different. This difference is due to the second harmonic [217, 236].

In the simplified model (3.15) the period of simple cycles is independent of the value of the parameter c_2 over a wide range of values. This proves that the same law is observed in the initial equation. The period is close to that predicted by the simplified system. It may be suggested that a constant period is typical for many two-component systems in the vicinity of the bifurcation point.

Various authors who are engaged in investigations of dissipative structures note that the emerging structures do not depend on many parameters and correspond to intrinsic properties of nonlinear systems. Their independence of the initial data ("forgetting" details of the initial data [3, 13]) or boundary conditions (localization effects [23]) was pointed out several times. Here we see a new type of parameter independence of a process. The parameter c_2 determines the frequency of the oscillations of the spatially homogeneous solution (3.9). Dissipative processes make that the frequency of the modulation of the oscillations of the entire system (which is determined by the cycle period) does not depend on c_2.

8.2. Other self-similar and spatially symmetric solutions

We have considered several domains of the parameters where the simple cycles and the singular points of a two-mode system can be compared with the solutions of a partial differential equation. Decreasing l results in an improvement of the quantitative agreement between these solutions. However, even for $l = \pi$ there are domains of the parameters which cannot be predicted by a two-mode system involving only the zeroth and first harmonics. They show which types of the space–time ordering can be typical for large l in this and other distributed systems. Let us consider one such domain.

In the system (3.12) an interesting phenomenon may be observed. From initial data of a general form without any spatial symmetry a change to even self-similar solutions of the form (8.2) [$W(x, t) = W(l - x, t)$, $\rho_{2m+1} = 0$, $m = 0, 1, 2, \ldots$] occurs. The domain where this takes place lies in the interval $0 < c_1 \lesssim 1.2$. In fig. 8.1 it is denoted as the region of even self-similar solutions. Unlike most open nonlinear systems where a spontaneous loss of symmetry occurs [3, 13] we can observe here *spontaneous appearance of symmetry*. As $t \to \infty$ the solution has a symmetry which is absent in the initial data. An even solution satisfies the condition of the absence of flow at the point $x = l/2$. Therefore, we can obtain it by considering the asymptotic behaviour of solutions of problem (3.12) in a region twice as short. As $t \to \infty$ the nonlinear system disintegrates into two similar noninteracting subsystems. More complex symmetric solutions corresponding to disintegration into a larger number of noninteracting parts may prove to be stable in regions with longer lengths.

An explanation for this phenomenon, based on a more complex three-mode system (involving variation of the zeroth, first and second harmonics) was proposed in refs. [108, 217, 238]. A typical

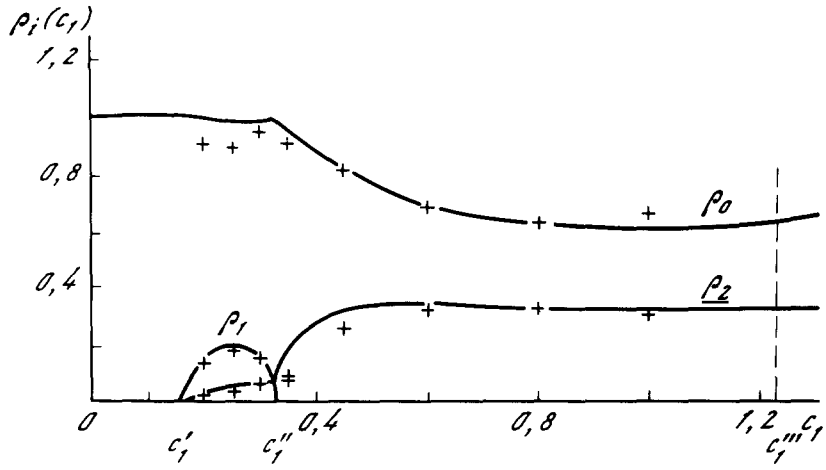

Fig. 8.3

picture of the variation of the parameters of the self-similar solution with increasing c_1 is shown in fig. 8.3. Here the step in c_1 is 0.01; $c_2 = -10$, $l = \pi$. The solid lines correspond to the solutions of the three-mode system, the markers to the solutions of the partial differential equation. It is seen that they agree well. When $c_1 = c_1'$ the spatially homogeneous solution loses its stability, and the self-similar solution emerges, to become even in the interval $c_1'' < c_1 < c_1'''$. An analysis of the stability of singular points in the three-mode system enables us to determine c_1' and c_1''', and their coordinates determine $\rho_0(c_1)$ and $\rho_2(c_1)$ in this range of parameters with a high accuracy. These results agree well with the values obtained for the partial differential equation.

There are analogs of the attractors of a simplified finite-dimensional model in the Kuramoto–Tsuzuki equation. The question arises: Do the unstable points and cycles have infinite-dimensional analogs? The answer is yes. Let us give some examples.

It turns out that there are infinitely many types of solutions with a spatial symmetry regardless of the length l. In refs. [103, 237] the conditions were formulated under which some Fourier coefficients in the solutions of problem (3.12) are zero throughout the entire process for $0 < t < \infty$. Let us put a sequence of integers $\{L\}$ in correspondence to the initial distribution $W_0(x)$ so that if $n \notin \{L\}$ then $\rho_n(0) = 0$. In other words, $\{L\}$ contains all harmonics with nonzero amplitude (maybe not only them).

The following statements are valid.

Lemma I. If the sequence $\{L\}$ is such that for any integers $m \in \{L\}$, $n \notin \{L\}$ the condition $m \pm n \notin \{L\}$ holds, then all the Fourier coefficients in the solutions of problem (3.12) with their number $n \notin \{L\}$ are zero for $0 < t < \infty$.

Lemma II. If the sequence $\{L\}$ is such that:
(1) for all $m \in \{L\}$, $n \notin \{L\}$ the condition $m \pm n \notin \{L\}$ holds,
(2) for all m, $n \notin \{L\}$ the condition $m \pm n \notin \{L\}$ holds,
then all the Fourier coefficients in the solutions of problem (3.12) with their number $n \notin \{L\}$ are zero for $0 \le t < \infty$.

A sequence of the form $\{0, m, 2m, \ldots\}$, where m is any natural number, satisfies the conditions of lemma I. From this lemma it follows, in particular, that only even solutions can emerge in the evolution of even initial data. The sequence $\{1, 3, 5, 7, \ldots\}$ satisfies lemma II.

But what will happen if the initial data corresponding to different sequences $\{L\}$ are put in a domain of given length? From the linear analysis of the spatially homogeneous solution (3.9) it follows that if

$$(\pi m/l) < -2(1 + c_1 c_2)/(1 + c_1^2)\,, \tag{8.4}$$

a spatially inhomogeneous solution splitting the region into m similar noninteracting parts can emerge. If m is sufficiently large the solution will tend to the spatially homogeneous solution (3.9), preserving its spatial symmetry, as $t \to \infty$. The larger l, the more different values of m satisfy inequality (8.4), and hence, the higher the dimension of the simplified system imitating the properties of the original problem.

In ref. [237] examples of solutions with different spatial symmetries are numerically constructed. As a rule, they are unstable. However, solutions corresponding to a sequence $\{L\}$ converge to the same asymptotic symmetric solution regardless of the specific form of the initial data (only the type of their symmetry is important).

Even the simplest two-mode system (3.14) has a finite-dimensional analog of odd solutions with $\{L\} = \{1, 3, 5, \ldots\}$. It is the solution

$$\rho_1 = \sqrt{4(1 - k^2)/3}\,, \quad \dot{\varphi}_1 = \omega = -3c_2\bar{\rho}_1^2/4 - c_1 k^2\,, \quad \rho_0 = 0 \quad (k \le 1)\,,$$

which is unstable against perturbations with $\rho_0 \neq 0$. When $l \lesssim 4\pi - 5\pi$ the values of $\bar{\rho}_1$ and ω are in good agreement with odd solutions of the partial differential equation [239].

8.3. *Space–time order without analog in a two-mode system. The problem of constructing a complete set of self-similar solutions*

Comparing figs. 7.12 and 8.1 shows that the second domain of parameters in which the solutions of the original problem and the simplified two-mode system are qualitatively different, is that where $c_2 \to -\infty$. In the simplified system there is a stable singular point, while in the distributed system a simple cycle (i.e. a solution of the type (8.3) whose projection onto the (ρ_0, ρ_1)-plane makes one revolution per period) is stable. Its period slows down as c_2 decreases and becomes constant when $c_2 \lesssim -400$. The cycle family in this domain of parameters is shown in fig. 8.4. Here the solutions of the original problem and the equation

$$W_t = W + (1 + \mathrm{i}c_1)W_{xx} - \mathrm{i}c_2|W|^2 W \tag{8.5}$$

turn out to be close to each other. In spite of the fact that the spatially homogeneous solutions of the latter equation increase infinitely as $t \to \infty$, its analysis may prove to be useful.

Since $|W| \sim |c_2|^{-1/2}$ as $c_2 \to -\infty$ in this parameter domain, $\rho_0(t)$ and $\rho_1(t)$ are close to zero. An analog of such a solution in the two-mode system must be near the origin of the coordinates, where the Ω value is strictly positive [see formula (7.6)], and hence there are no stable cycles. This explains different behaviour of the solutions of the original problem and of the simplified model.

Calculations show [103] that when $c_1 = 3$, $c_2 \to -\infty$ and $l = \pi$ the first three to four Fourier coefficients of the function W are comparable in magnitude. To describe such solutions in eq. (3.12) one should take at least four harmonics into consideration.

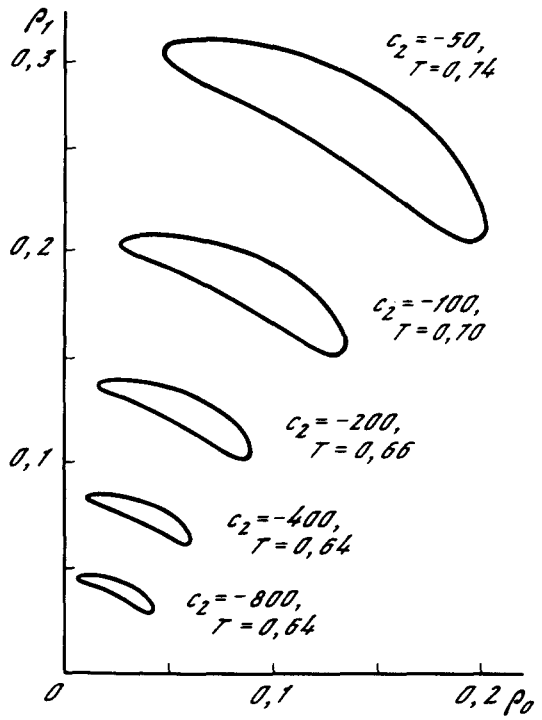

Fig. 8.4

In ref. [240] a simplified two-mode system for eq. (8.5) was studied in detail. The stochastic regimes and the ordered solutions of various types were obtained numerically. It is possible that they have analogs in eq. (8.5). So it would be interesting to investigate this question.

We have discussed above how the solutions of problem (3.12) change for different c_1 and c_2 when the domain length is fixed. In many cases, however, it is important to know how the solution changes with a variation of l. Analysing such a problem for stationary dissipative structures has resulted in the discovery of the so-called *zone structure*. It has been proved that as the domain length increases structures may appear and disappear (in the last case the spatially homogeneous solution becomes stable again) [241]. Such effects were discovered in investigations of the heterogeneous-catalytic wire reaction model,

$$\theta_t = D_1\theta_{xx} - g\theta + f(1-\eta)\exp(\theta/(1+\beta\theta)),$$

$$\eta_t = D_2\eta_{xx} - v\eta + k(1-\eta)\exp(\theta/(1+\beta\theta)).$$

Here θ characterizes the temperature, and η the conversion depth.

Examples in which the solutions of problem (3.12) change as l increases were given in refs. [102, 242]. The numerical results presented in fig. 8.5 allow us to estimate the boundaries of the range in which the two-mode system is applicable. It is shown how the parameters of self-similar solutions [$\rho_n(t)$ for $t \to \infty$] behave for different l. Here $c_1 = 2$, $c_2 = -1$, and the l values for which the calculations were performed are marked by the vertical dashes. When $l = \pi\sqrt{5/2} \approx 5$ the spatially homogeneous solution

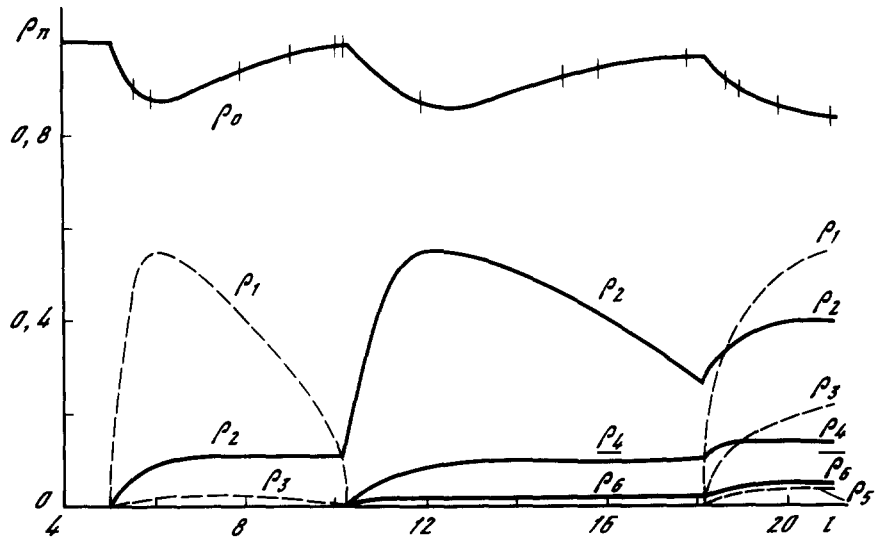

Fig. 8.5

loses its stability, after which the asymptotic behaviour is determined by a self-similar solution of the form (8.2). In the beginning the zeroth and first harmonics have maximal amplitudes. Here the simplified model (3.15) describes the behaviour of the system well. Then the first harmonic decreases, but the model (3.15) can be used by putting $k = 2\pi/l$. From $l \approx 18$ the number of harmonics with comparable amplitudes quickly increases. For $l \approx 22$ a complex oscillatory regime can be observed in the system. The question about simple efficient models in this parameter domain remains open.

We have discussed above the analogs of the simplest attractors of dynamic systems in problem (3.12). However, in dynamic systems different attractors may co-exist for the same values of the parameters. It is natural to assume that in nonlinear media several types of ordering can simultaneously exist as well.

One or other of them will be observed depending on the initial data. Experiments with Couette–Taylor flow showed that more than a hundred different stable regimes may be observed for certain parameter values. Among them are periodic and multi-frequency regimes, and a few types of chaos [32]. Therefore, the question arises: What is the complete set of dissipative structures that are possible in a given distributed system? To answer this question one needs to construct a whole set of solutions of a certain type for the equations under investigation, and then "the selection rule" must be established, i.e., the question of the stability of each solution should be settled. (The important problem which seldom can be solved is determining the regions of attraction of different solutions.)

An example of nonlinear dissipative systems for which the above questions are settled is provided by media described by eq. (2.1). In this case only unbounded solutions or stationary structures can exist as $t \to \infty$. The stationary structures are determined by the solutions of the equation

$$T_{xx} + Q(T) = 0\,, \tag{8.6}$$

which is a simple conservative dynamic system (that describes the motion of a material point in a given potential). As we have already mentioned, the question about the stability of different solutions can

also be settled analytically – all the solutions with several extrema at an inner point of the segment are unstable [29].

A complete set of self-similar solutions of the form (8.2) can be constructed for the Kuramoto–Tsuzuki equation when $c_1 = c_2$. In ref. [109] it was shown that the equation for the function $R(x)$ could be reduced to the form (8.6), and by using elliptic integrals analytical solutions could be obtained. However, searching for all the solutions of the boundary value problem requires special algorithms. To solve this problem a graphical method was proposed in ref. [239]. Numerical calculations showed that here [as in the system (2.1)] the simplest solution in which the function $R(x)$ has a minimum number of extrema proved to be stable [239].

It would be very important to construct numerical algorithms or approximate analytical methods to enable one to build a full set of stationary structures in reaction–diffusion systems and all the self-similar solutions of the Kuramoto–Tsuzuki equation in domains of a given length. However, at the present time this problem does not seem to be solved yet.

The equations determining self-similar solutions of various partial differential equations may prove to be rather complex and describe stochastic regimes. In this case we talk about *spatial chaos* in nonlinear systems.

An example of such a chaos is given by the solutions of the Kuramoto–Sivashinskii equation (3.21) of the form

$$u(x, t) = -c^2 t + v(x) .$$

Their configuration is determined by the equation

$$\frac{d^3y}{dx^3} + \frac{dy}{dx} = c^2 - \frac{y^2}{2} , \quad -\infty < x < \infty \quad (y = dv/dx) . \tag{8.7}$$

In ref. [243] it is shown that for small c^2 there are a periodic and an infinite set of quasi-periodic solutions, while for large c^2 the solution is unique and has a conical form. Numerical computations for intermediate values of c^2 suggest that below $c^2 \approx 1.6$ for every speed c^2 there is a continuum of odd quasi-periodic solutions or a Cantor set of chaotic solutions wrapped by infinite sequences of conic solutions.

Spatial chaos may arise in dissipative nonlinear media where sources and sinks are periodic functions of a spatial coordinate, for example, in the system described by the equation

$$A_t = \mu A + A_{xx} - A^3 + \nu \sin kx . \tag{8.8}$$

If $\nu = 0$ such media have trigger properties, and the elementary structures are described by the formula

$$D(x) = \pm\sqrt{\mu}\, \tanh[(\tfrac{1}{2}\mu)^{1/2} x] .$$

A simplified finite-dimensional model may be proposed by assuming that when $\nu \neq 0$ the solution will represent a set of N elementary structures interacting with each other according to a certain law. The evolution of the system will be described by N ordinary differential equations connecting the coordinates $x_1, \ldots, x_N$ of the elementary structures [244].

The existence of terms with fourth and higher derivatives may also lead to the emergence of stationary chaotic solutions. Such solutions, for example, were discovered in the equation [244]

$$A_t = \mu A + A_{xx} - A^3 - A_{xxxx} . \tag{8.9}$$

Creation of a chaotic spatial structure in many physical problems is of great interest. The classical problem of solid state physics is the problem of electrons passing through a crystal lattice with a periodic potential. The result of the considerations is that the electron moves like a wave whose parameters depend on the crystal characteristics. Now let us assume that we have managed to create a chaotic irregular lattice. The remarkable result is that in this case the electron motion is qualitatively different. It proves to be localized in a certain domain of space. The irregularities may have very small amplitude. It is important that they should be chaotic. This phenomenon called Anderson localization, has very great theoretical and applicational importance [245].

Another physical problem is connected with the study of and the search for so-called "*turbulent crystals*" [247] or quasi-crystals. The simplest example of such a crystal is a lattice at the nodes of which atoms of several substances alternate in a chaotic manner. Examples of figures which can fill a plane in an aperiodic way have been known in modern geometry [246]; however, crystals of such a kind have been discovered only in recent years [248].

Ideas about chaotic spatial structures have recently been used more and more extensively in astrophysics, the theory of elementary particles, and the theory of magnetism. Therefore we may expect that investigations of nonlinear dissipative media where chaotic spatial structures can exist will also experience progress.

Let us note that, when studying spatial chaos in eqs. (8.7), (8.8) and (8.9), we meet conservative dynamic systems [in eq. (8.8) with periodic external perturbation]. This enables us to use many results obtained in investigations of spatial chaos in Hamiltonian systems [156]. Further investigations will seem to allow a few basic general scenarios of the development of spatial chaos.

Now we shall turn our attention to a class of problems connected with analysing space–time order. At the present time the studies of these problems have only begun. Analysing self-similar solutions leads us to the necessity of studying boundary value problems for systems of ordinary differential equations or for elliptic equations in the multi-dimensional case. However, some nonlinear equations have particular solutions whose construction proves to be more complex. The solutions of Kuramoto–Tsuzuki-type equations are an example. Similar problems arise in searching for breathers in systems close to integrable, i.e., solutions which are close in form to one or several solitons whose amplitude periodically varies with time [250].

In this chapter we have discussed the example of a change from a simple few-mode system to a partial differential equation. The change has proved to be very efficient since the influence of the harmonics not involved in the simplified model is weak (in our case it is connected with the small length of the domain). The basis for the finite-dimensional model has been obtained from the solution of the linearized problem.

However, recently some interesting problems have appeared where the change to finite-dimensional systems is made in a different manner. In these cases nonlinear media are described by partial differential equations which are close to fully integrable systems [35]. Equations of such a kind arise, for example, in nonlinear optics. As the basis a set of solitons (solutions of the nonlinear equation) is used. Finite-dimensional systems of low dimension are also very efficient here. We shall consider these problems later on when discussing stochastic regimes in such systems.

9. Diffusion-induced chaos and other stochastic regimes in nonlinear dissipative media

In recent years it has been shown that for many dissipative systems it is typical to have, beyond the temporal or spatial stochasticity discussed above, a more complex spatial–temporal chaos. It has turned out that in reaction–diffusion systems with the simplest oscillatory kinetics stochastic regimes may exist. Since in this case a concentrated system behaves in a regular way and its complicated behaviour is connected with the effect of the diffusion terms, the phenomenon has been called *diffusion-induced chaos*. Now it arouses great interest for several reasons.

Reaction–diffusion-type models where the concentrated system shows self-oscillation (for example, has one or more limit cycles) are widespread. They appear in the analysis of oscillation reactions, in some ecology problems, or in physical models. In each case experiments for the investigation of diffusion-induced chaos would be very important. They could lead to the discovery of a new class of turbulent regimes.

The theoretical (and, possibly, experimental) study of diffusion-induced chaos appears to be simpler and easier than an analysis of few-mode chaos in many hydrodynamic systems. In most hydrodynamics problems multi-dimensional effects prove to be highly important. Because of this circumstance as well as the difficulties of numerical simulation of turbulent flows an assessment of the results in this field made ten years ago is still valid: "... for the complete Navier–Stokes equations not only do we not know a single turbulent solution but we are not even aware if one exists. What a stochastic attractor must look like is also unclear" [251]. Even when we know that in a given experiment the turbulent flow is determined by an attractor of low dimension it is usually impossible to construct simple finite-dimensional models that would describe the phenomenon.

The situation proves to be different in the case of diffusion-induced chaos. It has been shown that there are some simple and efficient dynamic systems describing spatial–temporal chaos in reaction–diffusion-type systems. At the same time eq. (3.12), which can describe diffusion-induced chaos, is a simplified model of some hydrodynamic systems [96, 98], and an analysis of this phenomenon may possibly enable us to obtain some insight in hydrodynamic turbulence.

An analysis of diffusion-induced chaos proves very useful from the mathematical physics point of view. The solutions of most partial differential evolution equations that have been studied by now behave in a rather simple way; as $t \to \infty$ they converge to stationary, time-periodic or other self-similar solutions. However, when nonlinear mathematical models, whose number quickly grows, are analysed we frequently encounter stationary stochastic regimes. Diffusion-induced chaos is a prototype of such regimes.

9.1. Diffusion-induced chaos in small regions

In the first numerical calculations of problems (3.8) and (3.21) (or their analogs with periodic boundary conditions) complex aperiodic behaviour of the solutions was observed as well as in a study of the Brusselator model. It allowed one to consider diffusion-induced chaos (or diffusion-induced chemical turbulence) as a new type of stochasticity in chemical reactions running in distributed systems.

We distinguish two types of such regimes: phase and amplitude turbulence. If we observe the motion of the point $u(\bar{x}, t)$, $v(\bar{x}, t)$ over the (u, v)-plane it turns out that in the first case for different $\bar{x}$ the trajectories are close to the same limit cycle which characterizes the concentrated system. However, their phases (the point positions on the cycle) may chaotically change when the spatial coordinate x varies. To describe such a situation it is natural to use the Kuramoto–Sivashinskii equation (3.21).

For amplitude turbulence the trajectories of each point $u(\bar{x}, t)$, $v(\bar{x}, t)$ over the (u, v)-plane for different $\bar{x}$ may essentially differ and behave chaotically. In a certain range of parameters this type of diffusion-induced chaos can be described by eq. (3.8).

Further analysis of stochastic regimes in distributed systems resulted in the formulation of several questions.

How is the phenomenon of diffusion-induced chaos connected with strange attractors of dynamic systems of low dimension? "An important and as yet unsettled problem is to find the connection between diffusion-induced chaos and known types of chaos in systems with several degrees of freedom" [104].

What is a scenario for the transition from ordered regimes to chaos when the system parameters change?

What numerical algorithms are efficient for investigating such regimes?

It is natural to begin the discussion of these questions with the simplest case of small regions.

Earlier the simplest attractors of two-mode systems were compared with one- and two-frequency regimes in eq. (3.12) for $l = \pi$ $(k = 1)$ (see figs. 7.12 and 8.1). Let us extend this comparison and consider more complex solutions. According to refs. [103, 217, 253] we consider the solutions of problem (3.12) for $c_1 = 5$ change. We shall increase the value of c_2 by moving towards the region of diffusion-induced chaos from below. By analogy with the two-mode system it may be expected that here period-doubling bifurcations occur.

An ideal way to determine a scenario for the transition to chaos would be to find the whole bifurcation diagram. However, this usually cannot be done while studying partial differential equations. Therefore, we search for different types of ordering that are typical for one of the known scenarios of the transition to chaos, and the simplest finite-dimensional models that describe the picture under observation.

For $c_1 = 5$ and $c_2 = -10.0$ the simple cycle S^1 determines the asymptotic behaviour of the solutions of the partial differential equation. As the parameter c_2 increases the stable cycle S^2 and then S^4 appear (fig. 9.1). We recall that the cycle in problem (3.12) is a solution of the form (8.3). For $c_2 = -7.4$ there is a stable cycle S^8, and for $c_2 = -7.35$ S^{16} appears. We shall again look for the values of local maxima of the function $\rho_0(t)$. We plot the values of the nth maximum, M_n, along the abscissa and of the $(n+1)$st maximum, M_{n+1}, along the ordinate, where $n = 1, 2, \ldots$. The points (M_n, M_{n+1}) lie with high accuracy on continuous unique curves, shown in fig. 9.2. Therefore, we may use a family of one-dimensional maps

$$M_{n+1} = f(M_n, c_2) \tag{9.1}$$

as a simplified model that describes the picture we observe.

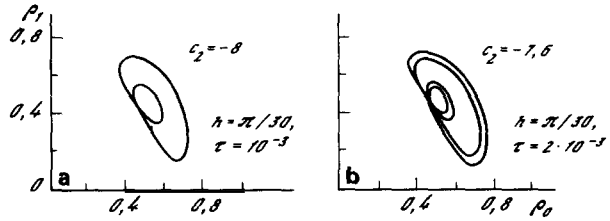

Fig. 9.1

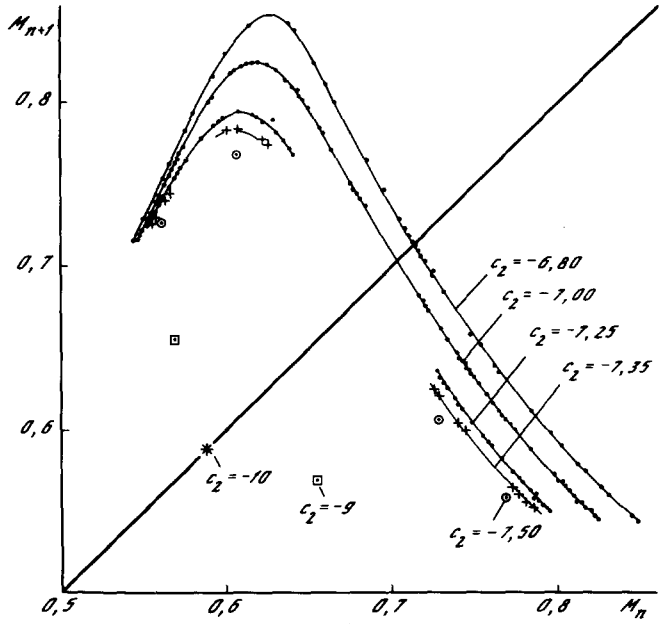

Fig. 9.2

From fig. 9.2 it is seen that these one-dimensional maps have a smooth vertex, and the amplitude of the function grows as c_2 increases. The family of maps (4.2) has the same properties. Transition to chaos in (4.2) occurs as a result of a cascade of period-doubling bifurcations. Then an inverse cascade of period-doubling bifurcations is observed which leads to a sequence of transitions $\chi^{2n} \to \chi^n$. Smoothness of the vertex brings about the occurrence of a "window structure" – in any vicinity of chaotic regimes there are stable cycles. After the first cascade stable cycles appear that do not belong to the type S^{2^n}. It may be expected that the properties of this family of maps will be close to those of the family (9.1).

The computations carried out in refs. [217, 218, 253] show that as c_2 increases in the partial differential equation the noisy cycles χ^4, χ^2 and χ^1 successively appear. Due to the limited accuracy of the computations solutions with $\sim 3 \times 10^2$ different maxima are considered as aperiodic. The map f $[M_{n+1} = f(M_n)]$ for one of the solutions of the type χ^2 is shown in fig. 9.2 ($c_2 = -7.25$). Between aperiodic solutions stable complex cycles exist indeed; one of them is shown in fig. 9.3.

The fact that a map which is close to one-dimensional can be distinguished is suggestive of the low dimension (of order $3 + \varepsilon$, $\varepsilon \ll 1$) of the attractor in the initial problem, and it greatly simplifies our investigation. In order to construct the function f, 100–300 elements of the sequence $\{M_n\}$ are sufficient. To obtain the simplest stochastic characteristics with the same accuracy much larger samples are needed. [For example, in this case constructing the histogram with step $\sim 10^{-3}$ would require $\sim 10^5$ local maxima of the function $\rho_0(t)$.] Using the results of the theory of one-dimensional maps we may forecast different types of ordering and stochastic regimes in the family of maps (9.1). It is natural to search for them in the initial problem for nearby values of the parameter. (We recall that the points of $\{M_n, M_{n+1}\}$ do not lie, in fact, strictly on a curve; they are located in its vicinity. Besides, the function (9.1) is known only approximately because the sample is finite.)

So far we increased the parameter c_2, moving towards the region of complex solutions from below. Now we shall act differently and decrease c_2, moving in from the ordered regimes above. The family of one-dimensional maps that appear in this case is shown in fig. 9.4. We have seen that in families with a

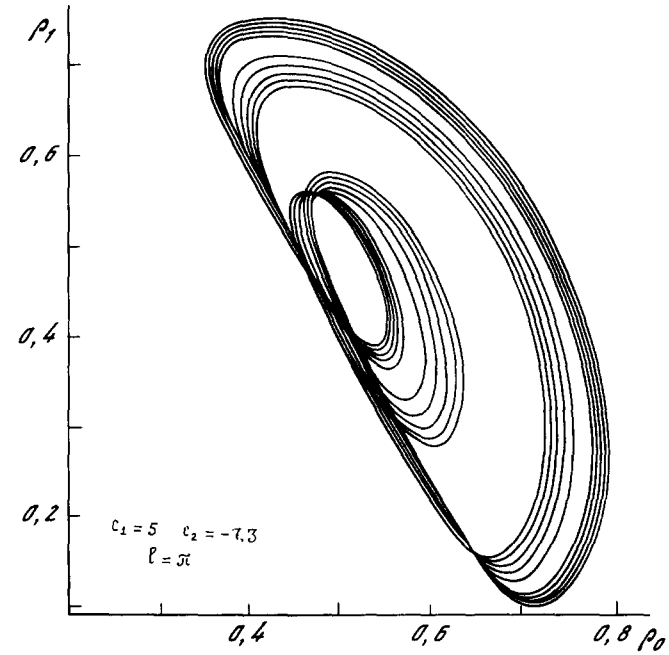

Fig. 9.3

sharp vertex the scenario of the transition to chaos may be very complex. In our computations for $c_2 = -4.1$ and $c_2 = -4.16$ the respective stable cycles S^1 and S^2 were observed; however, the transition to stochastic regimes was not studied in detail. The stochastic regimes that appear later on generate one-dimensional maps. First the function f has one sharp maximum as in the case of a two-mode system (see fig. 7.23).

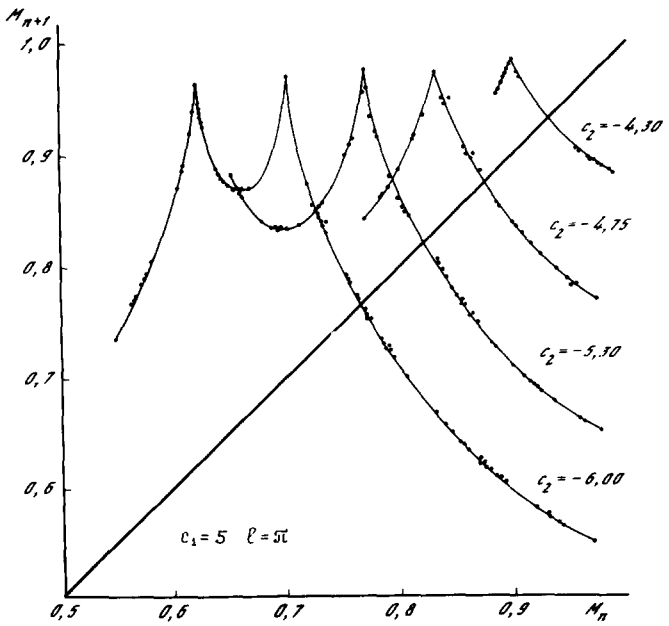

Fig. 9.4

As c_2 decreases in the simplified model (3.15) the maps remain continuous and unique, and have only one sharp maximum. In the partial differential equation the function f behaves in a more complex way. If we decrease c_2 the solution changes so that the function f will first have a minimum ($c_2 \approx -5.3$) and then another sharp maximum ($c_2 \approx -6.0$). (A similar phenomenon was observed in some systems of ordinary differential equations and specifically in the Lorenz system for certain values of the parameters [137].) For $c_2 \approx -6.0$ the uniqueness disappears, and the solution of the partial differential equation is still aperiodic. Then the reconstruction occurs once more, after which the function becomes smooth and unique (fig. 9.2).

Now we consider the parameter range $c_1 \lesssim 1.2$ (region III in fig. 7.12). In the two-mode system we can observe here aperiodic solutions in which the function $M_{n+1}(M_n)$ does not determine one-dimensional maps. It turns out not to be due to an increase of the dimension of the attractor. Let us explain the situation.

When systems of N ordinary differential equations are investigated the location of the intersection points of trajectories and a crossing surface as well as the corresponding $(N-1)$-dimensional maps are often considered [in the system (3.15) the local maxima of ρ_0 lie on the surface $\dot{\rho}_0 = 0$]. If the surface is chosen wrongly, some turns will not intersect it while others may intersect it several times. In this case the properties of the map and the original equations are essentially different.

Solutions of the system (3.15) in the given parameter range have, in fact, such a form that on some turns the function $\rho_0(t)$ achieves a local maximum several times. (The reason is the appearance of a stable singular point on line EF [217].) If we take this fact into account and throw away "spare" elements from the sequence $\{M_n\}$ the remaining points will determine a one-dimensional map. A similar picture is observed in the partial differential equation.

Figure 9.5 shows a typical aperiodic solution projected onto the (ρ_0, ρ_1)-plane in the considered parameter range. It is seen that on different turns $\rho_0(t)$ has a different number of maxima. For some values of the parameters the points $\{M_n, M_{n+1}\}$ fill the whole parts of the plane, for example, as is shown in fig. 9.6.

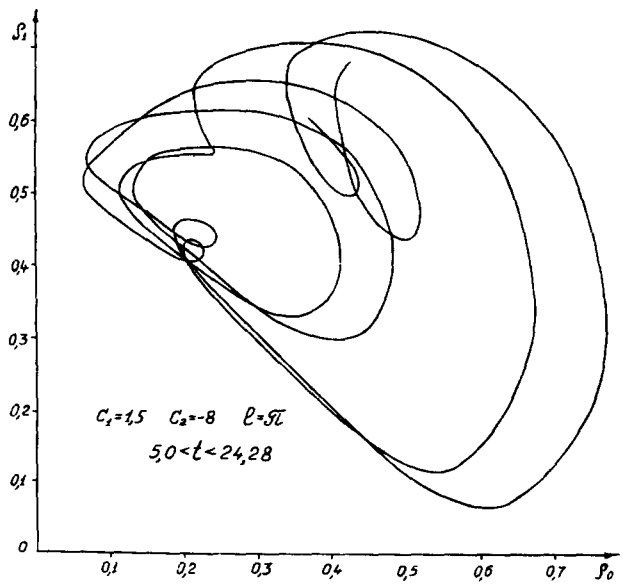

Fig. 9.5

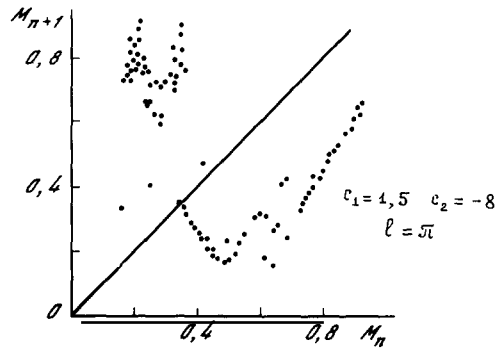

Fig. 9.6

Some other scenarios of the transition to chaos may be implemented in eq. (3.8). In ref. [242] the Cauchy problem ($-\infty < x < \infty$) is considered in detail for eq. (3.8) with initial data in the form

$$W(x, 0) = 1 + 0.2\cos(qx) \tag{9.2}$$

(which is equivalent to the second boundary value problem with the condition that flow is absent on the boundaries of the interval $[0, \pi/q]$).

The behaviour of the solution was investigated for $t \to \infty$ depending on two parameters c_0 and q ($c_1 = -c_2 = 1/c_0$). Putting $c_0 = 0.25$ and decreasing q (which is equivalent to increasing the length of the region) the authors observed the appearance of a limit cycle as a result of a Hopf bifurcation (in the variables ρ_n; in the original variables a two-torus appears from the limit cycle), then the appearance of a two-torus (a three-torus in the original variables) and a chaotic regime.

In this work the solution was processed in various ways; however, the following approach proved most successful. The quantity $|W(x, t)|^2$ was expanded in a Fourier series, $|W(x, t)|^2 = \Sigma_m \alpha_m(t)\cos(mqx)$. Then the behaviour of the points $A_1, A_2, \ldots$ such that $\alpha_0 = 0.01$ and $d\alpha_0/dt > 0$ was considered on the trajectory (an analog of the Poincaré section in an infinite-dimensional system). The point H was chosen in the (α_1, α_2)-plane and a reference system was introduced such that it allowed comparison between the projections of the points $A_1, A_2, \ldots$ onto the (α_1, α_2)-plane,

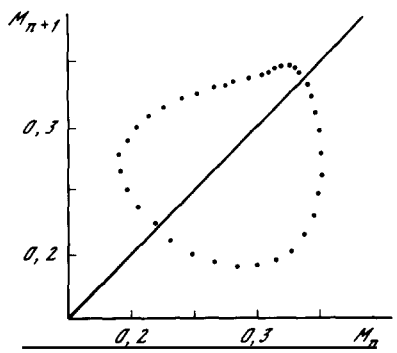

Fig. 9.7

$\bar{A}_1, \bar{A}_2, \ldots$, and the sequence of angles $\theta_1, \theta_2, \ldots$. Then we constructed the maps

$$\theta_{n+1} = F(\theta_n) . \tag{9.3}$$

It turned out that the function F determined a map of the circle onto itself with high accuracy.

Such maps appear in the second boundary value problem (3.12) too if we again distinguish local maxima of $\rho_0(t)$ and plot $M_{n+1} = f(M_n)$ for sufficiently large regions [103, 217]. A typical picture in this case is shown in fig. 9.7 ($c_1 = 4$, $c_2 = -4$, $l = \pi/0.51$). It is natural to choose the point H within the torus section.

In ref. [242] it is shown that the transition to chaos in a partial differential equation, as in the circle map (5.24), is caused by the fact that for a certain value of q the map (9.3) becomes noninvertible [178, 179].

Diffusion-induced chaos in eq. (3.12) was studied in detail in ref. [254]. Here initial conditions of the form (9.2) were considered, the value of $1/c_0 = c_1 = -c_2 = 4$ was fixed and the value of q was decreased. It was shown that in this problem bifurcations connected with the loss of symmetry or with the interaction of symmetric solutions were important too. Such a mechanism by which complicated solutions arise is also of importance in the two-dimensional analog of eq. (3.8) [103, 217]. Below we shall consider it in more detail.

In ref. [254] the standard technique for computing the Lyapunov exponents [197] was employed. The partial differential equation was replaced by a finite-dimensional system; therefore the methods developed for ordinary differential equations could be used. It was shown that diffusion-induced chaos in the partial differential equation in the considered range of parameters was characterized by positive Lyapunov exponents. (Note that these computations require a high accuracy because not a single one of the calculated positive Lyapunov exponents exceeds 0.05.) For example, for $q = 0.95$ the largest Lyapunov exponents were $\lambda_1 = 0.0431$, $\lambda_2 = 0.001\,12$, $\lambda_3 = 0.000\,48$, $\lambda_4 = -0.909$, while the dimension was $d_L = 3.0474$.

Remark. Questions dealing with computational techniques used for the investigation of diffusion-induced chaos are important, and the basic sources of information are numerical experiments.

A purely implicit difference scheme with a second-order approximation of the boundary conditions [255] was used in refs. [108, 217]. (In these problems the approximation of the boundary conditions turned out to be very essential [238].) With the nonlinearity involved a simple iteration method was applied, while the three diagonal matrix algorithm [255] was used for solving the linear system.

For the problem under investigation we usually need rather long computation times (strongly dependent on c_1 and c_2 and quickly increasing with increasing region length), so that the system could achieve a steady regime. The choice of steps in time and space usually requires test computations. The Galerkin method turns out to be very efficient – a good approximation to the equation requires a small number of harmonics. At the same time the errors introduced into the solutions by the difference and the spectral approximations turn out to be different. (In the first case the symmetry of the solutions of the original equation is not maintained, and this fact is very essential in an analysis of unstable spatially symmetric solutions.)

In refs. [242, 254] a pseudospectral method based on a fast Fourier transform algorithm was used. In the first case 64 harmonics were taken, in the second case 32. A system of ordinary differential equations was solved by the predictor–corrector method [20].

9.2. Chaos in systems with transport

Let us consider one generalization of the Kuramoto–Tsuzuki equations. In refs. [256–258] a phenomenological model of so-called "*open flows*" (such as flows in tubes, channels, etc.) is proposed. It is given by the equation

$$\psi_t = a\psi - v\psi_x + b\psi_{xx} - c|\psi|^2\psi\,, \quad 0<x<\infty\,, \quad \psi(0,t)=\varepsilon(t)\,, \quad \psi(x,0)=\psi_0(x)\,, \tag{9.4}$$

where $\varepsilon(t)$ is weak random noise; $a=a_1+ia_2$, $b=b_1+ib_2$ and $c=c_1+ic_2$ are complex coefficients, while v is a real coefficient; all coefficients are supposed to be piecewise but may be different in different regions.

For $c=0$, $\varepsilon(t)=0$ in the Cauchy problem with $-\infty<x<\infty$ the solution is determined by the explicit formula

$$\psi(x,t)=\frac{e^{at}}{(2\pi bt)^{1/2}}\int_{-\infty}^{\infty} dx'\,\psi_0(x')\exp[-(x-vt-x')/4bt]\,.$$

From the above formula it follows that three types of behaviour of the solutions of the linear problem are possible as $t\to\infty$.

1. $a_1<0$. The solution here is absolutely stable; $|\psi(x,t)|\to 0$, uniformly in x.
2. $a_1 - v^2b_1/(4|b|^2)>0$. The solution is absolutely unstable, $\psi(x,t)\to\infty$ at each point x.
3. $a_1 - v^2b_1/(4|b|^2)<0$, $a_1>0$. The solution is spatially or convectively unstable.

In case 3

$$\lim_{t\to\infty}|\psi(x,t)|\to 0\,, \qquad \lim_{t\to\infty}|\psi(X+vt,t)|\to\infty\,,$$

for some value v' and fixed arbitrary values of x and X.

If in problem (9.4) there is a region on the left where the solution is spatially unstable, the weak noise is of importance. When it is absent $\psi(x,t)\to 0$ as $t\to\infty$ at each point. In the presence of noise right-running waves are generated whose amplitude grows with time. When the amplitude $|\psi(x,t)|$ becomes sufficiently large, the nonlinearity becomes essential, and a chaotic regime develops. Numerical calculations show that in spite of the complex form and aperiodicity of the solution all the Lyapunov exponents may be nonpositive [258].

Describing such regimes requires the introduction of new quantitative characteristics of chaos, in particular, the *velocity-dependent Lyapunov exponents* $\lambda(v', x_1, x_2)$,

$$\lambda(v',x_1,x_2)\equiv\lim_{t\to\infty}\frac{1}{t}\ln\left|\frac{\zeta(v',x_1,x_2,t)}{\zeta(v',x_1,x_2,0)}\right|\,,$$

$$\zeta(v',x_1,x_2,t)\equiv\left(\int_{x_1+v't}^{x_2+v't}|\delta\psi(x,t)|^2\,dx\right)^{1/2}\,,$$

where $\delta\psi(x,t)$ is the solution of the equation that describes the evolution of a small perturbation $\delta\psi(x,0)$ in the region (x_1,x_2); it is an analog of the equation of variations.

The calculations presented in refs. [256, 257] show that chaotic space–time regimes of different types are possible in nonlinear dissipative media with transport ($v \neq 0$). Experimental investigation of such behaviour in open systems would be very interesting.

9.3. *Few-mode chaos in a hydrodynamic problem*

Above we have discussed diffusion-induced chaos that is described by the Kuramoto–Tsuzuki equation. Such regimes seem to be typical for many reaction–diffusion-type systems and some hydrodynamics problems. The stochastic regimes play an important role in other dissipative media too. It appears very helpful to use the ideas developed in the study of dynamic systems of low dimension. Consider the following example.

In the literature it has repeatedly been mentioned that the Lorenz system is not applicable to the physical situation for whose description it was proposed because an increase in the number of harmonics qualitatively changes the behaviour of the solutions depending on the parameter. However, it has been shown that the same differential equations may serve as an efficient model in other problems, in particular, in laser physics [13]. It is of interest to investigate nonlinear media and physical systems where the properties of chaotic regimes prove to be like those in the Lorenz model, which have been studied in detail.

One such system, called a thermosyphon, was proposed in ref. [259]. The thermosyphon is a torus filled with an incompressible fluid and mounted in a vertical position. Gravity acts in the vertical direction (fig. 9.8). Such systems are interesting in terms of some engineering problems arising in energy technology.

The fluid in the thermosyphon is heated from below and cooled from above (the wall temperature varies as $T = T_0 + W\cos\varphi$). The fluid density linearly depends on the temperature, the fluid velocity is determined by the Navier–Stokes equation

$$\frac{\partial \boldsymbol{v}}{\partial t} + (\boldsymbol{v}\cdot\nabla)\boldsymbol{v} = -\frac{1}{d_0}\nabla p + [1 + \delta(T_0 - T)]\boldsymbol{g} + \nu\nabla^2\boldsymbol{v}\,,$$

and the temperature distribution by the thermal conductivity equation

$$\partial T/\partial t + \boldsymbol{v}\cdot\nabla T = \chi\nabla^2 T\,.$$

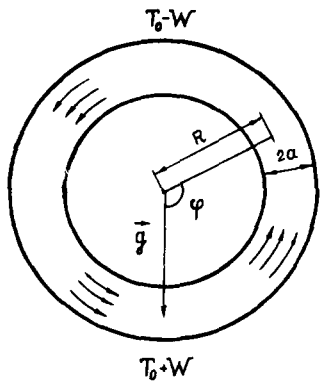

Fig. 9.8

These equations are studied by the Galerkin method (in the simplest approximation it yields the Lorenz system). A series of statements about the properties of the ensuing systems of equations are proved.

The calculations show that in this case increasing the number of modes does not change the scenario of the transition to chaos. It remains the same as in the Lorenz model. The quantity W may play the role of a control parameter.

Regardless of the number of harmonics chaotic regimes are well described by one-dimensional maps like those in the Lorenz system.

9.4. Spatial–temporal chaos in systems close to an integrable system

Stochastic spatial–temporal regimes are typical for a number of nonlinear optics problems. A large class of such nonlinear media is considered in the reviews [78, 260]. Their specific feature is that they are close to a completely integrable system – the cubic Schrödinger equation. The equation itself may be reduced to a certain linear equation by the inverse scattering method, and its solution in an unbounded region for $t \to \infty$ is a set of solitons. The appearance of sources and dissipative terms in such equations can lead to a very complex spatial–temporal behaviour of the solutions.

In accordance with ref. [78] we discuss one physical system of such a type. We consider laser beam propagation through a ring resonator filled with matter with a nonlinear coefficient of refraction (fig. 9.9).

The electric field of an incident wave may be represented in the form

$$E_{\text{in}} = A(x)\, e^{i(kz-\omega t)} + \text{c.c.},$$

and the field in the ring resonator in the form

$$E = F(x, z, t)\exp(ikz - i\omega t) + B(x, z, t)\exp(-ikz - i\omega t) + \text{c.c.}$$

Using adiabatic elimination of the atomic variables [13, 78] and asymptotic methods we may obtain an equation for the wave amplitude B in the form

$$2i\frac{\partial B}{\partial z} + \frac{2i}{c}\frac{\partial B}{\partial t} + \gamma L_1\left(\frac{\partial^2 B}{\partial x^2} + \frac{\partial^2 B}{\partial y^2}\right) + \beta L_1 N(BB^*)B = 0, \tag{9.5}$$

where $N(I)$ is a function determined by the properties of the nonlinear medium. Usually $N(I) =$

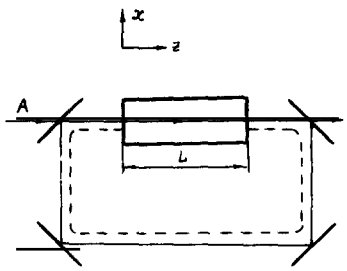

Fig. 9.9

$-1/(1+2I)$ (*saturable nonlinearity*); for small I it becomes the "*Kerr nonlinearity*" $N(I) = -1 + 2I$. In this case eq. (9.5) transforms to the cubic Schrödinger equation.

If the amplitude of the incident wave is independent of time, the quantity $t - z/c$ can be replaced by an integer index n which indicates how many times the wave passed through the ring resonator. Then we obtain the following problem:

$$B_n(x, 0) = \sqrt{T}A(x) + R\,e^{ikL}B_{n-1}(x, \zeta = z/L = 1), \quad B_0 = 0. \tag{9.6}$$

The coefficients R and T, which are less than unity, are determined by the resonator properties, and the coefficients $B_n(x, \zeta)$ change, when ζ varies from 0 to 1, according to the equation

$$2iB_{n\zeta} + \gamma(B_{nxx} + B_{nyy}) + \beta N(B_n B_n^*)B_n = 0. \tag{9.7}$$

This problem is equivalent to the *infinite-dimensional map* $B_n(x, 0) \to B_{n+1}(x, 0)$, which indicates how the amplitude B changes after every passage through the resonator.

In the plane wave case when there is no Laplacian in eq. (9.7) it can be solved explicitly, and the problem is reduced to investigating a two-dimensional map of the complex plane into itself,

$$B_{n+1} = a + R\exp[ikL + i\beta N(B_n B_n^*)/2]B_n, \quad B_n \equiv B_n(\zeta = 0).$$

In this map the coefficient $R^2 < 1$ is responsible for the contraction of the phase volume, a for the transport, and the exponent for rotation. It is clear that in such a map there may occur fixed points, cycles, or chaotic attractors. The involvement of various instabilities leads to an increase of the dimension of the map.

Two-dimensional maps arise also in the case when the spatial profile is close to a soliton solution,

$$B = G_s(y, \zeta, \lambda, \gamma) = S(\lambda y, \lambda)\,e^{i[(\lambda^2-1)\zeta/2+\gamma]},$$

where $S(\theta, \lambda)$ is a real even solution of the equation

$$S_{\theta\theta} - S + \frac{1}{\lambda^2}[1 + N(S^2)]S = 0,$$

tending to zero as $\theta \to \infty$; λ determines the soliton amplitude and width, and γ the phase. It may be expected that after each passage through the resonator the form of the solution will remain the same while the parameters γ and λ change. Instead of an infinite-dimensional map it yields a two-dimensional map $(\lambda_n, \gamma_n) \to (\lambda_{n+1}, \gamma_{n+1})$. (Its specific form is given in ref. [78].) Interesting more complex patterns of spatial ordering are observed when the characteristics of the incident wave or the system parameters are varied. The existence of solutions close to solitons proves very useful in these cases. It helps to describe complex processes in nonlinear media with the aid of dynamic systems of low dimension.

Numerical experiments have shown that in ring resonators where the intensity of the incident wave A is constant the transition to chaos may be connected with a cascade of period-doubling bifurcations with intermittency, or with the Ruelle–Takens scenario [261].

Complex cycles and stochastic regimes were observed also in a ring resonator with absorption [in this case eq. (9.7) would include dissipative terms] when the amplitude of the incident wave was modulated

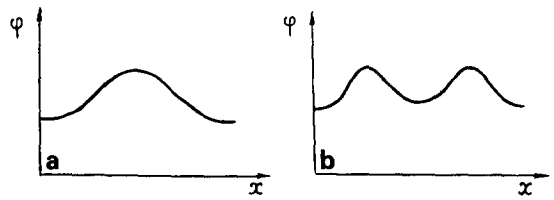

Fig. 9.10

in time, $A(t) = A_0 \Sigma_n \operatorname{sech}(t - nt_r)$ [99]. The energy losses and the pumping in the ring resonator were determined by the boundary conditions while the nonlinear medium could be described by integrable equations. It is interesting, however, to consider nonlinear media which are close to completely integrable ones and where there are dissipative processes and sources explicitly dependent on time. Such is, for example, the sine-Gordon equation with an inducing force, and damping,

$$\varphi_{tt} - \varphi_{xx} + \sin\varphi = \varepsilon[-\alpha\varphi_t + \Gamma \sin\omega t], \quad 0 < \varepsilon \ll 1,$$
$$\varphi(x + L, t) = \varphi(x, t), \quad \varphi(x, t = 0) = \varphi_{in}(x), \quad \varphi_t(x, t = 0) = v_{in}(x). \tag{9.8}$$

In ref. [262] it was discussed how a stochastic temporal regime emerged and how the spatial ordering in the system changed as the amplitude of the inducing force Γ increased. For $L = 24$, $\varepsilon = 0.1$, $\varepsilon\alpha = 0.04$, $\omega = 0.87$ and with increasing $\varepsilon\Gamma$, $0 < \varepsilon\Gamma < 0.116$, the solutions grew more complex in the following way.

For small values of $\varepsilon\Gamma$ and $t \to \infty$ the function $\varphi(x, t)$ proves to be spatially homogeneous and periodically varying in time with the frequency of the inducing force. Then it loses its homogeneity, and a profile arises whose typical form and location are as shown in fig. 9.10a. However, the solution still changes with frequency ω.

Then, as the parameter Γ increases, quasi-periodic regimes appear and the amplitude of the fourth spatial harmonic starts growing. As Γ increases further, temporal chaos appears, in which "turbulent peaks" alternate with the "laminar" intervals. The amplitudes of the second and fourth harmonics become comparable [for a certain instant of time the function $\varphi(x, t)$ is shown in fig. 9.10b].

In ref. [262] the Lyapunov exponents were calculated and the analogs of the Poincaré section, the temporal spectrum of the solution and other characteristics of the stochastic solutions were constructed. The correlation exponent in the investigated chaotic regimes changed in the interval $3.5 \lesssim \nu \lesssim 4.5$.

In the analysis of problem (9.8) the fact that the system is close to completely integrable was used. The inverse scattering method was applied by constructing the linear equation in which the "potential" changes while the "energy levels" λ remain fixed. Here at each instant of time a similar transformation is performed, the "potential" is constructed and the eigenvalues are determined. But they change in time. From the function $\lambda(t)$ we may judge how close the solution is to a set of solitons. It enables us to construct simplified efficient models.

Stochastic regimes were discovered also in media described by the equation

$$q_t + iq_{xx} - 2i|q|^2 q = (\varepsilon_1 - \varepsilon_2|q|^2)q + \varepsilon_3 q_{xx} - (\varepsilon_0/T) \sum_{n=-\infty}^{\infty} \exp(2\pi i n t/T).$$

In this case we can also construct dynamic systems of low dimension which allow us to describe chaotic regimes [264].

9.5. *A priori estimates of the dimension of the attractor*

When processes are studied in nonlinear media where stochastic regimes are observed, the dimension of the strange attractor is usually estimated in the course of a numerical or physical experiment. Recently, however, mathematical theories have been developed which allow a priori estimates of the dimension of the attractor in partial differential equations. Appropriate studies are discussed in the review [19].

We note here two important results. For the two-dimensional system of the Navier–Stokes equations it has been shown (specifically, for zero boundary conditions) that the Hausdorff dimension of the attractor may be estimated from above,

$$\dim U \leq C(\mathrm{Re})^4 .$$

For the reaction–diffusion system of equations,

$$u_t = \nu a\, \Delta u - f(x, u) + \lambda u , \quad u|_{\partial\Omega} = 0 , \quad \Omega \subset \mathbb{R}^n ,$$

where $u = (u_1, \ldots, u_m)$, $f = (f_1, \ldots, f_m)$, while the matrix a, of order m with constant coefficients, is such that the matrix $(a + a^*)/2$ is positive definite and its minimal eigenvalue exceeds μ_0, i.e.,

$$\mu_0 |u|^{p_0} - C \leq f(x, u)u \leq \mu_1 |u|^{p_0} + C , \quad p_0 > 2 ,$$

and

$$\sum_{i,k=1}^{m} \frac{\partial f_k}{\partial u_i}\, \xi_i \xi_k \geq 0 ,$$

it has been shown that

$$\dim U \leq C\lambda^{n/2} \nu^{-n/2} , \quad \lambda > 1 , \ \nu > 0 . \tag{9.9}$$

In the cases when the diffusion coefficient is constant the estimate (9.9) shows how the dimension of the attractor changes as the length of the region increases.

It may be expected that theoretical investigations of diffusion-induced chaos and other stochastic regimes in nonlinear media will be intensified in the immediate future.

10. Elementary types of ordering in two-dimensional systems

Multi-dimensional effects are essential for the investigation of many open systems and reaction–diffusion systems have to be analysed in two-dimensional and three-dimensional domains. An idea of the possible types of ordering in such nonlinear media is given by the two-dimensional analog of the Kuramoto–Tsuzuki equation,

$$W_t = W + (1 + \mathrm{i}c_1)(W_{xx} + W_{yy}) - (1 + \mathrm{i}c_2)|W|^2 W . \tag{10.1}$$

This equation is used in the theory of wind waves on water [96], for the investigation of dissipative structures in active media and in oscillating chemical reactions [101], and in some morphogenesis models [5]. We note that eq. (10.1) describes a narrower class of two-component systems than the Kuramoto–Tsuzuki equation in one-dimensional problems. Since in the two-dimensional case both the length and the direction of the wavevector are important, the number of unstable modes increases and models, more complicated than eq. (10.1), appear [121].

In some studies major attention is paid to the Cauchy problem for this equation. An extensive list of such publications is given in ref. [101]. Usually they deal with self-similar solutions (spiral waves, as a rule), defined in infinite domains and having *phase singularities* (i.e. points where $|W| \to 0$, and the phase φ, $W = \rho\, e^{i\varphi}$, is not defined [265]).

Comparing the analytical results with numerical or physical experiments leads to a number of problems. First, it is necessary to find out how quickly self-similar solutions can be obtained. Second, we always have to deal with bounded domains, while the solution does not have the property of localization.

That is why we are interested in an alternative approach – an analysis of solutions of eq. (10.1) for small two-dimensional domains. In this case we could use the results obtained for simplified models and one-dimensional equations. Within such an approach a more thorough analysis might be performed, getting beyond the scope of a single class of solutions, and the main types of ordering interesting for more complex problems could be revealed.

According to refs. [103, 217] we consider the following boundary value problem,

$$\begin{aligned} &W_t = W + (1 + ic_1)(W_{xx} + W_{yy}) - (1 + ic_2)|W|^2 W\,, \quad 0 \le x \le l\,, \quad 0 \le y \le l\,, \\ &W(x, y, 0) = W_0(x, y)\,, \quad W_x(0, y, t) = W_x(l, y, t) = W_y(x, 0, t) = W_y(x, l, t) = 0\,. \end{aligned} \tag{10.2}$$

We shall be interested in the behaviour of its solutions for different values of c_1 and c_2 in the case of small domains. In the numerical computations given below $l = \pi$ and the initial data are asymmetric, of the form

$$W_0 = u_0 + iv_0 = 0.1 \sum_{m,n=0}^{4} \cos(\pi m x/l) \cos(\pi n y/l)[1 + i/(m+1)]\,.$$

In such a formulation only the simplest symmetric solutions are essential, namely

(a) *spatially homogeneous solutions*

$$W(x, y, t) = \exp(-ic_2 t)\,, \tag{10.3}$$

(b) *one-dimensional solutions*

$$W(x, y, t) = W(x, t) \quad \text{or} \quad W(x, y, t) = W(y, t)\,,$$

(c) *solutions symmetric with respect to one of the diagonals*

$$W(x, y, t) = W(y, x, t) \quad \text{or} \quad W(x, y, t) = W(l - y, l - x, t)\,.$$

We shall discuss the following questions. Will the one-dimensional solutions of problem (10.2) be stable against two-dimensional perturbations? Does this problem have solutions for which there is no one-dimensional analog? In what way do the two-dimensional structures get complicated when the parameters c_1 and c_2 are varied?

10.1. A simplified finite-dimensional system

The analysis of various simplified models plays an important role in investigations of one-dimensional problems. To construct such models in two-dimensional problems it is convenient to present the solutions in the form

$$u(x, y, t) = \sum_{m,n=0}^{\infty} a_{mn}(t) \cos(\pi m x/l) \cos(\pi n y/l) ,$$

$$v(x, y, t) = \sum_{m,n=0}^{\infty} b_{mn}(t) \cos(\pi m x/l) \cos(\pi n y/l) ,$$

and to write down a system of equations which connects the Fourier coefficients $a_{mn}(t)$ and $b_{mm}(t)$,

$$\begin{aligned} \dot{a}_{mn} &= a_{mn} - (a_{mn} - c_1 b_{mn}) k^2 (m^2 + n^2) - (u_{mn} - c_2 v_{mn}) , \\ \dot{b}_{mn} &= b_{mn} - (c_1 a_{mn} + b_{mn}) k^2 (m^2 + n^2) - (c_2 u_{mn} + v_{mn}) , \quad k = \pi/l , \end{aligned} \tag{10.4}$$

where u_{mn} and v_{mn} are known functions of $\{a_{ij}\}$ and $\{b_{ij}\}$. Below we shall use the notation ρ_{mn}: $\rho_{mn}^2 = a_{mn}^2 + b_{mn}^2$. Simplified models may be obtained from this infinite system by keeping a finite number of equations. This may be done in various ways, for example, by dismissing the harmonics a_{mn} and b_{mn} with $m \geq p$ or $n \geq p$. The simplified system thus obtained will be called *the system with* $N = p$; it contains $2p^2$ equations.

We shall now consider a simplified model with $N = 2$, which contains 8 ordinary differential equations. We can decrease the number of equations by going over to the variables ρ_{mn} and θ_{mn} with the aid of the formulas $a_{mn} = \rho_{mn} \cos \varphi_{mn}$, $b_{mn} = \rho_{mn} \sin \varphi_{mn}$, $\theta_{mn} = \varphi_{mn} - \varphi_{00}$. The equation for φ_{00} may be solved separately. It means that the functions $a_{mn}(t)$, $b_{mn}(t)$ change in a more complicated way than $\rho_{mn}(t)$ and $\theta_{mn}(t)$. In particular, the singular points $\rho_{mn} = \text{const.}$, $\theta_{mn} = \text{const.}$ correspond to periodic solutions of $a_{mn}(t)$, $b_{mn}(t)$; the limit cycles correspond to two-frequency regimes. Therefore, below the solutions of a simplified system for which $\rho_{mn} = \text{const.}$ will be called *singular points*, and the solutions for which $\rho_{mn}(t)$ are periodic will be called *limit cycles*.

In the simplified model with $N = 2$ there is an analog of the simplest symmetric solutions. The singular point $\rho_{00} = 1$, $\rho_{mn} = 0$, $m + n \neq 0$, corresponds to the homogeneous solution (10.3). The solutions of the simplified system for which $a_{mn} = 0$, $b_{mn} = 0$, $n \neq 0$, correspond to the one-dimensional solutions, in y, of (10.2).

The solutions of problem (10.2) that are symmetric with respect to the diagonal of the square, $x = y$, may be compared with the integral curves where $a_{mn} = a_{nm}$, $b_{mn} = b_{nm}$. Such solutions of the system of ordinary differential equations are also called *symmetric*.

Let us see how the type of the solutions changes for the simplified system as the parameter c_2 decreases. We consider the line $c_1 = 1.5$. In the system of eight ordinary differential equations the

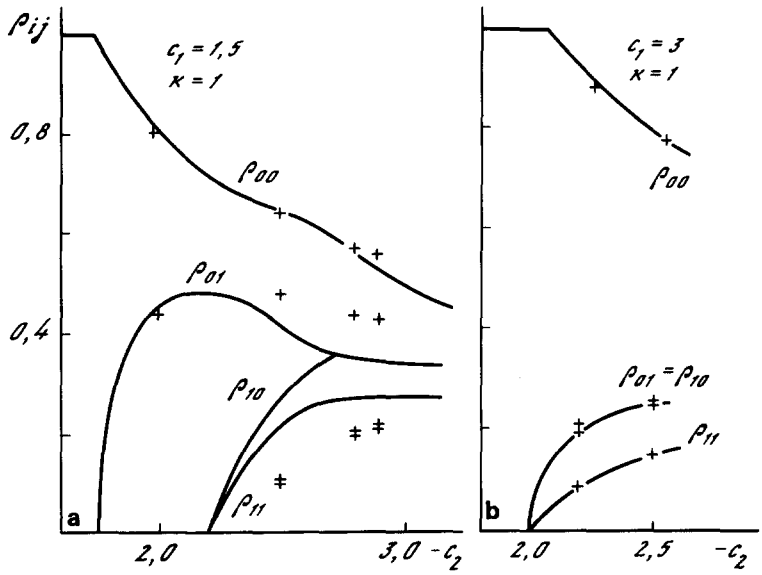

Fig. 10.1

homogeneous solution loses its stability, the stable singular point with $\rho_{00} \neq 1$ appears. The value of c_2 at which bifurcation occurs coincides with the critical value of the parameter for the partial differential equation. In the ensuing singular point $\rho_{mn} = 0$ for $m \neq 0$. We note that in the system another singular point appears simultaneously for which $\rho_{mn} = 0$ for $n \neq 0$. In this case the system with $N = 2$ becomes simplified and transforms into the system of ordinary differential equations (3.15), considered in chapter 7 [$\xi = a_{00}^2 + b_{00}^2$, $\eta = a_{01}^2 + b_{01}^2$, $\theta = 2(\varphi_{00} - \varphi_{01})$].

As c_2 decreases further, the point with $\rho_{mn} = 0$ for $m \neq 0$ loses its stability, and the asymptotic behaviour is determined by the singular point with $\rho_{mn} \neq 0$ (see the solid lines in fig. 10.1). Then for a certain value of c_2, ρ_{01} becomes exactly equal to ρ_{10}, after which the computations converge to a symmetric solution with $a_{01} = a_{10}$, $b_{01} = b_{10}$.

For $c_2 \approx -3.3$ a Hopf bifurcation occurs and a symmetric limit cycle develops [$\rho_{01}(t) = \rho_{10}(t)$]. The position of the singular point which lost its stability and examples of symmetric cycles are shown in fig. 10.2a. For $c_2 \approx -3.7$ the cycle loses its symmetry. Two projections of such a type of solution are shown in fig. 10.2b. The sequence of bifurcations observed conditionally may be presented as shown in scheme

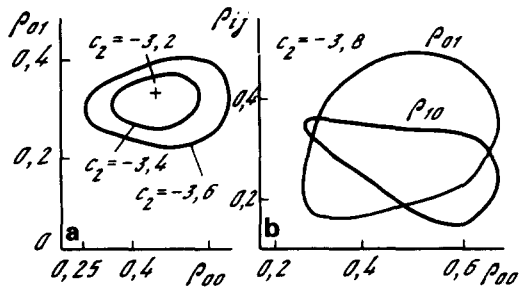

Fig. 10.2

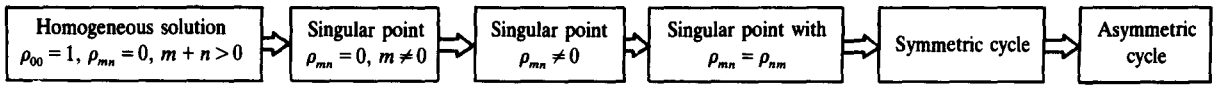

Scheme 2.

2. In this sequence most bifurcations are associated with the loss or appearance of symmetry, which is an essential difference between the two- and one-dimensional problems.

The first transition in this sequence is connected with the appearance of a singular point with $\rho_{mn}=0$, $m\neq 0$. The critical value of the parameter at which this transition occurs is determined by equality (7.8) as in the one-dimensional case. The situation, however, may be more complicated. We may verify this by observing how the solution changes along the line $c_1=3.0$ (fig. 10.1). How the solutions defining the asymptotic behaviour of a simplified system with $N=2$ become more complex is schematically shown in scheme 3.

It is important to note that a singular point with $\rho_{01}=\rho_{10}$ appears for a value of the parameter c_2 where points with $\rho_{mn}=0$, $m\neq 0$, may emerge. A symmetric solution is obtained for a general form of the initial data (spontaneous appearance of symmetry). The cause of this phenomenon can be understood using methods from bifurcation theory.

10.2. Loss of stability of a spatially homogeneous solution

We consider problem (10.2) near the critical values of the parameters for which the homogeneous solution (10.3) loses its stability. The respective results are shown by markers in fig. 10.1. As $t\to\infty$ the asymptotic behaviour is determined by solutions with $\rho_{mn}=\text{const.}$, $m,n=0,1,2,\ldots$. As in the simplified model with $N=2$, the solution arising is one-dimensional on the line $c_1=1.5$ and symmetric on $c_1=3$. Both the types of solution and their quantitative characteristics coincide in these two problems.

The periodic solutions of the partial differential equation are an analog of the singular points in the simplified model. The following lemma is valid.

Lemma. If a self-similar solution of the form

$$W(x,y,t)=R(x,y)\exp[\mathrm{i}\omega t+\mathrm{i}a(x,y)] \tag{10.5}$$

satisfies eq. (10.2) it has $\rho_{mn}=\text{const.}$, $\theta_{mn}=\text{const.}$, where $m,n=0,1,2,\ldots$ (ρ_{mn} and θ_{mn} are determined by the Fourier coefficients a_{mn}, b_{mn} as in the simplified system). The converse is also true: if the harmonic amplitudes and the phase shifts between the harmonics are constant in a solution of problem (10.2), it may be written in the form (10.5).

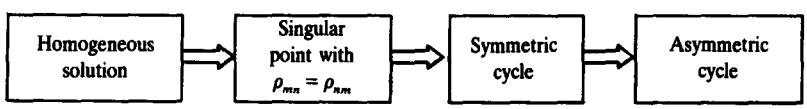

Scheme 3.

The self-similar solutions appearing after the loss of stability of the homogeneous solution are close to it. Therefore, it is natural to use asymptotic methods for its analysis. We write eq. (10.2) in the variables ρ and φ:

$$u = \rho \cos\varphi\,, \quad v = \rho \sin\varphi\,,$$

$$\rho_t = \rho - \rho^3 + (\rho_{xx} - \rho\varphi_x^2 + \rho_{yy} - \rho\varphi_y^2) - c_1(2\rho_x\varphi_x + \rho\varphi_{xx} + 2\rho_y\varphi_y + \rho\varphi_{yy})\,, \tag{10.6}$$

$$\rho\varphi_t = -c_2\rho^3 + (2\rho_x\varphi_x + \rho\varphi_{xx} + 2\rho_y\varphi_y + \rho\varphi_{yy}) + c_1(\rho_{xx} - \rho\varphi_x^2 + \rho_{yy} - \rho\varphi_y^2)\,.$$

We shall search for a solution in the form of a series in the small parameter ε that characterizes the deviation of c_2 from the critical value $\bar{c}_2$ at which the solution (10.3) loses its stability,

$$\rho = 1 + \varepsilon r_1(x, y) + \varepsilon^2 r_2(x, y) + \varepsilon^3 r_3(x, y) + \cdots\,,$$

$$\varphi = (-\bar{c}_2 + \varphi_1\varepsilon + \varphi_2\varepsilon^2 + \varphi_3\varepsilon^3 + \cdots)t + \varepsilon a_1(x, y) + \varepsilon^2 a_2(x, y) + \cdots\,, \tag{10.7}$$

$$c_2 = \bar{c}_2 + \omega_1\varepsilon + \omega_2\varepsilon^2 + \omega_3\varepsilon^3 + \cdots\,, \quad \varphi_i, \omega_i = \text{const.}\,.$$

We substitute formulas (10.7) into eqs. (10.6) and equalize terms with the same power of ε. This yields systems of equations for the successive determination of $r_n(x, y)$, and $a_n(x, y)$. We may show that [217]

$$r_1 = A\cos kx + B\cos ky\,, \qquad a_1 = -2Lr_1/k^2 + \text{const.}$$

The higher-order equations are soluble if their right-hand sides are orthogonal to all nontrivial solutions of the corresponding homogeneous equations (the *Fredholm alternative*).

The solubility conditions for the second- and third-order equations allow us to determine the values of A and B. The small parameter ε has been determined earlier to within a factor. Further we shall assume that $\varepsilon = |c_2 - \bar{c}_2|^{1/2} + \cdots$. This simplifies the relations for A and B,

$$A(XA^2 + YB^2 - \alpha Z) = 0\,, \qquad B(YA^2 + XB^2 - \alpha Z) = 0\,, \tag{10.8}$$

where

$$X = \frac{2L^4}{3k^6} - \frac{3L^2}{2k^2} + \frac{5k^2}{4} + \frac{k^4}{4} + L^2\,, \quad Z = \frac{|c_1|}{1 + c_1^2}\,,$$

$$Y = \frac{4L^2}{k^2} + L^2 - k^2 + \frac{k^4}{4}\,, \quad \alpha = \operatorname{sign} c_1 \cdot \operatorname{sign}(\bar{c}_2 - c_2)\,.$$

From formulae (10.8) it is clear that $X + Y > 0$, $Z > 0$; also it may be verified that $X > 0$.

It is easy to find that for $\alpha = -1$ the system of equations (10.8) has only trivial solutions. It corresponds to the parameter range where the homogeneous solution (10.3) is stable. Therefore, the bifurcation in the system under investigation is always supercritical [84]. For $\alpha = 1$ the system of equations (10.8) has nine solutions,

$$\begin{aligned}
&\text{(a)}\quad A = B = 0\,,\\
&\text{(b)}\quad A = 0\,,\quad B = \pm(Z/X)^{1/2}\,,\\
&\text{(c)}\quad B = 0\,,\quad A = \pm(Z/X)^{1/2}\,,\\
&\text{(d)}\quad \text{if } X \neq Y\,, \text{ then } A^2 = B^2 = Z(X+Y)\,.
\end{aligned} \tag{10.9}$$

Relations (10.9) show that in the general case ($X \neq Y$) the solutions appearing after branching will be either one-dimensional or symmetric. This conclusion is confirmed by computations.

Bifurcation theory methods may also be used to investigate in which parameter ranges some or other solution is stable. In refs. [103, 217] it is shown that the one-dimensional solution is stable for negative K and the symmetric self-similar solution for positive K,

$$K = \frac{2L^4}{3k^6} - \frac{11L^2}{2k^2} + \frac{9k^2}{4}\,,\quad L = \frac{-2-k^2}{2c_1}\,,\quad k = \pi/l\,. \tag{10.10}$$

The numerical results usually agree well with the asymptotic theory up to $\varepsilon^2 \sim 0.1$.

10.3. Complication of the solutions of the partial differential equation

In the initial problem an elementary attractor of the system of ordinary differential equations (a stable singular point) corresponds to a complex auto-wave process described by a self-similar solution of the form (10.5). We note that a *spiral wave* is a particular case of this solution, which may be written as

$$W = R(r)\exp[\mathrm{i}\omega t + \mathrm{i}S(r) + \mathrm{i}m\varphi]\,,\quad x = r\cos\varphi,\ y = r\sin\varphi\,. \tag{10.11}$$

Formula (10.11) coincides with (10.5) if $R(x, y) = R(r)$, $a(x, y) = S(r) + m\varphi$. The real and imaginary parts of the self-similar solution of problem (10.2), $u(x, y, t)$ and $v(x, y, t)$ periodically change in time; however, the modulus $R = (u^2 + v^2)^{1/2}$ does not depend on time. A typical form of the function $R(x, y)$ in a symmetric and an asymmetric solution in a square with side $l = \pi$ is shown in fig. 10.3.

Let us see how the solutions of the partial differential equation become complicated. On the line $c_1 = 1.5$ the sequence is as shown in scheme 4. The first two bifurcations coincide with those in the simplified system with $N = 2$. The parameters of the singular point with $\rho_{mn} = 0$ for $n \neq 0$ coincide within a few percent with the characteristics of the one-dimensional self-similar solutions. However, in problem (10.2) the sequence of transitions is simpler on the whole: it has no analogs of symmetric singular points and symmetric limit cycles.

On the line $c_1 = 3$ the sequence of bifurcations in the simplified system and the initial problem is the same – as in scheme 3. The parameters of the self-similar solutions and the singular points here are in good agreement (fig. 10.1).

We consider solutions of the partial differential equations for which the functions R and a are periodic in time, $\rho_{mn}(t + T) = \rho_{mn}(t)$, $\theta_{mn}(t + T) = \theta_{mn}(t) + 2\pi p_{mn}$, $p_{mn} = 0, \pm1, \pm2, \ldots$. Such solutions are the analog of the limit cycles in the system with $N = 2$. We note that the functions u and v are not periodic – a stationary two-frequency regime is observed in the system. A similar situation occurred in the simplified model too.

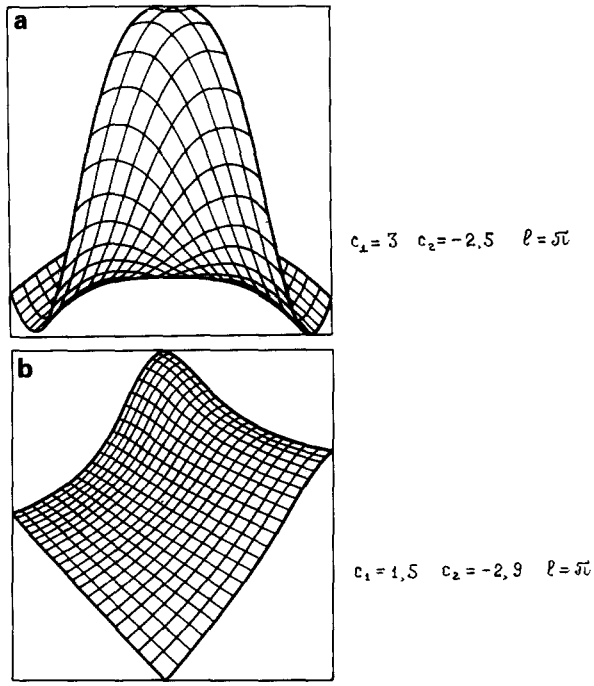

Fig. 10.3

Such types of two-dimensional solutions are rather complex. In order to reveal how they are qualitatively reconstructed we should consider their projections onto some finite-dimensional spaces. In this case the projections on the (ρ_{10}, ρ_{01})-plane are most illustrative. They are shown in fig. 10.4 together with plots of the functions $\rho_{mn}(t)$.

The projection of the solution shown in fig. 10.4a lies entirely above the diagonal $\rho_{10} = \rho_{01}$. During the whole period the directions x and y are inequivalent. We shall call it a *solution of type I*. The projection of the solution shown in fig. 10.4b is a closed curve which lies on both sides of the diagonal. This line is nearly symmetric with respect to the straight line $\rho_{10} = \rho_{01}$. The directions x and y "exchange" their positions every half period, $R(x, y, t + T/2) \approx R(y, x, t)$. Such solutions are of *type II*.

It is important to point out that the solutions of types I and II are qualitatively different. The transition between them superficially resembles a period-doubling bifurcation: for a small change in the parameter c_2 the period of the solution becomes twice as large, and the function $\rho_{00}(t)$ is near $\rho_{00}(t + T/2)$ (fig. 10.4a,b). However, $\rho_{01}(t)$ and $\rho_{10}(t)$ behave differently: during part of the period the function $\rho_{10}(t)$ in the bottom figure (solution of type II) repeats the behaviour of $\rho_{10}(t)$ in the upper

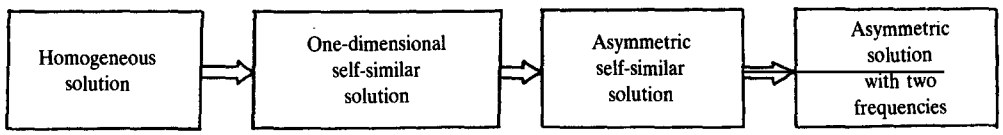

Scheme 4.

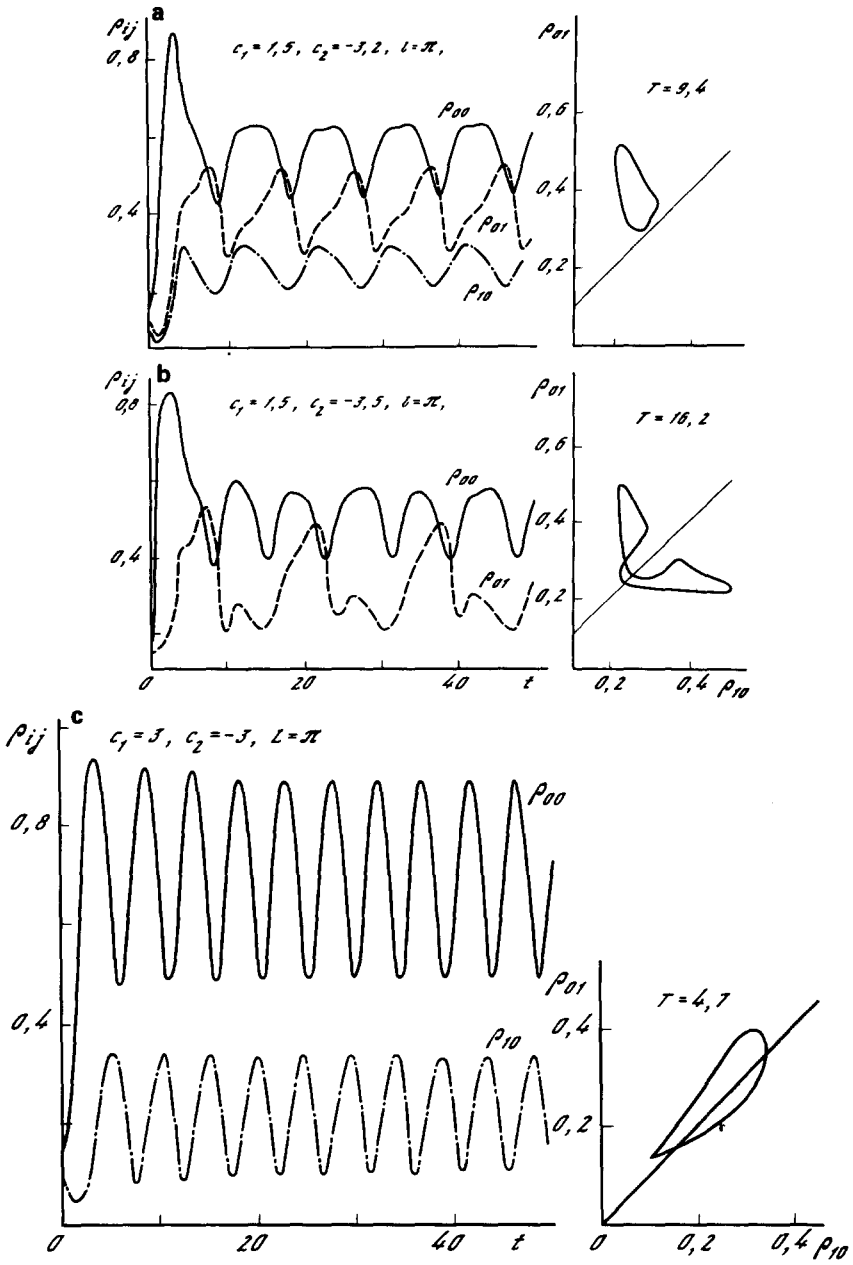

Fig. 10.4

figure, and in the remaining part of the period it repeats the behaviour of $\rho_{01}(t)$. In the vicinity of the transition point the period of the cycle sharply increases.

In the simplified system with $N = 2$ such transitions were not observed. Their appearance may be explained by the concept of a finite-dimensional model. Let there exist for a certain value of the parameter c_2 in the system with the sufficiently large N two stable singular points located symmetrically with respect to the plane $\rho_{mn} = \rho_{nm}$ and not situated in it. As c_2 decreases even further the amplitude of

the oscillation increases, and the cycles approach the symmetry plane from different sides. Due to the uniqueness of the solutions, they may touch each other, and hence the plane $\rho_{mn} = \rho_{nm}$, only at a singular point. The period of each cycle must increase infinitely as the parameter c_2 reaches the value c_2^* ($c_2 = c_2^*$). After the transition ($c_2 < c_2^*$) the cycles become qualitatively reconstructed. While before, being on the limit cycle, the point rotated about one equilibrium state, now it visits the neighbourhood of each of them.

We note that when $c_2 = c_2^*$ in the finite-dimensional system a homoclinic trajectory appears, while the system itself has a special symmetry [if $\{\rho_{mn}(t),\ \theta_{mn}(t)\}$ is a solution then $\{\rho_{nm}(t),\ \theta_{nm}(t)\}$ is a solution too]. This suggests that in this case methods developed for analysis of the Lorenz system may be employed [137].

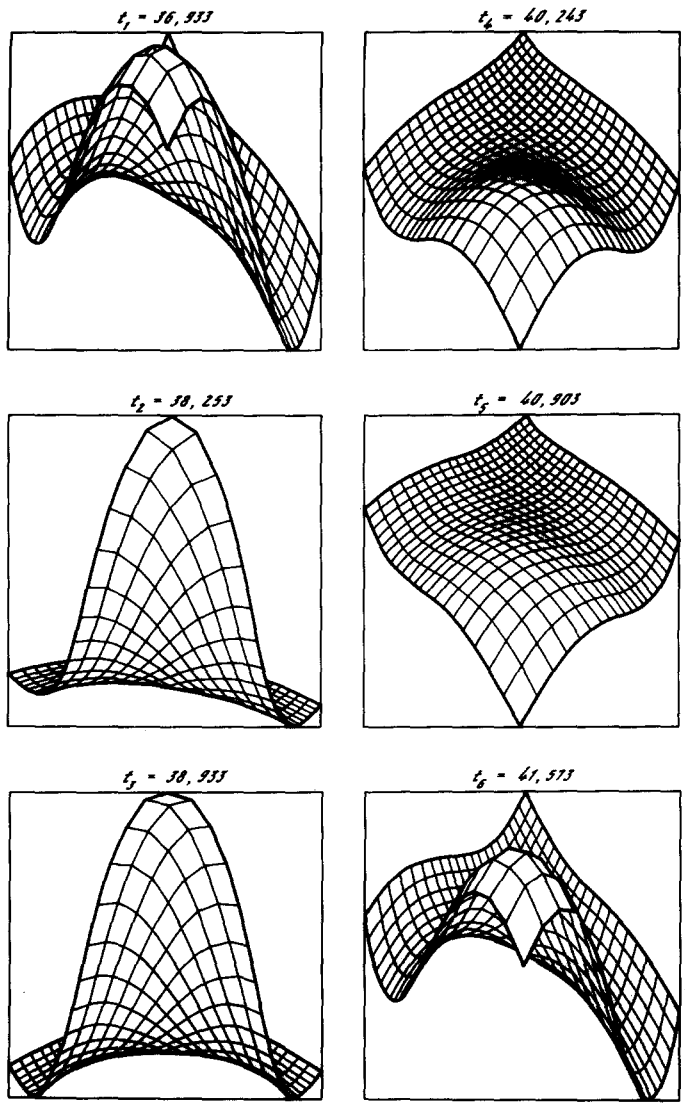

Fig. 10.5

We recall that along with the solution shown in fig. 10.4b there is a symmetric solution $\tilde{W}(x, y, t) = W(y, x, t)$. Therefore, the solutions of problem (10.2) may become further complicated in the same way in strong dependence on the symmetry. Such a mechanism, sometimes called "*anomalous doubling bifurcations*", is rather general and typical for many systems with symmetry [118].

Quite a different picture is observed for $c_1 = 3$. This is due to the fact that in this case the Hopf bifurcation results in a symmetric self-similar solution, such as occurs in the simplified system with $N = 2$. Figures 10.4c and 10.5 show asymmetric solutions with a periodic function R, which can neither be referred to type I nor to type II. It is of great importance that the asymptotic behaviour of the two-dimensional system (10.2) may be determined by analogs of limit cycles. In fact, it is a widespread opinion that in active nonlinear media the leading centres and spiral waves are the basic forms of ordering. In problem (10.2) they are a particular case of two-dimensional self-similar solutions in which the variables are separated once again. In fact, in a certain range of parameters the self-similar solutions determine the asymptotic behaviour of the process. However, in a wide range of values of c_1, c_2 and l they are unstable; here a more complicated ordering arises. It is described by solutions with periodically changing functions R and a. It is natural to expect that such solutions will be observed in many open dissipative systems near the bifurcation point.

As the parameter c_2 decreases further the solutions of one- and two-dimensional problems become aperiodic. In the one-dimensional case the complication on both lines $c_1 = 1.5$ and $c_1 = 3$ is connected with a sequence of period-doubling bifurcations. In the two-dimensional case solutions without ordering observed during computations are also obtained. Examples of such solutions are discussed in refs. [103, 217]. However, diffusion-induced chaos and scenarios of its appearance in two-dimensional systems require further study.

11. New trends in the theory of dissipative structures

For the investigation of nonlinear dissipative processes it may prove very useful to construct simplified models of the phenomenon with the least possible number of degrees of freedom and then to study these models in detail. The results obtained in analysing one- and two-dimensional maps, and systems of several differential equations play an important role in the formulation of modern ideas about the processes in nonlinear systems. They proved very helpful in an analysis of ordering in nonlinear media.

The question arises whether at present there exist other simple models which play an important part in the analysis of complex ordering and chaotic regimes in nonlinear media. Let us describe some of them.

11.1. Complex ordered and stochastic regimes in discrete systems

Discrete systems are widely used for simulating processes in continuous media. To solve partial differential equations difference schemes with derivatives replaced by finite differences are often used (both temporal and spatial coordinates are discretized). However, can discrete systems describe such types of ordering which have not yet been encountered? Can they directly be used as models of some phenomena? To answer these questions it is natural to consider the simplest case when not only the spatial and temporal coordinates are discrete but the function itself acquires only discrete values. An

idea of how rich and unusual the world of such systems is can be gained from the game called "*Life*", which was proposed by the mathematician John Conway from Cambridge University [266]. The name of this game is due to the fact that it simulates the growth, decay and various changes in the population of live organisms.

An infinite board with cells is considered. In the game played on this board the time is discrete ($t = 1, 2, \ldots$). A cell may be *alive* or *dead*. The change of the state of the cell at time $t + 1$ is defined by the states of its neighbours at time t (each cell has 8 neighbours, four of them share a side with it and the other four only a corner). The rules of the game are as follows.

If a cell is dead at time t it becomes alive at $t + 1$ if and only if exactly three of its eight neighbours were alive at t.

If a cell was alive at t it will be dead at time $t + 1$ if and only if less than two or more than three of its neighbours were alive at t.

These rules are very simple. Having a checked sheet of paper we may watch the evolution of elementary configurations. The behaviour of large associations over a long period may be watched by using a computer.

As we shall verify below there is a close analogy between the processes in nonlinear dissipative media and this discrete system. Therefore, it is natural to put the following questions. What basic types of structures (i.e. configurations that determine the behaviour of associations over long times) may exist in such a system? Which laws govern the organization of structures here? Can they interact and what will this lead to?

Stationary structures, i.e. those independent of time, are the simplest. Examples of them are given in fig. 11.1 (we draw a solid dot at the center of a live cell).

Using these stationary structures we may obtain many others. Indeed, if we have such a structure, the configuration obtained by a rotation by 90° will also be stationary. In this figure the four configurations in the right bottom corner show how certain structures may be made longer up to any size. It should be stressed that these structures are *localized*. Being separated by two dead cells, they do not influence each other. We may say that the stationary structures repeat themselves at each step in time. But there are other configurations that repeat themselves in N steps. For brevity we shall call them N-cycles.

Examples of 2-cycles are shown in fig. 11.2. Since 2-cycles are also localized, they are all presented in the same region. During the evolution of various associations the 2-cycle shown in the second line and called the *traffic light* is often encountered.

Many different periodic configurations are known [266]. Efficient algorithms, however, that would allow the construction of configurations with a given period N seem not to have been developed as yet.

Fig. 11.1

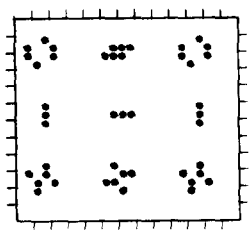

Fig. 11.2

In nonlinear dissipative media the structures are interesting not only as they are. They determine the behaviour of the system as $t \to \infty$ for different initial data. Is this so in the discrete system under investigation? The answer is positive.

The system of cells described by the game "Life" develops irreversibly. Indeed, the configuration at time t fully determines the future (states at $t+1$, $t+2$, etc.). But the past of the system cannot be restored from its present. The picture here is exactly the same as in one-dimensional maps, only a given configuration may have infinitely many pre-images. (We may use the localization property and situate a set of localized single cells or pairs of them so that they would not influence the given configuration and one another. It is clear that they will all disappear on the next step, by no means influencing the future of the system.)

The evolution of randomly given initial data frequently leads to the appearance of simple localized structures and traffic lights. However, more complex types of evolution are also possible, for example, when cycles of large period with complex form appear in symmetric configurations (fig. 11.3).

In the Life game there are configurations which can move across a plane. One of them is a *glider* (fig. 11.4a, the stationary structure here is taken as a reference point). Every four steps it repeats itself, shifting by one cell down and to the right. (It is clear that due to the symmetry there are gliders moving along both diagonals in both directions.) Four different "phases" of the glider are shown in fig. 11.4a.

By the way, some configurations may move along a line other than a diagonal. For example, such are the three *ships* shown in fig. 11.4b. (Let us note that not every configuration of such a type will be a

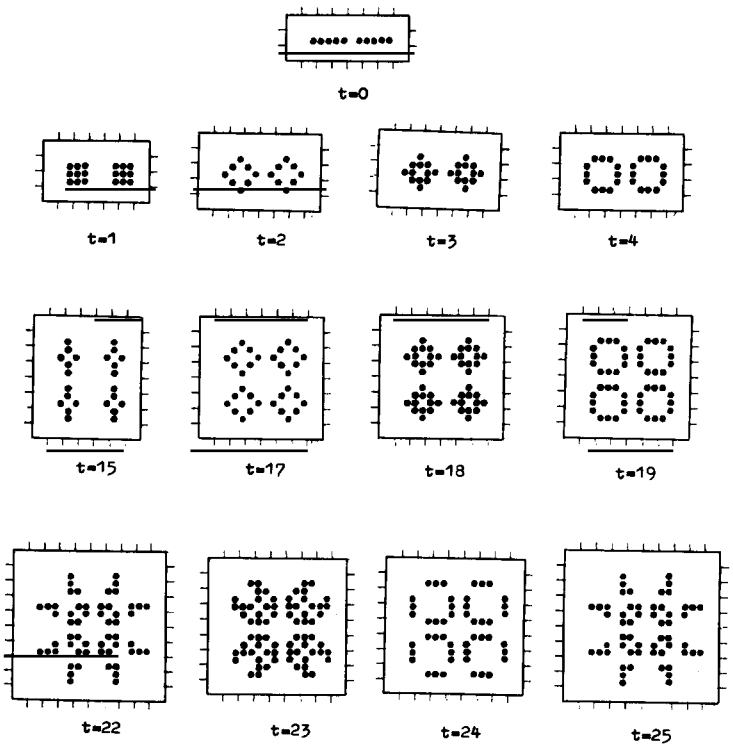

Fig. 11.3

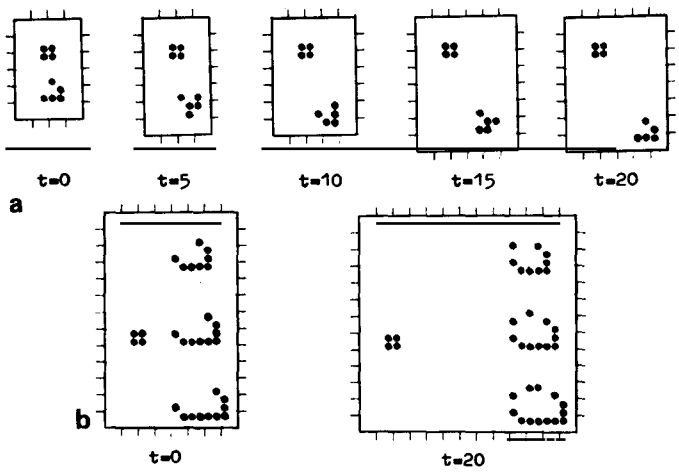

Fig. 11.4

"ship".) So, we have gliders and ships. The question arises: What happens when they collide with each other or with a stationary structure? The collisions may be of various types depending on the glider course and its phase at the time of collision.

The collision of two gliders or of a glider with a stationary structure may lead to their "*annihilation*" (fig. 11.5), or a whole set of traffic lights and stationary structures may be generated (fig. 11.6). Let us note two laws. If symmetry has appeared in the configuration (for example, with respect to the vertical

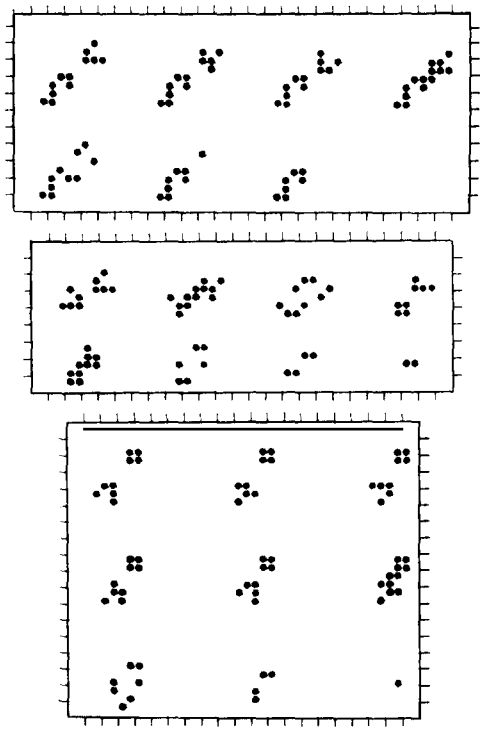

Fig. 11.5

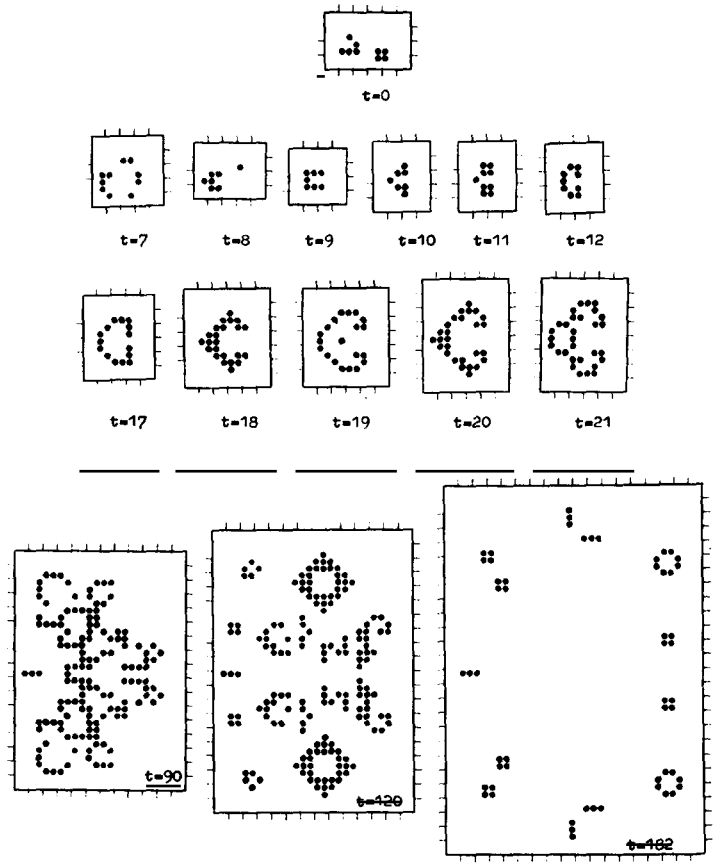

Fig. 11.6

or horizontal axis), it will be preserved during the evolution (see steps 7, 8, 9). If the configuration remains localized in an $N \times N$ square all of the time, it is a collection of stationary structures and cycles whose period does not exceed 2^{N^2}. Indeed, each cell may be in one of two states and in total there are N^2 cells in the square; therefore for $t > 2^{N^2}$ the configuration will be repeating itself.

When considering continuous media we discussed resonant excitation – initial data that resulted in a more complex evolution of solutions than in other cases. There is an analog of such a behaviour in the Life game. Let us note the configuration shown in fig. 11.7. Arising cells occupy a larger and larger part of the plane, several gliders evolve and this association will develop further (fig. 11.7). No other configuration consisting of five cells leads to such a complicated behaviour.

As a rule, the evolution of randomly taken configurations results in the appearance of a collection of stationary structures, traffic lights, gliders. The total number of cells proves to be limited as $t \to \infty$. However, for some initial data the situation may qualitatively change. Such a behaviour is typical for some biological systems, in particular evolution processes. An unlikely event may qualitatively change the behaviour of the system, leading to the appearance of new forms. This is why "*cellular automata*" (the Life game belongs to this class of models) are used in ecological models, in the simulation of morphogenesis, and in other biological problems [11].

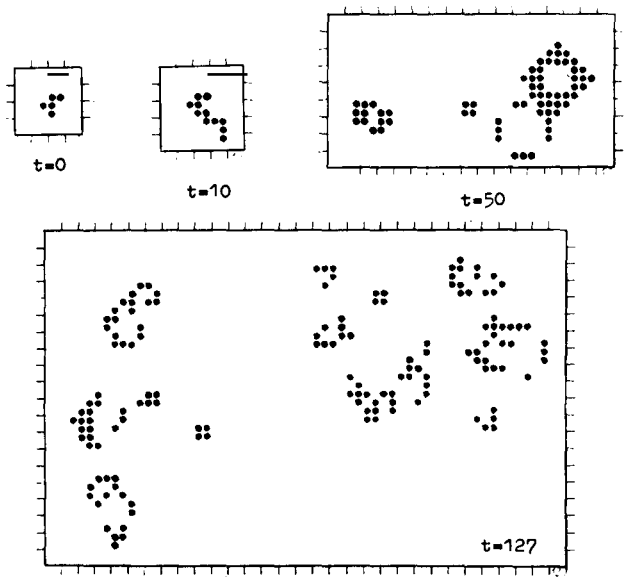

Fig. 11.7

The larger the area the association occupies, the more complex the behaviour it may show. Therefore configurations infinitely growing in space are of great interest. One of them, called a "*catapult*" or a "*glider gun*", was proposed by R. Gosper, in 1970. It is seen that every 30 steps the catapult repeats itself and produces a glider (fig. 11.8). The glider gun fills the space by a stream of gliders. There is an even more complex association of cells which moves forward, leaving behind a large collection of traffic lights and stationary structures. One of these is the "*puffer train*" shown in fig. 11.9. The search for such configurations requires the application of special algorithms [267].

The above mentioned examples show that in the discrete system under discussion there is a great number of different types of ordering, which define the asymptotic behaviour of some set of configurations (in this sense they prove to be equivalent to attractors of dynamic systems). However, we may prove more – in the Life game there are arbitrarily complex types of ordering, this discrete system proves to be equivalent to a *universal computer* [266].

We may consider a computer as a finite set of elementary logical elements that perform the operations "and", "or", "not" and that are connected by wires in a certain way. A set of pulses coding a sequence of 0's and 1's are running along these wires.

The glider gun in the Life game plays the part of a generator of such pulses. The existence of a glider in the stream may be interpreted as a one and its absence as a zero. The collision of gliders by which they annihilate allows the construction of the element "not" by directing two streams at a right angle (if a glider exists at a certain place in the first stream, then after the collision the glider will disappear at this place in the other stream). Other elements are constructed in a more complex way [266].

The equivalence of the Life game to a computer has many interesting consequences. The idea naturally arises to compare the computer in this discrete system to available computers. The considered hypothetical computer has two important merits – it consists of simple identical elements, each of them being connected with near neighbours only. The size of the logical elements decreases in every new generation of computers. Constructing small elements of the type considered, for example, on the

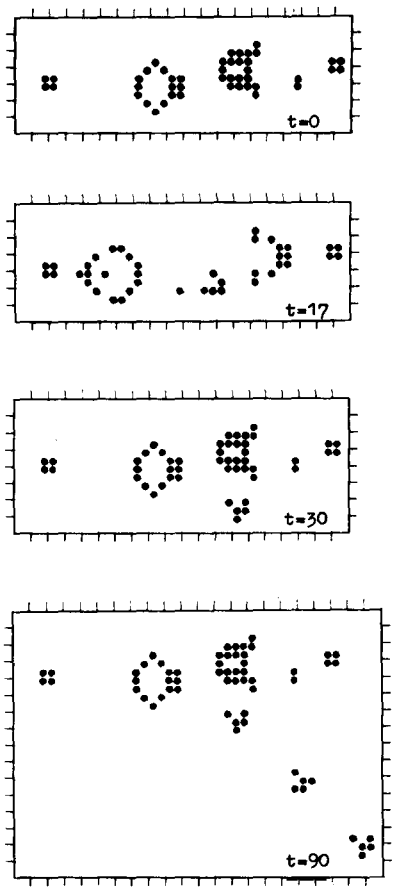

Fig. 11.8

molecular level, is considerably simpler than traditional integral circuits. Some investigations show that the molecules of certain compounds have the qualities required for the construction of a computer [268].

Here two essential objections arise. On the molecular (all the more, atomic) level quantum effects are appreciable. What restrictions do they impose on such computer systems? Of special interest are systems characterized by a minimal level of energy dissipation (or, ideally, by dissipationless processes). We recall that the evolution of configurations in the Life game is irreversible. Are there reversible dissipative systems with the properties of universal computers? The latest studies have shown that both objections may be turned down. Quantum mechanical systems with reversible properties can, in principle, be constructed [269].

The Life game and other systems of this type, called cellular automata, allowed new insight into many physical phenomena. (A cellular automaton is a set of identical cells, every one of which develops according to certain rules.) Using differential equations for the description of many complex processes involves serious difficulties; for example, some types of turbulent flows, packings of molecules consisting of long chains (in particular, DNA molecules whose description involves self-avoiding random walks), self-reproduction, growth and development processes typical for biological systems.

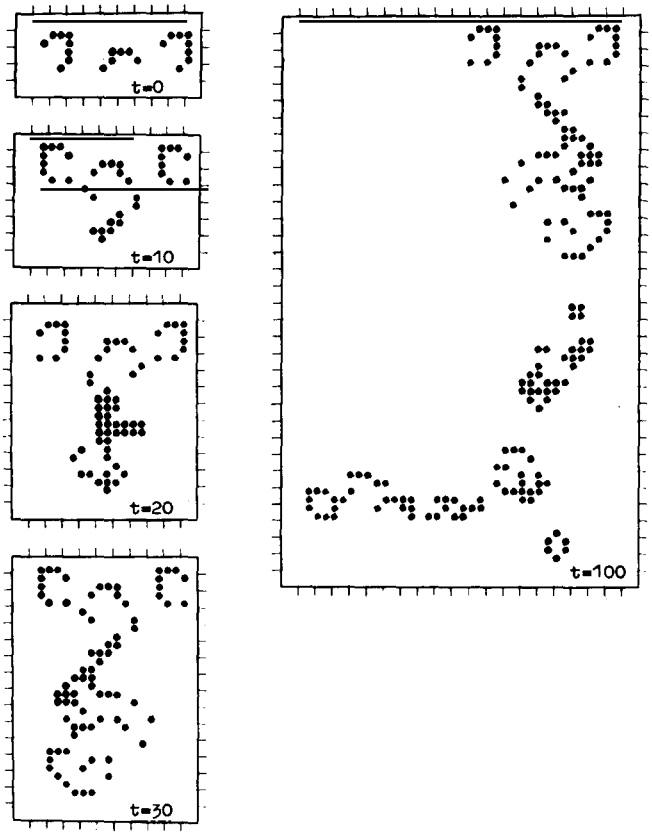

Fig. 11.9

In 1948 John von Neumann suggested that in modelling these phenomena cellular automata and direct computer simulation are most efficient. His theory of automaton self-reproduction showed the great potentialities of such an approach [270]. Recently it has been extended by S. Wolfram and other authors [271, 272]. They have come to the conclusion that some real systems may be arranged in the same way as the Life game. Depending on the initial data processes of any complexity may be implemented in them.

Here, the concepts and ideas of algorithm theory may be employed. The behaviour of any system can be modelled, in principle, by imitating its evolution step by step. In most cases, however, a simpler way may be found. For example, to multiply a number by 2^n on a computer it is not necessary to add it to itself 2^n times; we may simply shift its representation in the memory by n binary digits. Systems for which such simpler algorithms exist are called computationally reversible. It is this property that helps to distinguish a small set of order parameters in the description of the natural phenomena or to pass to a simpler statistical description.

The hypothesis by S. Wolfram suggests that many physical systems and their models, which cannot yet be described in a simple way, are *computationally irreversible* [272]. The only way to analyse such systems is to carry out physical or numerical experiments. In ref. [273] it is shown that there is a system of 10 nonlinear partial differential equations describing a medium which is equivalent to the Life game or other automata of this type.

Investigations of cellular automata lead to a paradoxical conclusion. In a medium of elementary identical elements an ordering of any complexity may exist. The evolution of some configurations may look like the emergence and interaction of elementary structures, and the appearance, as a result, of more complex structures, their interaction and so on. If after a certain stage the configuration appears to be localized in a bounded domain the development stops and a stationary regime is set up.

The Life game belongs to a more complicated class of automata. However, there are a number of simpler automata with cells in one of k states, located along a straight line [272]. The rules determining their evolution may be written in the form

$$a_i^{(t)} = f\left(\sum_{j=-r}^{j=r} \alpha_j a_{i+j}^{(t-1)}\right), \tag{11.1}$$

where $a_i(t)$ is the state of the ith cell at time t. The set of possible rules is very wide. The basic types of automata can be studied by considering a narrower class, the so-called *legal adding automata*. An automaton is called *legal* if

$$f(0) = 0, \qquad f(a_{i-r}, \ldots, a_{i+r}) = f(a_{i+r}, \ldots, a_{i-r}). \tag{11.2}$$

It is *adding* when all $\alpha_j = 1$.

Using the rule that determines an automaton we may find its code by the formula

$$C_f = \sum_{n=0}^{(2r+1)(k-1)} k^n f[n], \tag{11.3}$$

where k is the number of states in which each cell may occur.

In an analysis of dissipative dynamic systems and asymptotic regimes in nonlinear media with processes developing in a finite time, periodic and stochastic regimes were distinguished. Their analogs exist among automata too. In ref. [273] four types of legal adding automata were distinguished.

1. Regardless of initial data the transition to a homogeneous state occurs in a limited number of steps.

2. In the second class of automata the evolution leads to localized stationary configurations or N-cycles. They are analogs of singular points or limit cycles in dynamic systems.

3. Chaotic initial configurations in automata of the third class lead to chaotic temporal behaviour.

If the initial states are localized the evolution of each cell can normally be predicted using a rather simple algorithm. If we put the time t along one axis and the state of the elements at t along the other axis, the appearing pattern can be considered as a fractal structure. Figure 11.10 shows this pattern for two automata, whose codes are also indicated.

4. For the automata of the fourth class (to which the Life game belongs) there is no simple algorithm that would allow a prediction of the evolution of localized initial configurations. One of the features of such automata is the variety of behaviour for different initial states.

The results given in ref. [272] show that automata of the fourth class are encountered very seldom. Of the legal adding automata they constitute six percent for $k = 2$, $r = 2$ and seven percent for $k = 3$, $r = 1$. As the complexity of the automata grows (with increasing k and r) this fraction will increase.

By analogy with the analysis of fractals or strange attractors it is convenient to describe various automata by quantitative characteristics. We shall discuss some of them in accordance with the results in

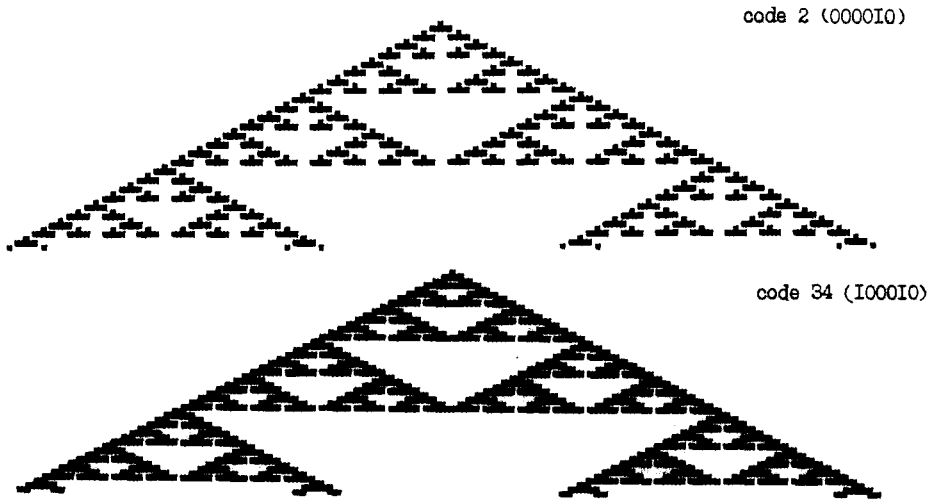

Fig. 11.10

ref. [272]. Consider a sequence of X elements by assuming that each cell occurs at one of k states and introduce the quantities

$$s^{(x)}(X) = \frac{1}{X} \log_k \left(\sum_{j=1}^{k^X} \theta(p_j^{(x)}) \right), \tag{11.4}$$

where $\theta(p) = 1$ for $p > 0$ and $\theta(0) = 0$, $p_j^{(x)}$ are the probabilities of different configurations of X elements,

$$s_\mu^{(x)}(X) = -\frac{1}{X} \sum_{j=1}^{k^X} p_j^{(x)} \log_k p_j^{(x)} . \tag{11.5}$$

We call the quantities $s^{(x)}(X)$ and $s_\mu^{(x)}(X)$, respectively, the *spatial set entropy* and the *spatial measure entropy*, and the limits

$$d^{(x)} = \lim_{X \to \infty} s^{(x)}(X), \qquad d_\mu^{(x)} = \lim_{X \to \infty} s_\mu^{(x)}(X) \tag{11.6}$$

the *set dimension* and the *measure dimension*.

The nonordered initial configuration in which all possible sets of elements occur with nonzero probability yields $d^{(x)} = 1$; for a homogeneous configuration $d^{(x)} = 0$.

By analogy with the quantities describing the spatial behaviour of configurations we may introduce temporal characteristics of cellular automata in the form

$$\begin{aligned} &s^{(t)}(T) = \frac{1}{T} \log_k \left(\sum_{j=1}^{k^T} \theta(p_j^{(t)}) \right), \qquad s_\mu^{(t)}(T) = -\frac{1}{T} \sum_{j=1}^{k^T} p_j^{(t)} \log_k p_j^{(t)} , \\ &d^{(t)} = \lim_{T \to \infty} s^{(t)}(T), \qquad d_\mu^{(t)} = \lim_{T \to \infty} s_\mu^{(t)}(T), \end{aligned} \tag{11.7}$$

and the spatial–temporal characteristics

$$s^{(t,x)}(T,X)=\frac{1}{T}\log_k\Big(\sum_{j=1}^{k^{XT}}\theta(p_j^{(t,x)})\Big),$$

$$s_\mu^{(t,x)}(T,X)=-\frac{1}{T}\sum_{j=1}^{k^{XT}}p_j^{(t,x)}\log_k p_j^{(t,x)}, \tag{11.8}$$

$$h=\lim_{\substack{T\to\infty\\X\to\infty\\T/X\to\infty}}s^{(t,x)}, \qquad h_\mu=\lim_{\substack{T\to\infty\\X\to\infty\\T/X\to\infty}}s_\mu^{(t,x)}(T,X).$$

In the automaton given by the formula $a_i^{t+1}=F[a_{i-r}^t,\ldots,a_{i+r}^t]$ the excitation can propagate over a distance rT in a time T. For longer times, however, the excitations in many automata propagate with smaller velocities. Let $\|F^T\|$ denote the maximal value of R for which the state of cell i depends only on cells $i-R,\ldots,i+R$. Then the maximum propagation speed may be defined as

$$\lambda_+=\overline{\lim_{T\to\infty}}\|F^T\|/T \quad (\lambda_+\le r). \tag{11.9}$$

The relationships between the quantitative characteristics of cellular automata are discussed in ref. [272].

For large characteristic times and steady regimes the values of the characteristics (11.4)–(11.9) prove to be different for different classes of cellular automata.

Since any configurations in class 1 cellular automata tend to be a homogeneous state, their spatial and temporal dimensions tend to zero. The average propagation speed $\bar{\lambda}$ in class 2 cellular automata vanishes over long times as the temporal dimensions for such automata also vanish, $d_\mu^{(t)}=h_\mu=0$. At the same time the spatial dimensions in the case of irregular initial data will be different from zero.

For class 3 cellular automata the average propagation speed $\bar{\lambda}$ is positive, and the state of a single cell affects a growing number of its neighbours with time. The spatial and temporal measure entropies, $s_\mu^{(x)}(X)$ and $s_\mu^{(t)}(T)$, are also different from zero and usually tend to constant values over long times. The behaviour of class 4 cellular automata may be quite different for different initial data. Therefore, the quantitative characteristics of various configurations in such automata may be just the same as in any of the above three classes.

The behaviour of cellular automata is diverse, and their theory has been developed rapidly. This class of mathematical objects is interesting also because they represent exactly soluble models. They may be studied without using approximate methods (when investigated on computers) and simplified models.

Let us note two classes of physical phenomena whose analysis is performed using cellular automata. Experimental investigation of the Belousov–Zhabotinsky reaction shows that over certain characteristic times several types of ordering and chaotic regimes may arise. Their study with the aid of reaction–diffusion systems proves to be rather difficult due to the need to consider many components, incomplete knowledge of various reaction rates and the existence of several small parameters in the resulting equations. This led the authors of ref. [274] to the idea of using a cellular automaton as a phenomenological model.

As in the investigation of diffusion-induced chaos they suggested that a concentrated system shows self-oscillatory dynamics while diffusion processes are a cause for a complex spatial–temporal behaviour.

We shall assume that in the one-dimensional case the system can be split into identical cells. The state of the nth cell at time t is defined by a nonnegative function $A(n, t)$. The value of $A(n, t+1)$ is determined by the preceding state according to the rule

$$A'(n,t) = \alpha[A(n+1,t) + A(n-1,t)]/2 + (1-\alpha)A(n,t)\,, \quad A(n,t+1) = F(A'(n,t))\,. \tag{11.10}$$

The nonlinear function $F(x)$ is given by

$$F(x) = \begin{cases} 1\,, & \text{if } 1.5 \le x\,, \\ 0\,, & \text{if } 0.5 \le x < 1.5\,, \\ M\,, & \text{if } x < 0.5\,. \end{cases} \tag{11.11}$$

The coefficient $0 \le \alpha \le 1$ characterizes the value of the diffusion coefficient. When diffusion is absent ($\alpha = 0$) the system (11.10) describes an oscillatory regime. (Assuming that $M > 1.5$ we may verify that the automaton (11.10) has the cycle $0 \to M \to 1 \to 0 \to \cdots$.) In ref. [274] steady regimes were considered for different M and α. It was shown that in such a system cycles of period 3, wave processes, and complex turbulent regimes might exist. Their further analysis, and an investigation of the quantitative characteristics of diffusion-induced chaos in this model are of great interest.

Another trend of research where cellular automata are of growing importance deals with new methods of investigating continuous media. At the present time numerical experiments are widely used to investigate complex multi-dimensional problems of aerodynamics and plasma physics. To solve these problems most perfect numerical techniques and powerful computers are used. Enhancing the accuracy of experimental installations, and optimizing aerodynamic vehicles usually involve large amounts of computations.

One of the approaches to accelerate computations and go over to an analysis of more complex objects is to use parallel computations. In many problems of mathematical physics it is more economic to exploit, instead of one huge processor, a large number of simpler and cheaper processors that operate simultaneously. If the number of such processors is sufficiently large and they perform elementary operations the computations may be considered as the evolution of a cellular automaton. The question arises: What automata may be used to simulate systems of nonlinear partial differential equations (first, of all, the equations of ordinary and magneto-hydrodynamics)? Since spatial derivatives occur in the equations the relationships among the cells/processors are also rather simple – only nearest neighbours need to be connected. In the two-dimensional case it is convenient to fill the plane with identical triangular, square or hexagonal cells.

As in the construction of the usual difference schemes [275] cellular automata of such a type are built according to the momentum, energy, or angular momentum conservation laws. A sampling of particles is introduced, each of the particles may be in one of the nodes of a square (hexagonal) lattice. It is usually assumed that two identical particles cannot occur in a node. Then one should determine according to which laws collisions between these particles may take place, and a method is indicated to calculate the pressure, velocity and density in this flow by knowing the behaviour of the "*lattice gas*".

Specifically, in ref. [275] it is shown that an automaton defined on a hexagonal lattice enables one to simulate the Navier–Stokes equations and may be used for the creation of a parallel computer. In this

publication a reference list of previous works is given. Providing the particles with a quantum of vector potential, introducing more complex rules of particle scattering and using again hexagonal cells allows one to employ this approach for simulating the magnetohydrodynamics equations [276].

An example of computations in the hydrodynamic case with the aid of a two-dimensional cellular automaton consisting of 2^{16} cells (256×256) and 130 thousand particles is given in ref. [277]. Note also the publication [278], where estimates are obtained for the parameters of cellular automaton systems. These are necessary to calculate hydrodynamic flows for large Reynolds numbers. The conclusion drawn by the authors turns out to be pessimistic. However, a comparison between the efficiencies of cellular automata and the usual numerical techniques can be really made only after the construction of dedicated computers aimed at such an approach.

One such computer, which includes 65 636 simple processor elements and has a performance of 2.5 billion operations with a floating point, has been designed by now [279]. The system has an interesting feature, as follows. For the simulation of some partial differential equations it is sufficient that each cell in a two-dimensional geometry is connected with six nearest neighbours. In many cases, however, many more connections are required. In order to implement such a system and reserve a structure appropriate for various cellular automata we should build these computers in a multi-dimensional space. Specifically, the connections in the computer described in ref. [279] are arranged in the same way as on a cubic lattice in 12-dimensional space (every vertex in such a cube has 12 neighbours, and in total the cube has 4096 vertices). Computers with such a structure were designed mainly to solve problems of artificial intelligence. They may possibly prove useful also for certain classes of hydrodynamic problems, which can be efficiently simulated using cellular automata.

11.2. Complex ordering and chaos in spatially inhomogeneous systems

Most reaction–diffusion systems were investigated under the assumption that sources and sinks did not explicitly depend on the spatial coordinate. Meanwhile in many physical systems this condition is not satisfied. Spatial inhomogeneity results in many interesting effects. We shall illustrate some of them by considering two nonlinear spatially inhomogeneous systems.

As a result of the study of the thermal effect of laser radiation upon chemically active media a new field, "*laser thermochemistry*", has emerged [280]. It has turned out that the dynamics of thermochemical processes may be extremely complex even in the case when continuous laser radiation of low power is incident upon a medium. This is mainly due to two factors. First, the processes are not isothermal: since the rates of chemical processes strongly depend on the temperature and the laser radiation continuously introduces thermal energy into the system, the reaction rates may change. If the temperature variation rate is higher than the reaction rates the process will be quite far from isothermal ("macroscopic irregularity"). Second, it is essential when there is a feedback between the temperature variation rate and the reaction rates. The appearance of this feedback may be due to either a heating effect of the reactions or a change in the optical properties of the medium if the chemical composition varies during the reaction. In the latter case the absorption characteristics also change, which influences the amount of energy introduced into the system.

Laser thermochemistry may prove to be the field where experimental studies of nonstationary spatially localized processes, complex time ordering, and diffusion-induced chaos will be rather simple.

One of the simplest problems of laser thermochemistry is modelling the heating of a thermally thin plane ($h^2 \ll \alpha\tau$, where h is the plane thickness, τ is the characteristic time of temperature variation, α is the thermal conductivity) in air by laser irradiation (fig. 11.11). In some cases this process is described

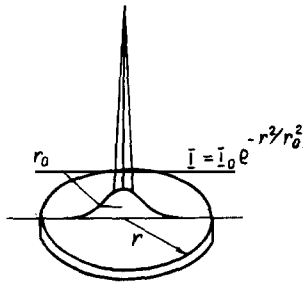

Fig. 11.11

by the following boundary value problem:

$$\frac{\partial T}{\partial t} = \frac{c}{r}\frac{\partial}{\partial r}\left(r\frac{\partial T}{\partial r}\right) + I\,e^{-r^2/r_0^2} + \frac{\alpha}{X}e^{-1/T} - \beta\,e^{-\kappa/T} - \delta T\,,$$

$$\frac{\partial X}{\partial t} = \frac{d}{X}e^{-1/T} - \gamma\,e^{-\kappa/T}\,, \quad 0 < r < R\,, \tag{11.12}$$

$$\left.\frac{\partial T}{\partial r}\right|_{r=0} = \left.\frac{\partial T}{\partial r}\right|_{r=R} = 0\,, \qquad T\Big|_{t=0} = T_0(r)\,, \qquad X\Big|_{t=0} = X_0(r)\,.$$

Here r is the distance from the centre of symmetry, R is the radius of the sample, t is the time, T is the temperature, X is the oxide thickness, I is the intensity, r_0 is the effective radius of the radiation beam (fig. 11.11). The radiation intensity distribution is written in Gaussian form. The third and fourth terms in the first equation take account of the energy released by metal oxidation and of the absorption by oxide evaporation. The last term describes the heat exchange with the ambient air. The second equation in (11.12) describes the variation in the oxidized layer thickness due to metal oxidation and oxide evaporation. The dimensionless constants c, α, β, κ, δ, d, γ describing the thermophysical properties of the substance, the kinetics of the oxidized layer, the energy release and heat losses are connected with the corresponding "dimensional" parameters by relations given in ref. [281].

If $r_0 \gg R$ and the characteristic spatial scale of variations in the temperature T and the layer thickness X exceeds R, the equations turn into the dynamic system

$$\frac{dT}{dt} = I + \frac{\alpha}{X}e^{-1/T} - \beta\,e^{-\kappa/T} - \delta T\,, \qquad \frac{dX}{dt} = \frac{d}{X}e^{-1/T} - \gamma\,e^{-\kappa/T}\,. \tag{11.13}$$

The system can have one stable point, $T(t) \to \text{const.}$, $X(t) \to \text{const.}$ as $t \to \infty$, or trigger properties: for some initial data $T \to T_1$, $X \to X_1$, as $t \to \infty$ while for other data $T \to T_2$, $X \to X_2$ as $t \to \infty$. A stable limit cycle may exist in this system as $T(t) \to T_c(t)$, $X(t) \to X_c(t)$ as $t \to \infty$, where $T_c(t) = T_c(t + \bar{\tau})$, $X_c(t) = X_c(t + \bar{\tau})$ and $\bar{\tau}$ is the period of the solution. All these regimes were observed experimentally [282].

At the same time experiments show [287] that for inhomogeneous irradiation the heating dynamics of a metal sample becomes complicated: when the beam is sharply focused, chaotic oscillations of the temperature are observed. This explains the interest in problem (11.12).

In ref. [283] the parameters are chosen so that for large values of I in the system (11.13) there is a stable singular point, and for intermediate values a limit cycle. For small intensities the temperature drops and the characteristic times of the processes sharply increase. The existence of heat conduction

leads to interactions between all these systems with different properties. This is typical for problems with spatially inhomogeneous parameters.

Suppose we vary the intensity I and the beam radius r_0 so that the total radiation power $P = \pi r_0^2 I$ remains constant. Physically this means that we change the focusing of the laser beam.

First a transition process is observed. The heat sinks prove to be inessential at low temperatures, and the properties of the system (11.12) are similar to those of the heat conduction equation with a nonlinear source. From the theory of such equations it follows that in some cases the half-width of the temperature profile may decrease. In ref. [66] an experiment is described where the half-width decreases a few times. Then the restricting factors become important, and a heat wave propagates from the centre along the radius, and behind this wave the oxide thickness increases. After this processes are initiated with characteristic times several orders of magnitude longer.

The main types of steady regimes are shown in fig. 11.12. A fixed value of P corresponds in the $(I, 1/r_0^2)$-plane to a straight line. When I is sufficiently large, stationary dissipative structures appear in the system. Typical behaviour of $T(r)$ and $X(r)$ is shown in the figure. The structures appearing are effectively localized. In this case the localization is associated with sink effects.

Decreasing the intensity I leads to the development of a periodic oscillatory regime. Then a cascade of period-doubling bifurcations is observed, $S^p \to S^{2p}$. Diffusion-induced chaos emerges. Here we may also construct a family of one-dimensional maps with a smooth vertex.

Decreasing the laser beam intensity still further leads to a situation where the temperature oscillations become more relaxing. The solution acquires new properties.

We discuss them by the example of the following calculations: $I = 1.8$; $r_0 = 1.0$; $c = 0.1$; $\alpha = 9.0$; $\beta = 0$; $\kappa = 0.6$; $\delta = 9.0$; $d = 0.894$; $\gamma = 1.0$. The variations of the temperature and the thickness of the oxide layer with time at different points of the sample are shown in fig. 11.13. It is seen that at $r = 0.03$

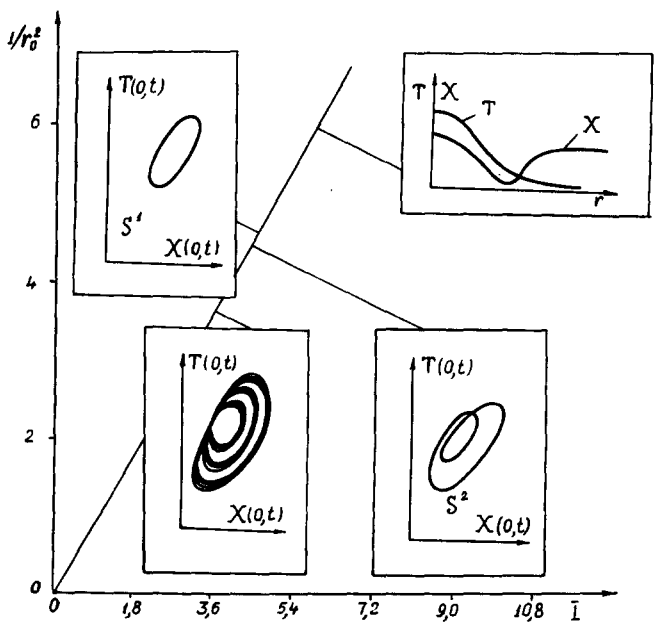

Fig. 11.12

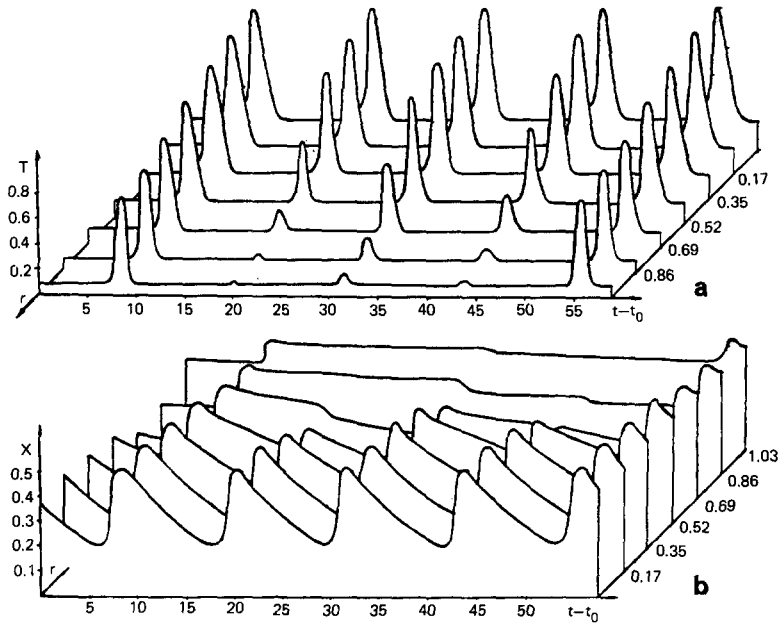

Fig. 11.13

maxima of the temperature with an amplitude $T_{max} > 0.9$ appear with a period $\tau \approx 12.5$. At $r = 0.35$ they appear with a period $\approx 2\tau$, and at $r = 0.86$ with period 4τ. Analogously the time dependence of the oxide thickness varies with the radius. At $r = 0.03$ the oxide thickness varies with a period τ, at the edge of the sample with period 4τ (fig. 11.13). The observed picture significantly differs from the auto-wave processes in systems with spatially homogeneous parameters. It is usually pointed out in the theory of oscillations that a nonlinear dissipative system may behave as a generator [86]. Here an open distributed system behaves as a *frequency divisor* as well: thermal pulses of large amplitude appear with different frequencies at different points of the system.

From the model (11.12) it follows that by switching the laser off ($I = 0$ for $t > t^*$) we may create complex spatial distributions of the oxide thickness. Examples of such distributions and other properties of this model are discussed in ref. [285].

The spatial dependence of the source in eqs. (11.12) is explained by the fact that a Gaussian beam and a rather large sample are taken. Such models are also of interest when thermodiffusion processes are analysed.

In ref. [286] a mixture of two gases contained in a thin cuvette is considered. The cuvette is illuminated by a narrow beam of radiation, which is absorbed by the heavy component. An elementary model of such processes includes the heat conductivity equation and the diffusion equation,

$$
\begin{aligned}
&T_t = T_{xx} + b[I_n(x)\, e^{-T_0/T} - (T - T_n)]\,,\\
&\nu n_t = n_{xx} + \alpha\left(\frac{n(1-n)}{T}\, T_x\right)_x\,, \quad \alpha, b > 0\,, \quad 0 < x < R\,,\\
&I_n(x) = I \exp[-(x - x_c)^2/r_0^2]\,,\\
&T|_{t=0} = T_n\,, \quad n|_{t=0} = n_0\,, \quad T_x|_{x=0,R} = 0\,, \quad n_x|_{x=0,R} = 0\,.
\end{aligned}
\tag{11.14}
$$

There is a conservation law for the second equation, which is not typical for the problems considered earlier of the theory of dissipative structures. Moreover, it may be shown that in the homogeneous problem (I_n = const.) the homogeneous solution is stable and oscillations are impossible.

Applying the averaging technique to eqs. (11.14) we can obtain an approximate model – a system of two ordinary differential equations where stable limit cycles may occur [286].

Numerical calculations revealed oscillations in the nearby domain of parameters in the initial problem. The localization of oscillatory processes was demonstrated – as the length of the domain R increased the oscillations at the boundary did not disappear, remaining at the centre. In spite of the equality of the heat conductivity and diffusion coefficients (for $\nu = 1$) the length of the localization domain in the concentration proves to be several times as large as that in temperature. This is due to the lack of a sink in the second equation; therefore the absorbing component from the illuminated region concentrates in its vicinity.

Thus, the existence of distributed parameters qualitatively changes the properties of the system. We may expect that later other interesting phenomena will be found in reaction–diffusion systems with spatially inhomogeneous parameters.

References

[1] A. Turing, Philos. Trans. R. Soc. London B 237 (1952) 37.
[2] C.A. Villee and V.G. Dethier, Biological Principles and Processes (Saunders, London, 1971).
[3] G. Nicolis and I. Prigogine, Self-Organization in Nonequilibrium Systems. From Dissipative Structures to Order through Fluctuations (Wiley, New York, 1977).
[4] A.J. Lichtenberg and M.A. Liberman, Regular and Stochastic Motion (Springer, Berlin, 1983).
[5] B.N. Belintsev, Usp. Fiz. Nauk 111 (1983) 54.
[6] A. Gierer and H. Meinhardt, Kybernetik 12 (1972) 30.
[7] H. Meinhardt, Ber. Dtsch. Bot. Ges. 87 (1974) 101.
[8] A. Gierer, Prog. Biophys. Molec. Biol. 37 (1981) 1.
[9] P.K. Maini, J.D. Murray and G.F. Oster, in: Lecture Notes in Mathematics, Vol. 1151 (Springer, Berlin, 1985) p. 252.
[10] R. Thom, Stabilité Structurelle et Morphogenèse (Benjamin, New York, 1972).
[11] V.Z. Alad'ev, in: Parallel Processing of Information and Parallel Algorithms (Valgus, Tallin, 1981).
[12] B.B. Mandelbrot, Fractals, Form, Chance and Dimension (Freeman, San Francisco, 1977).
[13] H. Haken, Synergetics, An Introduction, 2nd enlarged Ed., Springer Series in Synergetics, Vol. 1 (Springer, Berlin, 1978).
[14] H. Haken, Advanced Synergetics. Instability Hierarchies of Self-Organizing Systems and Devices, Springer Series in Synergetics, Vol. 20 (Springer, Berlin, 1983).
[15] Yu.M. Romanovskii, N.V. Stepanova and D.S. Chernavskii, Mathematical Biophysics (Nauka, Moscow, 1984) (in Russian).
[16] H. Haken, ed., Dynamics of Synergetic Systems (Springer, Berlin, 1977).
[17] A.N. Tikhonov. Mat. Sbor. 31 (73) (1952) 575.
[18] A.B. Vasil'eva and V.F. Butuzov, Asymptotic Expansions for Solutions of Singularly Perturbed Equations (Nauka, Moscow, 1973) (in Russian).
[19] A.B. Babin and M.I. Vishik, Usp. Mat. Nauk 38 (1983) 133.
[20] A.A. Samarskii, Introduction in Computational Methods (Nauka, Moscow, 1982) (in Russian).
[21] N.V. Zmitrenko, S.P. Kurdyumov and A.P. Mikhailov, in: Itogi Nauki i Tekhniki. Sovremennye Problemy Matematiki. Noveishie Dostizheniya 28 (VINITI, Moscow, 1987) p. 3 (in Russian).
[22] A.A. Samarskii, N.V. Zmitrenko, S.P. Kurdyumov and A.P. Mikhailov, Dokl. Akad. Nauk SSSR 227 (1976) 321.
[23] S.P. Kurdyumov, in: Contemporary Problems of Mathematical Physics and Computational Mathematics (Nauka, Moscow, 1982) p. 217.
[24] A.A. Samarskii, V.A. Galaktionov, S.P. Kurdyumov and A.P. Mikhailov, Regimes with Peaking in Problems of Quasilinear Parabolic Equations (Nauka, Moscow, 1987) (in Russian).
[25] G.G. Elenin and K.E. Plokhotnikov, preprint 91 (IPMatem AN SSSR, Moscow, 1977).
[26] H. Haken, ed., Chaos and Order in Nature (Springer, Berlin, 1984).
[27] A. Brandstäter, J. Swift, H.L. Swinney, A. Wolf, E. Jen and P.J. Crutchfield, Phys. Rev. Lett. 51 (1983) 1442.
[28] J.C. Roux, Physica D 7 (1983) 57.
[29] T.I. Zelenyak, Qualitative Theory of Boundary Value Problems of Quasilinear Parabolic Second-Order Equations (Izd. NGU, Novosibirsk, 1972) (in Russian).

[30] D. Henry, Geometric Theory of Semilinear Parabolic Equations. Lecture Notes in Mathematics, Vol. 840 (Springer, Berlin, 1981).
[31] J.F.G. Auchmuty, in: Lecture Notes in Mathematics, Vol. 322 (Springer, Berlin) p. 357.
[32] H.L. Swinney, Physica D 7 (1983) 3.
[33] M. Feigenbaum, Los Alamos Science 1 (1980) 4.
[34] R.P. Feynman, R.B. Leighton and M. Sands, The Feynman Lectures on Physics (Addison-Wesley, Reading, 1963).
[35] A.S. Monin, Usp. Fiz. Nauk 150 (1986) 61.
[36] H.L. Swinney and J.P. Gollub, eds, Hydrodynamic Instabilities and the Transition to Turbulence, Topics in Applied Physics, Vol. 45 (Springer, Berlin, 1981).
[37] A.N. Kolmogorov, I.G. Petrovskii and N.S. Piskunov, Byull. MGU 1, No. 6 (1937) 1.
[38] D.G. Aronson and H.F. Weinberger, in: Partial Differential Equations and Related Topics, Lecture Notes in Mathematics, Vol. 446 (Springer, Berlin, 1975) p. 5.
[39] A.N. Tikhonov and A.A. Samarskii, Equations of Mathematical Physics (Nauka, Moscow, 1964) (in Russian).
[40] S.E. Shnol', in: Mathematical Modelling of Biological Processes (Nauka, Moscow, 1979) p. 5 (in Russian).
[41] N.P. Erugin, Textbook for a General Course on Differential Equations (Nauka i Tekhnika, Minsk, 1979) (in Russian).
[42] G.B. Whitham, Linear and Nonlinear Waves (Wiley, New York, 1974).
[43] V.P. Starr, Physics of Negative Viscosity Phenomena (Mir, Moscow, 1971) (in Russian).
[44] V.E. Zakharov, Zh. Eksp. Teor. Fiz. 62 (1972) 1745.
[45] B.A. Trubnikov and S.K. Zhdanov, Phys. Rep. 154 (1987) 201.
[46] O.A. Oleinik, A.S. Kalashnikov and Chzhoe Yuie-lin, Izv. Akad. Nauk SSSR, Ser. Mat. 22 (1958) 667.
[47] V.A. Galaktionov, S.P. Kurdyumov and A.A. Samarskii, Diff. Uravn. 17 (1981) 1826.
[48] L.K. Martinson and K.B. Pavlov, Zh. Vychisl. Mat. Mat. Fiz. 12 (1972) 1048.
[49] A.S. Kalashnikov, Zh. Vychisl. Mat. Mat. Fiz. 14 (1974) 891.
[50] S.P. Kurdyumov, A.P. Mikhailov and K.E. Plokhotnikov, preprint 22 (IPMatem AN SSSR, Moscow, 1977).
[51] J.B. Keller and S. Antman, eds., Bifurcation Theory and Nonlinear Eigenvalue Problems (Benjamin, New York, 1969).
[52] A.A. Samarskii, G.G. Elenin, N.V. Zmitrenko, S.P. Kurdyumov and A.P. Mikhailov, Dokl. Akad. Nauk SSSR 237 (1977) 1330.
[53] G.G. Elenin, S.P. Kurdyumov and A.A. Samarskii, Zh. Vychisl. Mat. Mat. Fiz. 23 (1983) 380.
[54] V.A. Galaktionov, V.A. Dorodnitsyn, G.G. Elenin, S.P. Kurdyumov and A.A. Samarskii, in: Itogi Nauki i Tekhniki. Sovremennye Problemy Matematiki. Noveishie Dostizheniya 28 (VINITI, Moscow, 1987) p. 95 (in Russian).
[55] S.P. Kurdyumov, G.G. Malinetskii, Yu.A. Poveshchenko, Yu.P. Popov and A.A. Samarskii, Dokl. Akad. Nauk SSSR 251 (1980) 836.
[56] M.M. Ad'yutov, U.V. Klokov and A.P. Mikhailov, Diff. Uravn. 19 (1983) 1107.
[57] S.P. Kurdyumov, E.S. Kurkina, A.B. Potapov and A.A. Samarskii, Dokl. Akad. Nauk SSSR 274 (1984) 1071.
[58] S.P. Kurdyumov, E.S. Kurkina, A.B. Potapov and A.A. Samarskii, Zh. Vychisl. Mat. Mat. Fiz. 26 (1986) 1189.
[59] A.B. Potapov, preprint 8 (IPMatem AN SSSR, Moscow, 1986).
[60] S.P. Kurdyumov, E.S. Kurkina, G.G. Malinetskii and A.A. Samarskii, Dokl. Akad. Nauk SSSR 251 (1980) 587.
[61] S.P. Kurdyumov, E.S. Kurkina, G.G. Malinetskii and A.A. Samarskii, Dokl. Akad. Nauk SSSR 258 (1981) 1084.
[62] S.P. Kurdyumov, E.S. Kurkina and O.V. Tel'kovskaya, preprint 189 (IPMatem AN SSSR, Moscow, 1986).
[63] N.V. Zmitrenko and A.P. Mikhailov, Inertia of Heat (Znaniye, Moscow, 1982) (in Russian).
[64] N.V. Zmitrenko, S.P. Kurdyumov, A.P. Mikhailov and A.A. Samarskii. Pis'ma Zh. Eksp. Teor. Fiz. 26 (1977) 620.
[65] N.V. Zmitrenko, S.P. Kurdyumov and A.A. Samarskii, preprint 153 (IPMatem. AN SSSR, Moscow, 1980).
[66] V.A. Bobyrev, F.V. Bunkin, N.A. Kirichenko, B.S. Luk'yanchuk, A.A. Lyalin and S.A. Ubaidullaev, preprint 298 (IOFiz AN SSSR, Moscow, 1985).
[67] N.V. Zmitrenko and S.P. Kurdyumov, Zh. Prikl. Mekh. Tekh. Fiz. No. 1 (1977) 3.
[68] L.V. Ovsyanikov, Group-theoretical Analysis of Differential Equations (Nauka, Moscow, 1978) (in Russian).
[69] N.H. Ibragimov, Groups of Transformations in Mathematical Physics (Nauka, Moscow, 1983) (in Russian).
[70] V.A. Galaktionov, S.P. Kurdyumov, A.P. Mikhailov and A.A. Samarskii, Dokl. Akad. Nauk SSSR 248 (1979) 586.
[71] V.A. Galaktionov, S.P. Kurdyumov and A.A. Samarskii, Mat. Sbor. 124 (1984) 163.
[72] V.A. Galaktionov and A.A. Samarskii, Mat. Sbor. 121 (1983) 87.
[73] S.P. Kurdyumov, G.G. Malinetskii, Yu.A. Poveshchenko, Yu.P. Popov and A.A. Samarskii, Diff. Uravn. 17 (1981) 1875.
[74] B.N. Belintsev, L.V. Belousov, L.V. Zaraiskii and M.V. Volkenshtein, Dokl. Akad. Nauk SSSR 281 (1985) 708.
[75] A.M. Zamorzaev, E.I. Galyarskii and A.F. Palistrant, Color Symmetry, its Generalizations and Applications (Shtinitsa, Kishinev, 1979) (in Russian).
[76] E.N. Lorenz, J. Atmos. Sci. 20 (1963) 130.
[77] M.C. Cross and A.C. Newell, Physica D 10 (1984) 299.
[78] A. Aceves, H. Adachihara, C. Jones, J.C. Lerman, D.W. McLaughlin, J.W. Moloney and A.C. Newell, Physica D 18 (1985) 85.
[79] F.H. Busse, Ann. Rev. Fluid Mech. 10 (1978) 435.
[80] N.O. Weiss, F. Cattaneo and C.A. Jones, Astrophys. Fluid Dyn. 30 (1984) 305.
[81] A.D. Bryuno. Local Method of Nonlinear Analysis of Differential Equations (Nauka, Moscow, 1978) (in Russian).
[82] R. Gilmore, Catastrophe Theory for Scientists and Engineers (Wiley, New York, 1981).

[83] Ya.G. Panovko and N.I. Gubanova, Stability and Oscillations of Elastic Systems (Nauka, Moscow, 1979) (in Russian).
[84] G. Ioss and D.D. Joseph, Elementary Stability and Bifurcation Theory (Springer, New York, 1980).
[85] V.I. Arnold, Additional Chapters in the Theory of Ordinary Differential Equations (Nauka, Moscow, 1978) (in Russian).
[86] A.A. Andronov, A.A. Vitt and S.E. Khaikin, Theory of Oscillations (Nauka, Moscow, 1981).
[87] M.M. Vainberg and V.A. Trenogin, Bifurcation Theory for Solutions of Nonlinear Equations (Nauka, Moscow, 1969).
[88] D.D. Joseph, Stability of Fluid Motions, Springer Tracts in Natural Philosophy, Vols 27, 28 (Springer, Berlin, 1976).
[89] J.E. Marsden and M. McCracken, The Hopf Bifurcation and its Applications (Springer, Berlin, 1976).
[90] B.D. Hassard, N.D. Kazarinoff and Y.H. Wan, Theory and Applications of Hopf Bifurcation, London Math. Soc. Lecture Note Series, Vol. 41 (Cambridge Univ. Press, Cambridge, 1981).
[91] B.B. Kadomtsev, Cooperative Phenomena in Plasma (Nauka, Moscow, 1976) (in Russian).
[92] O.M. Phillips, J. Fluid Mech. 106 (1981).
[93] A.C. Newell and J.A. Whitehead, J. Fluid Mech. 38 (1969) 279.
[94] Y. Kuramoto and T. Tsuzuki, Prog. Theor. Phys. 54 (1975) 687.
[95] Y. Kuramoto and T. Tsuzuki, Prog. Theor. Phys. 52 (1974) 1399.
[96] A.A. Andronov and A.A. Fabrikant, in: Nonlinear Waves (Nauka, Moscow, 1979) (in Russian).
[97] M.I. Rabinovich and A.A. Fabrikant, Zh. Eksp. Teor. Fiz. 77 (1979) 617.
[98] K. Stewartson and J.T. Stuart, J. Fluid Mech. 48 (1971) 529.
[99] K.J. Blow and N.J. Doran, Phys. Rev. Lett. 52 (1984) 526.
[100] H. Koppel and L.N. Howard, Stud. Appl. Math. 52 (1973) 291.
[101] P.S. Hagan, SIAM J. Appl. Math. 42 (1982) 762.
[102] T.S. Akhromeyeva, S.P. Kurdyumov, G.G. Malinetskii and A.A. Samarskii, Dokl. Akad. Nauk SSSR 279 (1984) 591.
[103] T.S. Akhromeyeva, S.P. Kurdyumov, G.G. Malinetskii and A.A. Samarskii, in: Mathematical Modelling. Processes in Nonlinear Media (Nauka, Moscow, 1986) (in Russian).
[104] Y. Kuramoto, Suppl. Prog. Theor. Phys. 64 (1978) 346.
[105] S.-K. Ma, Modern Theory of Critical Phenomena (Benjamin, New York, 1979).
[106] P.K. Newton and L. Sirovich, Quart. Appl. Math. 43 (1986) 535.
[107] J.B. McLaughlin and P.C. Martin, Phys. Rev. A 12 (1975) 186.
[108] T.S. Akhromeyeva and G.G. Malinetskii, Diff. Uravn. 21 (1985) 657.
[109] V.S. Berman and U.A. Danilov, Dokl. Akad. Nauk SSSR 258 (1981) 67.
[110] S.C. Müller, T. Plesser and B. Hess, Physica D 24 (1987) 87.
[111] G.R. Ivanitskii, V.I. Krinskii and E.F. Sel'kov, Mathematical Biophysics of the Cell (Nauka, Moscow, 1978) (in Russian).
[112] T. Kakutani, Suppl. Prog. Theor. Phys. 55 (1974) 97.
[113] T. Taniuti, Suppl. Prog. Theor. Phys. 55 (1974) 1.
[114] Y. Kuramoto and T. Tsuzuki, Prog. Theor. Phys. 55 (1976) 356.
[115] T. Yamada and Y. Kuramoto, Prog. Theor. Phys. 56 (1976) 681.
[116] D. Michelson, Physica D 19 (1986) 89.
[117] B. Nikolaenko and B.S. Scheurer, Physica D 12 (1984) 391.
[118] Y. Kuramoto, Chemical Oscillations, Waves and Turbulence (Springer, Berlin, 1984).
[119] A. Scott, Active and Nonlinear Wave Propagation in Electronics (Wiley-Interscience, New York, 1970).
[120] K. Yamafuji, K. Toko, J. Nitta and K. Urahama, Prog. Theor. Phys. 66 (1981) 143.
[121] A. Nitzan and P. Ortoleva, Phys. Rev. A 21 (1980) 1735.
[122] S.A. Kashchenko and U.S. Kolesov, Dokl. Akad. Nauk SSSR 281 (1985) 1307.
[123] P. Manneville, J. Physique Lett. 44 (1983) 903.
[124] H.S. Greenside Jr, W.M. Coughran and N.L. Schryer, Phys. Rev. Lett. 49 (1982) 726.
[125] R.M. May, Nature 261 (1976) 459.
[126] M.J. Feigenbaum, J. Stat. Phys. 19 (1978) 25.
[127] M.J. Feigenbaum, J. Stat. Phys. 21 (1979) 669.
[128] E.B. Vul, Ya.G. Sinai and K.M. Khanin, Usp. Mat. Nauk 39 (1984) 3.
[129] K.I. Babenko and V.I. Petrovich, Dokl. Akad. Nauk SSSR 277 (1984) 265.
[130] P. Manneville and Y. Pomeau, Physica D 1 (1980) 219.
[131] P. Collet and J.P. Eckmann, Iterated Maps on the Interval as Dynamical Systems (Birkhäuser, Basel, 1980).
[132] M. Reed and B. Simon, Methods of Modern Mathematical Physics 1. Functional Analysis (Academic Press, New York, 1972).
[133] M.V. Yakobson, in: Itogi Nauki i Tekhniki. Sovremennye Problemy Matematiki. Fundamental'nye Napravleniya 2 (VINITI, Moscow, 1985).
[134] S.V. Ershov and G.G. Malinetskii, preprint 166 (IPMatem AN SSSR, Moscow, 1987).
[135] D. Singer, SIAM J. Appl. Math. 35 (1978) 260.
[136] J. Yorke and E. Yorke, J. Stat. Phys. 21 (1979) 263.
[137] C. Sparrow, The Lorenz Equations: Bifurcations, Chaos and Strange Attractors (Springer, Berlin, 1982).
[138] C. Grebogi, E. Ott and J.A. Yorke, Phys. Rev. Lett. 48 (1982) 1507.

[139] C. Grebogi, E. Ott and J.A. Yorke, Physica D 7 (1983) 181.
[140] T.Y. Li and J.A. Yorke, Am. Math. Month. 82 (1975) 985.
[141] A.N. Sharkovskii, Ukr. Mat. Zh. 16 (1964) 61.
[142] A.N. Sharkovskii, V.A. Maistrenko and E.Yu. Romanenko, Difference Equations and their Applications (Naukova Dumka, Kiev, 1986) (in Russian).
[143] N. Metropolis, M.L. Stein and P.R. Stein, J. Comb. Theory Ser. A 15 (1977) 25.
[144] K. Coffman, W.D. McCormic and H.L. Swinney, Phys. Rev. Lett. 56 (1986) 999.
[145] M.V. Jakobson, Commun. Math. Phys. 81 (1981) 39.
[146] J.D. Farmer, Phys. Rev. Lett. 55 (1985) 351.
[147] J. Coste and N. Peyraud, Physica D 5 (1982) 415.
[148] I.B. Bokolishvili and G.G. Malinetskii, preprint 112 (IPMatem AN SSSR, Moscow, 1987).
[149] G. Mayer-Kress and H. Haken, J. Stat. Phys. 26 (1981) 149.
[150] K. Tomita and T. Tsuda, Suppl. Prog. Theor. Phys. 69 (1980) 185.
[151] Ya.B. Pesin, in: Itogi Nauki i Tekhniki. Sovremennye Problemy Matematiki. Fundamental'nye Napravleniya 2 (VINITI, Moscow, 1985) 123 (in Russian).
[152] Ya.G. Sinai, in: Nonlinear Waves (Nauka, Moscow, 1979) p. 192.
[153] I.P. Kornfel'd and Ya. G. Sinai, in: Itogi Nauki i Tekhniki. Sovremennye Problemy Matematiki. Fundamental'nye Napravleniya 2 (VINITI, Moscow, 1985) p. 7.
[154] D. Ruelle, Am. J. Math. 98 (1976) 619.
[155] R. Bowen and D. Ruelle, Invent. Math. 29 (1975) 181.
[156] G.M. Zaslavskii, Stochasticity of Dynamical Systems (Nauka, Moscow, 1984) (in Russian).
[157] L.A. Bunimovich, in: Itogi Nauki i Tekhniki. Sovremennye Problemy Matematiki. Fundamental'nye Napravleniya (VINITI, Moscow, 1985) p. 173.
[158] L.A. Bunimovich and Ya.G. Sinai, in: Nonlinear Waves (Nauka, Moscow, 1979) p. 212.
[159] T.S. Akhromeyeva and G.G. Malinetskii, Zh. Vychisl. Mat. Mat. Fiz. 27 (1987) 202.
[160] Z. Nitecki, Differentiable Dynamics (MIT Press, Cambridge, MA, 1971).
[161] J. Guckenheimer and P. Holmes, Nonlinear Oscillations, Dynamical Systems and Bifurcations of Vector Fields (Springer, Berlin, 1983).
[162] J.D. Farmer, E. Ott and J.A. Yorke, Physica D 7 (1983) 153.
[163] M. Henon, Commun. Math. Phys. 50 (1976) 69.
[164] D.L. Hitzl and F. Zele, Physica D 14 (1985) 305.
[165] B. Derrida, A. Gervois and Y. Pomeau, J. Phys. A 12 (1979) 269.
[166] P. Collet and Y. Levy, Commun. Math. Phys. 93 (1984) 461.
[167] M. Misiurewicz, in: Nonlinear Dynamics (NY Acad. Sci., New York, 1980) p. 348.
[168] L.D. Landau, Dokl. Akad. Nauk SSSR 44 (1944) 339 [English transl. in Collected Papers].
[169] E.B. Gledzer, F.V. Dolzhanskii and A.M. Obukhov, Hydrodynamic Systems and their Applications (Nauka, Moscow, 1981) (in Russian).
[170] D. Ruelle and F. Takens, Commun. Math. Phys. 20 (1971) 167.
[171] D.G. Aronson, M.A. Chory, G.R. Hall and R.P. McGehee, Commun. Math. Phys. 83 (1982) 303.
[172] J. Moser, Lectures on Hamiltonian Systems, Memories Am. Math. Soc., No. 81 (1968).
[173] V.I. Arnold, V.V. Kozlov and A.I. Neishtadt, in: Itogi Nauki i Tekhniki. Sovremennye Problemy Matematiki. Fundamental'nye Napravleniya 3 (VINITI, Moscow, 1985) p. 5.
[174] B.V. Chirikov, Phys. Rep. 52 (1979) 265.
[175] S. Smale, Bull. Am. Math. Soc. 73 (1967) 747.
[176] S. Ostlund, D. Rand, J. Sethna and E. Siggia, Physica D 8 (1983) 303.
[177] V.I. Arnol'd, V.S. Afraimovich, Yu.S. Il'yashenko and L.P. Shil'nikov, in: Itogi Nauki i Tekhniki. Sovremennye Problemy Matematiki. Fundamental'nye Napravleniya 5 (VINITI, Moscow, 1986).
[178] M.J. Feigenbaum, L.P. Kadanoff and S.J. Shenker, Physica D 8 (1983) 303.
[179] S.J. Shenker, Physica D 5 (1982) 405.
[180] J. Stavans, F. Heslot and A. Libchaber, Phys. Rev. Lett. 55 (1985) 596.
[181] K. Kaneko, Prog. Theor. Phys. 69 (1983) 1427.
[182] V.S. Anishchenko, Stochastic Oscillations in Radiophysical Systems (Izd. Saratovskogo Univ., Saratov, 1986) (in Russian).
[183] A.S. Dmitriev and A.I. Panas, Zh. Tekh. Fiz. 56 (1986) 1864.
[184] P. Cvitanovic, M.H. Jensen, L.P. Kadanoff and I. Procaccia, Phys. Rev. Lett. 55 (1985) 343.
[185] Seung-hwan Kim and S. Ostlund, Phys. Rev. Lett 55 (1985) 1165.
[186] Y.M. Gu, M. Tung, J. Yuan, D.H. Feng and L.H. Narducci, Phys. Rev. Lett. 52 (1984) 701.
[187] C. Grebogi, E. Ott and J.A. Yorke, Phys. Rev. Lett. 56 (1986) 1011.
[188] C. Grebogi, E. Ott and J.A. Yorke, Phys. Rev. Lett. 57 (1986) 1284.
[189] B.R. Gelbaum and J.M.H. Olmsted, Counterexamples in Analysis (Holden-Day, San Francisco, 1964).
[190] Ya.B. Zeldovich and D.D. Sokolov, Usp. Fiz. Nauk 146 (1985) 4933.

[191] I.M. Sokolov, Usp. Fiz. Nauk 150 (1986) 729.
[192] T.A. Witten and L.M. Sander, Phys. Rev. B 27 (1983) 5686.
[193] Du-Yand Zhong-can, Yae Gang and Hao Bai-lin, Phys. Rev. Lett. 57 (1986) 3203.
[194] F. Takens, in: Lecture Notes in Mathematics, Vol. 898 (Springer, Berlin, 1981) p. 366.
[195] G.G. Malinetskii and A.B. Potapov, preprint 101 (IPMatem AN SSSR, Moscow, 1987).
[196] H.S. Greenside, A. Wolf, J. Swift and T. Pignataro, Phys. Rev. A 25 (1982) 3453.
[197] G. Benettin, L. Galgani, A. Giorgilli and J.M. Strelcin, Meccanica 15 (1980) 9.
[198] P. Grassberger and I. Procaccia, Physica D 9 (1983) 189.
[199] V.I. Oseledec, Trudy Mosk. Mat. Obshch. 19 (1968) 179.
[200] J. Kaplan and J. Yorke, in: Functional Differential Equations and the Approximation of Fixed Points, Proc. (Bonn, 1978), Lecture Notes in Mathematics (Springer, Berlin, 1978) p. 228.
[201] A. Wolf, J.B. Swift, H.L. Swinney and J. Vastano, Physica D 16 (1985) 285.
[202] H.G.E. Hentschel and I.P. Procaccia, Physica D 8 (1983) 435.
[203] F. Takens, in: Nonlinear Dynamics and Turbulence (Pitman, London, 1983) p. 314.
[204] M. Sano and Y. Sawada, Phys. Rev. Lett. 55 (1985) 1082.
[205] R. Fenstermacher, H.L. Swinney and J.P. Gollub, J. Fluid Mech. 94 (1978) 103.
[206] I.M. Yavorskaya, Yu.N. Belyaev and A.A. Monakhov, Dokl. Akad. Nauk SSSR 237 (1977) 804.
[207] B. Malraison, P. Atten, P. Berge and M. Dubois, J. Physique Lett. 44 (1983) 897.
[208] M. Giglio, S. Musazzi and U. Perini, Phys. Rev. Lett. 53 (1984) 2402.
[209] M. Bonetti, R. Meynart, J.P. Boon and D. Olivari, Phys. Rev. Lett. 55 (1982) 492.
[210] P.R. Gromov, A.B. Zobin, M.I. Rabinovich and A.M. Reiman, M.M. Sushchik, in: Chisl. Metody Mekh. Splosh. Sredy 17, No. 2 (1986) 30.
[211] V.S. Afraimovich and L.P. Shil'nikov, in: Qualitative Theory of Dynamical Systems (Izd. Gor'kovskogo Univ., Gor'ky, 1983) p. 3 (in Russian).
[212] V.S. Afraimovich, in: Nonlinear Waves (Nauka, Moscow, 1987) p. 189 (in Russian).
[213] D.V. Anosov, in: Itogi Nauki i Tekhniki. Sovremennye Problemy Matematiki. Fundamental'nye Napravleniya 1 (VINITI, Moscow, 1985) p. 151.
[214] V.S. Afraimovich, V.V. Bykov and L.P. Shil'nikov, in: Trudy Mosk. Mat. Obshch. 44 (1982) 150.
[215] V.S. Afraimovich, V.V. Bykov and L.P. Shil'nikov, Dokl. Akad. Nauk SSSR 234 (1977) 336.
[216] L.P. Shil'nikov, Dokl. Akad. Nauk SSSR 160 (1965) 558.
[217] T.S. Akhromeyeva, S.P. Kurdyumov, G.G. Malinetskii and A.A. Samarskii, In: Itogi Nauki i Tekhniki. Sovremennye Problemy Matematiki. Noveishie Dostizheniya 28 (VINITI, Moscow, 1986) p. 207.
[218] T.S. Akhromeyeva, S.P. Kurdyumov, G.G. Malinetskii and A.A. Samarskii, Dokl. Akad. Nauk SSSR 279 (1984) 1091.
[219] H. Henon, Physica D 5 (1982) 412.
[220] H. Yoshimura, Astrophys. J. 227 (1979) 1047.
[221] G.E. Williams, Sci. Am. 225 (1985) No. 2.
[222] A.A. Ruzmaikin, Comments Astrophys. 9 (1981) 85.
[223] F. Crauze and K.H. Radler, Magnetohydrodynamics of Mean Fields (Mir, Moscow, 1984) (in Russian).
[224] N.I. Kliorin and A.A. Ruzmaikin, Magnitnaya gidrodinamika No. 2 (1982) 17.
[225] G.G. Malinetskii, A.A. Ruzmaikin and A.A. Samarskii, preprint 170 (IPMatem AN SSSR, Moscow, 1986).
[226] S.I. Vainshtein, Ya.B. Zel'dovich and A.A. Ruzmaikin, Turbulent Dynamo in Astrophysics (Nauka, Novosibirsk, 1980) (in Russian).
[227] A.I. Vol'pert and A.N. Ivanova, in: Mathematical Modelling. Nonlinear Differential Equations of Mathematical Physics (Nauka, Moscow, 1987) p. 103.
[228] C.A. Jones, N.D. Weiss and F. Cattaneo, Physica D 14 (1985) 161.
[229] A.C. Fowler, J.D. Gibbon and M.J. McGuiness, Physica D 7 (1983) 126.
[230] B.P. Belousov, in: Autowave Processes in Systems with Diffusion (IPFiz AN SSSR, Gor'ky, 1981) p. 176 (in Russian).
[231] A.M. Zhabotinsky, Self-oscillations of the Concentration (Nauka, Moscow, 1974) (in Russian).
[232] D. Gurel and O. Gurel, Oscillations in Chemical Reactions (Springer, Berlin, 1983).
[233] V.P. Gachok, in: Modern Problems of Biokinetics (Izd. MGU, Moscow, 1987) p. 78.
[234] Yu.S. Il'yashenko, Usp. Mekh. No. 1 (1982) 31.
[235] J.H. Curry, Commun. Math. Phys. 60 (1978) 193.
[236] T.S. Akhromeyeva and G.G. Malinetskii, USSR Comput. Math. Math. Phys. 25 (1985) 20.
[237] T.S. Akhromeyeva and G.G. Malinetskii, Diff. Uravn. 20 (1984) 1281.
[238] T.S. Akhromeyeva and G.G. Malinetskii, preprint 118 (IPMatem AN SSSR, Moscow, 1982).
[239] T.S. Akhromeyeva and G.G. Malinetskii, preprint 53 (IPMatem AN SSSR, Moscow, 1982).
[240] D.A. Russel and E. Ott, Phys. Fluids 24 (1981) 1976.
[241] A.N. Ivanova and N.E. Maganova, Zh. Vychisl. Mat. Mat. Fiz. 24 (1984) 1217.
[242] H.T. Moon, A. Huerre and L.G. Redekopp, Physica D 7 (1983) 135.
[243] G. Mayer-Kress, ed., Dynamics and Entropies in Chaotic Systems (Springer, Berlin, 1986).

[244] P. Coullet, C.E. Elphick and D. Repaux, Phys. Rev. Lett. 58 (1987) 431.
[245] F. Anderson, Usp. Fiz. Nauk 127 (1979) 19.
[246] M. Berger, Geometrie (Cedic/Fernand Nathan, Paris, 1977).
[247] D. Ruelle, Physica D 7 (1983) 43.
[248] D. Shechtman, I. Blech, D. Gratias and J.W. Cahn, Phys. Rev. Lett. 53 (1984) 1951.
[249] J.P. Eckman and D. Ruelle, Rev. Mod. Phys. 57 (1985) 617.
[250] K. Lonngren and A. Scott, eds, Solitons in Action (Academic Press, New York, 1978).
[251] J. Marsden, in: Lecture Notes in Mathematics, Vol. 615 (Springer, Berlin, 1977).
[252] Y. Kuramoto and T. Yamada, Prog. Theor. Phys. 56 (1976) 679.
[253] T.S. Akhromeyeva and G.G. Malinetskii, preprint 140 (IPMatem AN SSSR, Moscow, 1983).
[254] L.R. Keefe, Stud. Appl. Math. 73 (1985) 91.
[255] A.A. Samarskii, Theory of Difference Schemes (Nauka, Moscow, 1974) (in Russian).
[256] R.J. Deissler, J. Stat. Phys. 40 (1985) 371.
[257] R.J. Deissler, Physica D 25 (1987) 233.
[258] R.J. Deissler and K. Kaneko, Phys. Lett. A 120 (1987) 334.
[259] J.A. Yorke, E.D. Yorke and J. Mallet-Paret, Physica D 24 (1987) 279.
[260] J.-P. Eckmann and D. Ruelle, Rev. Mod. Phys. 57 (1985) 617.
[261] J.V. Moloney, Phys. Rev. Lett. 53 (1984) 556.
[262] A.R. Bishop, M.G. Forest, D.W. McLaughlin and E.A. Overman II, Physica D 23 (1986) 293.
[263] R.K. Bullough and P.J. Caudrey, eds, Solitons (Springer, Berlin, 1980).
[264] K. Nozaki and N. Bekki, Phys. Rev. Lett. 50 (1983) 1226.
[265] A.T. Winfree, The Geometry of Biological Time (Springer, Berlin, 1980).
[266] E.R. Berlekamp, J.H. Conway and R.K. Guy, Winning Ways for your Mathematical Plays (Academic Press, New York, 1982).
[267] R.Wm. Gosper, Physica D 10 (1984) 75.
[268] F.L. Carter, J. Vac. Sci. Technol. B 1 (1983) 959.
[269] R.P. Feynman, Usp. Fiz. Nauk 149 (1986) 671.
[270] J. von Neumann, Theory of Self-Reproducing Automata (Univ. Illinois Press, 1966).
[271] S. Wolfram, Rev. Modern Phys. 55 (1983) 601.
[272] S. Wolfram, Physica D 10 (1984) 1.
[273] S. Omohundro, Physica D 10 (1984) 128.
[274] Y. Oono and M. Kohmoto, Phys. Rev. Lett. 55 (1985) 2927.
[275] U. Frisch, B. Hasslacher and Y. Pomeau, Phys. Rev. Lett. 56 (1986) 1505.
[276] D. Montgomery and C.D. Doolen, Phys. Lett. A 120 (1987) 229.
[277] N. Margolus, T. Toffoli and G. Vichniak, Phys. Rev. Lett. 56 (1986) 1694.
[278] S.A. Orszag and V. Yakhot, Phys. Rev. Lett. 56 (1986) 1694.
[279] W.D. Hillis, Sci. Am. 256 (1987) No. 6.
[280] F.V. Bunkin, N.A. Kirichenko and B.S. Luk'yanchuk, Usp. Fiz. Nauk 138 (1982) 45.
[281] F.V. Bunkin, N.A. Kirichenko, S.P. Kurdyumov, G.G. Malinetskii and A.A. Samarskii, preprint 81 (IPMatem AN SSSR, Moscow, 1983).
[282] V.A. Bobyrev, F.V. Bunkin, N.A. Kirichenko, B.S. Luk'yanchuk and A.V. Simakin, Kvantovaya Elektron. 10 (1983) 793.
[283] T.S. Akhromeyeva, F.V. Bunkin, N.A. Kirichenko, S.P. Kurdyumov, G.G. Malinetskii and A.A. Samarskii, Dokl. Akad. Nauk SSSR 281 (1981) 55.
[284] K.I. Babenko and A.P. Afendikov, preprint 82 (IPMatem AN SSSR, Moscow, 1987).
[285] T.S. Akhromeyeva, F.V. Bunkin, N.A. Kirichenko, S.P. Kurdyumov, G.G. Malinetskii and A.A. Samarskii, Izv. Akad. Nauk SSSR Ser. Fiz. 51 (1987) 1154.
[286] F.V. Bunkin, N.A. Kirichenko, S.P. Kurdyumov, A.B. Potapov and A.A. Samarskii, preprint 40 (IPMatem AN SSSR, Moscow, 1986).
[287] V.A. Bobyrev, F.V. Bunkin, N.A. Kirichenko, B.S. Luk'yanchuk and A.B. Simakin, Pis'ma Zh. Eksp. Teor. Fiz. 32 (1980) 608.
[288] A.V. Gaponov-Grekhov and M.I. Rabinovitch, in: Nonlinear Waves. Structures and Bifurcations (Nauka, Moscow, 1987) p. 7.
[289] L.S. Young, Ergod. Theory Dyn. Syst. 2 (1982) 109.
[290] O.E. Lanford, in: Hydrodynamic Instabilities and the Transition to Turbulence (Springer, Berlin, 1981).
[291] S. Aubry and P.V. Le Daeron, Physica D 8 (1983) 381.
[292] I. Prigogine, From Being to Becoming: Time Complexity in the Physical Sciences (Freeman, San Francisco, 1980).
[293] M.A. Demidov, A.P. Mikhailov and V.V. Stepanova, Dokl. Akad. Nauk SSSR 281 (1985) 41.